Report No. FAA-SS-72-70

SST Technology Follow-On Program – Phase I

TEST AND ANALYSIS OF A QUADRUPLE REDUNDANT HORIZONTAL STABILIZER ACTUATION SYSTEM

L.R.Appleford, M.L.Beattie, C.W.King,
E.L.Maylor, D.R.Ryder

The Boeing Company
Commercial Airplane Group
P.O. Box 3707
Seattle, Washington 98124

D6-60270
April, 1972

FINAL REPORT

TASK 7

Prepared for

FEDERAL AVIATION ADMINISTRATION
Supersonic Transport Office
800 Independence Avenue, S.W.
Washington, D.C. 20590

The contents of this report reflect the views of The Boeing Company, which is responsible for the facts and the accuracy of the data presented herein. The contents do not necessarily reflect the official views or policy of the Department of Transportation. This report does not constitute a standard, specification, or regulation.

TECHNICAL REPORT STANDARD TITLE PAGE

1. Report No.	2. Government Accession No.	3. Recipient's Catalog No.
FAA-SS-72-70		

4. Title and Subtitle	5. Report Date
SST TECHNOLOGY FOLLOW-ON PROGRAM–PHASE I, Test and Analysis of a Quadruple-Redundant Horizontal Stabilizer Actuation System	April 1972
	6. Performing Organization Code
7. Author(s) L. R. Appleford, M. L. Beattie, C. W. King, E. L. Maylor, D. R. Ryder	8. Performing Organization Report No. D6-60270
9. Performing Organization Name and Address The Boeing Company Commercial Airplane Group P. O. Box 3707 Seattle, Washington 98124	10. Work Unit No.
	11. Contract or Grant No. DOT-FA-SS-71-12
12. Sponsoring Agency Name and Address Federal Aviation Administration Supersonic Transport Office 800 Independence Avenue S.W. Washington D. C. 20590	13. Type of Report and Period Covered Final Report–Task 7 Nine Months
	14. Sponsoring Agency Code

15. Supplementary Notes

Other documents prepared: D6-60271 and D6-60272

16. Abstract

An SST flight control system has been analyzed and tested as a technical follow-on to the cancelled U.S.A. supersonic transport program. The qudruple-redundant horizontal stabilizer actuation system was evaluated to determine static performance, dynamic stability, force synchronization, dynamic (flutter) stiffness, electronically compensated stiffness, static stiffness, bottoming loads, failure detection and effects, and high hydraulic flow rate effects. Conclusions are that the actuation system concept was feasible and that linear analysis methods accurately predict the linear characteristics of the system.

17. Key Words	18. Distribution Statement
Redundancy - flight control system Flight controls Horizontal stabilizer Actuation system Supersonic transport	"Approved for U.S. Government only. Transmittal of this document outside of U.S. Government must have prior approval of the Office of Supersonic Transport Development."

19. Security Classif. (of this report)	20. Security Classif. (of this page)	21. No. of Pages	22. Price
Unclassified	Unclassified	201	

Form DOT F 1700.7 (8-69)

CONTENTS

CONTENTS (Concluded)

FIGURES

FIGURES (Continued)

FIGURES (Concluded)

TABLES

SYMBOLS

A	area of main actuator piston, sq in.
AR	amplitude ratio, output magnitude/input magnitude
A_1	area of electric command servo piston, sq in.
C_L	leakage coefficient, cu in./sec/psi
CPC	channel processor circuit
D_H	structural damping of housing, lb-sec/in.
D_L	structural damping of load, lb-sec/in.
D_P	equivalent viscous damping of piston, lb-sec/in.
D_R	structural damping of rod, lb-sec/in.
EC	electric command
EC_{MV}	electric command servo input, mV
F_A	average of the force developed by four actuators
F_L	$\Delta P_L A$, load force, lb
F_O	force developed by one actuator
F_R	rated force (developed by one actuator at 4000 psid)
ΔF	ΔPA, piston differential force, lb
f_D	damped natural frequency, Hz
$G(s)$	actuator open-loop transfer function
$G_1(s)$	actuator closed-loop transfer function
$G_2(s)$	electric command servo and linkage transfer function
$H_2(s)$	stiffness compensation network transfer function
K	$\frac{K_{oil}K_H K_R}{K_{oil}K_H + K_H K_R + K_R K_{oil}}$, equivalent actuator spring, lb/in.

$K_A(0)$	AR_F/R_{PF}, equivalent actuator spring at s = 0, or static stiffness, lb/in.
$K_A(s)$	stiffness, lb/in.
$K_A(\infty)$	equivalent actuator spring at s = ∞, or frequency-independent dynamic stiffness, lb/in.
K_E	integral equalization gain, V/in.
K_{EC}	ratio of main valve displacement to electric command servo input, in./mV
K_F	stiffness compensation feedback gain, mV/in.
K_{FE}	proportional equalization gain, V/in.
K_H	housing spring constant, lb/in.
K_L	load spring constant, lb/in.
K_{oil}	$4\beta A^2/V$, oil spring constant, lb/in. β = oil bulk modulus, psi; V = effective oil volume, cu in.
K_P	main valve pressure gain, psi/in.
K_Q	ECSS forward path gain schedule as a function of Mach number and q_c
K_R	rod spring constant, lb/in.
K_S	EC synchronization shaft stiffness, lb/in.
K_{TOT}	$(K\ K_L)/(K + K_L)$, total system spring, lb/in.
K_V	no-load flow gain, main valve, cu in./sec/in.
K_1	no-load flow gain, electric command servovalve, cu in./sec/mV
K_2	electric command servo feedback gain, mV/in.
LVDT	linear variable differential transformer
M_H	housing mass, lb-sec^2/in.
M_L	load mass, lb-sec^2/in.
M_P	piston and rod mass, lb-sec^2/in.
P_{C_1}	actuator cylinder retract pressure, psi
P_{C_2}	actuator cylinder extend pressure, psi

$P_{L_{1(2,3, or 4)}}$	load pressure of No. 1 (2, 3, or 4) main actuator piston, psi
$P_{L_{aver}}$	average load pressure of all four actuators
P_R	actuator return pressure, psi
P_S	actuator supply pressure, psi
ΔP	differential pressure across main actuator piston, positive retract, psi
Q	pitch rate, deg/sec
q_c	impact pressure, lb/sq ft
R_E	command input gain schedule as a function of Mach number and qc
R_F	ratio of main valve displacement to rod displacement, in./in.
R_{IN}	ratio of main valve displacement to mechanical input displacement, in./in.
R_{PF}	effective pressure feedback gain including leakage, inverse pressure gain, and structural effects, in./psi
R'_{PF}	feedback gain of actuator pressure feedback device, in./psi
SSD	signal selection device
s	Laplace operator
$X_{p_{1(2,3, or 4)}}$	No. 1 (2, 3, or 4) main actuator control valve position
$X_{PFB_{1(2,3, or 4)}}$	No. 1 (2, 3, or 4) actuator pressure feedback piston position, in.
$X_{V_{1(2,3, or 4)}}$	No. 1 (2, 3, or 4) actuator main control valve position
X_{EC}	electric command servo piston displacement, in.
X_H	actuator housing displacement along rod axis, in.
X_{IN}	mechanical input, in.
X_L	load displacement, in.
X_p	piston displacement, in.
X_R	piston rod-end displacement, in.
X_{VC}	main valve command, in.
X_V/X_{EC}	ratio of main valve position to electric command servo output, in./in.

X_V/X_H	ratio of main valve position to housing position, in./in.
X_V/θ_M	ratio of main valve position to mechanical input arm position, in./deg
δ	stabilizer position, positive, trailing edge down, deg
δ_{COL}	angular travel of control column, deg
θ_B	mechanical input bus shaft position, deg
θ_B/X_{IN}	ratio of bus shaft position to mechanical input position, deg/in.
θ_M/θ_B	ratio of mechanical input position to bus shaft position, deg/deg
θ_M/X_R	ratio of mechanical input position to rod position, deg/in.
ζ	damping ratio
ζ_{CL}	damping ratio of closed-loop second-order poles (system damping ratio)
ζ_L	damping ratio of load (M_L, K_L)
ζ_O	damping ratio of open-loop second-order poles
ζ_{OD}	damping ratio of open-loop second-order poles, with load damping
ϕ	phase angle, ϕ_{XP_1}/ϕ_D
ω_a	break frequency of stiffness compensation lag, rad/sec
ω_B	break frequency of stiffness compensation lead, rad/sec
ω_c	actuator break frequency, loaded, rad/sec (inverse of closed-loop time constant)
ω_{CL}	natural frequency of closed-loop second-order poles, rad/sec
ω_D	$(KK_VR_{PF})/A^2$, dynamic stiffness break frequency, rad/sec
ω_{EC}	$(K_1K_2)/A$, electric command servo break frequency, rad/sec
ω_L	natural frequency of load, rad/sec
ω_O	natural frequency of open-loop second-order poles, rad/sec
ω_{OD}	natural frequency of open-loop second-order poles, with load damping, rad/sec
ω_S	$(K_VR_P)/A$, actuator no-load break frequency, rad/sec (or open-loop gain)

1.0 SUMMARY

The Boeing Company has successfully completed an SST technical follow-on program of flight control system analyses and tests for the Department of Transportation. Using a laboratory test rig (iron bird) built before cancellation of the SST program, the quadruple-redundant horizontal stabilizer actuation system was analyzed and tested to evaluate performance and feasibility of the system and to preserve the technical information for future airplanes.

The actuation system had four identical power control units, each consisting of an actuator (rated at 87,000 lb output force) and an integrated control module. The control module contained an electric command (EC) servo and linkage for summing the electrical commands with mechanical input commands. The laboratory test rig consisted of a section of the SST aft body containing the actuation system with a simulated "slab tail" horizontal stabilizer and geared elevators.

The results of the analysis and test program are given in sections 4.0 and 5.0. Based on these results, it is concluded that the tested system would have been feasible for the SST prototype airplane after certain deficiencies were corrected. Specific conclusions from the testing are as follows:

1. Linear Analysis

   A linear analysis program demonstrated the ability to predict the dynamic characteristics of a multiple-channel actuator system mounted in a flexible structure. The program predicted the stability and frequency response of the system with a good degree of correlation. The measured static stiffness did not agree well with the linear analysis due to discrepancies between the model and the test structure.

2. Static Performance

   Under various normal and failure operating conditions, the system would probably achieve the stabilizer position repeatability requirement of 0.050° by correcting the reduced EC servo pressure gain caused by the reduced land lengths of the EC servo pistons.

3. Stability Tests

   Stability tests demonstrated that the control system dynamic response characteristics compare favorably with the SST specifications and those predicted by theoretical analysis. Stability of each actuator was achieved by feeding back differential load pressure mechanically to the control valve. System stability was very sensitive to nonlinearities such as friction in the mechanical parts, demonstrating that special care in design of such devices is extremely important.

4. Force Synchronization

The four actuators were able to be adjusted to be within the specified tolerance band and, after being adjusted, the synchronization did not vary excessively outside of the acceptable tolerance band for actuator removal and replacement, temperature changes, operating time, load changes, or surface position. When in the electric command mode of operation without electrical equalization, the actuators did not stay synchronized. This was caused by tolerances in the electrical loops and clearly proved the need for electrical equalization to force the EC servos to track each other more precisely and keep the actuators in synchronization.

5. System Dynamic Stiffness Tests

Dynamic stiffness test results showed sufficient stiffness for flutter restraint during normal conditions. During large command, stall, and blowback conditions the system did not exhibit the specified stiffness and would have required hardware changes and continued flutter analysis and testing to ensure proper suppression of stabilizer flutter during these transient conditions. The very close match of all dynamic stiffness test data to first-order linear approximations showed that good computer methods can be readily developed to analyze stiffness and flutter during transient conditions.

6. System Static Stiffness Tests

Static stiffness test results showed wide variations in stiffness depending on load application position and pressure feedback malfunctions, number of actuators powered, and stabilizer position. It was concluded that it would be desirable to eliminate the complex structural influences on static stiffness and rely solely on internal pressure feedback or separate reaction structure and appropriate control linkage to ensure proper static stiffness.

7. Electrical Compensation System Stiffness

Electric stiffness compensation could be used to increase stiffness and improve repeatability and load droop without sacrificing the stability of the system.

8. Actuator Bottoming Loads

No impact loads approached the 87,000 lb force capability of the actuator. Acceleration loads when the valve was opened to start motion were higher than the bottoming loads. Unless fatigue loads become critical, snubbing would not be needed for these actuators.

9. Main Actuator Failure Detection and Effects

The main actuator relief/bypass valve that was used to limit the system performance loss after the hardover failure of any of the four actuators, signal this failure to the flight crew, and limit the maximum aerodynamic load that could be imposed

on the airplane tail performed all functions as expected. The testing showed that a delay circuit would have to be used on the failure detection system to avoid false failure indications.

10. EC Servo Failure Detection

The SST fail-operational concept limited failure transients to less than 0.1° for any single EC servo failure. The detection system, as designed, reliably detected EC servo failures without false indication at normal system operating levels.

11. High Hydraulic Flow Rates

Design of hydraulic control systems with a major portion of the pressure drop in the hydraulic lines is an acceptable way to reduce system weight. The analysis method used to predict transient hydraulic system behavior was in good agreement with test data.

2.0 INTRODUCTION

After cancellation of the U.S.A. supersonic transport program early in 1971, The Boeing Company proposed to the Department of Transportation a follow-on program to complete certain flight control system tests and evaluations to preserve technical information for support of design and development of future airplanes. The proposed program of laboratory tests and analyses of the quadruple-redundant horizontal stabilizer actuation system has been completed using a test rig assembled and checked out just before the SST program cancellation.

The most significant features of the actuation system were (1) the high force capability for the large aerodynamic loads, (2) the reliance on the actuator system stiffness (rather than mass balancing) to suppress flutter, (3) the four-channel integrated electronic stability augmentation servos needed because of the aerodynamic instability of the SST at subsonic speeds, and (4) the force voting and equalization between the four actuators to provide fail-operational/fail-safe redundancy.

The tests reported herein determined static performance, dynamic response, stability, force synchronization, bottoming loads, static stiffness, system dynamic (flutter) stiffness, electronically compensated stiffness, failure detection and effects, and high hydraulic flow rate effects at normal and abnormal operating conditions. A linear mathematical model of the actuation system and structure and a digital computer program are presented for analytically determining closed-loop stability, closed-loop frequency response, static and dynamic stiffness, and electronically compensated stiffness.

3.0 SYSTEM DESCRIPTIONS

3.1 PROTOTYPE SST PITCH AXIS FLIGHT CONTROL SYSTEM

Two fundamental decisions were instrumental in determining the flight control configuration for the SST:

1) The decision to incorporate a moderate-aspect-ratio delta wing with leading and trailing edge flaps for high lift/drag (to ensure good low-speed performance and low noise) required an aft tail surface for trim and control.

2) To optimize airplane payload/range performance (through reduced weight and drag), the airplane longitudinal balance placed the operating center-of-gravity (cg) range aft of the longitudinal stability neutral points for subsonic operation, resulting in an unstable configuration.

The requirement for minimum tail size dictated a high-rate, all-movable horizontal stabilizer with geared elevators. The elevators are slaved to stabilizer movement by means of constant-ratio mechanical linkage connected to the body structure such that the effective camber of the horizontal stabilizer is increased as a function of stabilizer deflection from neutral (see figs. 1 and 2).

The supersonic performance advantages of having the engines located on the trailing edge of the wing caused an airplane balance problem which would have required an extension of the fuselage forward to provide acceptable cg limits for stability. To shorten the fuselage and minimize tail size, thus saving weight and improving aerodynamic performance, it was elected to locate the cg aft of the maneuver neutral point at subsonic speeds. A highly reliable electronic stability augmentation system was therefore required for safety of flight. System redundancy was necessary to ensure that the occurrence of multiple failures resulting in loss of function would be an extremely remote possibility. The longitudinal axis was configured using a redundant electronic system as the primary means of control, with a single-thread mechanical backup system. The requirement for safety and thus high electronic integrity resulted in the development of two systems: (1) the hardened stability augmentation system (HSAS) and (2) the electric command and stability system (ECSS).

The longitudinal flight control system is shown schematically in figure 3. Pilot commands were transmitted from the pilots' controls by mechanical linkage and cables to the master servo. The master servo performed the function of a force-isolating boost servo and was connected mechanically to the control valves on the four stabilizer actuators. An artificial feel system was introduced near each control column, with spring centering at the master servo input. Pitch commands were also transmitted electrically via the four-channel HSAS and ECSS systems to the four electric command (EC) servos. The HSAS provided stabilization to ensure minimum safe handling qualities; the ECSS to ensure normal handling qualities. The output of the EC servos was mechanically summed with the output of the master servo at each surface actuator. Multiple load paths were provided from the control columns to the feel systems and from the master servo to the four stabilizer actuators. Each of the four actuators was powered by a separate, independent hydraulic system.

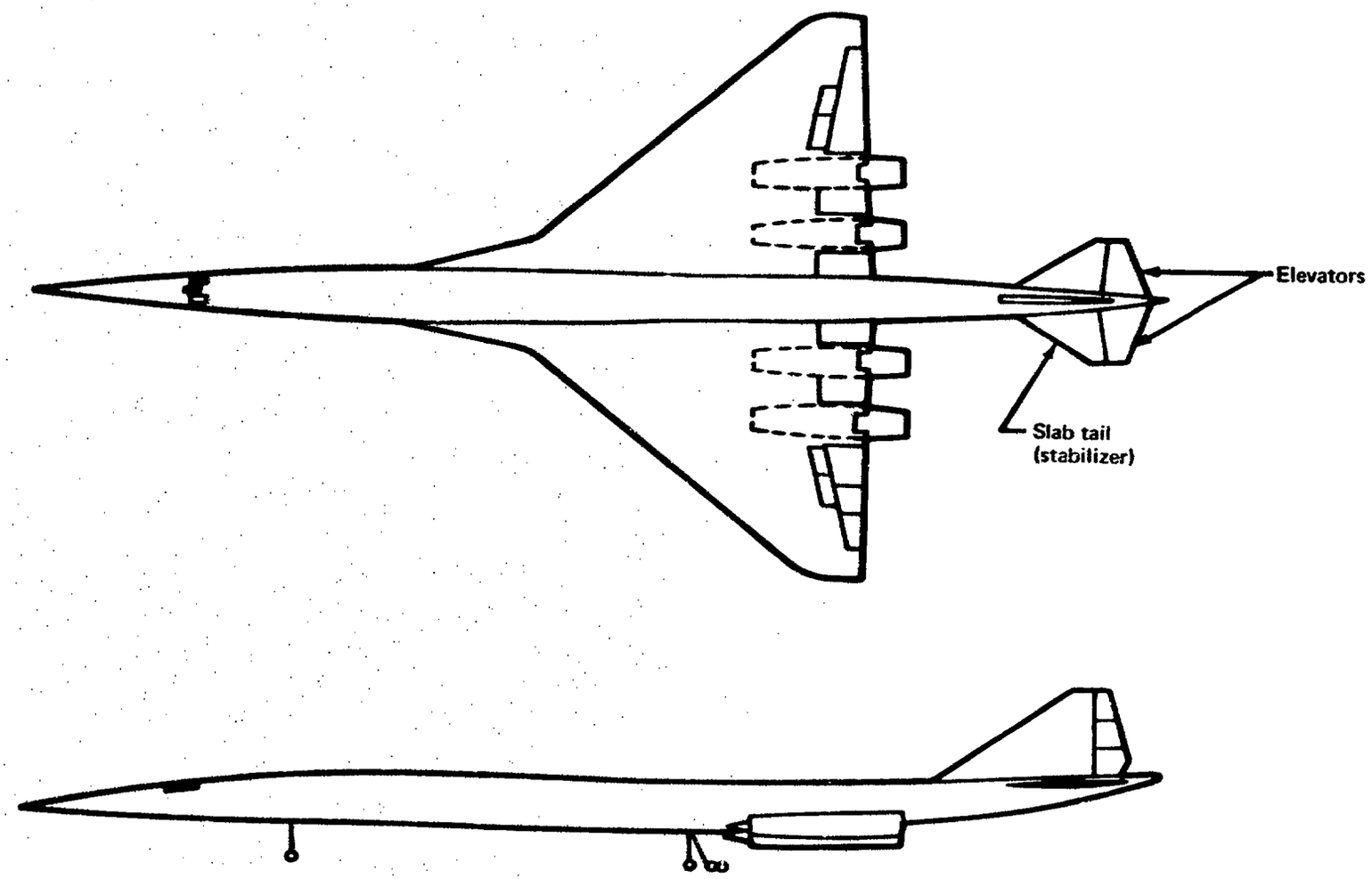

FIGURE 1.–PROTOTYPE SST

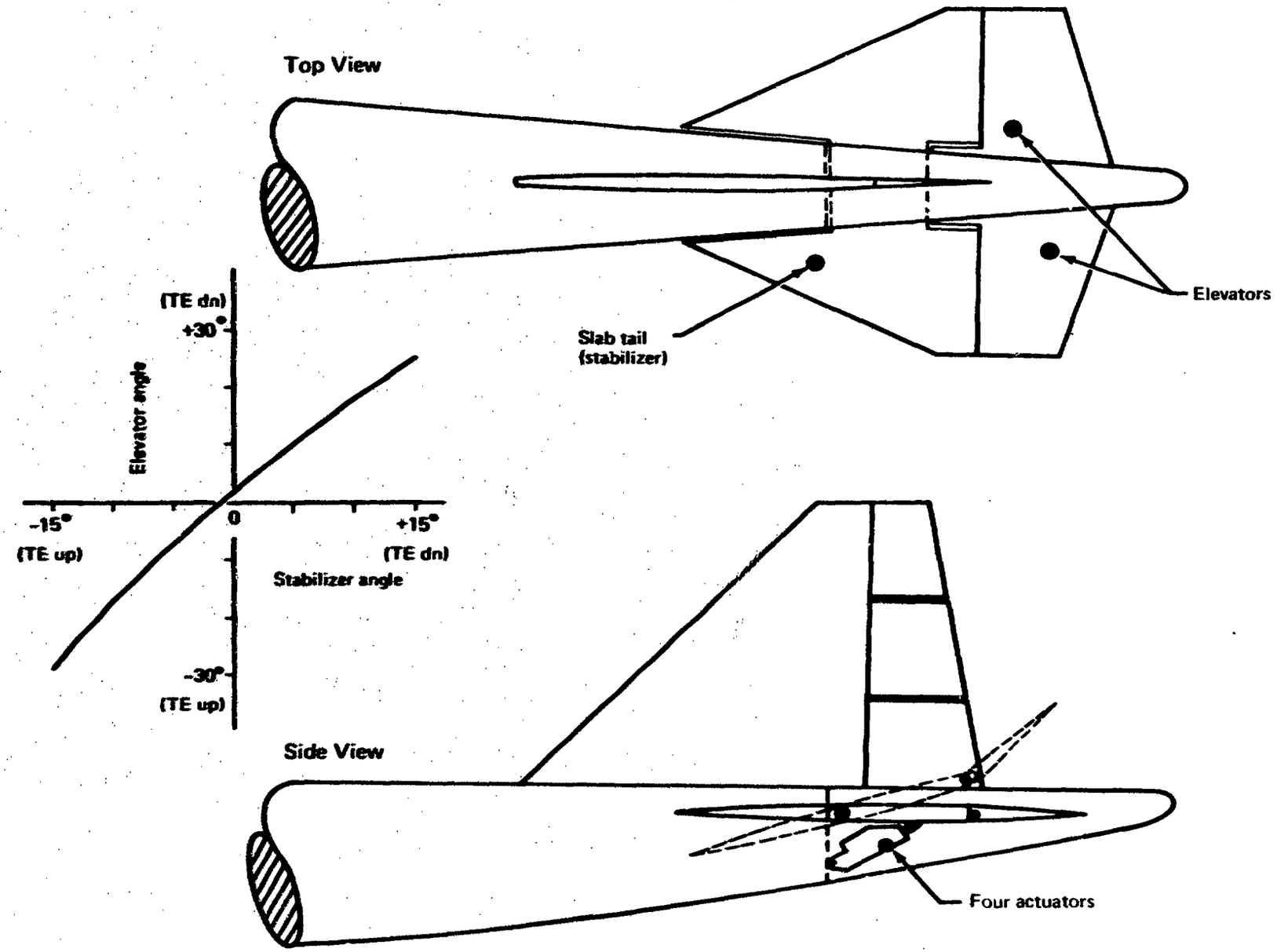

FIGURE 2.–SST LONGITUDINAL FLIGHT CONTROL SURFACES

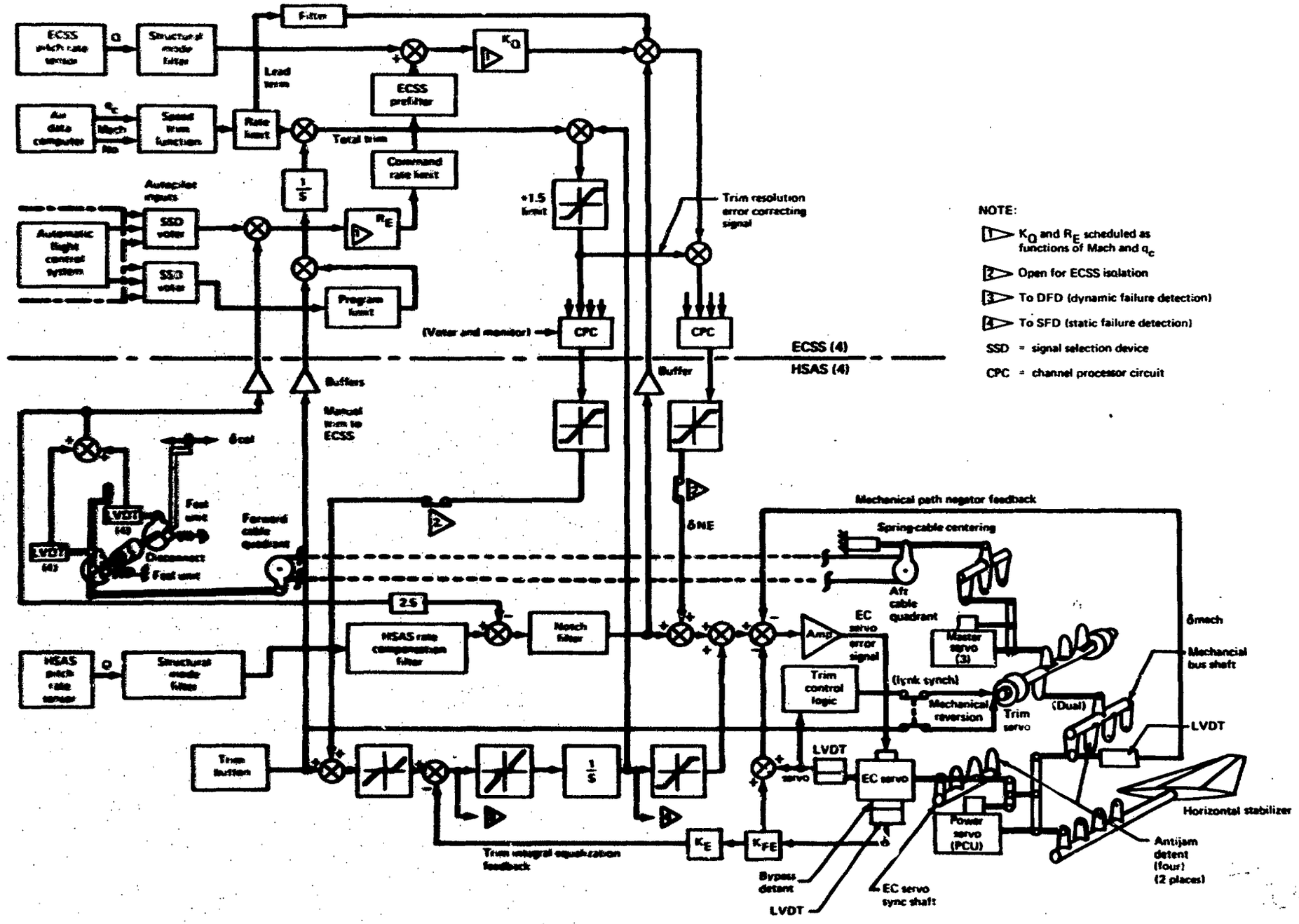

FIGURE 3.–SCHEMATIC OF LONGITUDINAL FLIGHT CONTROL SYSTEM

3.1.1 Mechanical System

Since the control cable system performed a backup control function only and was not needed for normal operation, it was designed as a single load path system to save weight and space and to minimize friction. Because good feel characteristics were required in the event of failure of the cable system, the major portion of the feel system was located at the control columns. A minor portion of the feel system spring centering was on the master servo input to center the master servo and thus preserve the HSAS integrity in the event of a cable break. The forward portion of the feel system was divided between pilot and copilot, with the detent portion of the system on the pilot's column.

A set of four position sensors were mounted on each column and their outputs summed to form the HSAS column command signals. A pilot-operated disconnect was placed between the two columns to retain control in the event of a column jam.

In the mechanical reversion mode, with the airplane cg at the median to forward location, a pilot could control the airplane safely without a stability augmentation system.

3.1.2 Pitch Trim Control System

The pitch trim control system utilized a servo actuator consisting of four ac servomotors rate summed to produce one output. Use of brakes, no-backs, and dual load path design avoided a single failure point anywhere in the system. The speed trim commands caused EC servo deflections, which were then offloaded through the "LINC-SYNC" path (see fig. 3) into the trim motor.

3.1.3 Hardened Stability Augmentation System (HSAS)

Since the HSAS was required for minimum safe airplane handling qualities, it had to be very reliable. The system design was based on the premise that the simplest design would be the most reliable. Functions such as gain scheduling that were nonessential for safe flight and reduced reliability were avoided. The HSAS design had to meet the following requirements:

- Four channels of electronics and hydraulics were required to meet reliability goals.
- Physical separation of channels was required, and channel interconnections were not allowed. No electronic cross-channel voting was allowed.
- Failure of the ECSS was not allowed to affect the HSAS operation.

Figure 3 shows the separation of HSAS and ECSS in the longitudinal flight control system. The column position sensors, feel units, column disconnects, and trim portions of the HSAS have been explained in the preceding sections.

The single cable system was made nonessential for safe flight by generating the total surface command electrically, and then subtracting the mechanical path command to create the EC servo command, i.e., the EC servo always supplied the difference between the desired surface command (electric command) and the mechanical path input. Hence, if the

mechanical path failed, the EC servo would command the correct surface position until it reached the limit of its authority. The mechanical path command was measured by the negator transducer. The output of this transducer is labeled the "mechanical path negator feedback" in figure 3.

The actuator piston of each EC servo drove the error linkage of its own main actuator and was also coupled to the other EC servo pistons by an external EC servo synchronization shaft. Antijam detents were provided so that any single EC servo piston or linkage jam would cause only one main actuator to have an erroneous command signal. The failure was isolated by depressurizing the hydraulic system to the failed actuator, thus allowing the system to continue operation on three channels.

Across each EC servo piston was a bypass valve (EC servo equalizer valve) set to operate when the pressure across the EC piston reached 292 psi. (See sec. 3.3.2.1 for a description of the electric command servo equalizer.)

Without equalization, command offsets and tolerances between HSAS channels would cause the equalizer valves to operate full stroke since EC servo position errors could not be satisfied with the output of the four channels connected by the relatively stiff synchronizing shaft and linkage.

Electrical and mechanical unbalances between the four EC servos were corrected by feeding back to the position loop a voltage proportional to the equalizer valve position. This voltage was also integrated electronically and fed back to provide the necessary steady-state balancing input. The equalizer signal drove the integrator through an electrical threshold. This threshold prevented the equalization integrators from eliminating the steady-state force capability of the servos. The equalization integrators also served as trim integrators.

Cross-channel failure monitoring was used at the points labeled "DFD" and "SFD." The DFD signal was used for dynamic failure detection and the SFD signal for static failure detection, i.e., the DFD signal should always have a steady-state value of zero as long as the servo and the equalization loops are operational. Cross-channel comparison of the SFD points detected the static channel offsets plus the dynamic offsets that filtered through the equalization integrators.

Mechanical reversion transients were minimized by offloading the EC servo position into the mechanical trim input. The servo offloading signal into the trim motors is labeled "LINC-SYNC" in figure 3. Any time the EC servo position exceeded a value of $\pm 0.25^\circ$ (equivalent surface) for a time interval longer than 2 sec, the trim motors were commanded to run in the direction the servos were displaced. As the trim motors ran, the mechanical path negator feedback caused the servos to retract towards center until the servo displacement was less than $\pm 0.2^\circ$. The EC synchronizing shaft compliance and EC servo equalizers kept the actual mechanical reversion transients to approximately $\pm 0.1^\circ$ when the servos were offloaded within the $\pm 0.2^\circ$ threshold.

3.1.4 Electric Command and Stability System (ECSS)

The ECSS augmented the basic airplane to provide normal handling qualities. Gain scheduling and additional sensors were allowed. Electronic cross-channel voting isolated ECSS failures from the HSAS. Limiters set to tolerable hardover values were downstream of all electronic voters to protect against any unknown system output hardover failure conditions. The ECSS was the only system nonessential for safety which interfaced with the HSAS.

3.1.5 Automatic Flight Control System

Autopilot flight director and control wheel steering modes were provided by the automatic flight control system. Autopilot functions were tied into the ECSS in a series fashion, with voting at the automatic flight control system output and ECSS input to isolate automatic flight control system failures from propagating into the ECSS/HSAS.

3.2 CONTROLS DEVELOPMENT (CODE) TEST RIG

For the purpose of conducting developmental and verification tests of the flight controls systems during the SST program, a controls development (CODE) test rig, or iron bird, was constructed. The portion of the CODE rig for the longitudinal control system included a 131-in. section of the aft body installed on a support structure, with a simulated horizontal stabilizer and elevators, a prototype actuation system, and a hydraulic power supply system. The following is a description of these CODE rig elements as used in the test program reported herein.

3.2.1 Structure

3.2.1.1 Support Structure

The steel structure (fig. 4) for supporting the aft body section was constructed on a foundation of concrete, steel, and piling. The aft body section was cantilever mounted from a vertical plane at airplane body station 3204.430, or 50.851 in. forward of the stabilizer hinge line. The support structure was designed as a highly rigid structure so that compliance of the aft body section and the actuation system could be referenced to essentially "grounded" structure.

3.2.1.2 Aft Body Section

The aft body section (figs. 5, 6, and 7) included all body structure elements from body station 3204.439 to 3335.04. The major features included the main bulkhead at station 3248 for support of the stabilizer hinges, the four actuators, and the brackets for the EC servo synchronization shaft and mechanical input bus shaft. Also included were the master servo mounting provisions forward of the 3248 bulkhead and the elevator anchor link attach point at station 3315.486. The section was built of aluminum regaged as necessary to duplicate the stiffness and strength of the airplane titanium structure. All dimensional features and tolerances were the same as those of the airplane.

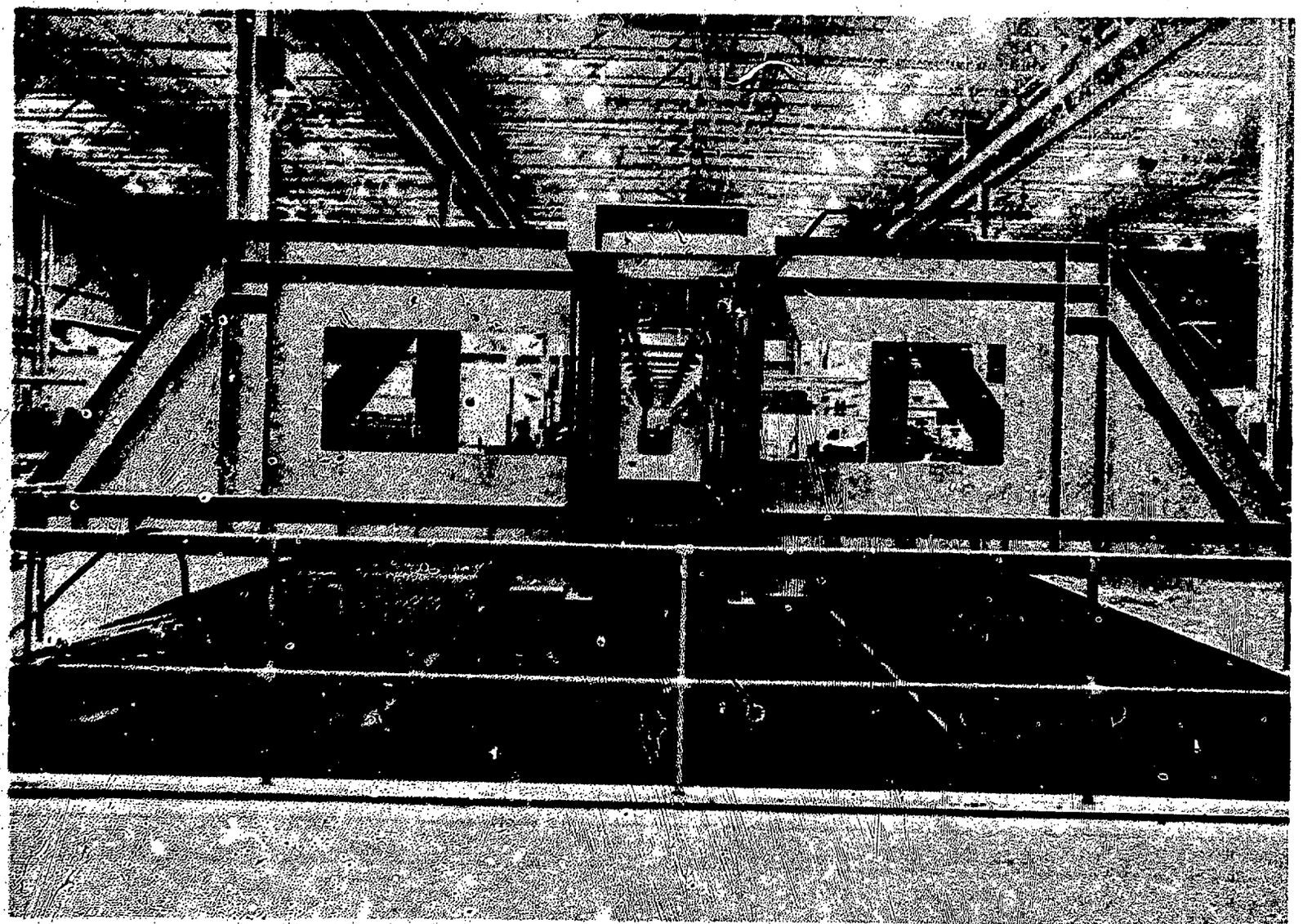

FIGURE 4.–CODE RIG SUPPORT STRUCTURE

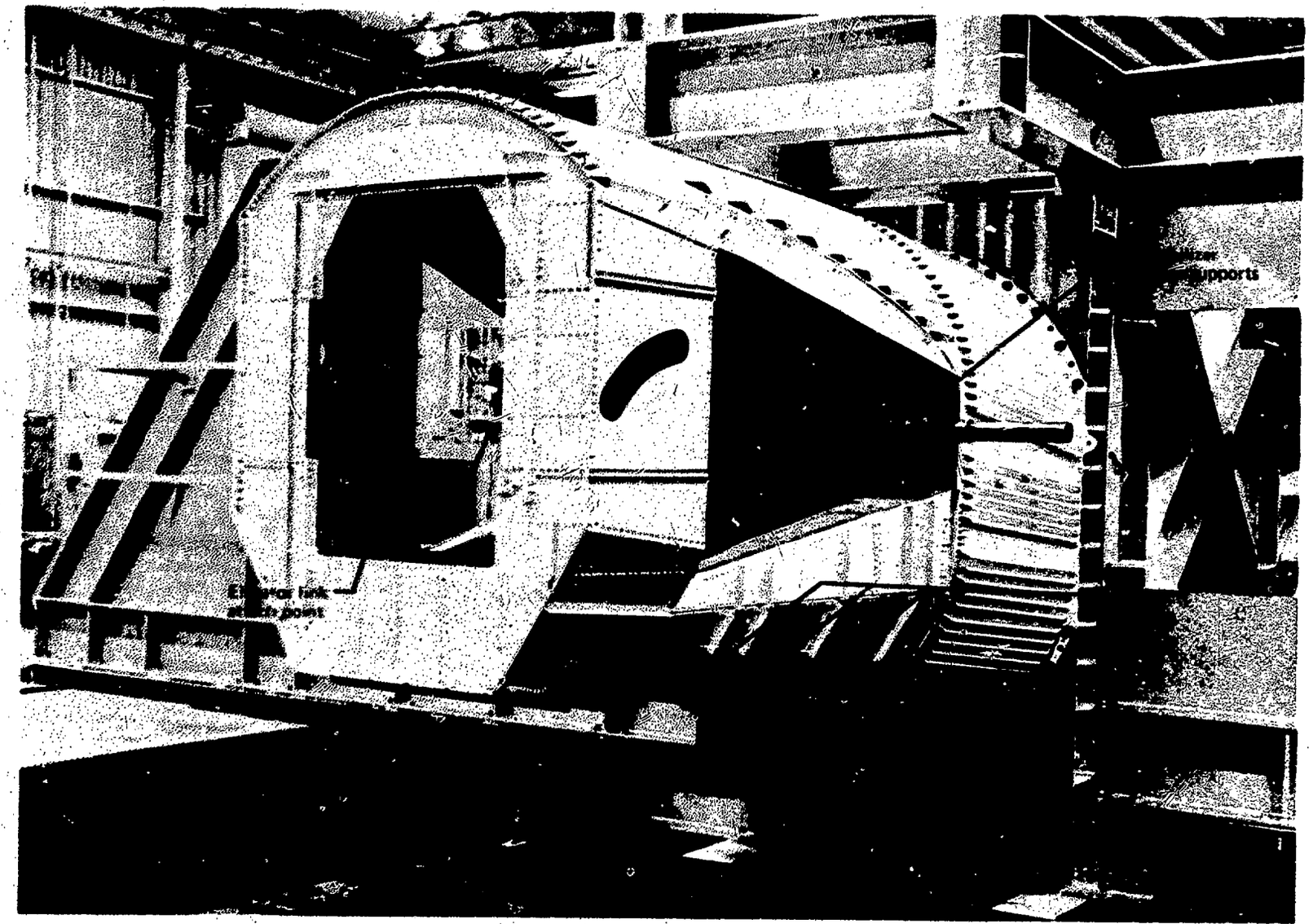

FIGURE 5.—AFT BODY SECTION

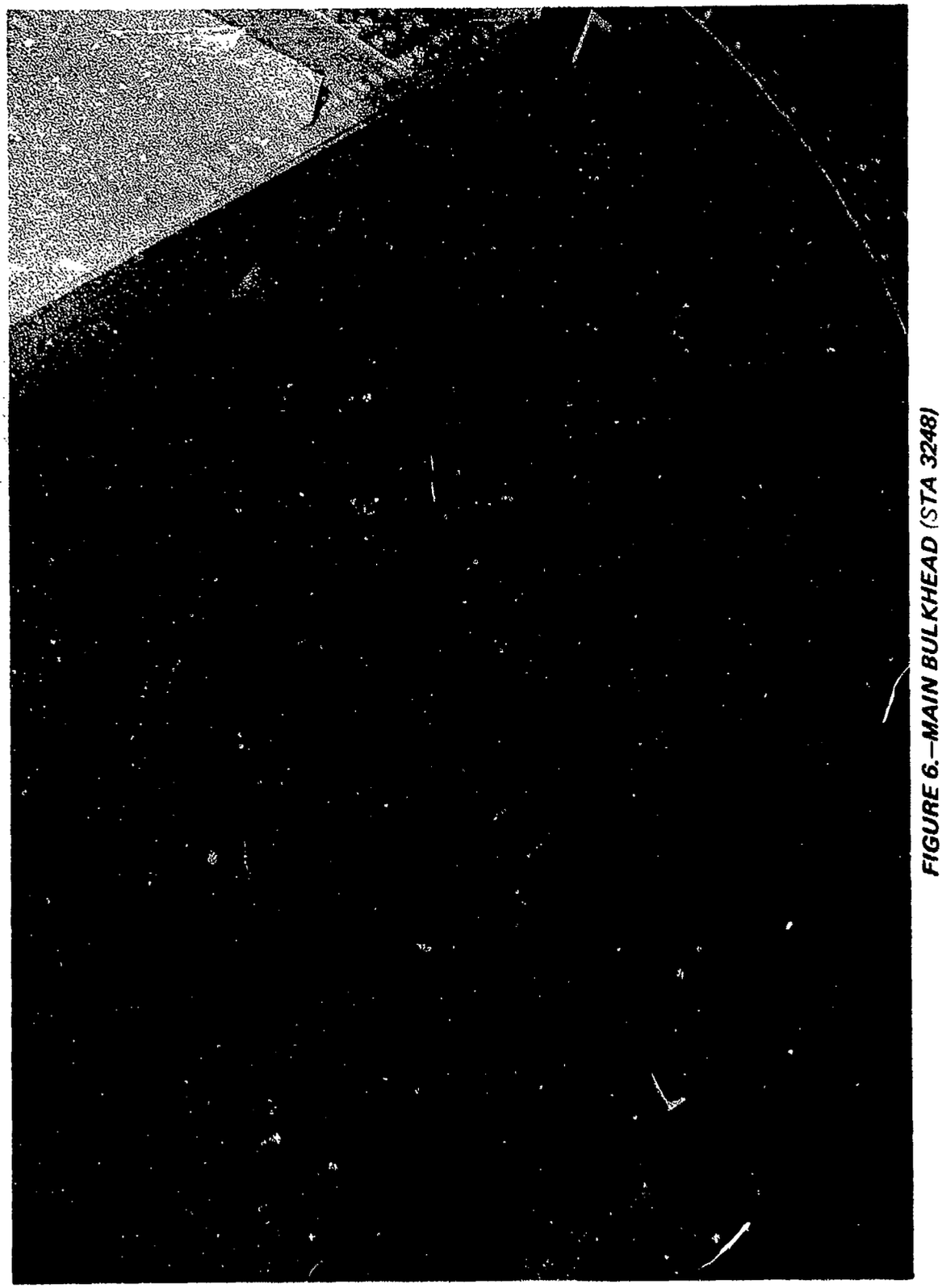

FIGURE 6.—MAIN BULKHEAD (STA 3248)

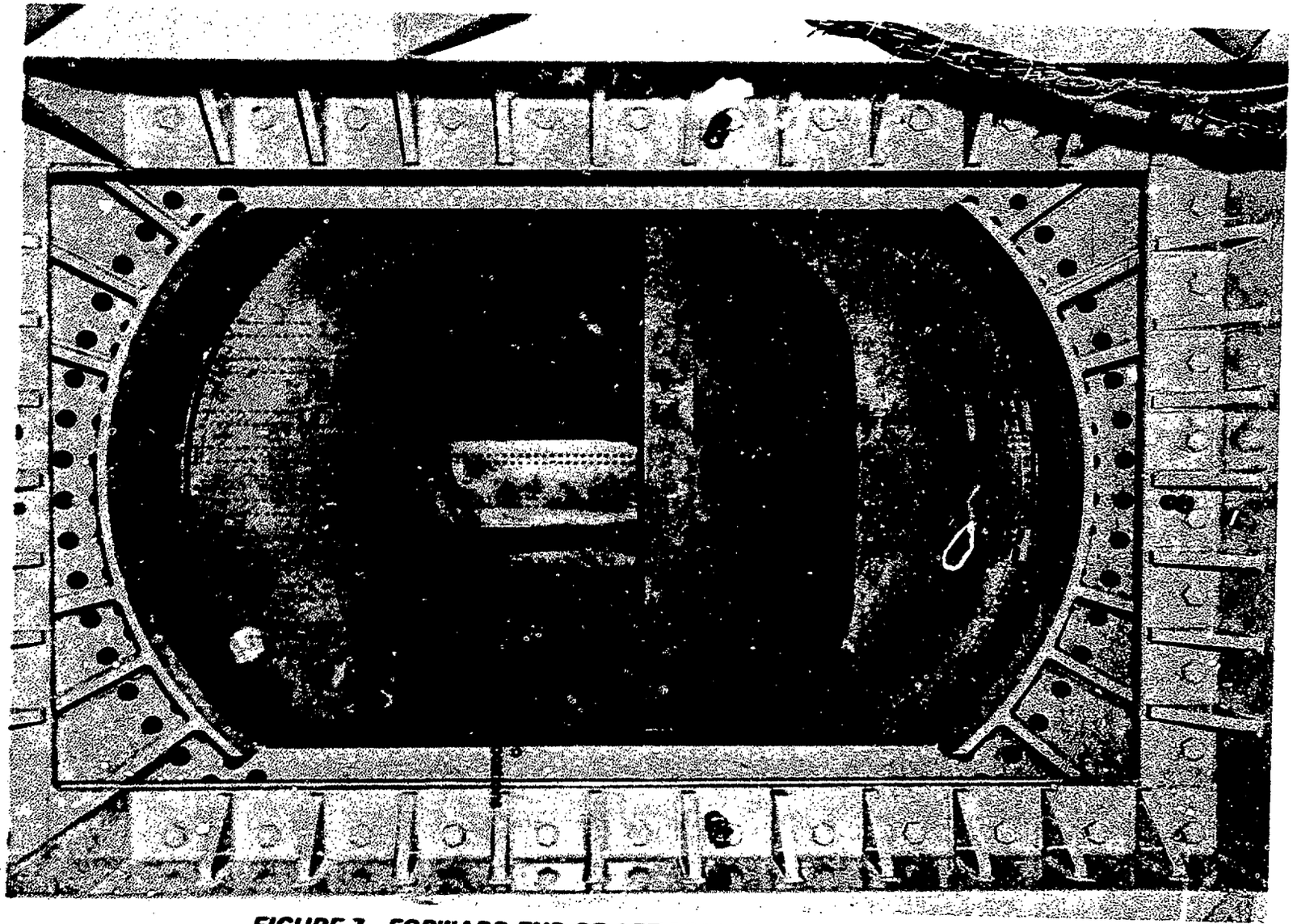

FIGURE 7.–FORWARD END OF AFT BODY SECTION–LOOKING AFT

3.2.1.3 Stabilizer and Elevators

The simulated stabilizer and elevators (figs. 8 and 9) were designed to have mass properties similar to those of the prototype with a stiffness to give the same first-mode natural frequency as predicted for the airplane surfaces. The stabilizer hinge fittings and actuator fittings were dimensionally equivalent to those of the airplane configuration, but the outline shapes and materials were altered to make the construction more economical.

The elevator installation included the anchor link to duplicate the airplane elevator gearing ratio. A pair of load beams were attached to the outboard edges of the stabilizer to distribute static hinge moment point loads.

3.2.2 Actuation System

The actuation system (figs. 10 and 11) consists of four actuators attached to the stabilizer. These four actuators contained an integrated EC servo and were commanded (1) mechanically by a mechanical actuator via the input bus shaft, and (2) electrically by the CODE servo electronics signaling the integrated EC servo.

3.2.2.1 Main Actuator

Each main actuator (fig. 12) has an output stroke of 17.4 in. and an effective area of 21.8 sq in. The nominal supply and return pressures are 4150 and 150 psi, respectively. The rated output force is 87,000 lb. The rated actuator velocity at 1000 psid pressure drop from the manifold pressure port to return port and 200° F supply temperature is 13.2 ±1.2 in./sec. The following paragraphs describe certain important components of the actuator.

Main Control Valve and Pressure Feedback—The main control valve (fig. 13) is a net lap, pilot-operated, slide and sleeve metering valve actuated by mechanical inputs to the pilot valve. A linear variable differential transformer (LVDT) position sensor enables the valve slide position to be measured when the actuator is pressurized.

The static pressure feedback device is internally summed with the actuator input (mechanical or electrical) so as to reduce the actuator's effective pressure gain.

Main Actuator Relief/Bypass Valve—The main actuator cylinder relief/bypass valve (figs. 14 and 15) is a pressure-operated slide valve on each main actuator cylinder. It is biased to its center position by preloaded springs and is actuated by comparing the main actuator cylinder pressures with the supply pressure (see fig. 16). When a cylinder pressure exceeds the supply pressure by 200 ±50 psi, the valve slide approaches one end of its travel and will begin to bypass. Flow will then occur from the high-pressure side to the low-pressure side of the main actuator cylinder. This is known as the "bypass" position (see fig. 17).

The valve will seek its center position when the supply and cylinder pressures are nearly equal. This will occur when the hydraulic supply pressure is zero or when a power control unit is misrigged with respect to the other units so that its cylinder pressure is equal to the supply pressure in a static condition. The center position of the valve is referred to as the "depressurized" or "equal-pressure" position.

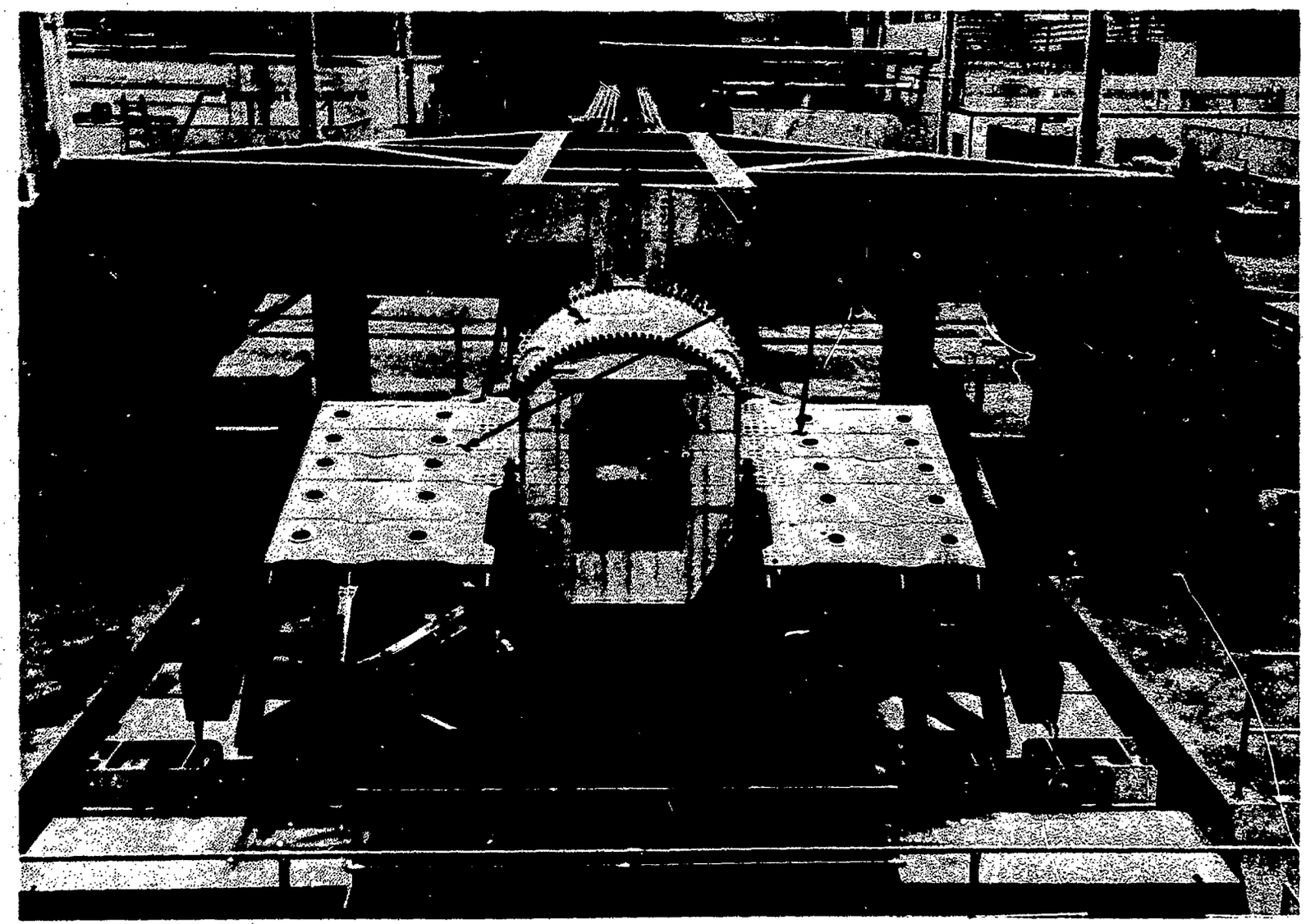

FIGURE 8.–CONTROLS DEVELOPMENT (CODE) TEST RIG

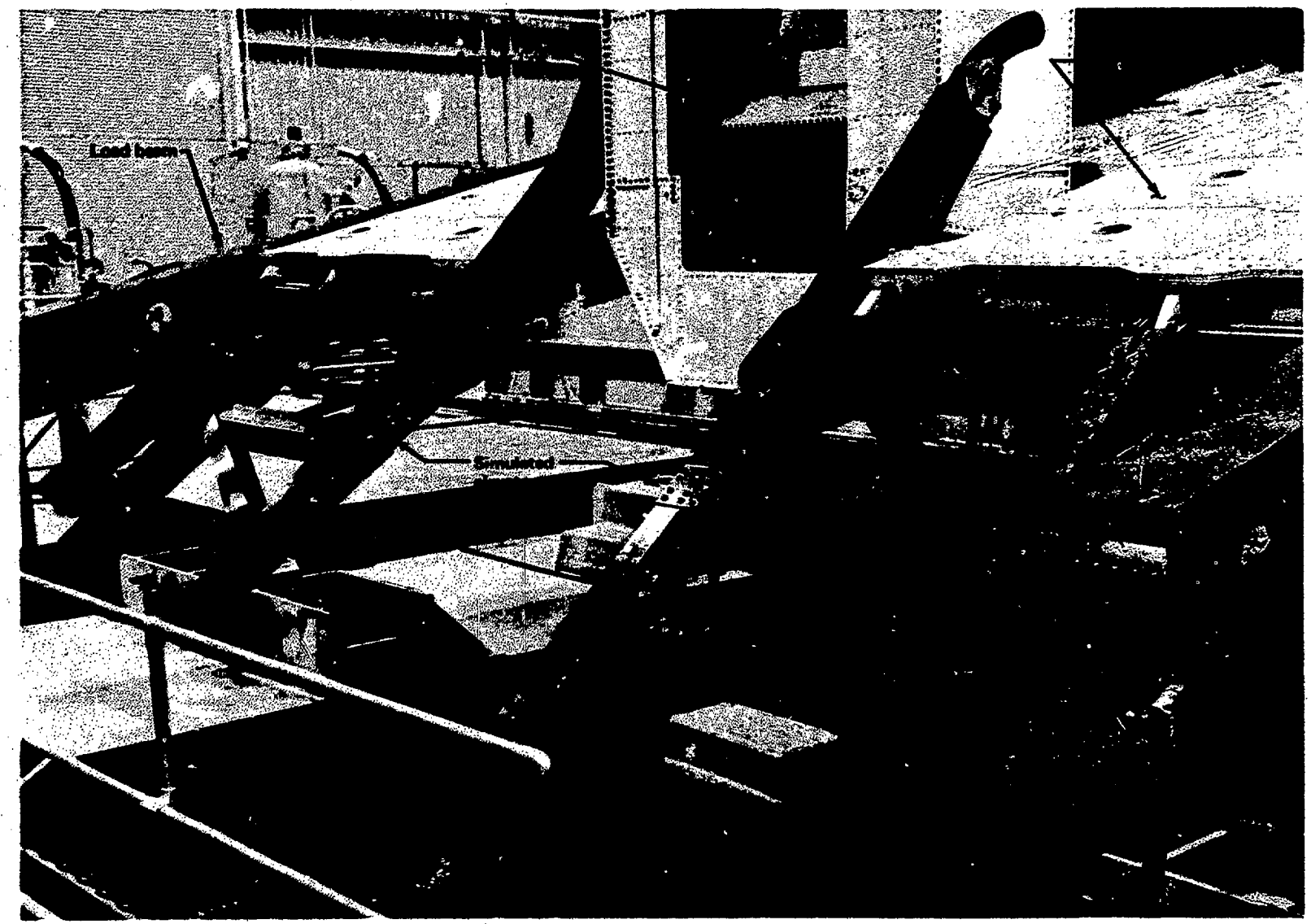

FIGURE 9.—SIMULATED STABILIZER AND ELEVATORS

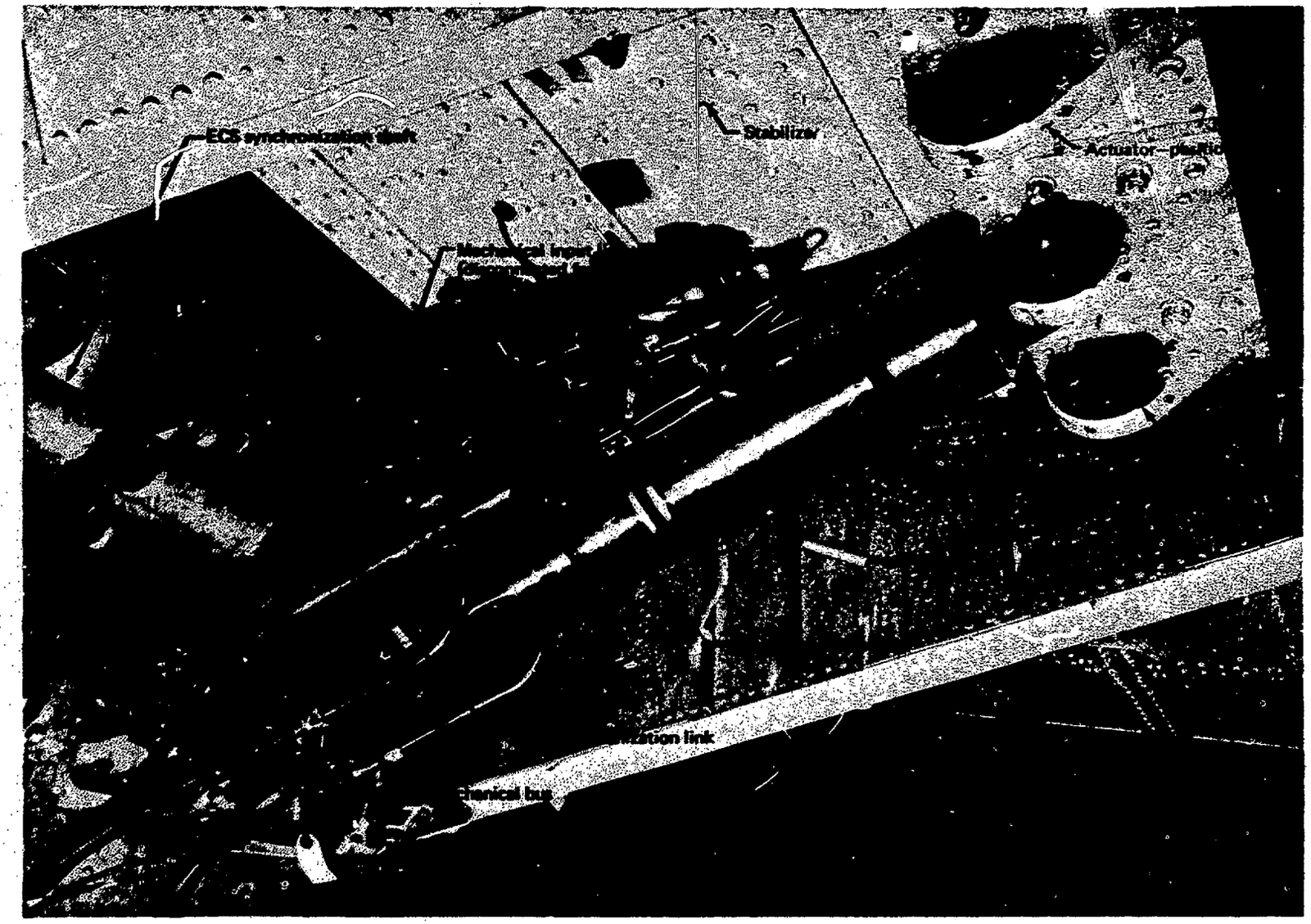

FIGURE 10.—ACTUATOR INSTALLATION

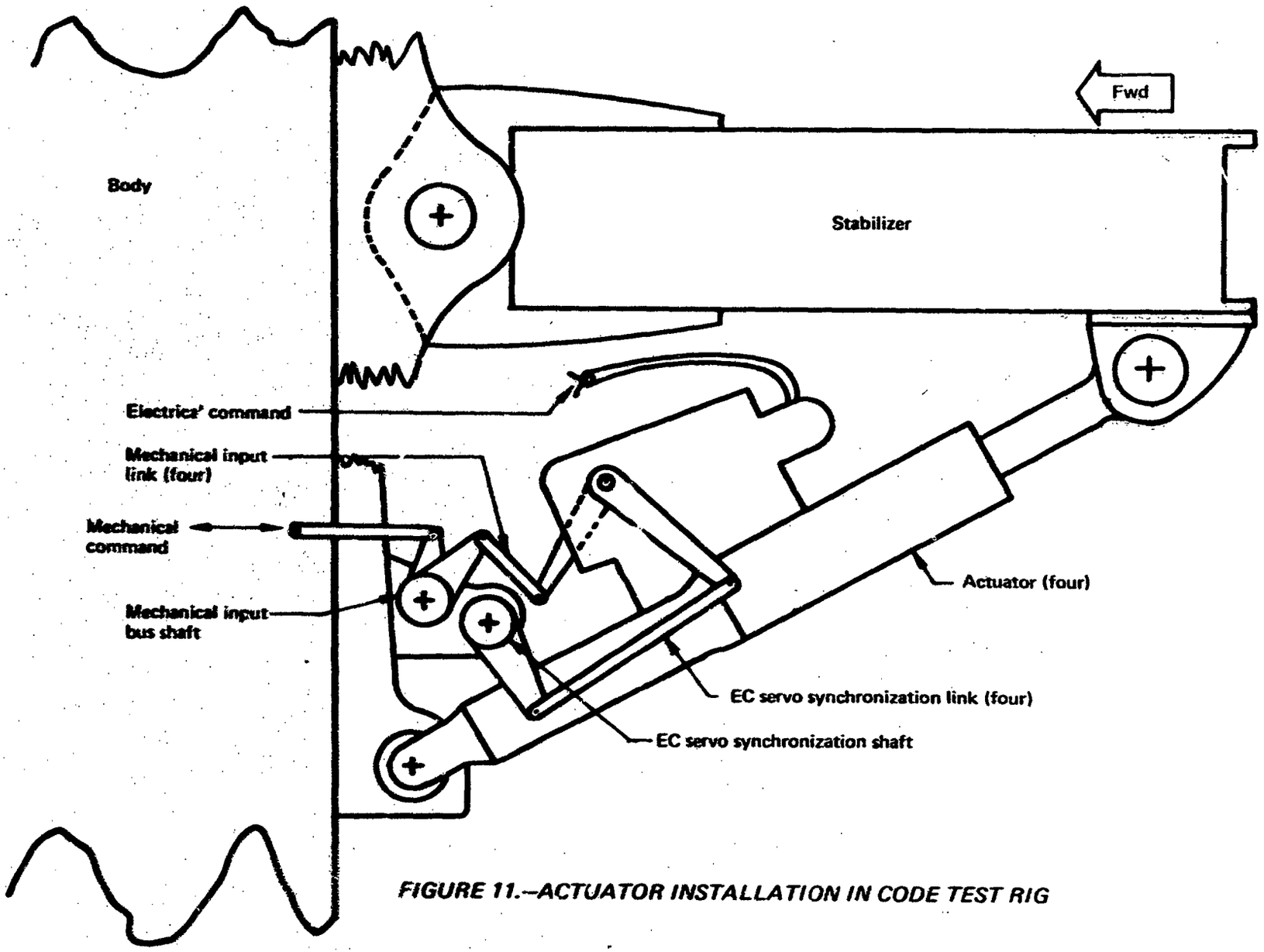

FIGURE 11.—ACTUATOR INSTALLATION IN CODE TEST RIG

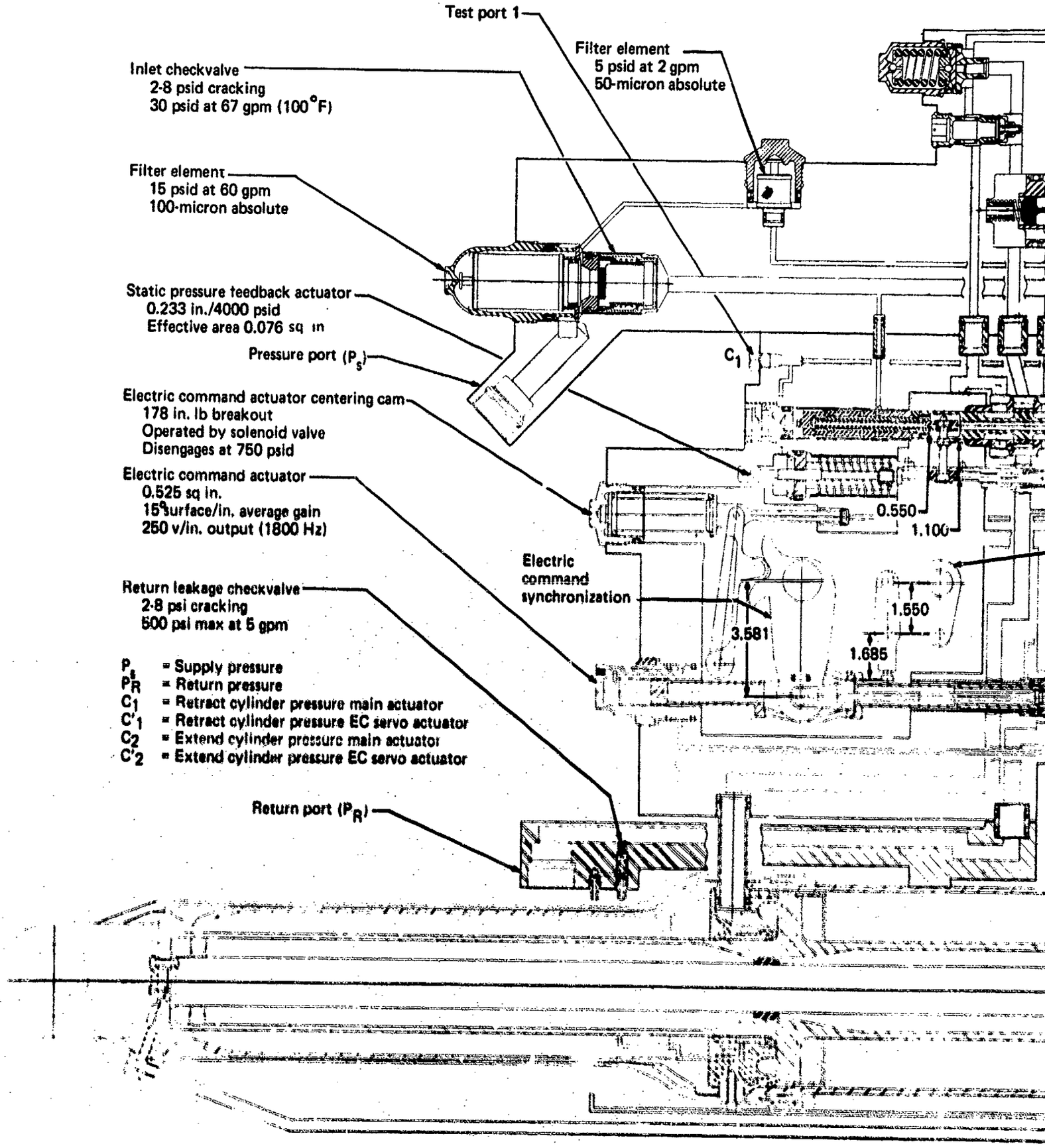
Test port 1
Filter element
5 psid at 2 gpm
50-micron absolute
Inlet checkvalve
2-8 psid cracking
30 psid at 67 gpm (100°F)
Filter element
15 psid at 60 gpm
100-micron absolute
Static pressure feedback actuator
0.233 in./4000 psid
Effective area 0.076 sq in
Pressure port (P_s)
C_1
Electric command actuator centering cam
178 in. lb breakout
Operated by solenoid valve
Disengages at 750 psid
Electric command actuator
0.525 sq in.
15° surface/in. average gain
250 v/in. output (1800 Hz)
0.550
1.100
Electric command synchronization
1.550
3.581
1.685
Return leakage checkvalve
2-8 psi cracking
500 psi max at 5 gpm
P_s = Supply pressure
P_R = Return pressure
C_1 = Retract cylinder pressure main actuator
C'_1 = Retract cylinder pressure EC servo actuator
C_2 = Extend cylinder pressure main actuator
C'_2 = Extend cylinder pressure EC servo actuator
Return port (P_R)

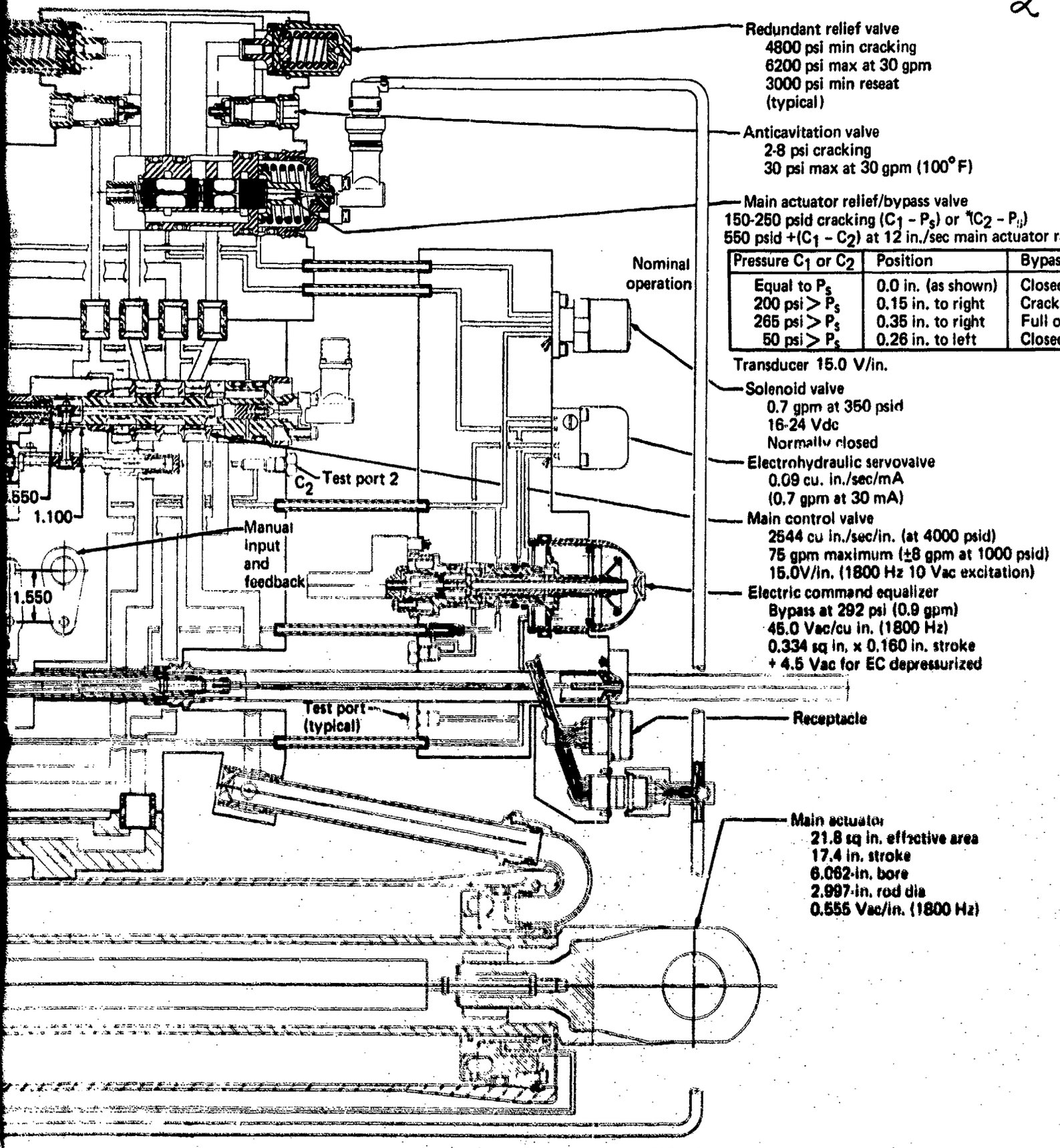

FIGURE 12.—MAIN ACTUATOR

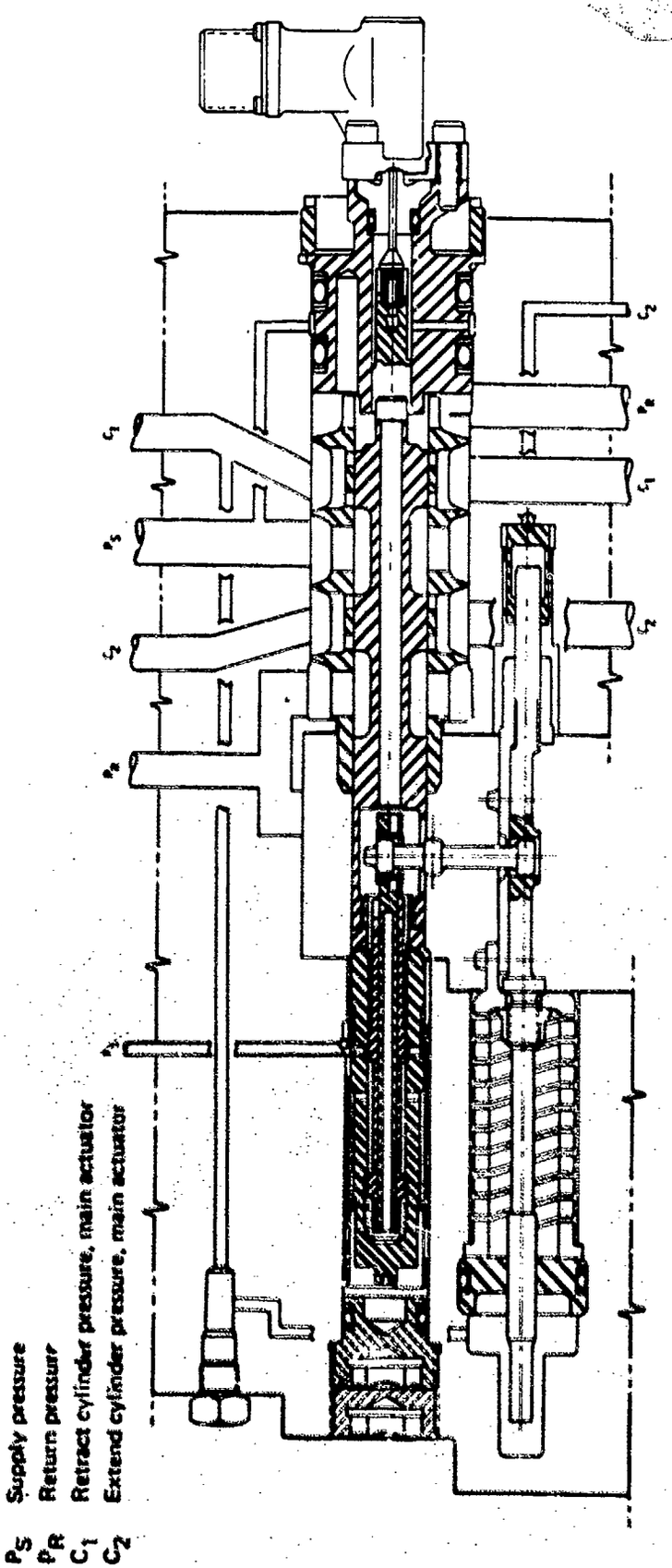

FIGURE 13.–MAIN CONTROL VALVE AND PRESSURE FEEDBACK

P_S Supply pressure
P_R Return pressure
C_1 Retract cylinder pressure, main actuator
C_2 Extend cylinder pressure, main actuator

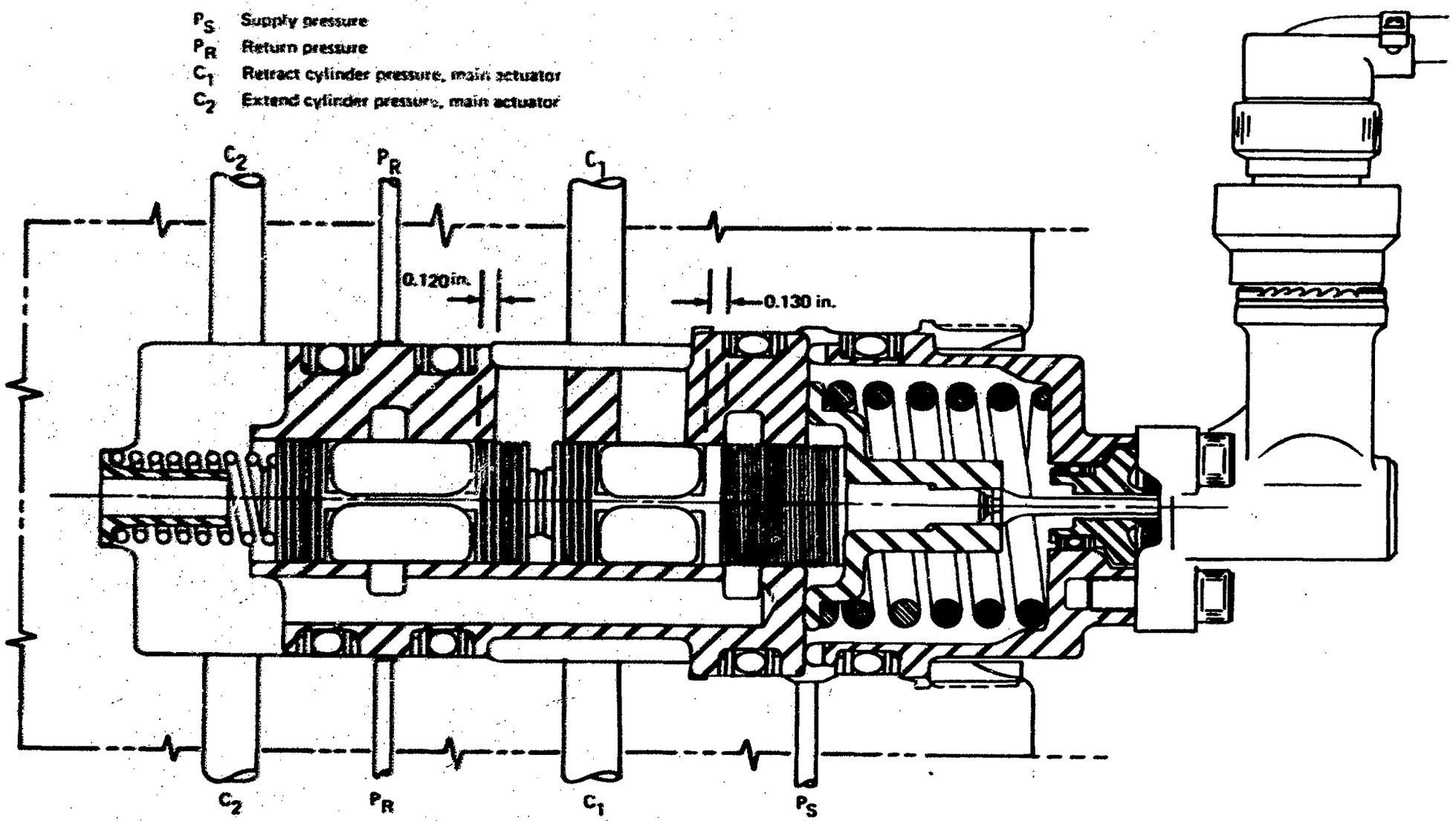

FIGURE 14.–MAIN ACTUATOR RELIEF/BYPASS VALVE–SHOWN CENTERED

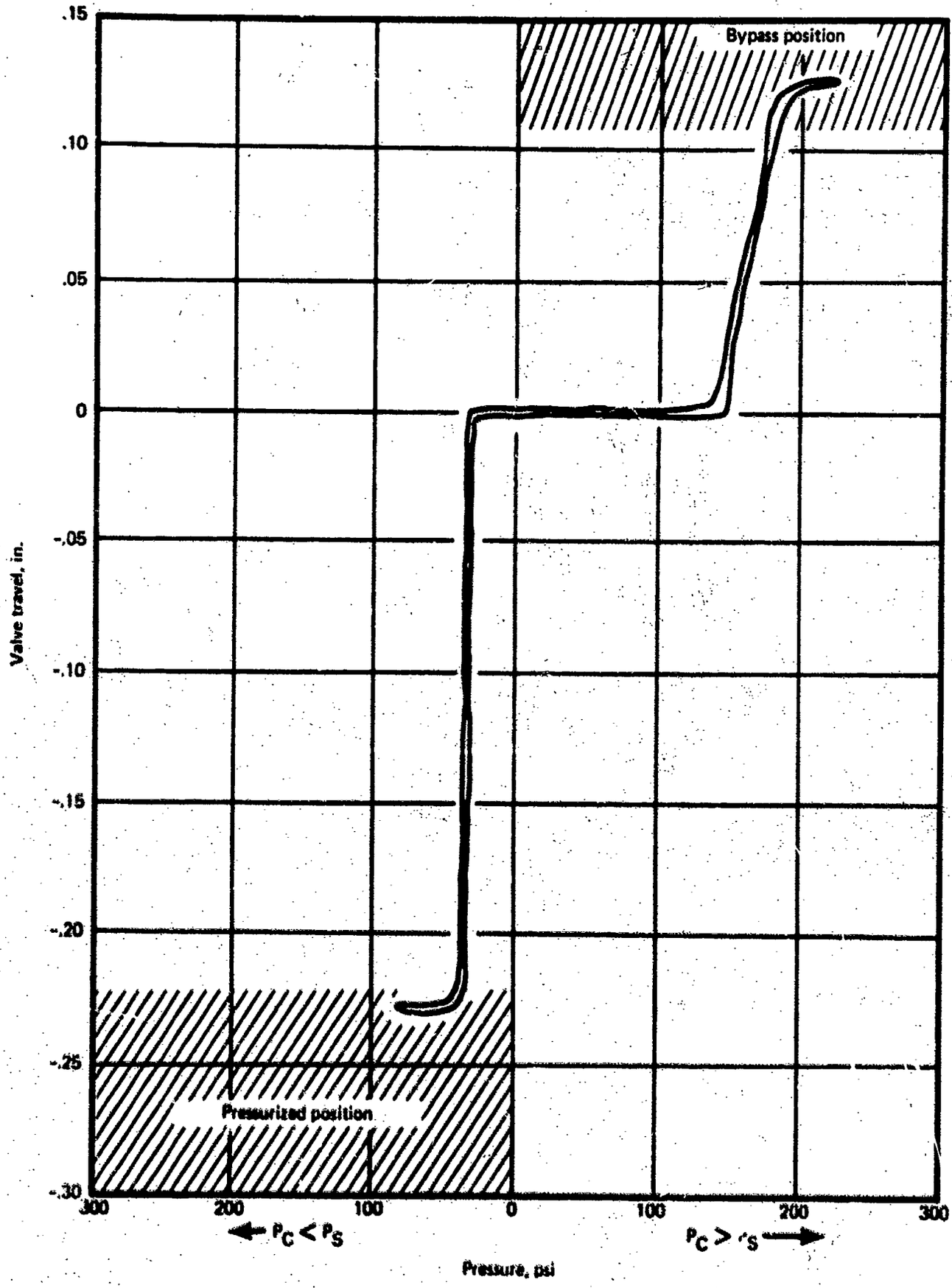

FIGURE 15.–MAIN ACTUATOR RELIEF / BYPASS VALVE

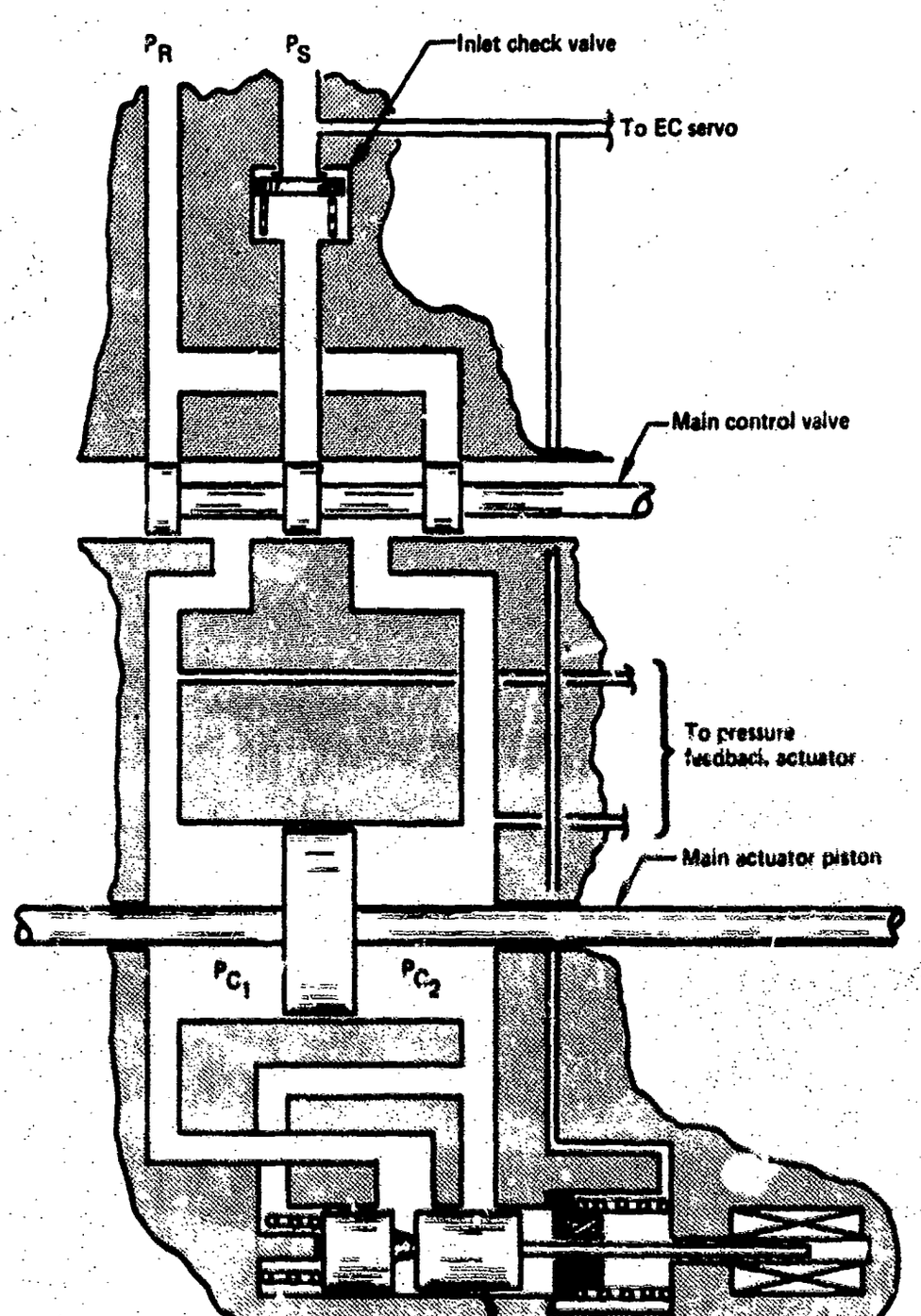

FIGURE 16.–MAIN ACTUATOR RELIEF/BYPASS VALVE SCHEMATIC

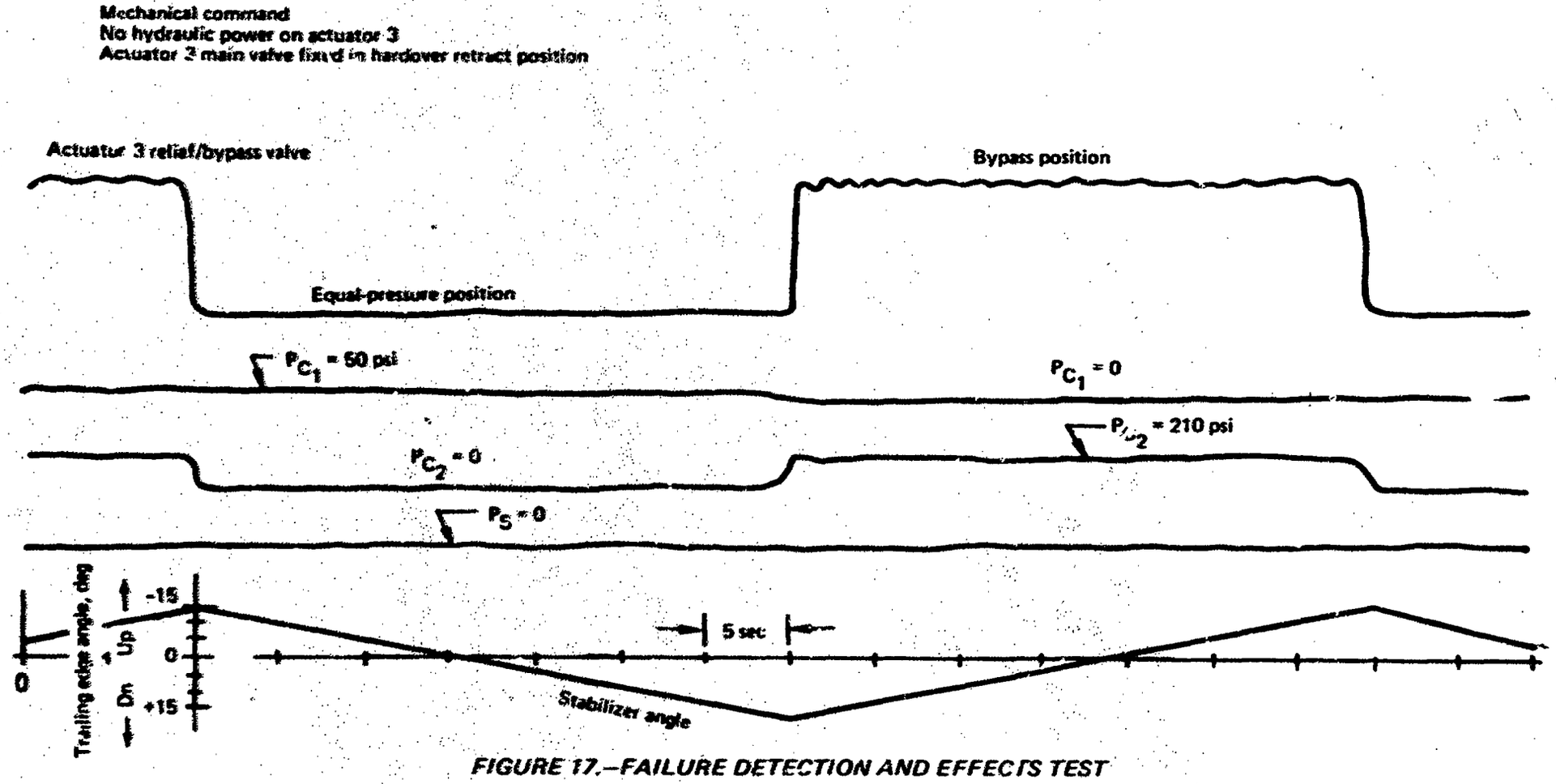

FIGURE 17.–FAILURE DETECTION AND EFFECTS TEST

The valve slide will also move in a direction opposite to that of the "over-pressure" position when the supply pressure exceeds the cylinder pressure. This position is the "pressurized" position.

Electric Command Servo Equalizer—The EC servo equalizer (fig. 18) is a spring-detented piston/valve that provides the following functions:

- When the EC supply pressure is on, the valve is preloaded to the zero position for EC servo differential pressures up to 285 psid. At or above 292 psid the bypass valve opens, allowing flow between both sides of the EC piston.

- When the EC supply pressure is off, the bypass valve is open.

An LVDT position sensor is attached to the valve to provide bypass and supply ON/OFF detection signals and to provide the equalization feedback signals to the EC servo electronics (see sec. 3.2.2.2).

Main Valve Input Linkage—The input linkage (fig. 19) mechanically sums the mechanical input, the electrical input (EC piston position), and the pressure feedback position. The output of the linkage is the input to the pilot slide of the main control valve. The linkage authority is such that the EC piston can command ±15°of stabilizer with the mechanical input at neutral, or +15° to -5° with the mechanical input at +10°, or +5° to -15° with the mechanical input at -10°. The linkage has the capacity to transmit at least 200 lb of chip shearing force to the pilot valve.

3.2.2.2 CODE Servo Electronics

The CODE servo electronics (CSE) (figs. 20, 21, and 22) provide the electric commands and related electronic functions to the EC servo. Each of the four CSE channels includes EC servo loop closing circuitry, static and dynamic failure monitors, negator loop, power supply, sensor excitation, test points, and demodulators for the actuator LVDTs. The block diagram on figure 20 shows a typical CSE channel.

3.2.2.3 EC Servo Synchronization Shaft

The high stiffness of the synchronization shaft forces the EC servo pistons to track each other closely, providing nearly equal commands to all four actuators (figs. 10 and 11). The antijam detents specified for the airplane shaft were omitted on the CODE rig EC servo synchronization shaft in the interest of economy.

3.2.2.4 Mechanical Input Bus Shaft

The bus shaft provides four identical mechanical input commands to the actuators from the single mechanical input actuator (master servo) (figs. 10 and 11). The antijam detents specified for the airplane bus shaft were omitted on the CODE rig for economy.

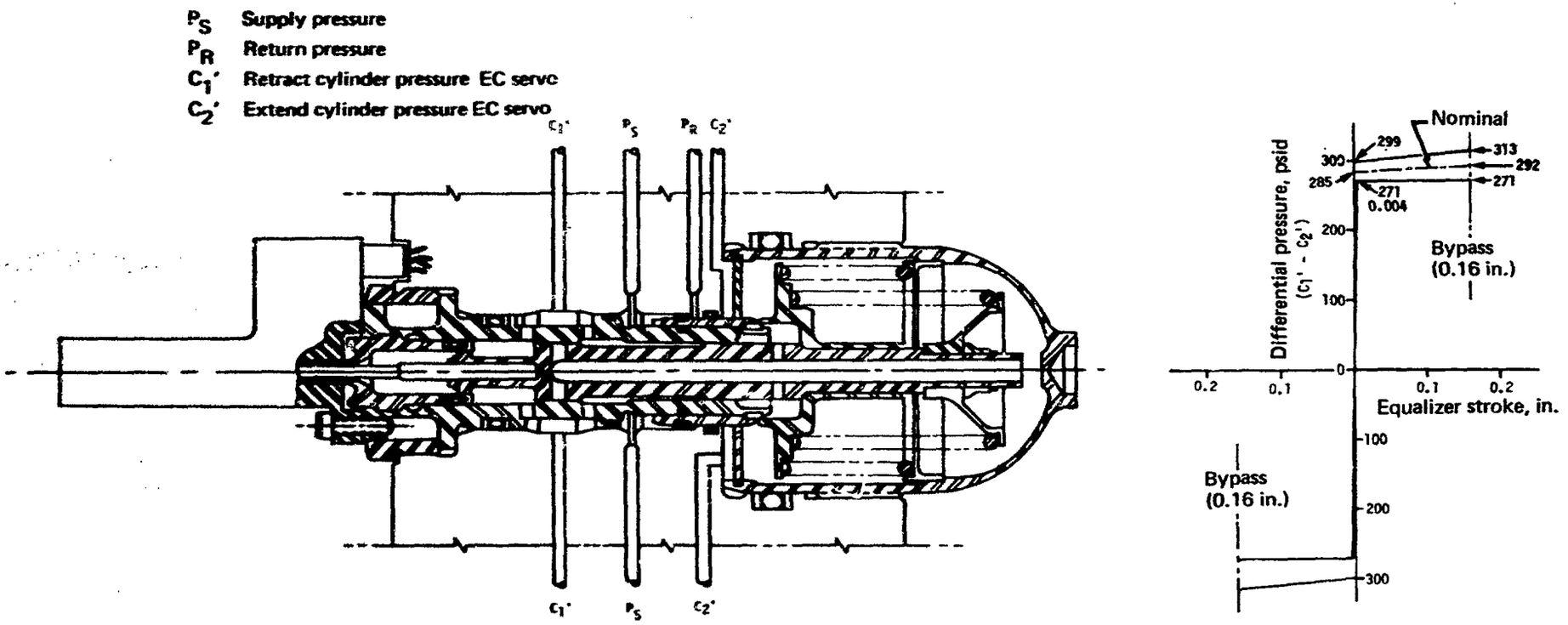

FIGURE 18.–ELECTRIC COMMAND SERVO EQUALIZER–SHOWN AT ZERO POSITION

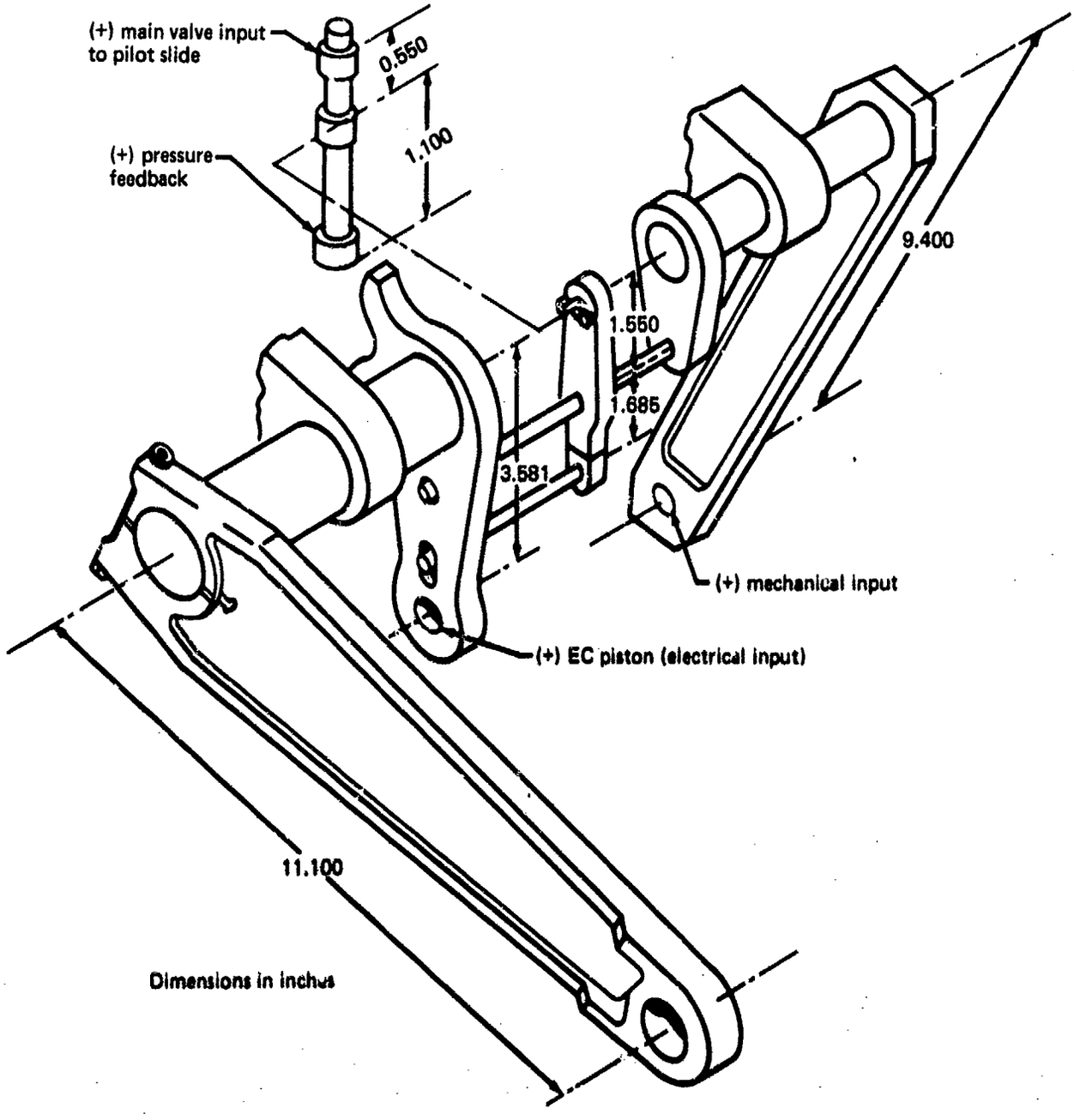

FIGURE 19.--MAIN VALVE INPUT SUMMING LINKAGE

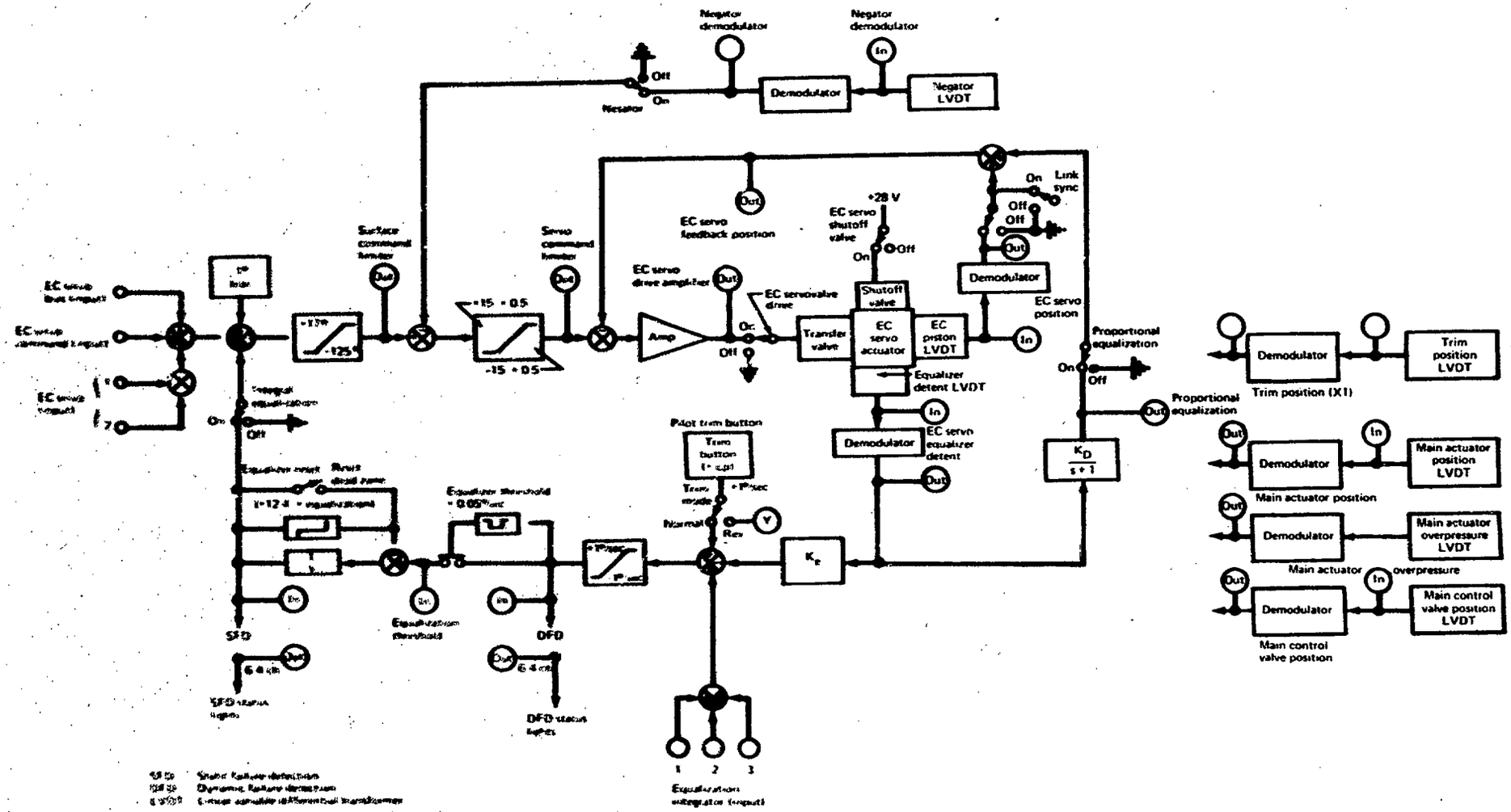

FIGURE 20.–PITCH CODE SERVO ELECTRONICS–FUNCTIONAL BLOCK DIAGRAM (SHOWING INPUTS AND TEST POINTS OF MONITOR AND CONTROL PANEL)

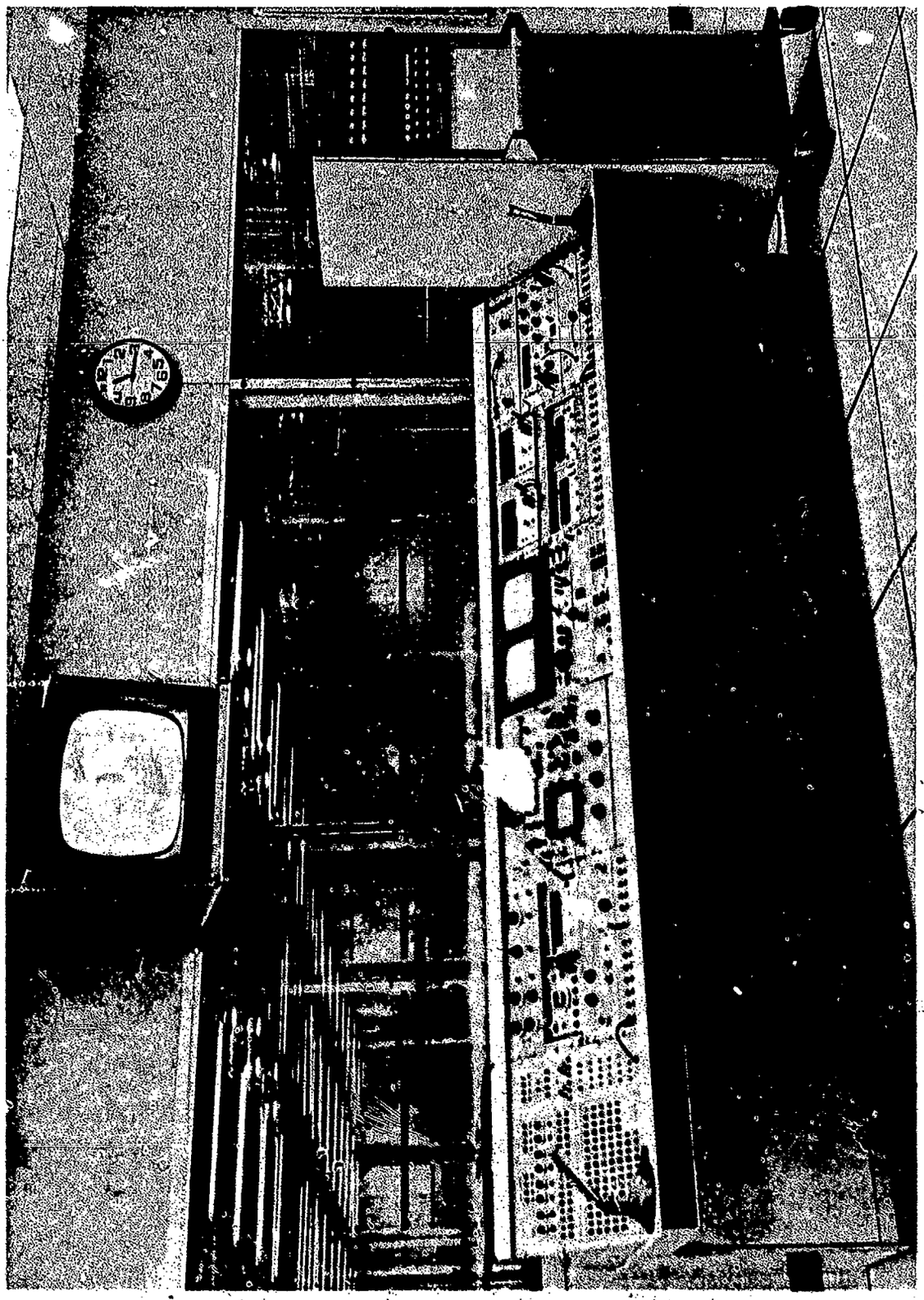

FIGURE 21.—CODE CONTROL CONSOLE

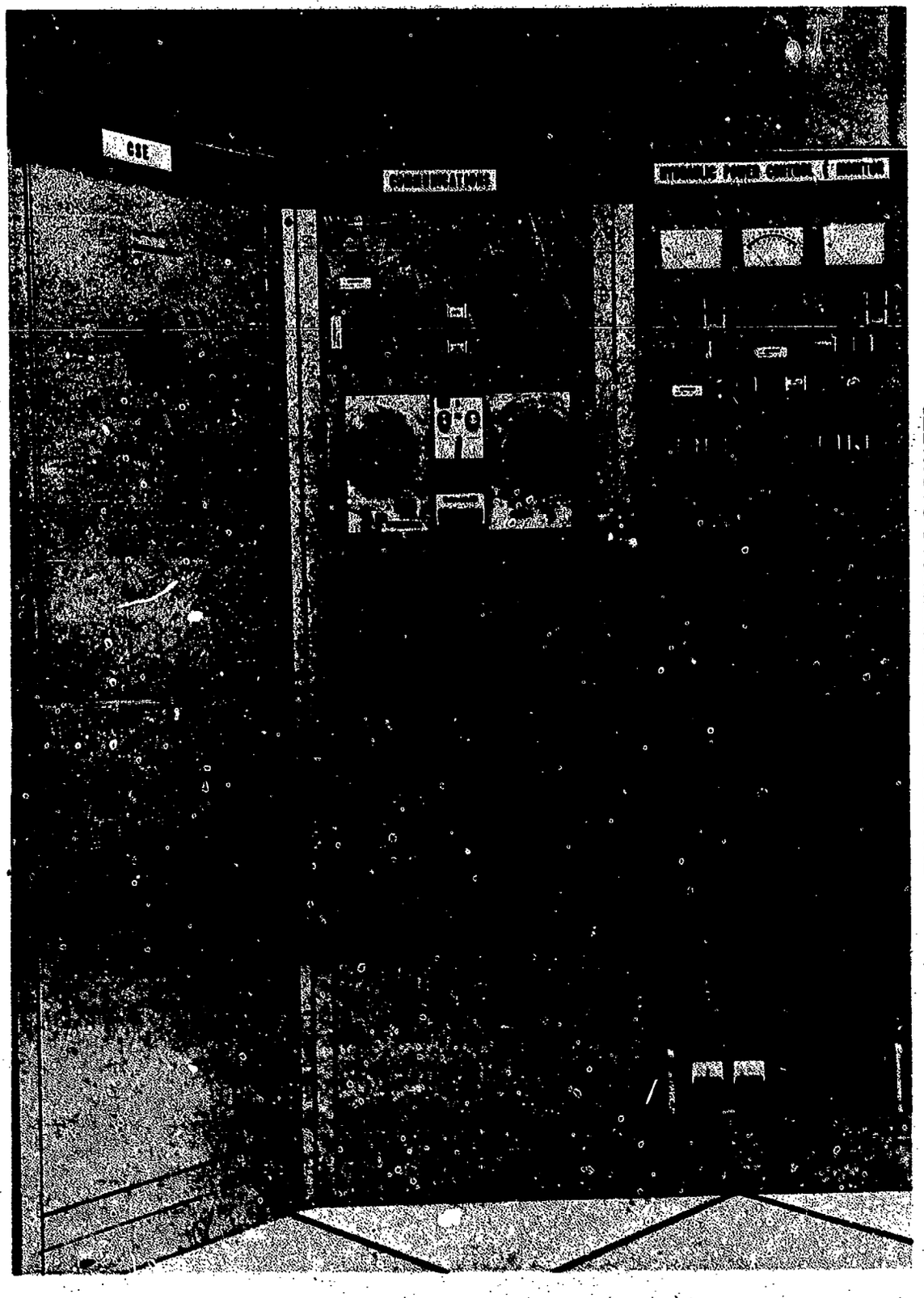

FIGURE 22.—CODE CONTROLS CABINETS

3.2.2.5 Mechanical Input Servo

The mechanical commands for the actuators were generated by a 3000-psi, 4.25-in.-stroke hydraulic powered position servo controlled by an electrohydraulic valve (fig. 23). The link connecting this mechanical servo to the bus shaft had a linear detent to prevent damage in the event of inadvertent bottoming of the main actuator control valve. This actuator simulated the master servo and trim actuator mechanical inputs.

3.3 HYDRAULIC POWER SUPPLY

3.3.1 Normal-Temperature Unit

The normal-temperature hydraulic power supply unit (figs. 24 and 25) provided the hydraulic power requirements to the CODE rig. This unit had two pumps, each rated at 60 gpm and 4000 psi, and could be connected to any combination of the four actuators in the rig. The heat exchanger and controls gave the unit the capability to supply up to 120 gpm of fluid at temperatures from 100° to 200° F. The pressure could be set at any value from 1500 to 5000 psi.

3.3.2 High-Temperature Unit

The high-temperature hydraulic supply unit (figs 24 and 25) was a modified normal-temperature unit using one pump rated at 60 gpm and 4000 psi. The heat exchanger and controls gave the unit the capability to provide fluid at temperatures from 100° to 375° F. The plumbing to the unit was arranged such that fluid could be supplied either to all four actuators in the rig or to a single actuator while the normal-temperature unit supplied the other actuators. The pressure setting of this unit could be adjusted from 1500 to 5000 psi.

3.3.3 Mechanical Input Servo Hydraulic Supply Unit

The hydraulic power required for the mechanical input servo was provided by an auxiliary portable hydraulic power cart. This unit was rated at 7 gpm and 3000 psi and could be adjusted at pressures from 1500 to 5000 psi.

3.3.4 Hydraulic Fluid

All three of the above hydraulic supply units used a hydraulic fluid per Boeing material specification BMS 3-10. Properties of BMS 3-10 are shown on figure 26,

3.4 LOAD SYSTEM

Certain tests required applying simulated aerodynamic loads up to a significant percentage of the actuation system's maximum hinge moment capability (fig. 27). The loads were provided by a pneumatically powered load system. Load links with force transducers were attached to the stabilizer load beams (see figs. 8 and 9) at any of five locations from 40.2 to 137.7 in. aft of the stabilizer hinge axis. The lower ends of the links were attached to levers that were pivoted to move parallel with the stabilizer. Two pneumatic actuators

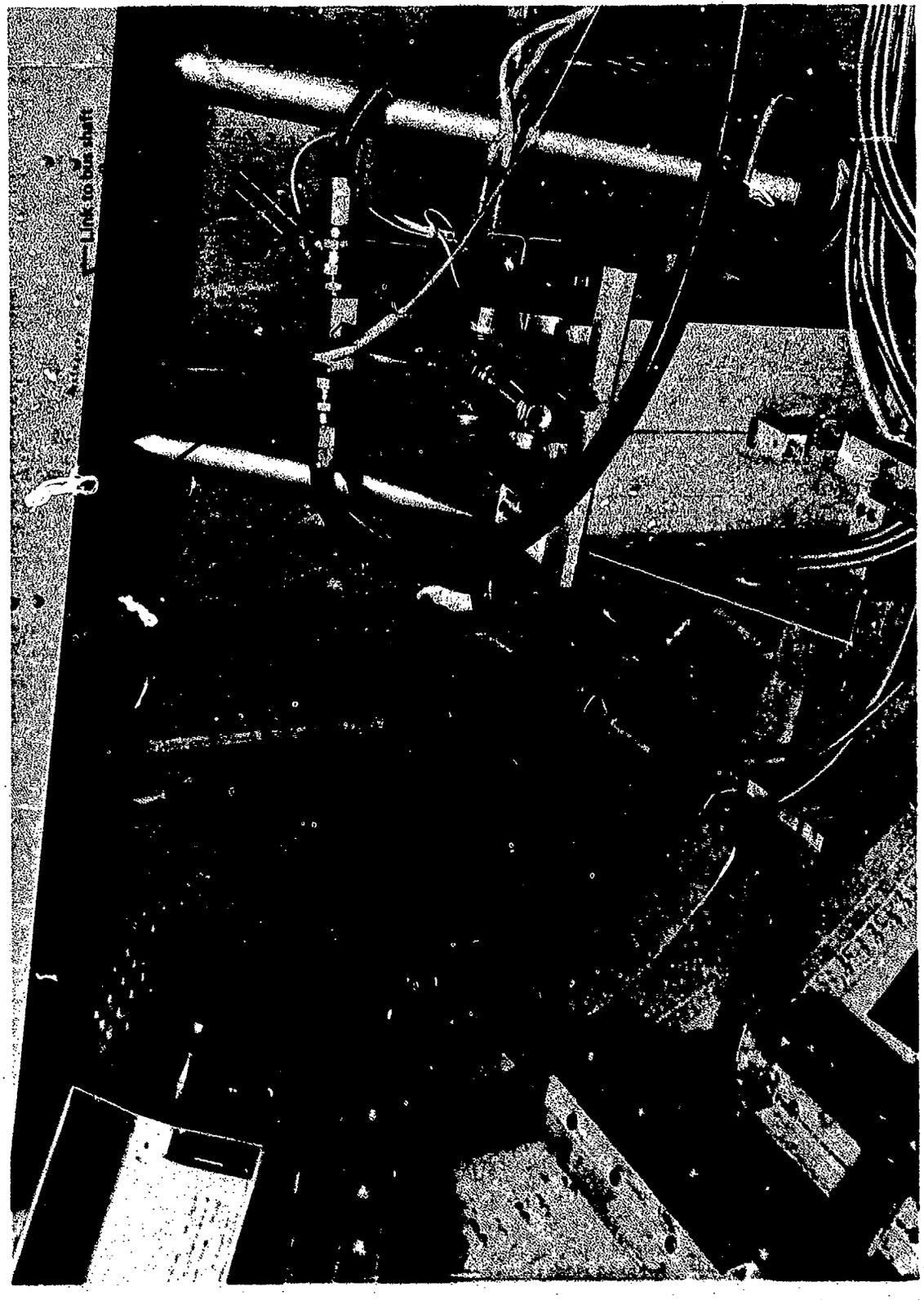

FIGURE 23.–MECHANICAL INPUT ACTUATOR

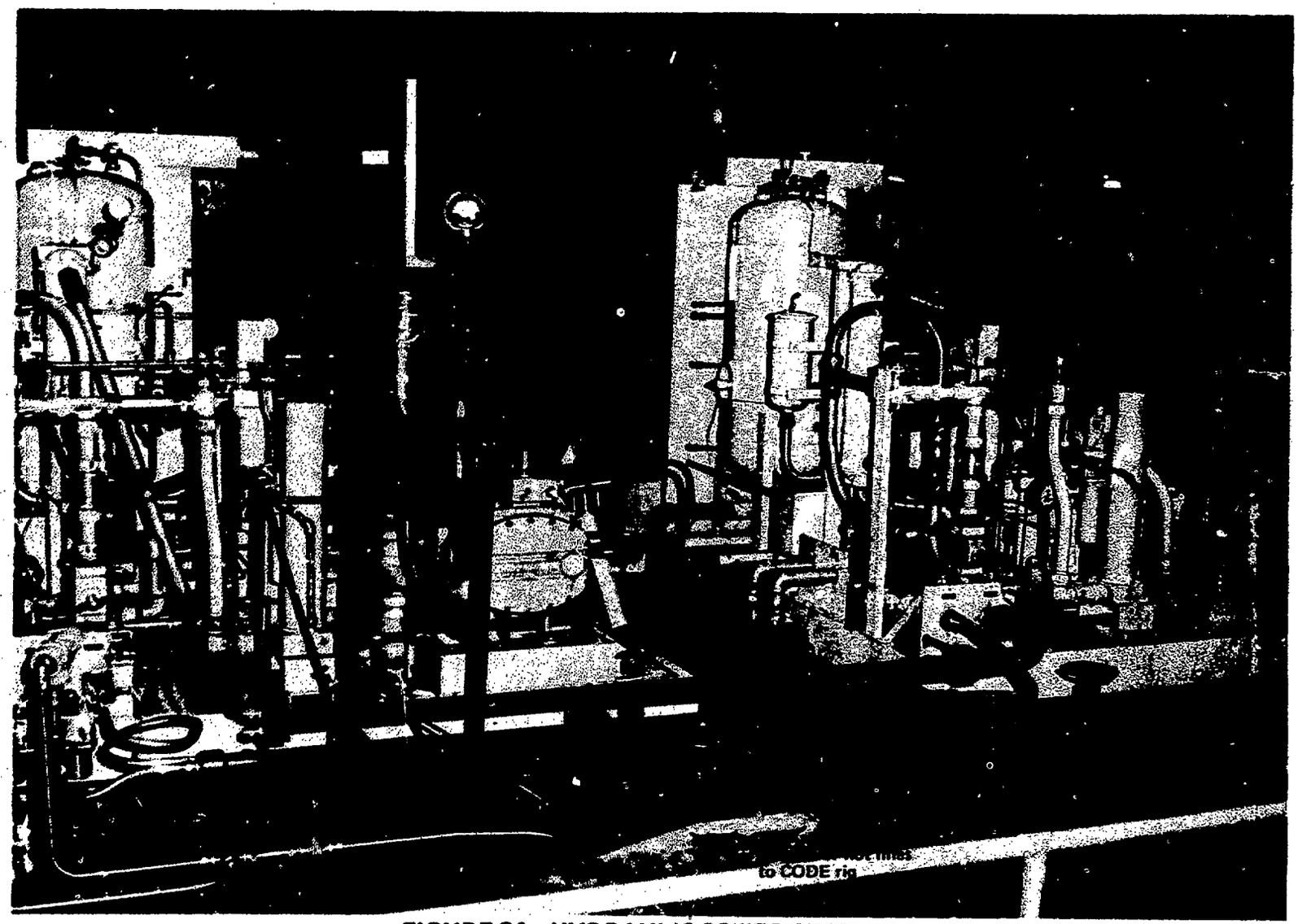

FIGURE 24.—HYDRAULIC POWER SUPPLIES

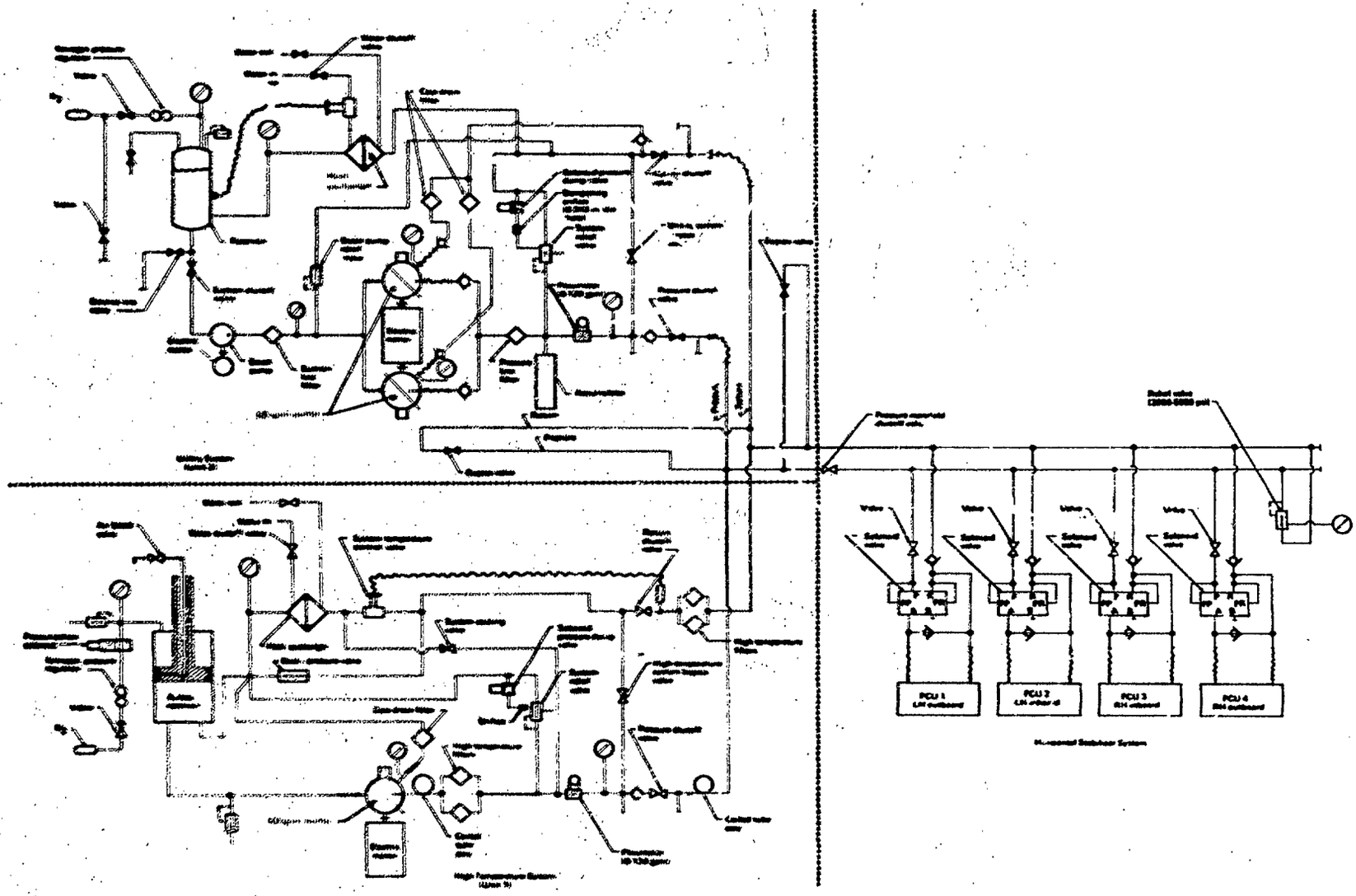

FIGURE 25.--HORIZONTAL STABILIZER HYDRAULIC POWER SYSTEM SCHEMATIC

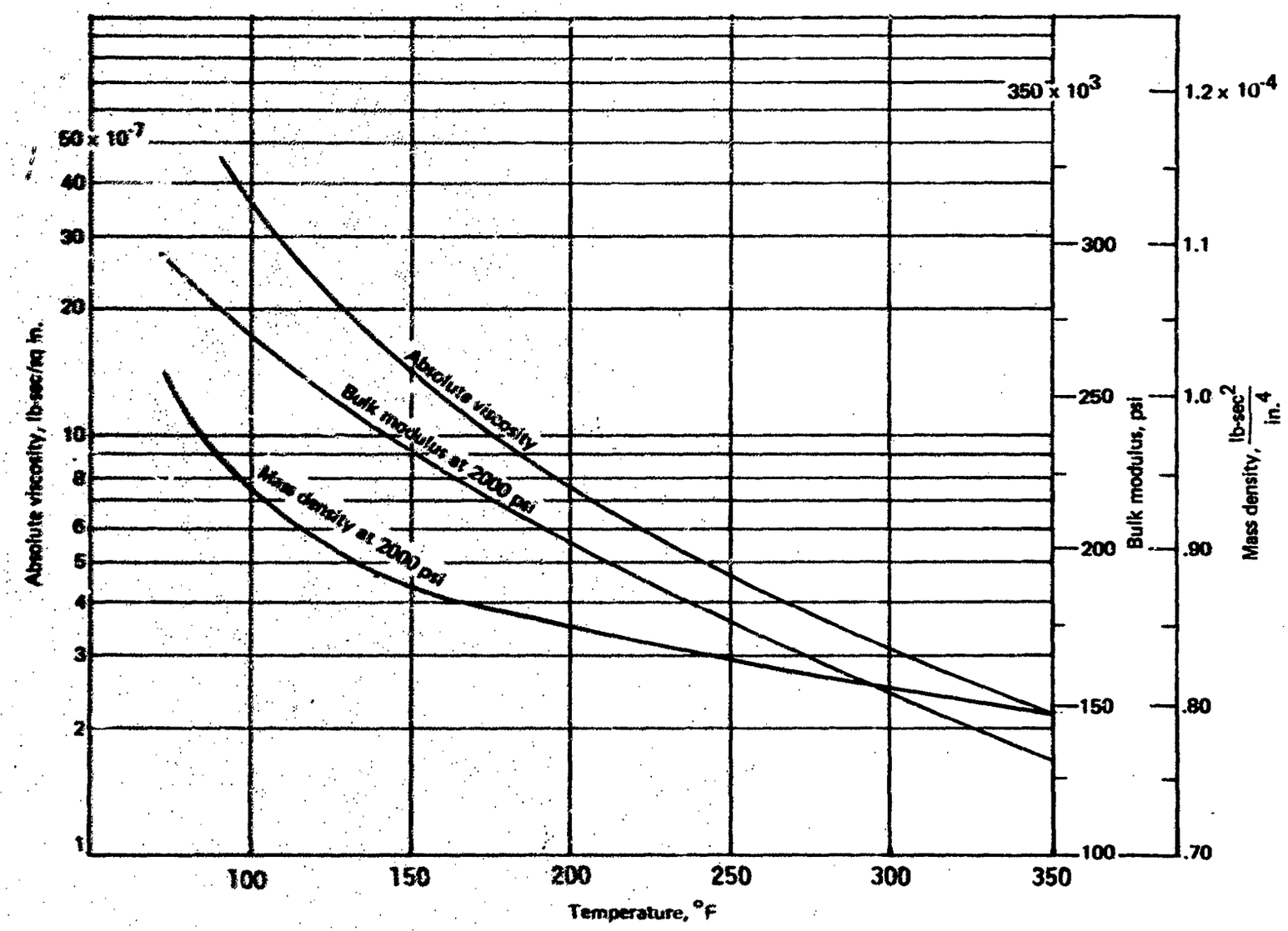

FIGURE 26.—BMS 3-10 HYDRAULIC FLUID PROPERTIES

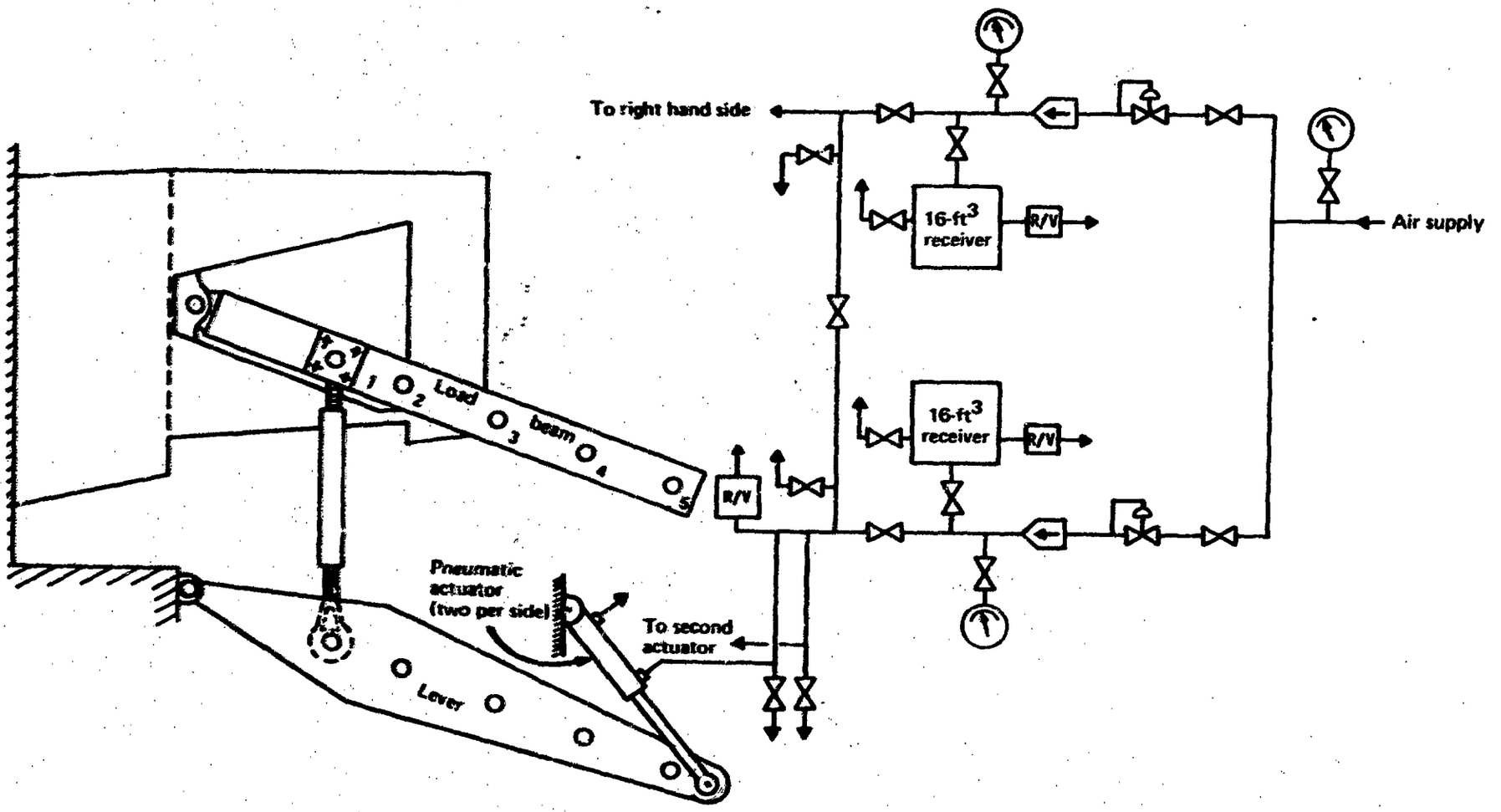

FIGURE 27.—LOAD SYSTEM—LEFT SIDE SHOWN

attached to each lever created hinge moments that tended to restore the stabilizer to the neutral position. By adjusting the pressure on the pneumatic actuators, hinge moments up to about 50% of the actuation system's maximum capability were available.

3.5 DATA ACQUISITION SYSTEM

3.5.1 General

The data acquisition system was an analog type located in the control room about 200 ft from the test rig. Data trunk lines were in iron conduit to minimize noise pickup between the data system and the test rig.

3.5.2 Data System Accuracy

The overall accuracy of recorded data was ±3% full scale. In some cases where digital readout was used, accuracy was ±1% full scale.

3.5.3 Certification and Traceability

All data system transducers, signal conditioners, amplifiers, recorders, and readouts were periodically certified per established Boeing procedures, and these certifications are traceable to the National Bureau of Standards.

3.5.4 Data System Equipment

The data system equipment (fig. 28), located in the control room, was mounted in eight standard 6-ft by 19-in. racks and interconnected through a system patch board with removable cords. The specific configuration used to accomplish a given test is recorded on a "Test Setup Record" and is part of the permanent record for that test plan (see document D6A-12305)

3.5.4.1 Transducers

- Pressure transducers--strain gage bridge type:
  - Standard Controls model 410-2, 0-5000 psi
  - Standard Controls model 650-2, ±5000 psid
- Position, angular
  - Computer Instrument Corp. model 7[illegible]5 film potentiometers
- Position, linear
  - Transteck model 242 and 243, dc to dc LVDTs

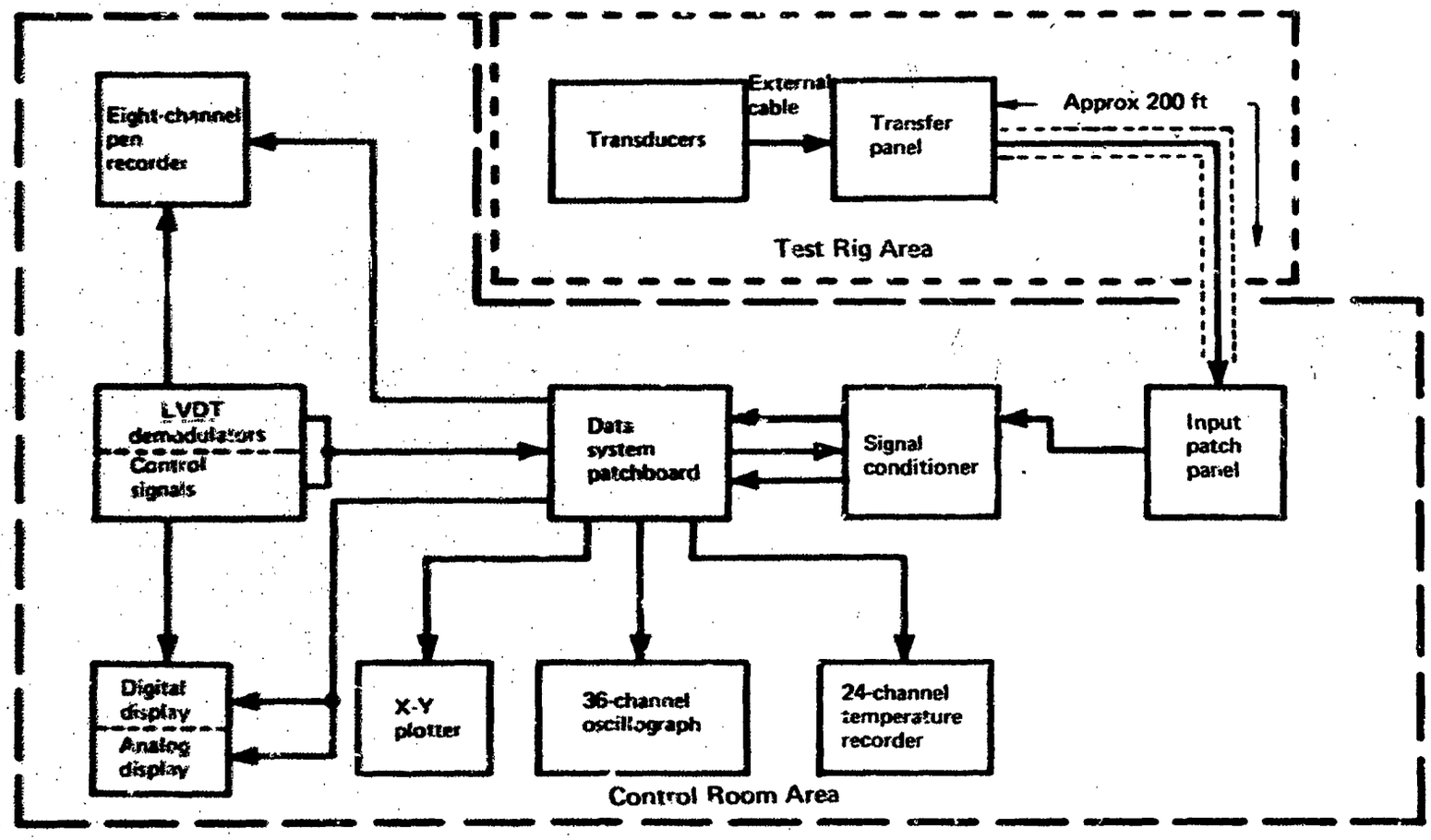

FIGURE 28.—DATA ACQUISITION SYSTEM BLOCK DIAGRAM.

- Force
  - Strain gage load cells–Baldwin, Lima, Hamilton
  - Boeing-applied strain gage installation on actuators
- Hydraulic flows
  - Impulse turbine type–Fisher Porter and Pottermeter
- Temperature
  - Chromel-alumel thermocouple probes–Comac and Thermoelectric

3.5.4.2 Signal Conditioners

- DC power and balance units, Sigma Systems model S.C. 61054
- DC signal amplifiers, Preston model 8300
- Integrators–flow meter, Anaden model PL-408

3.5.4.3 Recorders

- Directrite oscillograph–CEC model 5-133 data graph
- X-Y plotter–Mosley model 7001 AR
- Temperature strip chart–L&N Speedomax W

3.5.4.4 Readouts and Indicators

- Digital voltmeters
  - H.P. model 3460
  - N.L.S. model X-2
  - Preston model 723
- Oscilloscope, Tektronix model RM 503
- Frequency counter, Anaden model CF 600R

4.0 DESCRIPTION AND RESULTS OF LINEAR ANALYSIS PROGRAM

4.1 INTRODUCTION

The horizontal stabilizer actuation system was analyzed during the SST program using several digital programs and analog simulations. The linear analysis conducted during this program used one of the digital programs written prior to termination of the SST. It was used to predict the stability, frequency response, and stiffness of the quadruple actuation system installed in a complex structural model. In the following discussion, predicted dynamic performance is compared to illustrative test data.

The surface actuation system must meet four basic requirements:

- Adequate stability margin to guarantee stability.
- Frequency response (bandwidth) capability for controlling the airplane in all flight regimes.
- High stiffness to prevent surface flutter in all flight regimes. High static stiffness is also desired to minimize static error under load.
- In multiple-actuator installations, the synchronization of the actuators requires either low static stiffness or very tight manufacturing and installation tolerances.

The stiffness requirements are sometimes contradictory and not necessarily compatible, as explained in appendix A, and considerable theoretical analysis is required during the design phase to develop a satisfactory configuration. The SST analysis problem was complicated by the "flying-tail" concept, with its large aerodynamic forces, and by the need for a lightweight structure. Analysis of the problem required a mathematical model of the horizontal stabilizer and its surrounding support structure.

4.2 STRUCTURAL MODEL

The test structure is described and illustrated in section 3.2.1. The aft body section was intended to structurally duplicate the prototype airframe, but the stabilizer and elevators were simplifed, having mass properties similar to the prototype, with a stiffness to give the same first-mode natural frequency as the prototype. As illustrated in figures 6 through 9, the structure is symmetrical except for the mountings of the mechanical input bus shaft and the EC synchronizing shaft.

The structural model was developed as a symmetrical half-section, with attachment points for two actuators. Figure 29 illustrates the structural half-model, and shows the relative locations of the nodes used in the digital program. Nodes 1 through 32 contain mass terms, whereas the remaining 20 nodes contain spring constants only. No structural damping is included. The 52 by 52 structural matrix is included in appendix B for a neutral surface position ($\delta = 0$).

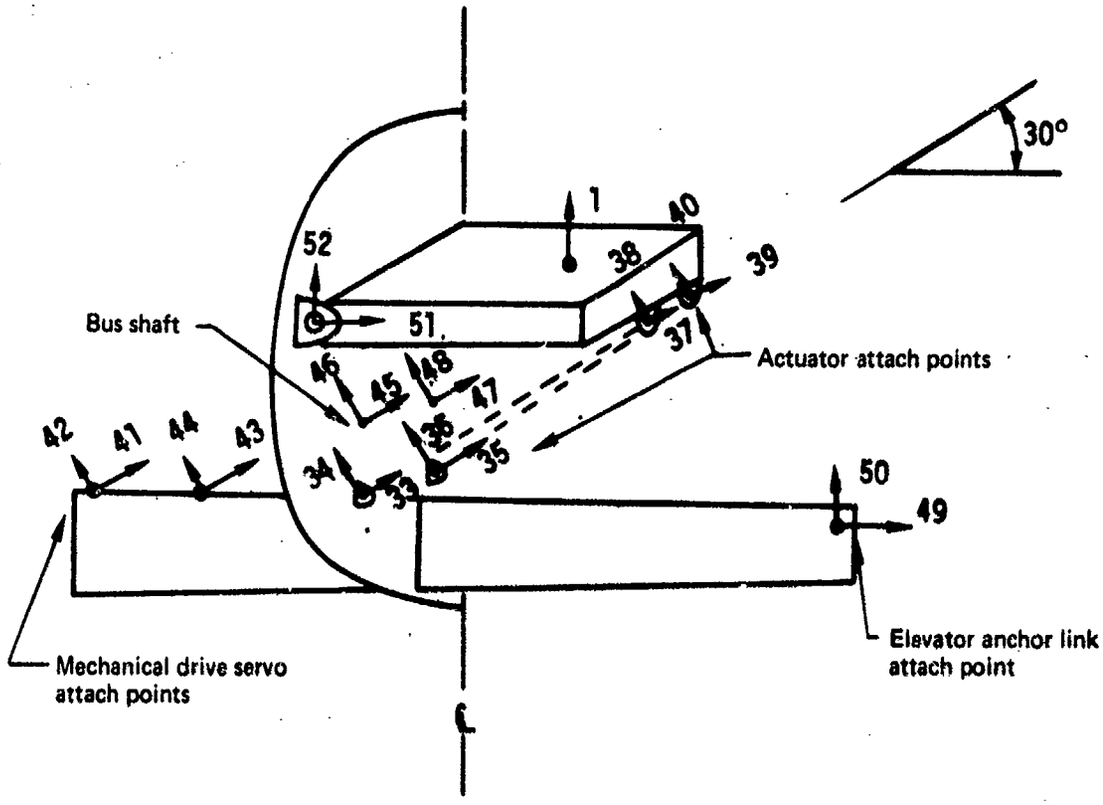

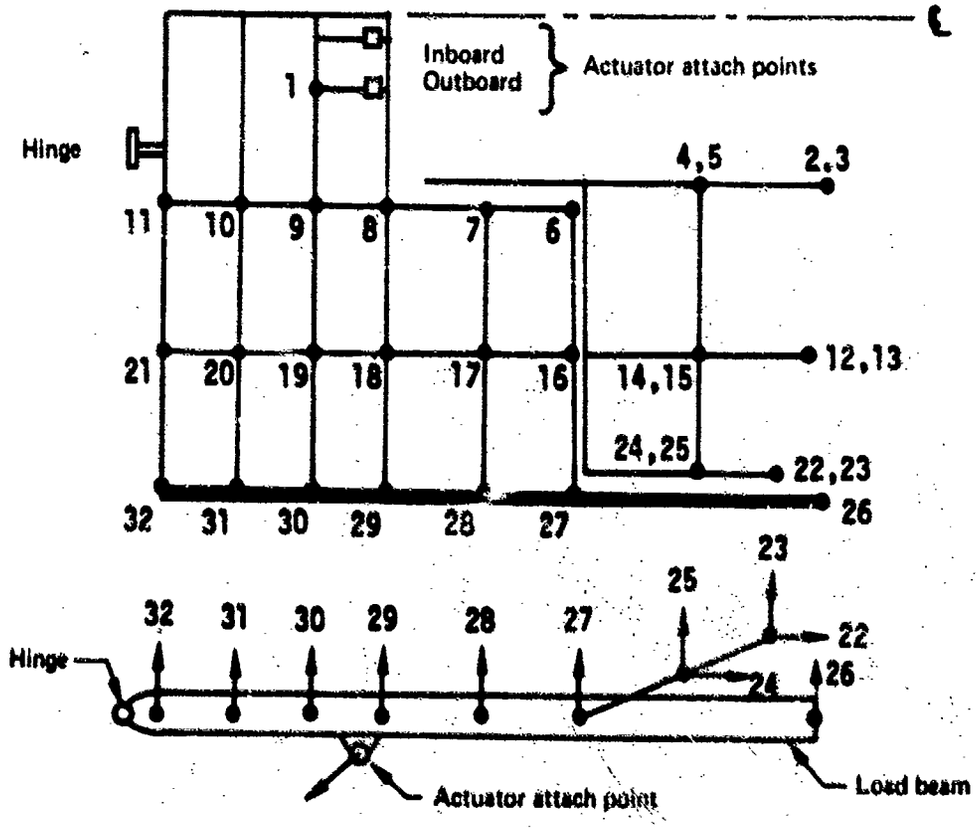

FIGURE 29.–DIGITAL PROGRAM NODE POINTS–SURFACE AT NEUTRAL

4.3 ACTUATOR MODEL

Referring to figure 29, attachment points are shown on the matrix for an outboard actuator (33, 34 and 37, 38) and in inboard actuator (35, 36 and 39, 40). The mechanical input is attached at 41, 42 and 42, 43. Movement of the bus shaft rotation points is represented by 45, 46 and 47, 48. An outboard actuator is shown connected to its respective node attachment points in figure 30.

The block diagram in figure 31 illustrates the linear model used for the outboard and inboard actuators. The model in figure 31 resembles the model analyzed in appendix A, except that the position feedback is now a function of actuator rotation, structural movement of the mechanical input actuator attachment, bus shaft movement, and the actuator housing. The simulated actuators may be commanded through either the mechanical input actuator or an EC servo. The actuator equations and their coupling to the structural matrix are summarized in figures 32 and 33. The constants for the actuator equations are summarized in table 1.

NOTE: There is a difference of sign convention between the above equations and those of appendix A. The former fit the structural convention in which positive indicates trailing edge up, whereas the latter conform to the convention of positive for trailing edge down. Therefore, most of the signs are reversed between the two sets of equations.

4.4 CLOSED-LOOP STABILITY

The details of developing the relationship between actuator stiffness and closed-loop stability are shown in appendix A. Stability depends on the static stiffness being less than the dynamic stiffness.

Structural damping is usually considered to be zero in preliminary analysis, since it is difficult to determine until the structure is designed and tested. Structural damping ratios are normally in the region 0.01 to 0.02, so neglecting structural damping adds a small margin of conservatism to the calculated actuation system stability margin.

The stability of the system with elevators removed was computed at a surface angle of 0.0°, and at -15.0° (trailing edge up) where the effective load mass is maximum. Oil temperatures of 150° and 350° F were assumed at each surface position. For comparison, an elevator-installed case was calculated at 150° F and 0.0°. The results are summarized and compared with measured test data in table 2. The system's natural frequency and damping ratio decrease as the surface is moved trailing edge up, but are almost independent of oil temperature.

The measured natural frequencies agree well with the theoretical frequencies, the former being lowered by approximately 0.5 Hz in all cases ($\approx 5\%$). The calculated damping ratios show the same incremental changes as the measured data, and would be nearly equal to the measured data if the structural damping contribution were assumed to be 0.01 in all theoretical cases.

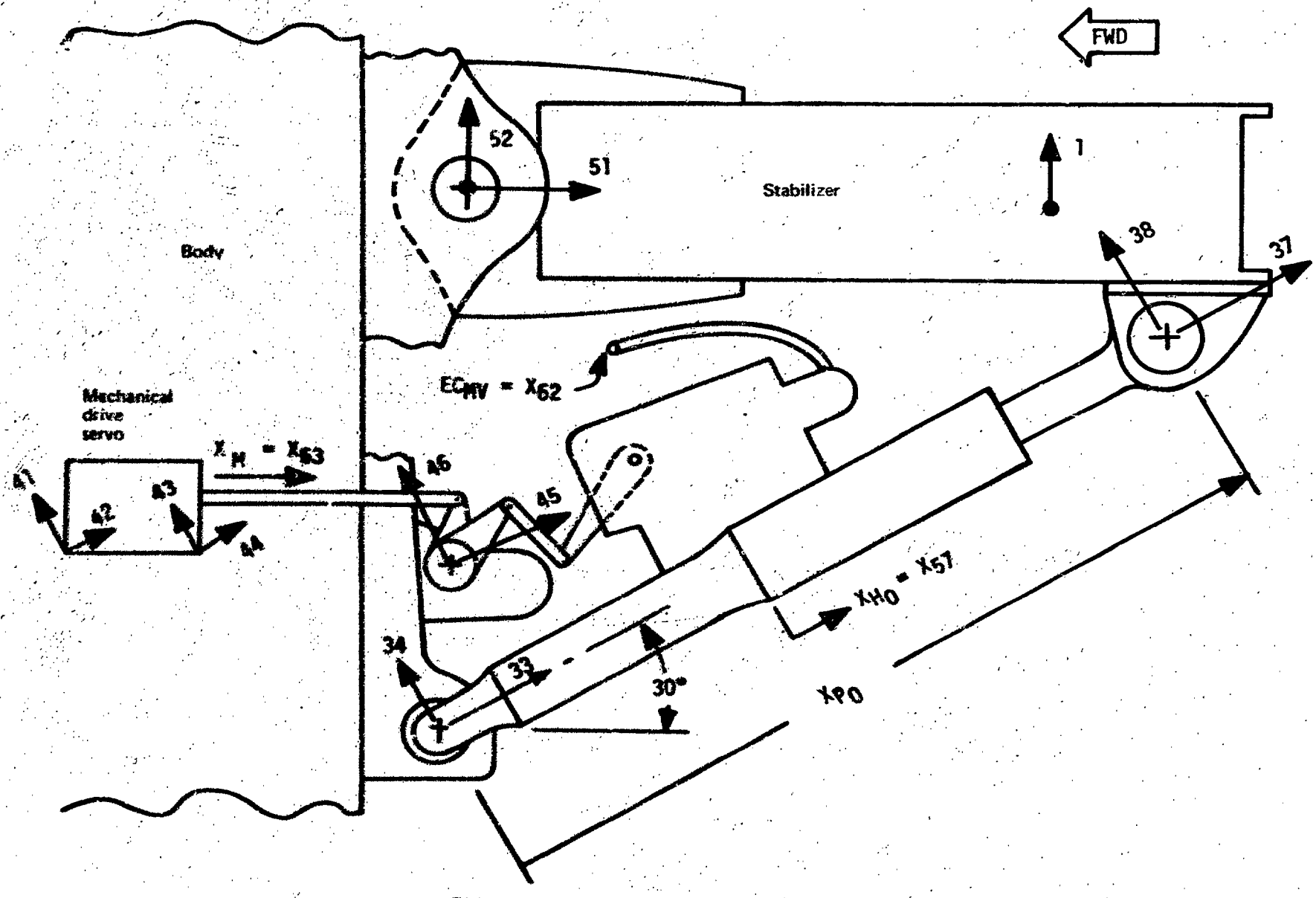

FIGURE 30.–OUTBOARD ACTUATOR

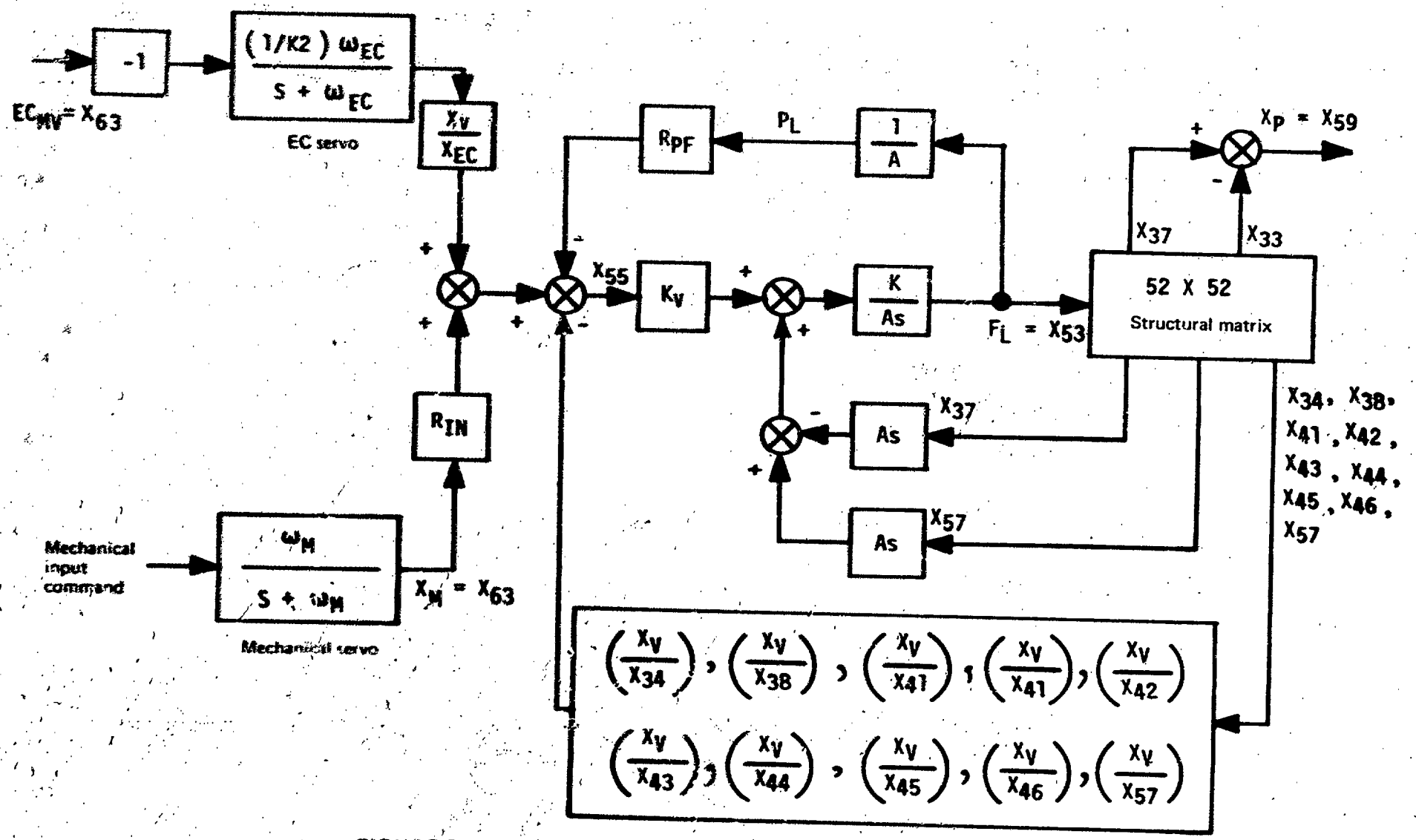

FIGURE 31.–BLOCK DIAGRAM OF ACTUATOR CONNECTION TO STRUCTURAL MATRIX–OUTBOARD

Row 33 Outboard Actuator Housing Attach Point

(Structural equation) - $K_H X_{H_O} = 0$

Row 35 Inboard Actuator Housing Attach Point

(Structural equation) - $K_H X_{H_I} = 0$

Row 37 Outboard Actuator Rod Attach Point

(Structural equation) - $F_{L_O} = 0$

Row 39 Inboard Actuator Rod Attach Point

(Structural equation) - $F_{L_I} = 0$

Row 53 Outboard Actuator Force

$$sX_{37} + \frac{s}{K_{RO}} X_{53} - \frac{K_V}{A} X_{55} - sX_{57} = 0$$

Row 54 Inboard Actuator Force

$$sX_{39} + \frac{s}{K_{RO}} X_{54} - \frac{K_V}{A} X_{56} - sX_{58} = 0$$

Row 55 Outboard Main Valve

$$\frac{X_V}{X_{34}} X_{34} + \frac{X_V}{X_{38}} X_{38} + \frac{X_V}{X_{41}} X_{41} + \frac{X_V}{X_{42}} X_{42} + \frac{X_V}{X_{43}} X_{43} + \frac{X_V}{X_{44}} X_{44}$$

$$+ \frac{X_V}{X_{45}} X_{45} + \frac{X_V}{X_{46}} X_{46} + R_{PF} X_{53} - X_{55} + \frac{X_V}{X_H} X_{57} + \frac{X_V}{X_{EC}} X_{61} + R_{IN} X_{63} = 0$$

Row 56 Inboard Main Valve

$$\frac{X_V}{X_{36}} X_{36} + \frac{X_V}{X_{40}} X_{40} + \frac{X_V}{X_{41}} X_{41} + \frac{X_V}{X_{42}} X_{42} + \frac{X_V}{X_{43}} X_{43} + \frac{X_V}{X_{44}} X_{44}$$

$$+ \frac{X_V}{X_{47}} X_{47} + \frac{X_V}{X_{48}} X_{48} + R_{PF} X_{54} - X_{56} + \frac{X_V}{X_H} X_{58} + \frac{X_V}{X_{61}} X_{61} + R_{IN} X_{63} = 0$$

Row 57 Outboard Housing

$$-K_H X_{33} + X_{53} + K_H X_{57} = 0$$

Row 58 Inboard Housing

$$-K_H X_{35} + X_{54} + K_H X_{58} = 0$$

FIGURE 32.–ACTUATOR EQUATIONS

Row 59 Outboard Piston

$$X_{33} - X_{37} + X_{59} = 0$$

Row 60 Inboard Piston

$$X_{35} - X_{39} + X_{60} = 0$$

Row 61 Electric Command Servo Piston (outboard = inboard)

$$sX_{61} + \omega_{EC}X_{61} - \omega_{EC}\frac{X_V}{EC_{MV}}X_{62} = 0$$

Row 62 Electric Command Servo Input

X_{62} = 361 mV/deg for EC input "on"

= 0 for EC input "off"

Row 63 Mechanical Servo Output

$sX_{63} + \omega_M X_{63} = \omega_M E_M$ for Mechanical Servo "on"

= 0, for Mechanical Servo "off"

Row 64 Scale Factor (to prevent computer overflow)

$$10^{-100}X_{64} = 0$$

FIGURE 32.–Concluded

Row 1				
•				
•	52 x 52 structural matrix			
•				
Row 52				
Row 53	Outboard actuator force	F_O		
Row 54	Inboard actuator force	F_I		
Row 55	Outboard main valve	X_{V_O}		
Row 56	Inboard main valve	X_{V_I}		= [Input]
Row 57	Outboard housing	X_{H_O}		
Row 58	Inboard housing	X_{H_I}		
Row 59	Outboard piston	X_{P_O}		
Row 60	Inboard piston	X_{P_I}		
Row 61	EC servo piston	X_{EC}	(outboard = inboard)	
Row 62	EC servo input	EC_{MV}	(outboard = inboard)	
Row 63	Mechanical servo	X_M		
Row 64	Scale factor			

Note: Signs do not agree with appendix A equations.

FIGURE 33.–MATRIX SUMMARY

TABLE 1.–ACTUATOR CONSTANTS FOR DIGITAL PROGRAM

A = area of main piston (21.8 $in.^2$)

EC_{mv} = electric command servo input (361 mV/deg of surface)

K = actuator spring (503,000 lb/in. at 150° F, 350,000 lb/in. at 350°F)

K_H = actuator housing spring (2.88×10^6 lb/in.)

K_{oil} = oil spring (1.14×10^6 lb/in. at 150°F, 0.57×10^6 lb/in. at 350°F)

K_R = rod spring (1.3×10^6 lb/in.)

K_{RO} = $\frac{K_R K_{oil}}{K_R + K_{oil}}$ = combined rod and oil springs (605,000 lb/in. at 150°F, 395, 000 lb/in. at 350°F)

K_V = no-load flow gain, main valve (1700 $in.^3$/sec/in.)

R_F = valve displacement due to actuator rod displacement, with no structural effects (0.136 in./in.)

R_{IN} = valve displacement due to mechanical input (0.6 in./in.)

R_{PF} = valve displacement due to load pressure feedback (2.75×10^{-5} in./psi, including inverse valve pressure gain of 750,000 psi/in.)

$\frac{X_{EC}}{EC_{mv}}$ = electric command servo gain (0.1732×10^{-3} in./mV)

$\frac{X_V}{X_{EC}}$ = gain of linkage from EC servo to main valve (1.247 in./in.)

$\frac{X_V}{X_H}$ = valve displacement due to actuator housing displacement (-0.0954 in./in.)

ω_{EC} = electric command servo pole or break frequency (4.77 Hz = 30 rad/sec)

ω_M = mechanical servo pole or break frequency (adjustable)

Main valve displacement constants due to respective structural node displacement:

$\frac{X_V}{X_{34}} = \frac{X_V}{X_{36}}$ = 0.355 in./in.

$\frac{X_V}{X_{38}} = \frac{X_V}{X_{40}}$ = 0.122 in./in.

$\frac{X_V}{X_{41}}$ = 0.284 in./in.

$\frac{X_V}{X_{42}}$ = 0.148 in./in.

$\frac{X_V}{X_{43}}$ = 0.212 in./in.

$\frac{X_V}{X_{44}}$ = 0.492 in./in.

$\frac{X_V}{X_{45}} = \frac{X_V}{X_{47}}$ = -0.424 in./in.

$\frac{X_V}{X_{46}} = \frac{X_V}{X_{48}}$ = -0.148 in./in.

TABLE 2.–COMPARISON OF COMPUTED AND MEASURED STABILITY

Configuration	Surface position (deg)	Oil temperature, °F	Feedback loop	Computed (no structural damping)		Measured from step response	
				System natural frequency, Hz	Damping ratio	System natural frequency, Hz	Damping ratio
Elevator off (four actuators)	0	150	Open	13.1	0.053	–	–
	0	150	[a]Rigid	13.05	0.040	–	–
	0	150	[b]Normal	13.1	0.013	12.5	0.025
	0	350		12.8	0.009	11.7	0.022
	[c] -.15	150		12.1	0.004	11.7	0.016
	[c] -.15	350		11.8	0	11.2	0.017
Elevator off (two actuators)	0	150		11.5	0.069	–	–
Elevator on (four actuators)	0	150		8.25	0.017	7.65	0.021

[a]Structural effects removed from position feedback

[b]Structural effects included

[c]δ = -.10 degrees on test

4.5 CLOSED-LOOP FREQUENCY RESPONSE

The closed-loop frequency response is one important indicator of the system's dynamic performance, and (1) shows the closed-loop servo break frequency more accurately than a step response, and (2) determines the presence or absence of resonant frequencies other than the system natural frequency, such as structural frequencies and hydraulic line frequencies.

The two cases in figures 34 and 35 illustrate the capability of the linear analysis to predict the frequency response of the hardware. Test conditions such as misrigging, surface position, and number of actuators powered do not change the predicted frequency response appreciably since the effects of the load and the servo break frequency are dominating.

4.6 STIFFNESS

As discussed in appendix A and section 5.4, the term "stiffness" in this report refers to the ratio of applied actuator force to actuator displacement regardless of frequency, and as such is described by a frequency-dependent transfer function.

The stiffness transfer function of the theoretical actuation system can be evaluated easily if the structure is assumed to be rigid. The static stiffness, frequency-independent dynamic stiffness, closed-loop servo break frequency, and dynamic stiffness break frequency (see fig. A-4) can be calculated according to the equations of appendix A, and a straight-line approximation plotted. For example, using oil temperatures of 150° and 350° F, and the constants in table 1, the stiffness frequency responses of figure 36 result.

Static stiffness of the actuation system is difficult to determine when flexible structure is included. With a flexible structure, the deflections of the structural feedback loop are dependent on the location and direction of load application. The load beam (fig. 29) was designed to simulate application of a normal aerodynamic load along the mean aerodynamic chord and to produce structural deflections similar to those derived from distributed aerodynamic loading. Loads were applied analytically to nodes 26 and 30 of figure 29, which approximated the load application positions on the test system as described in section 5.4.5. A comparison of various computed and measured system stiffness values is shown in table 3. Since the measured stiffnesses on each side of the test rig were unsymmetrical, stiffness values of the outboard and inboard actuators were averaged to obtain a value for comparison with the symmetrical calculation. The degree of correlation is not very good. The deflections of the loaded structure did not agree with computed values. These discrepancies are discussed in section 5.4.5.

4.7 ANALYSIS SUMMARY

The linear analysis program demonstrated the ability to predict the dynamic characteristics of a complex actuation system. The stability and frequency response results correlated well with the predicted data. Correlation between the predicted and measured static stiffnesses was not as good because of discrepancies between the mathematical model of the predicted airplane structure and the test structure. These discrepancies are discussed in section 5.4.5.

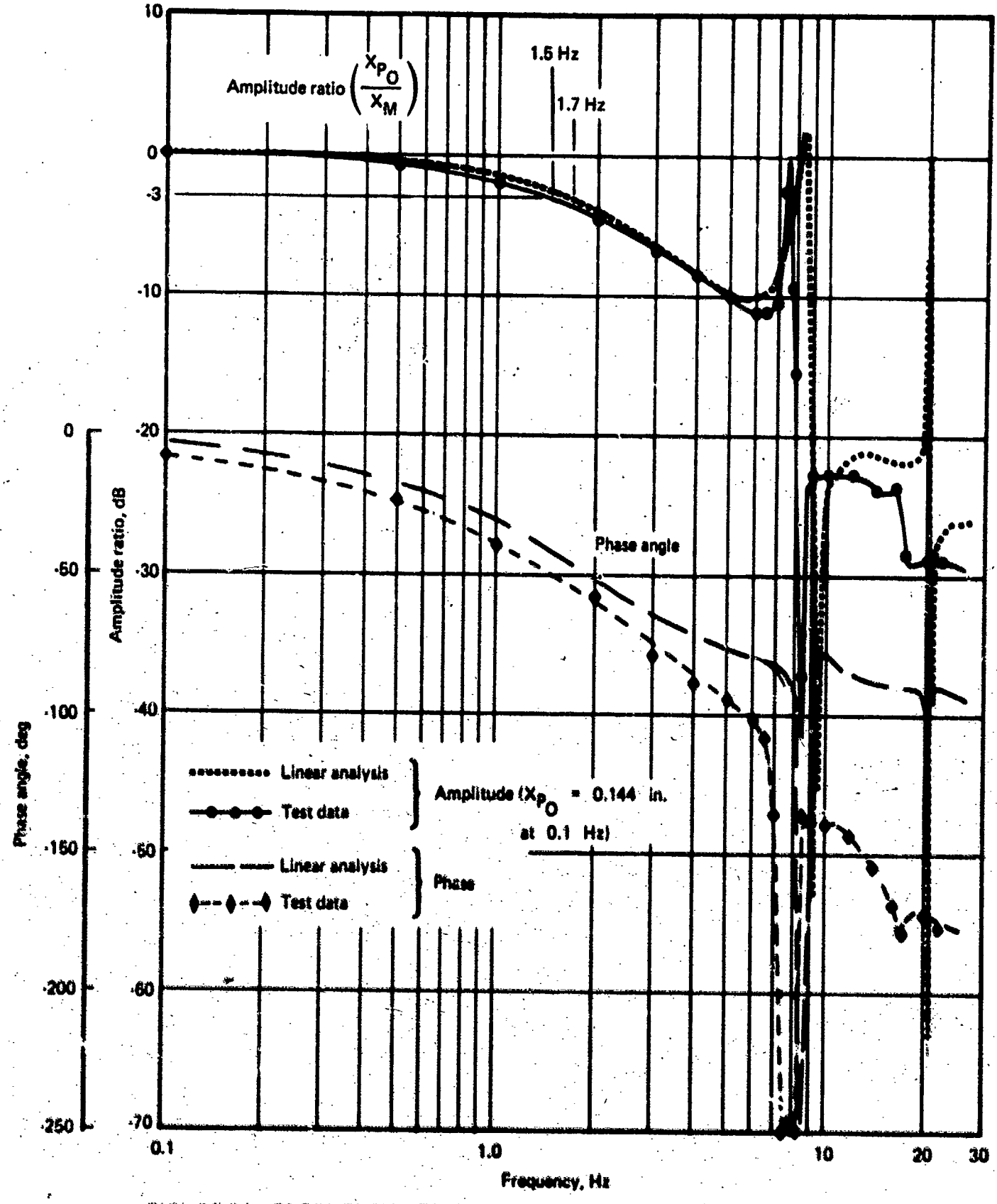

FIGURE 34.–FREQUENCY RESPONSE COMPARISON OF TEST DATA WITH LINEAR ANALYSIS–δ = 1, ELEVATOR INSTALLED

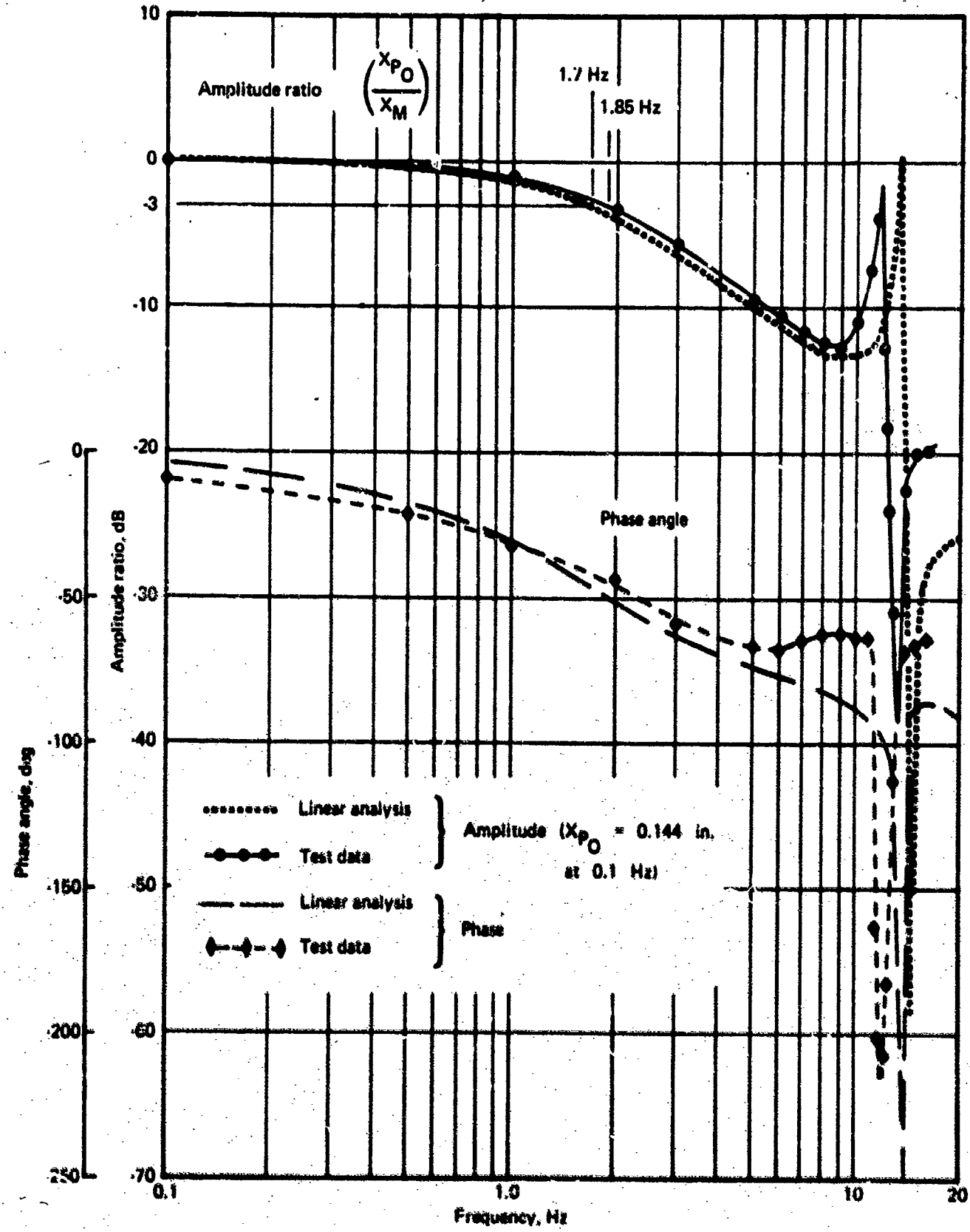

FIGURE 35.--FREQUENCY RESPONSE COMPARISON OF TEST DATA WITH LINEAR ANALYSIS-- δ = 0, ELEVATOR REMOVED

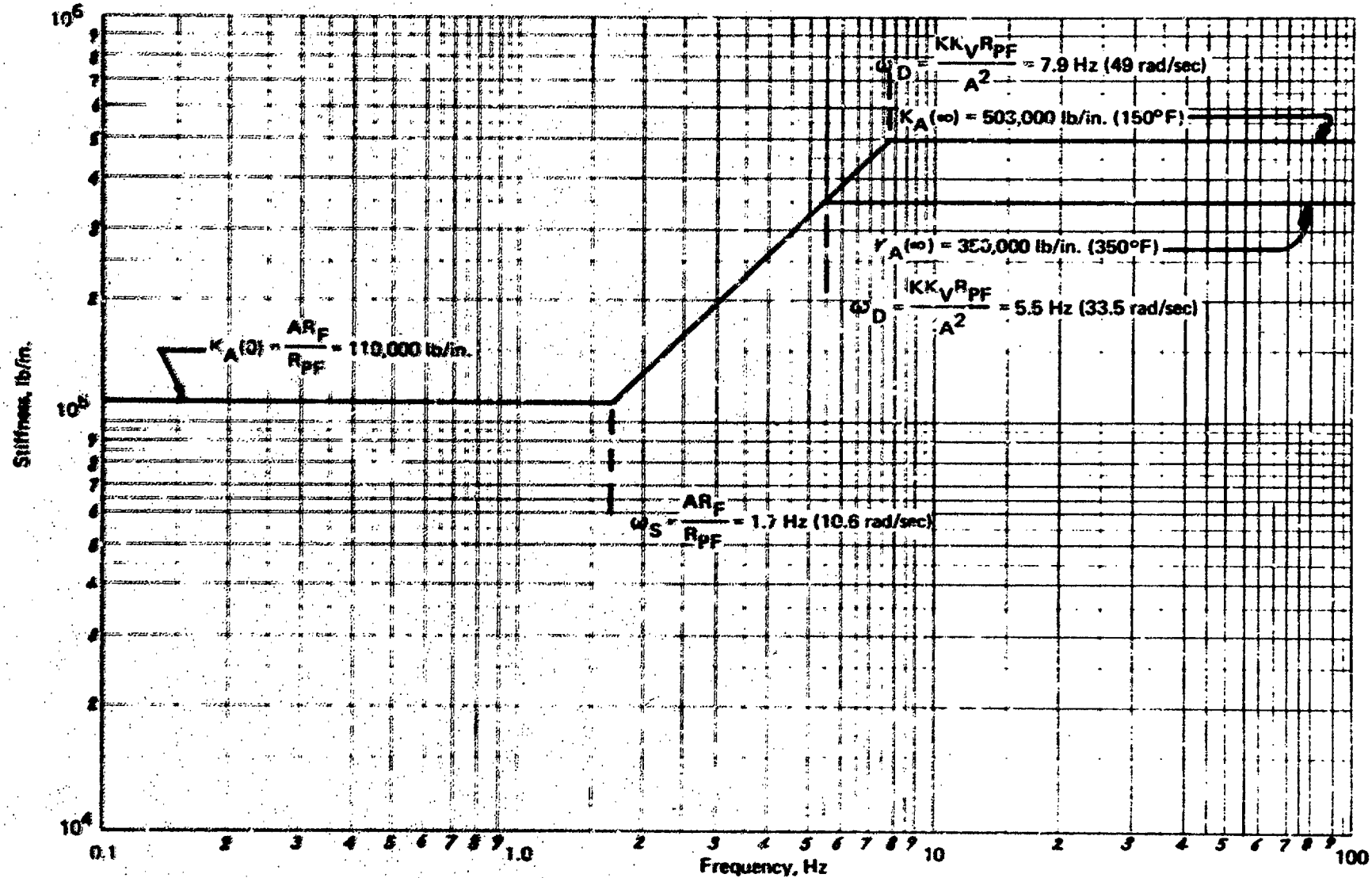

FIGURE 36.–THEORETICAL ACTUATION SYSTEM STIFFNESS FREQUENCY RESPONSE– NO STRUCTURAL EFFECTS

TABLE 3.–COMPARISON OF COMPUTED AND MEASURED STATIC STIFFNESS–FOUR ACTUATORS ON

Load	Surface position, deg	Feedback loop	Computed system static stiffness		Measured system static stiffness	
			Outboard actuator, lb/in.	Inboard actuator, lb/in.	Outboard actuator, lb/in.	Inboard actuator, lb/in.
–	0	[a]Rigid	110,000	110,000		
Distributed	0	Normal	225,000	225,000		
Force at node 26 (load position 4)	0	Normal	205,000	240,000		
Force at node 30 (load position 1)	0	Normal	250,000	260,000	[b]347,000	[b]340,000

[a]Structural effects removed from position feedback

[b]Average of two outboards and two inboards

The use of a half-section to represent a symmetrical section limited the capability of the analysis, since it could not be used to study unsymmetrical actuator operation. Neither could the effects of unsymmetrical structure be included.

The linear analysis could not predict the system static performance, since the friction forces (nonlinear) dominate at low frequencies. Static performance can be studied with a low-frequency, nonlinear simulation that does not include the complex structural matrix.

5.0 TEST RESULTS AND DISCUSSION

5.1 STATIC PERFORMANCE TESTS

"Static performance" (i.e., resolution, hysteresis, or repeatability) requirements of the SST actuation system were very exacting due to the necessity to suppress the limit cycle oscillations of the aerodynamically unstable airplane. Static performance may be measured by recording the system's hysteresis plot, as shown in figure 37. By traversing the loop very slowly to eliminate phase lag (dynamic effect), the plot represents static performance.

The allowable repeatablity values for the SST were based on human factors related to the peak-to-peak acceleration loads resulting from airplane limit cycling at the short-period frequency of 0.25 Hz. Table 4 lists the human factor classifications pertinent to the SST and the corresponding repeatability requirements. Preliminary analysis had shown that the production airplane values would be very difficult to achieve. However, the analysis included many assumptions, approximations, and linearizations of functions, and accurate values could only be obtained from flight tests. Therefore, the prototype airplane requirement was relaxed to 0.050°of peak-to-peak stabilizer travel (0.025 g peak to peak).

There are many hydraulic and mechanical factors as well as actuation system operating conditions which degrade static performance. Friction, linkage backlash, nonlinearity of system gains, lower hydraulic oil temperature, and input mismatches or misrigging causing force differentials all adversely affect the system's repeatability.

5.1.1 Hysteresis Test–Mechanical Commands

5.1.1.1 Test Objective

Testing was conducted to investigate static performance under probable operating conditions such as:

- Nominal rigging at various stabilizer positions and drive amplitudes
- Misrigging retract and extend directions
- Nominal rigging with hydraulic fluid temperature of 325° F
- Misrigging and hydraulic fluid temperature of 325° F
- Misrigging on one actuator and loss of hydraulic power to one other actuator

5.1.1.2 Test Description

Tests were conducted by commanding the actuators with the mechanical input servo. All tests were conducted with a triangle wave shape of ±0.5° or ±2.0° stabilizer travel at 0.02 cps. Various stabilizer displacements were obtained by biasing the command to the desired angle and superimposing the cyclic command.

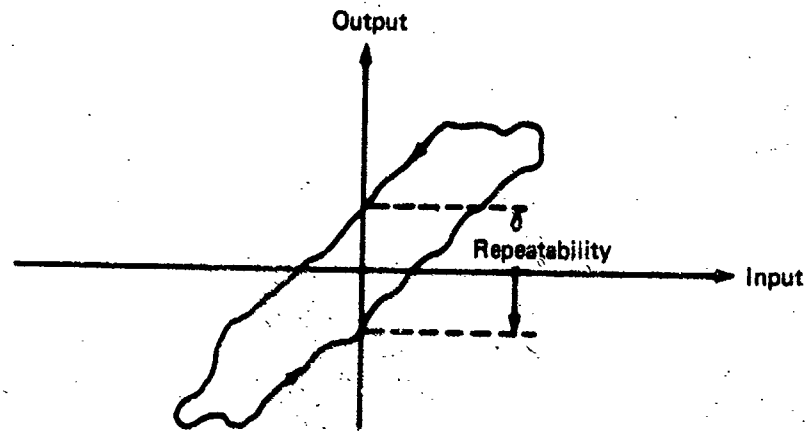

FIGURE 37.–SYSTEM HYSTERESIS PLOT

TABLE 4.–SST HUMAN FACTORS CLASSIFICATIONS

Repeatability, stabilizer (peak-to-peak, deg)	Limit cycle (peak-to-peak), g	Human factors classification	Established values for SST	
			Production airplane	Prototype airplane
0.008	0.004	Threshold of perceptibility	Goal	–
0.020	0.010	–	Requirement	–
0.040	0.020	Perceptible, but not unpleasant	–	–
0.050	0.025	–	–	Requirement

Note: All values are based on the SST short-period frequency of 0.25 Hz

Nominal rigging tests were conducted by adjusting the length of the input link from the bus shaft to each actuator to obtain an output force within 200 psid of the average load pressure of all four actuators. For these nominal rigging tests, the EC servo was off. Misrigging was simulated in channel four through the EC servo.

5.1.1.3 Test Results

The test results are shown in table 5. Representative hysteresis plots are shown in figure 38. Except for repeatability error magnitudes, as shown on table 5, all plots are similar in shape indicating no linkage binding or excessive friction.

Misrigging one actuator to produce the 800-psi allowable limit for force differential between actuators was expected to cause a degradation in repeatability, but the test results presented no clear trend of degradation. Although the rigging adjustments were within the prescribed limits, the variations within these limits were sufficient to masked expected degradations.

When hydraulic power to an actuator was turned off together with misrigging of another actuator to allowable limits, degradation was apparent, but only for ±2.0° excursions. Two cases were run for ±0.50° excursion, and the results were inconclusive. The reason for the large degradation at ±2.0° is not clear but may have been caused by backpressure in the unpressurized actuator. Since the main servovalve is piloted, the valves of unpressurized actuators do not follow the input command. If leakage is not equivalent to backdriving flow, backpressure must be built up in an unpressurized actuator to either cause the bypass valve to operate or to self-energize the pilot valve. This additional load would further degrade the repeatability.

An increase of oil temperature from 150° to 325° F caused a slight improvement in static performance. The higher temperature reduces the viscosity of the oil, which tends to reduce the friction within the actuator.

The performance degradation due to stabilizer position (trailing edge 10° up) could only be seen for test runs at a cyclic amplitude of ±2.0°. Some slight reduction in static performance was expected due to accumulation of minor geometry changes, such as a 10% reduction in moment arm and a 20% increase in actuator steady-state gain. These could, if added in the most adverse direction, account for 30% to 67% degradations.

5.1.1.4 Conclusion

The measured repeatability of 0.028° of stabilizer angle for four-channel operation at 325° with nominal rigging (vs the SST requirement of 0.050°) indicates that the system would meet the prototype airplane performance requirements during operation in the normal mode.

The small degradation in repeatability due to the combined effects of oil temperature, stabilizer position changes, cyclic command amplitudes, unpowered actuators, and misrigging indicate that the performance of the system would be sufficient to meet the overall design requirements of the prototype airplane. This is especially true in the case of small commands

TABLE 5.–ACTUATOR SYSTEM REPEATABILITY TEST RESULTS–MECHANICAL COMMAND

Conditions						Results
Cyclic amplitude, deg	Stabilizer angle, TE up	PCU 4 misrig		Oil temperature, °F	PCUs On	Repeatability, stabilizer deg
		Retract	Extend			
±0.5	0°	0		150	All 4	0.044
±2	0°	0		↓	↓	0.065
±0.5	-5°	0				0.032
±2	-5°	0				0.075
±0.5	-10°	0				0.040
±2	-10°	0				0.085
±0.5	0°	1/4°				0.046
±2	0°	↓				0.060
±0.5	-5°					0.068
±2	-5°					0.060
±0.5	-10°					0.056
±2	-10°					0.080
0.5	0°		1/4°			0.054
2	0°		↓			0.060
0.5	-5°					0.036
2	-5°					0.080
0.5	-10°					0.040
2	-10°					0.100
0.5	0	0		325		0.028
2	0	0		↓		0.065
0.5	-10°	0				0.066
2	-10°	0				0.105
0.5	0°	1/4°				0.044
2	0°	1/4°				0.050
0.5	0°		1/4°			0.034
0.5	0°	1/4°		150	1, 2, and 4 (3 off)	0.070
2	0°	1/4°		↓	↓	0.100
0.5	0°		1/4°			0.044
2	0°		1/4°			0.105

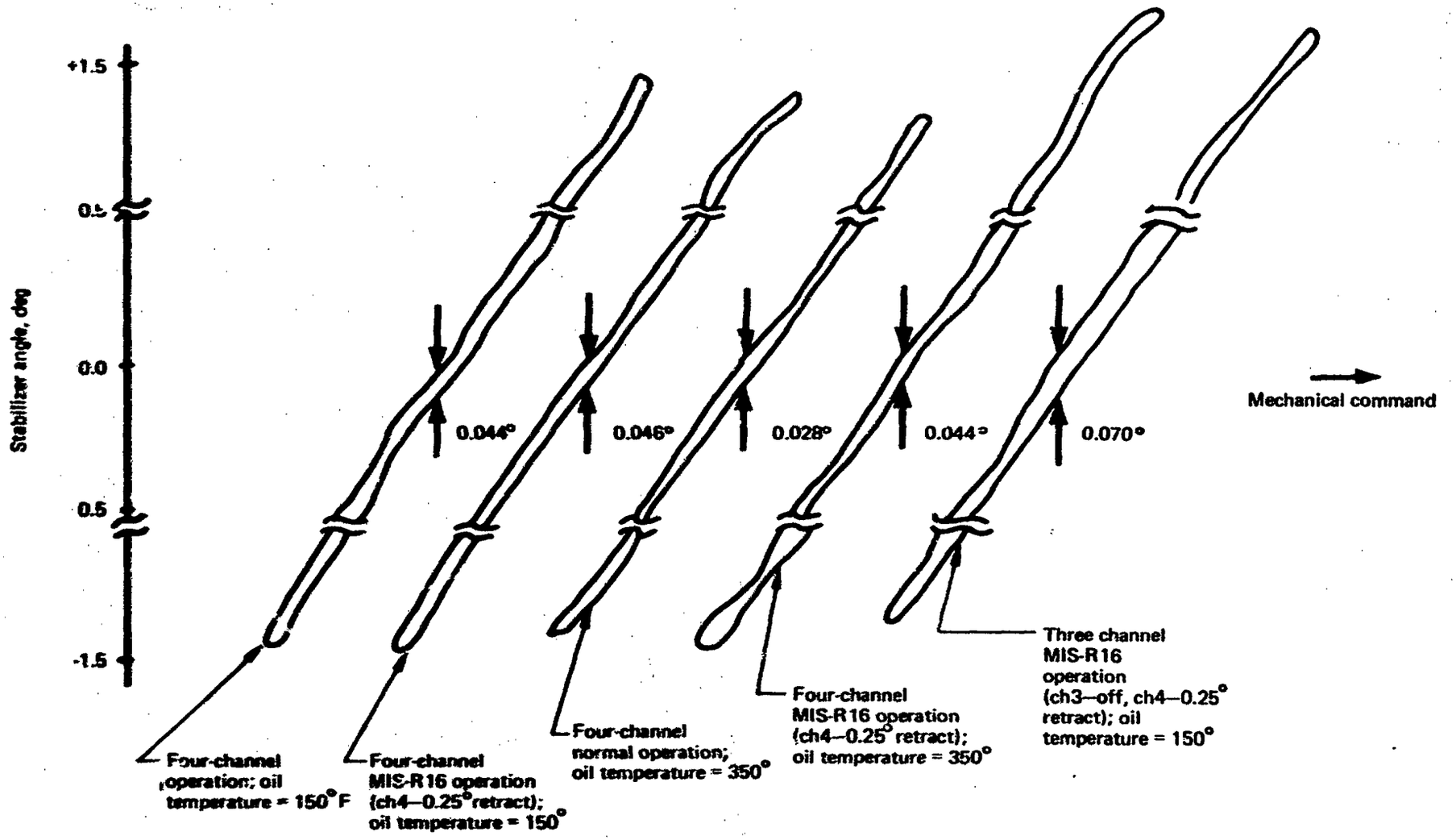

FIGURE 38.—ACTUATOR SYSTEM HYSTERESIS TEST RESULTS—MECHANICAL COMMAND

(±0.5°), which is considered the condition most often encountered. Larger travels at large stabilizer angles are the exception, and the larger hysteresis exhibited there is not considered typical for the major portion of high-speed flight.

5.1.2 Hysteresis Test—Baseline Electrical Commands

5.1.2.1 Test Objective

The objective of this test was to determine the baseline static performance of the actuation system commanded electrically for four-, three-, and two-channel operation with hydraulic fluid temperatures of 150° and 325° F.

5.1.2.2 Test Description

Tests were conducted by electrically commanding the actuator with a function generator. The command was applied to all four channels and the tests conducted with a triangle wave shape of ±1° stabilizer angle at 0.02 Hz.

Adjusting EC servo bias voltages on each channel obtained EC servo force synchronization within 25 psid for both the 150° and 325° F cases. For the three- and two-channel operation, the appropriate EC servo solenoid shutoff valves were closed; the hydraulic supply to the main actuator was left on.

5.1.2.3 Test Results

The test results are shown on table 6. Representative hysteresis plots of certain tests are shown on figure 39. Except for repeatability magnitude as shown on table 6, all X-Y plots were similar in shape.

The repeatability of the actuator system is significantly degraded for electrical input command over the mechanical command with four active channels. This degradation is attributed to the abnormally low servovalve pressure gain resulting from the EC servo piston leakage.

This abnormal performance resulted from a reduction of the EC servo piston land lengths by the actuator vendor to meet a friction requirement of 10 lb maximum. The reduced land lengths allowed more fluid leakage and decreased the effective pressure gain of the servovalve around null. Since static performance tests were conducted around null, some degradation and nonlinearity of the performance was expected. Unacceptably high EC servo friction had resulted from cocking of the EC servo pistons in the cylinders due to buckling of the compression loaded, asymmetric member connecting the EC servo pistons. A proper design fix on the connection member (instead of reducing land lengths) had been initiated by the vendor at the time of cancellation of the SST program.

Repeatability for three channels of EC servo operation was slightly degraded due to the load of the dead channel on the three active channels. Further degradation in surface repeatability was experienced with two-channel operation.

TABLE 6.–ACTUATION SYSTEM REPEATABILITY TEST RESULTS –±1° ELECTRICAL INPUT, NO OFFSETS

EC servo channels on	Hydraulic fluid temperature, °F	
	150	325
Repeatability, stabilizer deg		
1, 2, 3, 4	0.075	0.060
2, 3, 4	0.082	–
3, 4	0.10	0.090
1, 4	0.10	–
1, 2	–	0.10

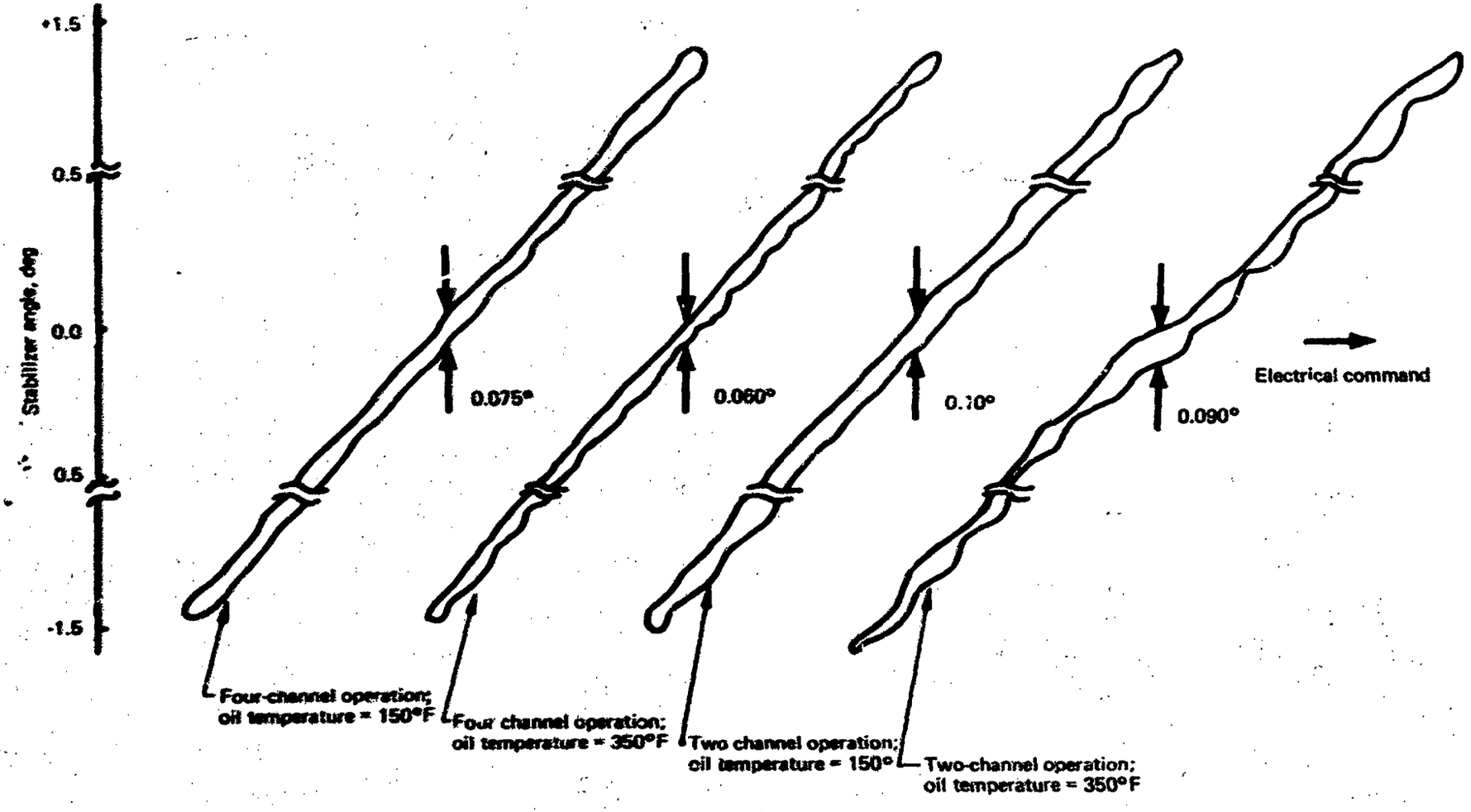

FIGURE 39.–ACTUATOR SYSTEM HYSTERESIS TEST RESULTS–ELECTRICAL INPUTS; NO OFFSETS

5.1.2.4 Conclusion

The measured repeatability under electrical commands at normal operating conditions very nearly met the SST required repeatability of 0.050°. Had the effective EC servo pressure gain met the specification requirement, the repeatability would certainly have been improved.

The small degradations in the repeatability due to the off-normal conditions of 150° F temperature and three- and two-channel operation are considered acceptable. The degradation in system performance, in the case of the two-channel operation which is classified as a double failure, the degradation in system performance would be compatible with the reduced airplane performance permitted for this failure condition.

5.1.3 Hysteresis Test–Electrical Commands With Equalization

5.1.3.1 Test Objectives

The first objective of this test was to determine static performance of the actuation system with steady-state electrical command offsets and the following equalization modes:

- No equalization
- Proportional equalization only
- Integral equalization only
- Proportional and integral equalization

The second test objective was to determine if the force differential between main actuators met the specification allowable of 130 psid with a steady-state electrical command offset without equalization.

5.1.3.2 Test Description

The performance tests were conducted by electrically commanding all four EC servos with a triangular wave shape of ±1°of stabilizer angle at 0.02 Hz. Superimposed on the command signal were +1° offsets to channels 1 and 3, and -1° offsets to channels 2 and 4.

The main actuator force differential tests were conducted by engaging all EC servo channels with equalization off and signaling one channel at a time with steady-state input of ±1°. The actuator pressure was manually recorded at 0.5° and 1° signal levels.

5.1.3.3 Test Results

Performance test results are shown in table 7 and figure 40. Four-channel repeatability degraded compared to the baseline data (see sec. 5.1.2). Degradation was due to the friction and force differential between the actuators caused by the EC servo output differences as allowed by the compliance of the synchronization shaft and linkage.

TABLE 7.–ACTUATION SYSTEM REPEATABILITY TEST RESULTS–±1° ELECTRICAL COMMANDS, WITH OFFSETS

EC servo channels on	Equalization mode			
	None	Proportional only	Integral only	Both
	Repeatability, stabilizer deg			
4	0.10	0.09	0.075	0.075
3	0.14	0.09	0.08	0.08
2	0.12 (1.57 dead zone)	0.10 (1.50 dead zone)	0.10	0.10

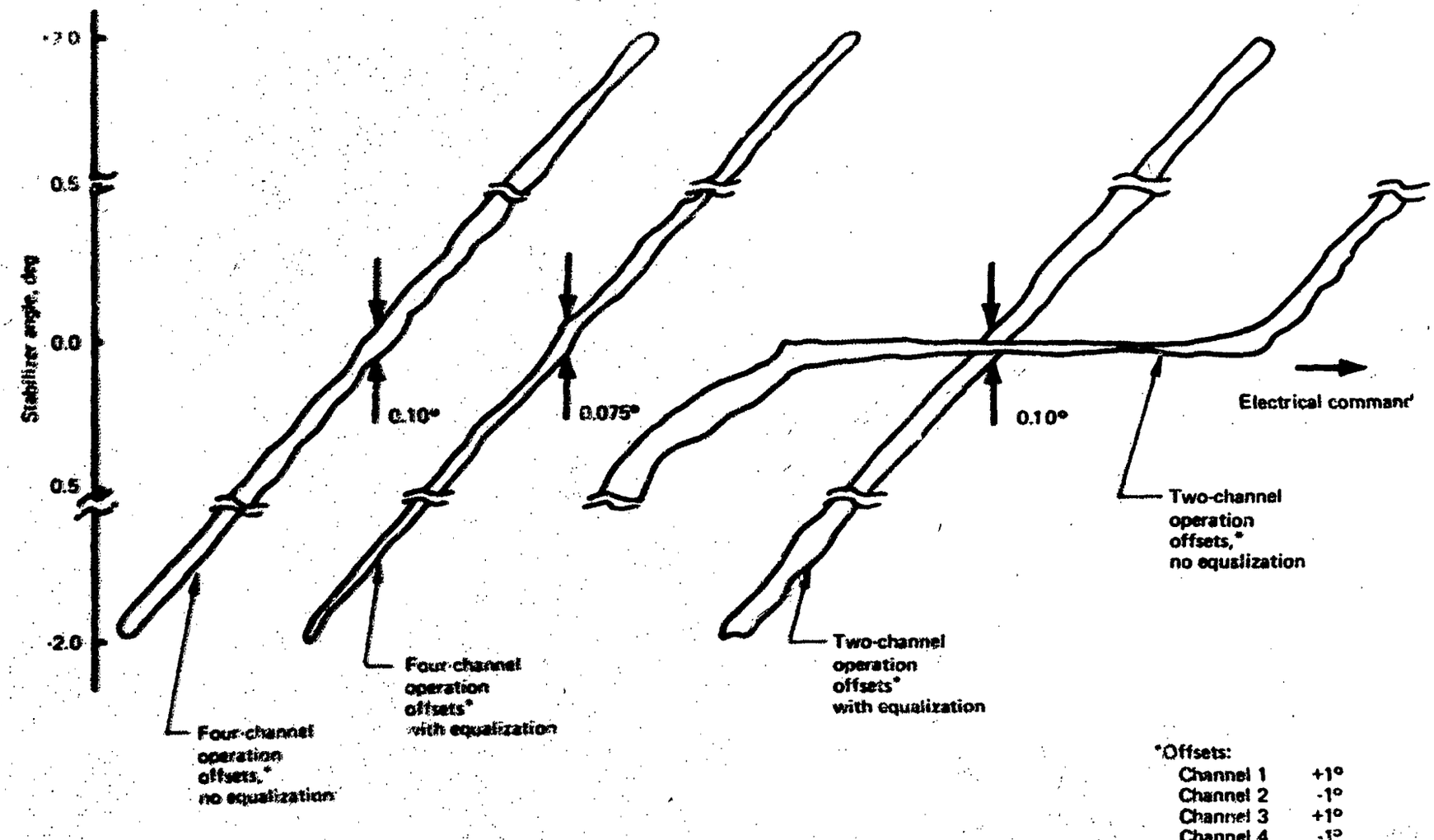

FIGURE 40.--ACTUATOR SYSTEM HYSTERESIS TEST RESULTS--ELECTRICAL COMMAND WITH OFFSETS

Further degradation with three-EC-servo-channel operation was due to the effect of the mechanical centering cam load of the depressurized channel on the three remaining EC servo actuators.

Two-channel operation with opposite offsets in the operating channels and equalization off produced a surface dead zone approximately equivalent to the value of electrical offsets. This resulted from the equalization detent and the centering cam acting as a mechanical third-channel voter.

Actuator repeatability improved when the proportional equalization loop was closed for four- and three-EC-servo-channel operation. The proportional loop prevented the equalization detent from bypassing and thereby slightly reduced the force difference between the EC servos.

Integral equalization further improved the system repeatability and eliminated the dead zone noted above. Integral equalization commanding the EC servos to move in the proper direction reduced the forces in the synchronizing shaft.

The main actuator incremental force differential due to the unequalized offsets was 820 psi and resulted from the deflections of the EC servo synchronization shaft and linkage as illustrated in figure 41. A typical stiffness value measured for a single channel being restrained by three channels was 8250 lb/in. Had the EC synchronization shaft stiffness (K_1) met the design requirement of 70,000 lb/in., the main actuator force differential would have been about 130 psid. A stiffer synchronizing shaft would also have resulted in even smaller surface transients due to failures.

5.1.3.4 Conclusions

The measured repeatability of 0.075° of stabilizer angle for four- and three-channel operation with offsets and equalization is essentially the same in comparison to the baseline repeatability data without offsets. Therefore, it is concluded that the tested equalization concept is feasible and could meet the established SST repeatability requirement of 0.050° of stabilizer by correcting the effective EC servo pressure gain (see sec. 5.1.2).

The 820-psid system main actuator force differential with offset electrical commands exceeded the 130-psid allowable. However, had the stiffness of the EC servo synchronization shaft and linkages met design requirements, the main actuator force synchronization would have been within allowable limits.

5.2 DYNAMIC PERFORMANCE AND STABILITY TESTS

A series of tests were performed to determine the dynamic response characteristics of the system. These consisted of step and frequency response tests using mechanical and electrical commands.

Tests were carried out at both 140° and 350° F. The 140° F tests provided a baseline definition of the stability of the system. A number of the tests were repeated at 350° F to evaluate the effect of increasing the fluid temperature on system stability. Increasing the

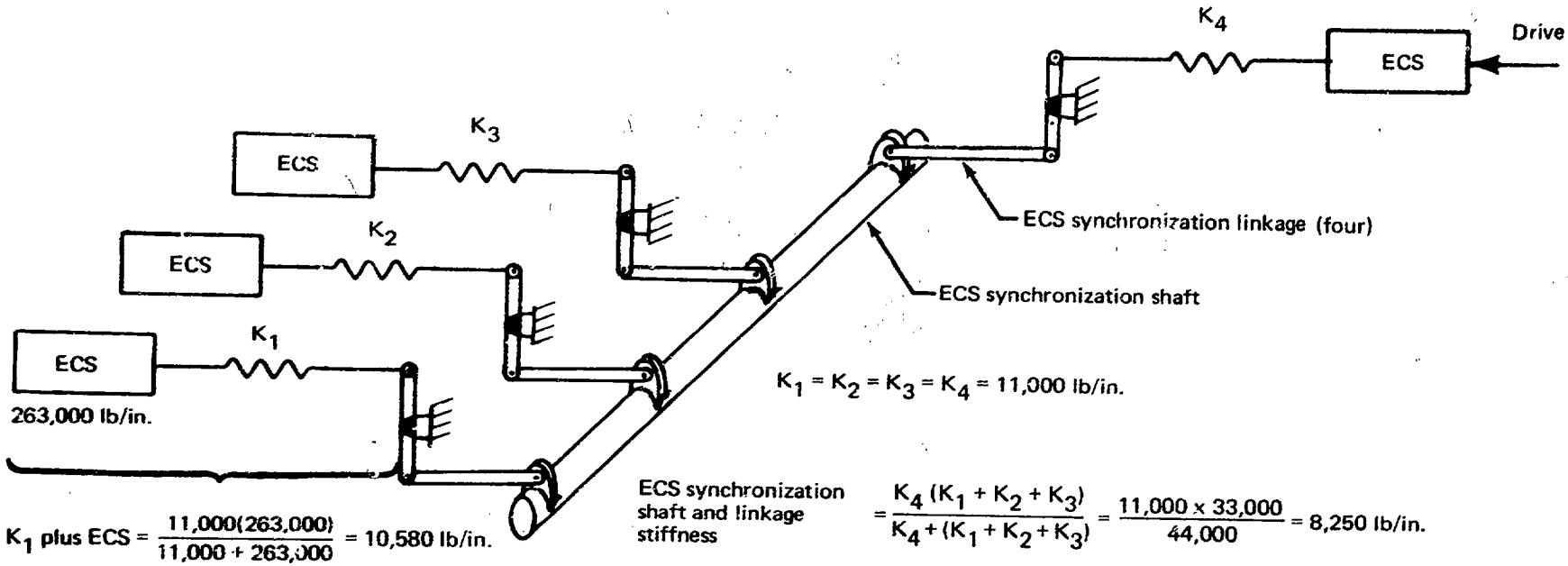

$$K_1 \text{ plus ECS} = \frac{11{,}000(263{,}000)}{11{,}000 + 263{,}000} = 10{,}580 \text{ lb/in.}$$

$$\text{ECS synchronization shaft and linkage stiffness} = \frac{K_4 (K_1 + K_2 + K_3)}{K_4 + (K_1 + K_2 + K_3)} = \frac{11{,}000 \times 33{,}000}{44{,}000} = 8{,}250 \text{ lb/in.}$$

$$\text{ECS max displacement} = \frac{\text{Equalizer force limit}}{\text{Stiffness}} = \frac{148 \text{ lb}}{8{,}250 \text{ lb/in.}} = 0.0179 \text{ in.}$$

Stabilizer command limit (due to ECS displacement
= (ECS to stabilizer gain)(ECS displacement)
= (15°/in.)(0.0179 in.) = 0.268° stabilizer

Max PCU force differential = (ECS displacement)(Linkage)(Main valve pressure gain)
= (0.0179 in.)(1.247)(37,000 psi/in.) = 820 psi

FIGURE 41.—EC SERVO (ECS) SYNCHRONIZATION SHAFT AND LINKAGE STIFFNESS

fluid temperature reduces its bulk modulus and hence reduces the dynamic stiffness of the actuators. Since the margin of stability of the system is directly proportional to dynamic stiffness, an increase in the fluid temperature tends to reduce the stability of the system.

All of the tests were at a no-load condition with small input perturbations in order to stay in the linear operating region so that the effects of the valve flow gain and flow-pressure coefficient on the system response at the point of their maximum influence could be examined. At no-load, the valve flow gain is at its maximum, giving the highest system gain. At small valve openings, the flow-pressure coefficient is at or near its minimum, giving a low damping ratio. Hence, for stability considerations, the no-load and small main actuator control valve opening conditions are very important.

The pressure feedback employed on each of the actuators is a means of providing system stability. Pressure feedback reduces the effective pressure gain of the installed actuator. Static stiffness of the actuator is directly proportional to the effective pressure gain, and the margin of stability is inversely proportional to the static stiffness. Thus, a decrease in the effective pressure gain of the installed actuator through pressure feedback will lower the static stiffness and increase the margin of stability.

Of particular interest is the effect of pressure feedback piston friction on actuator stability. Friction introduces pressure feedback piston hysteresis, which increases the actuator effective pressure gain. Jamming of the pressure feedback piston drastically increases the effective pressure gain. The SST design required system stability with two pressure feedback devices jammed.

At the beginning of these tests, the reflected load to the actuators had mass properties and a load stiffness with the same first-mode natural frequency as the SST prototype.

Because a failure of test structure representing the SST prototype elevators occurred during a frequency response test, the elevators were removed. It was recognized that, on some of the tests that followed, the change in spring-mass would not have any effect. On those tests where results would be affected by the removal of the elevators, the incremental changes could be accounted for in the analysis of test results.

5.2.1 Test Objectives

The objective of this test was to determine the dynamic response characteristics of the actuation system. The characteristics of interest were the system damping ratio, break frequencies of the main actuators and the electric command servos, the system damped natural frequency, and the first-mode damped natural frequency. These test data were then compared with analytical predictions.

5.2.2 Test Description

Theoretically, the system natural frequency and damping ratio can be determined by observing the time response of either the actuator rod position or load pressure. The load pressure traces were a more sensitive indicator of damping ratio, since pressure is proportional to rod acceleration. The load pressure traces were not identical on all four actuators,

and the system damping ratio was determined by averaging the ratios derived from each of the load pressure traces.

Frequency responses of the stabilizer position (left and right) were run, but the asymmetry of the structure caused the respective amplitude ratios to vary more than 2 to 1 in the region of the system natural frequency. Harmonics and subharmonics also appeared on the stabilizer positions. Therefore, the actuator rods were better suited for condition comparisons and comparison with the analytical results. Frequency responses are plotted using the number 1 rod position. The plots of the other rods were not identical, but the differences were negligible.

The system natural frequencies in the test results were read from the apparent peak of the frequency response plots, and are usually lower than the system natural frequencies read from the step response data in table 3 (sec. 4.0). The difference is attributed to the nonlinear effects in the frequency response data. For example, the data showed that the main valve position was exceeding the linear region of flow gain as the system natural frequency was approached.

Step response tests with nonlinearities in the pressure feedback loop were performed by attaching friction or locking devices to the pressure feedback pistons on one or more of the actuators. These devices were mechanical and could be adjusted to a given value. Before each test, a force vs displacement plot was made for the pressure feedback piston to establish that the friction device had been adjusted correctly (see figs. 42 and 43). A locking device was attached to the piston and clamped to the actuator body to simulate a jammed pressure feedback piston.

Frequency response tests were conducted using both mechanical and electrical commands with the test equipment illustrated in figure 44. One electrical command test was run after the EC loop gain had been increased from 30 to 60 rad/sec to evaluate the margin of stability of the EC servo. Selected tests were also conducted for various combinations of active (hydraulic power on) main actuators and various numbers of active EC servos.

A digital computer provided an analog command signal to the controls development test system. Specific parameters were measured and returned to the digital computer via the instrumentation system. Amplitude ratio and phase angle were computed and plotted automatically in the form of Bode diagrams. The computer program allowed the test engineer to specify the frequencies of interest, the amplitude of the command, and the parameters to be evaluated.

5.2.3 Test Results

The initial step and frequency response tests using mechanical commands were run with the elevators installed (figs. 45 and 46). From these tests it was determined that the system damping ratio, ζ, is 0.021, the break frequency is 1.8 Hz for the main actuators, the system damped natural frequency is 6.9 Hz, and the first-mode natural damped frequency is 7.9 Hz. These values compare very well with the predicted values. Tests were extended to 26 Hz to investigate a resonance expected at about 18 Hz. The test data do not show a resonance, but a discontinuity at approximately 18 Hz indicates the presence of a highly damped pair of

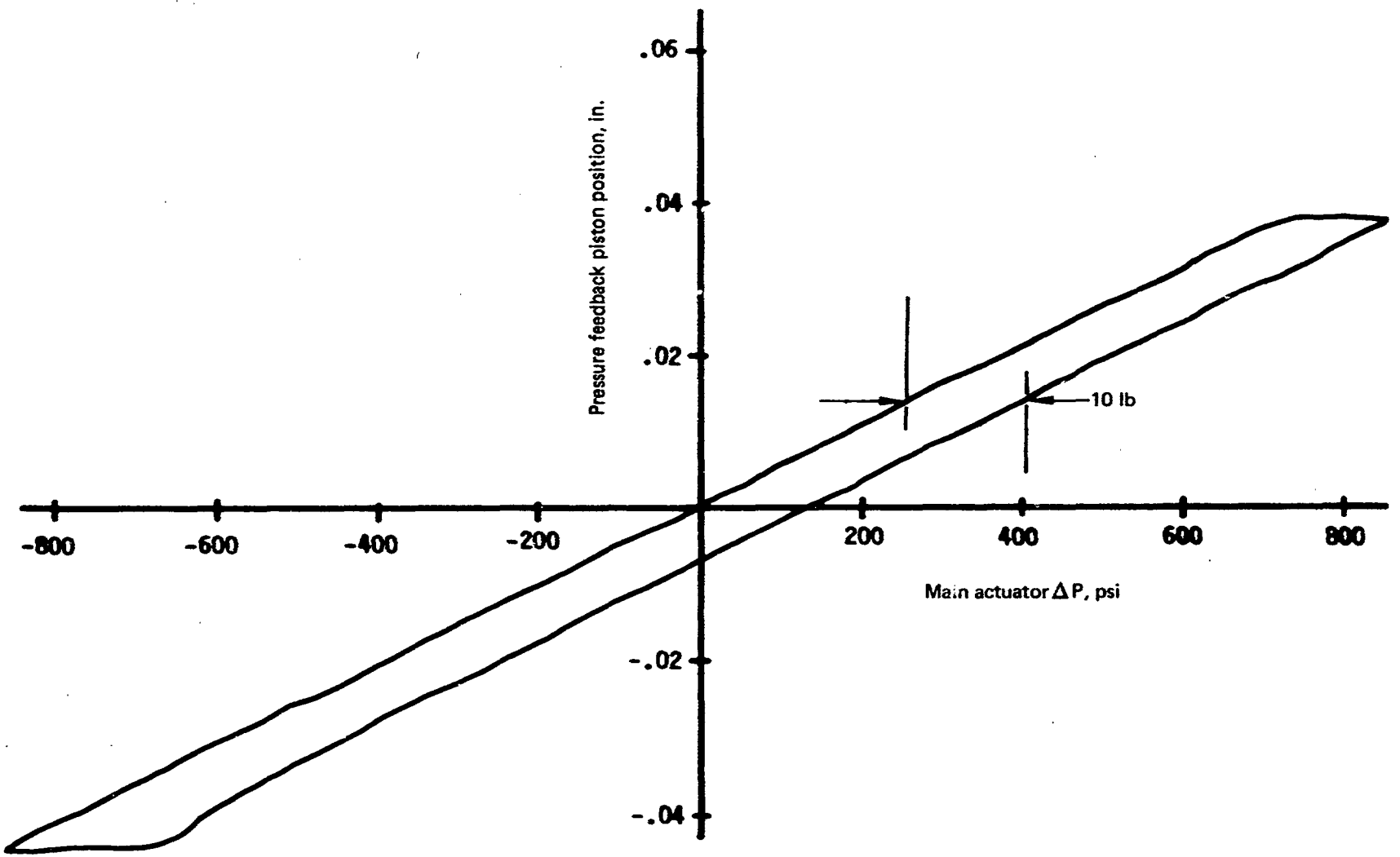

FIGURE 42.–STEP RESPONSE TEST–PRESSURE FEEDBACK PISTON FRICTION (10 LB)

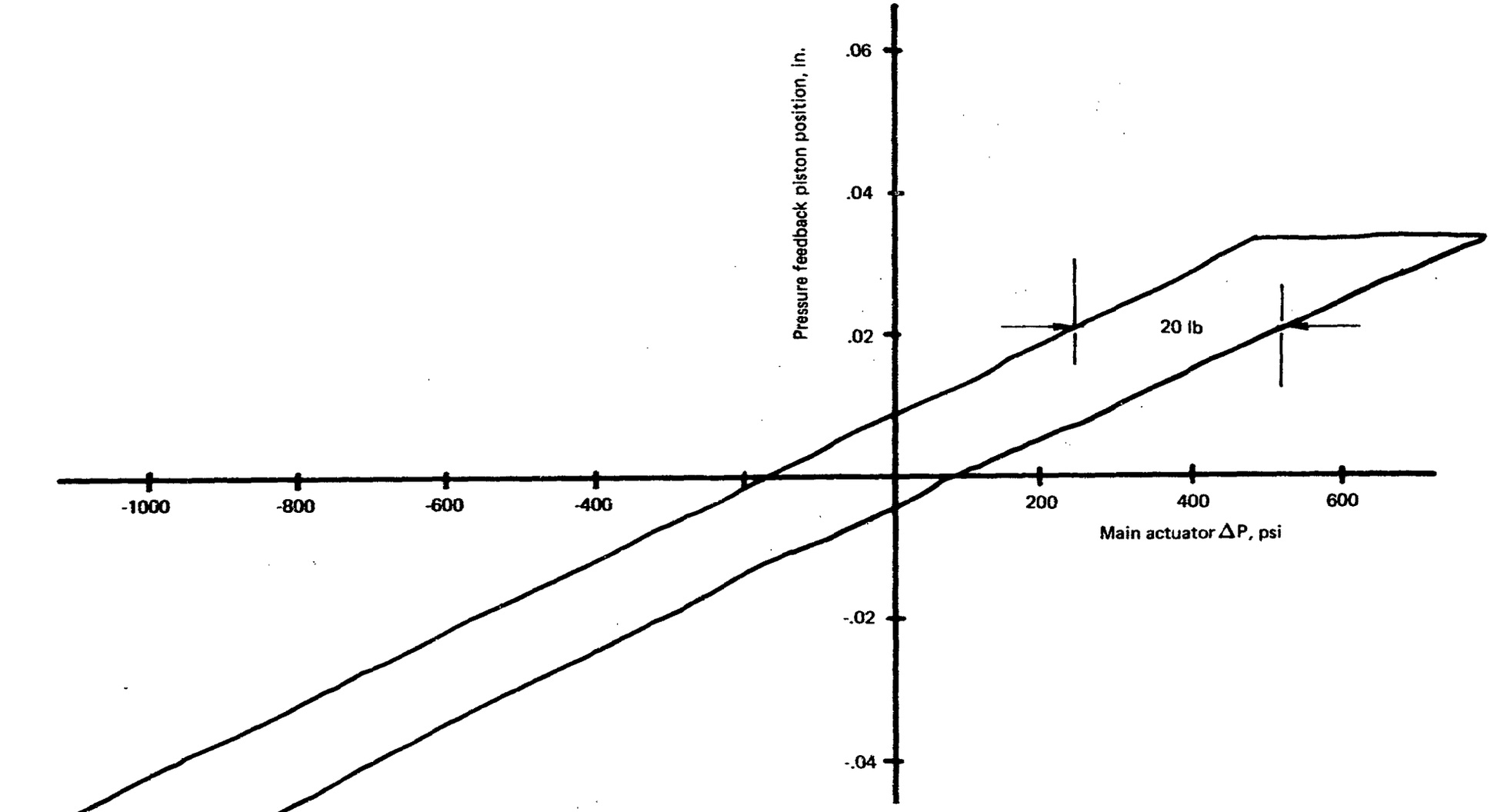

FIGURE 43.–STEP RESPONSE TEST–PRESSURE FEEDBACK PISTON FRICTION (20 LB)

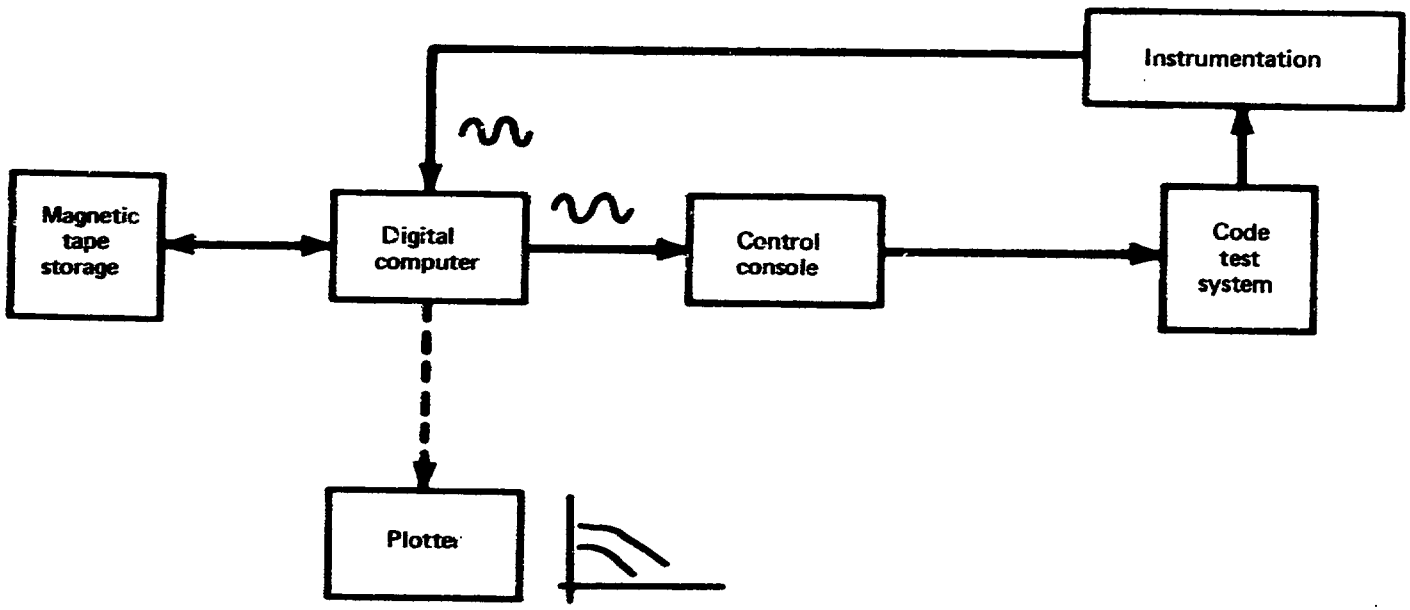

FIGURE 44.—FREQUENCY RESPONSE TEST EQUIPMENT

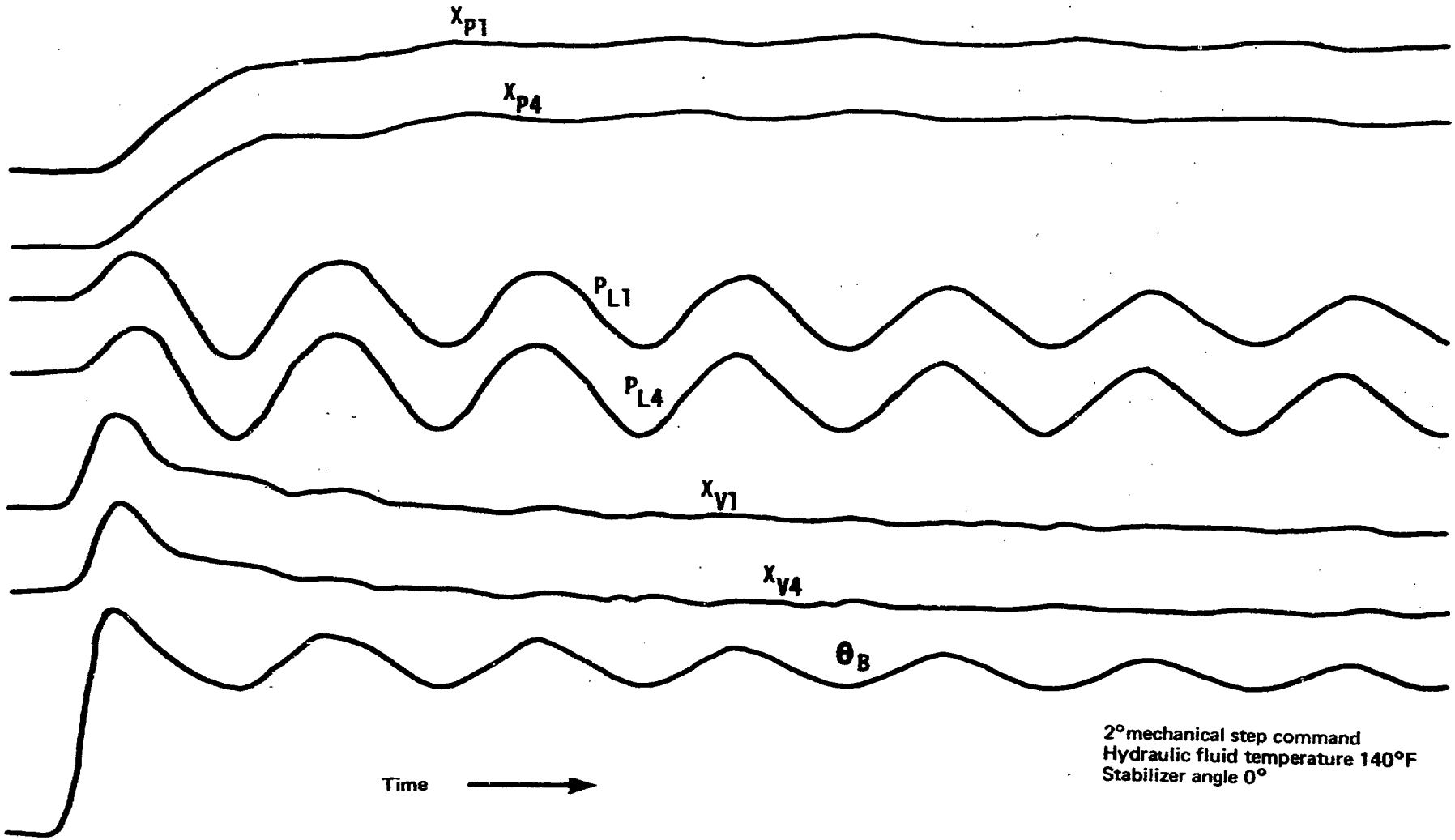

FIGURE 45.—STEP RESPONSE TEST—ELEVATORS INSTALLED, $\zeta = 0.021$

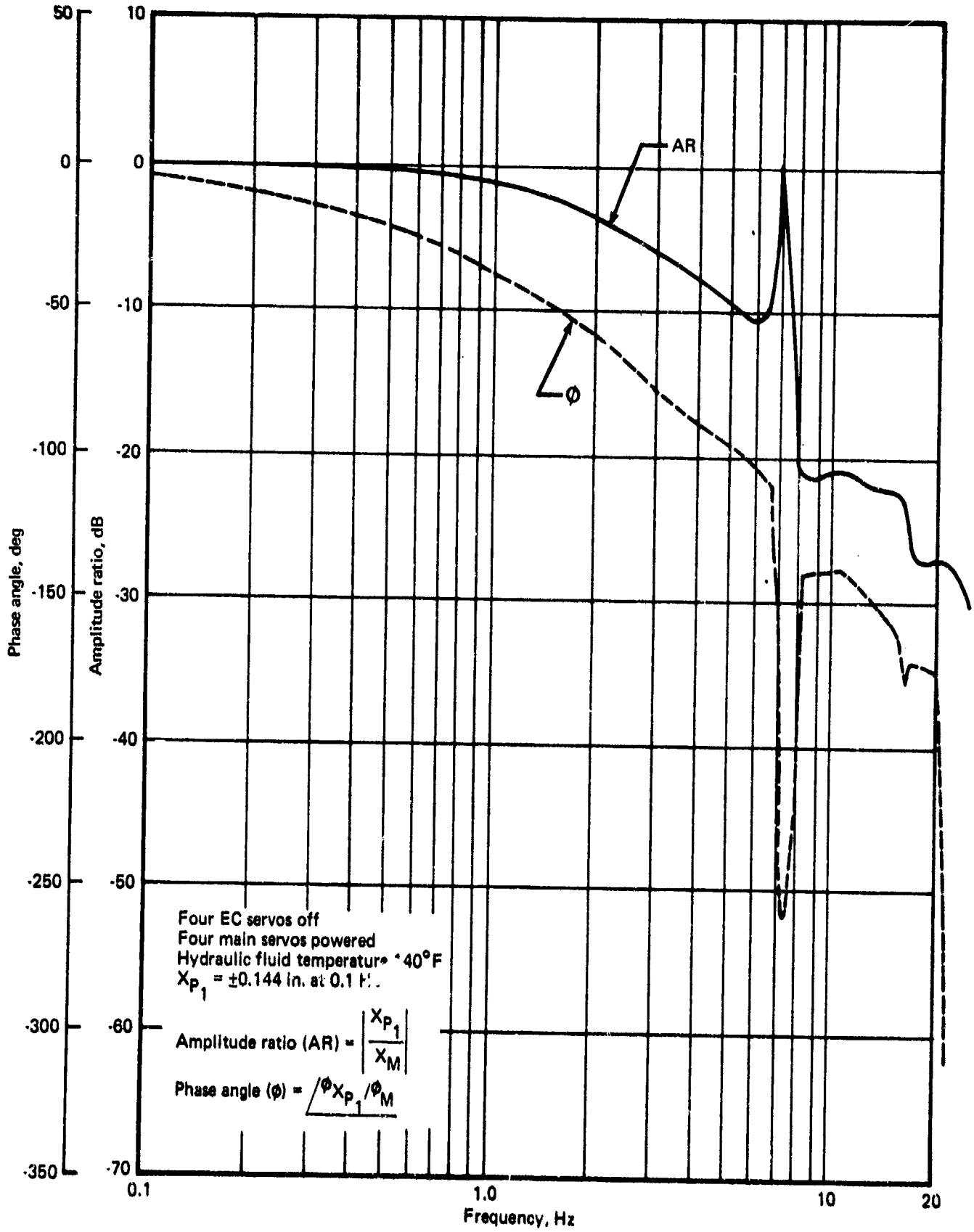

FIGURE 46.–CLOSED-LOOP FREQUENCY RESPONSE–MECHANICAL COMMAND, ELEVATORS INSTALLED

poles and zeros (see fig. 46). Frequencies above 16 Hz were eliminated after the initial testing because it was determined that the higher frequency modes were insignificant.

The system damped natural frequency and the first-mode natural damped frequency were each 1 Hz lower than the predicted values. This indicates that the spring-mass combination of the test system would have to be increased by approximately 23% to simulate the equivalent SST system. Examination of the mechanical input bus shaft response clearly shows that structural deflections affect the bus shaft. Response to these deflections constitutes an input to the valve in a destabilizing sense.

The difference between the measured damping ratio, ζ, of 0.021 and the theoretical value of 0.017 is largely due to the absence of the structural damping in the theoretical analysis.

Step and frequency response tests with the elevators removed showed that the modified system damped natural frequency, first-mode damped natural frequency, and system damping ratio were 11.5 Hz, 12.5 Hz, and 0.025, respectively. The break frequency of the main actuators is not affected by the change in the spring-mass of the load (see figs. 47 and 48). The change in the characteristics noted above are the result of a reduction in the load mass by approximately 75% and in the load spring by approximately 35%.

Increasing the hydraulic fluid temperature from 140° to 350° F reduced the system damped natural frequency from 11.5 to 11.0 Hz (see figs. 49 and 50). This reduction was a result of a lower oil spring rate due to the reduction in bulk modulus of the oil at higher temperatures. The increase in phase angle was due to the increased separation of the system natural damped frequency and load natural damped frequency.

With the stabilizer in the -10° (trailing edge up) position, the system damping ratio decreased slightly from 0.025 to 0.016 at 140° F and from 0.022 to 0.017 at 350° F (see figs. 47, 49, 51, and 52 and table 8). This is the result of increased static stiffness of the installed actuators at this stabilizer position, which offsets the increase in the damping ratio caused by the increased effective mass and the increased oil spring rate when the actuator piston is near the end of its stroke.

A frequency response test using an electric command established the electric command break frequency at 4.77 Hz and was in agreement with the predicted value (see fig. 53). The attenuation of the amplitude ratio and increased phase shift of the system were consistent with addition of the EC command first-order system. Increasing the EC command loop gain from 30 to 60 rad/sec did not significantly reduce the margin of stability of the EC servo (fig. 54).

When the friction was increased on two of the four pressure feedback pistons, the damping ratio of the system decreased as the magnitude of the friction force was increased (see figs. 55, 56, and 57). As shown in figure 55, a 10-lb friction force on two of the four pressure feedback pistons decreased the system damping ratio from 0.025 to 0.008. At a friction level of 20 lb on two pistons, as shown in figure 56, the system went into a limit cycle at its natural frequency. The magnitude of the differential pressures across the main actuator pistons varied by 600 and 750 psi, respectively, peak to peak on the actuators with

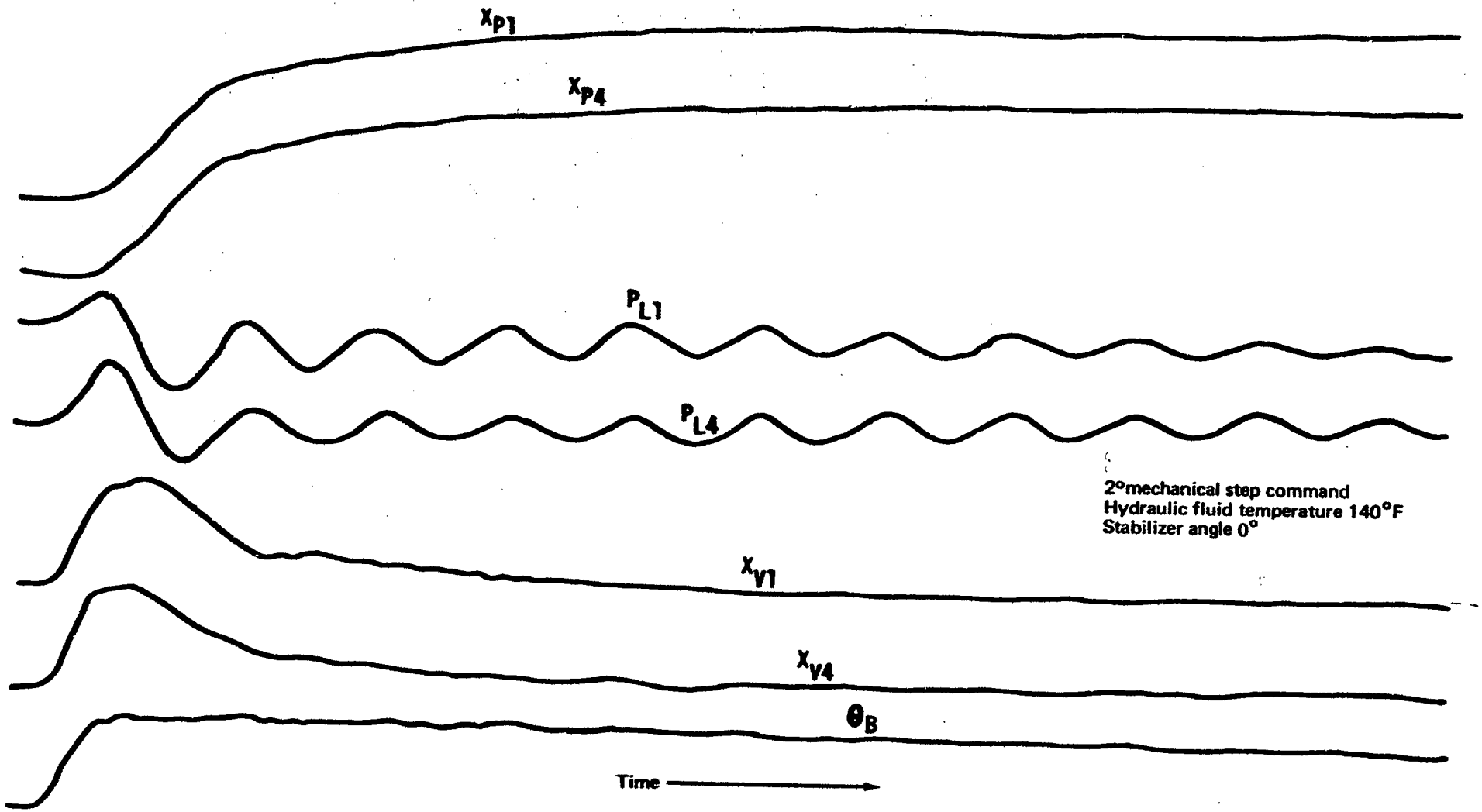

FIGURE 47.–STEP RESPONSE TEST–ELEVATORS REMOVED, $\zeta = 0.025$

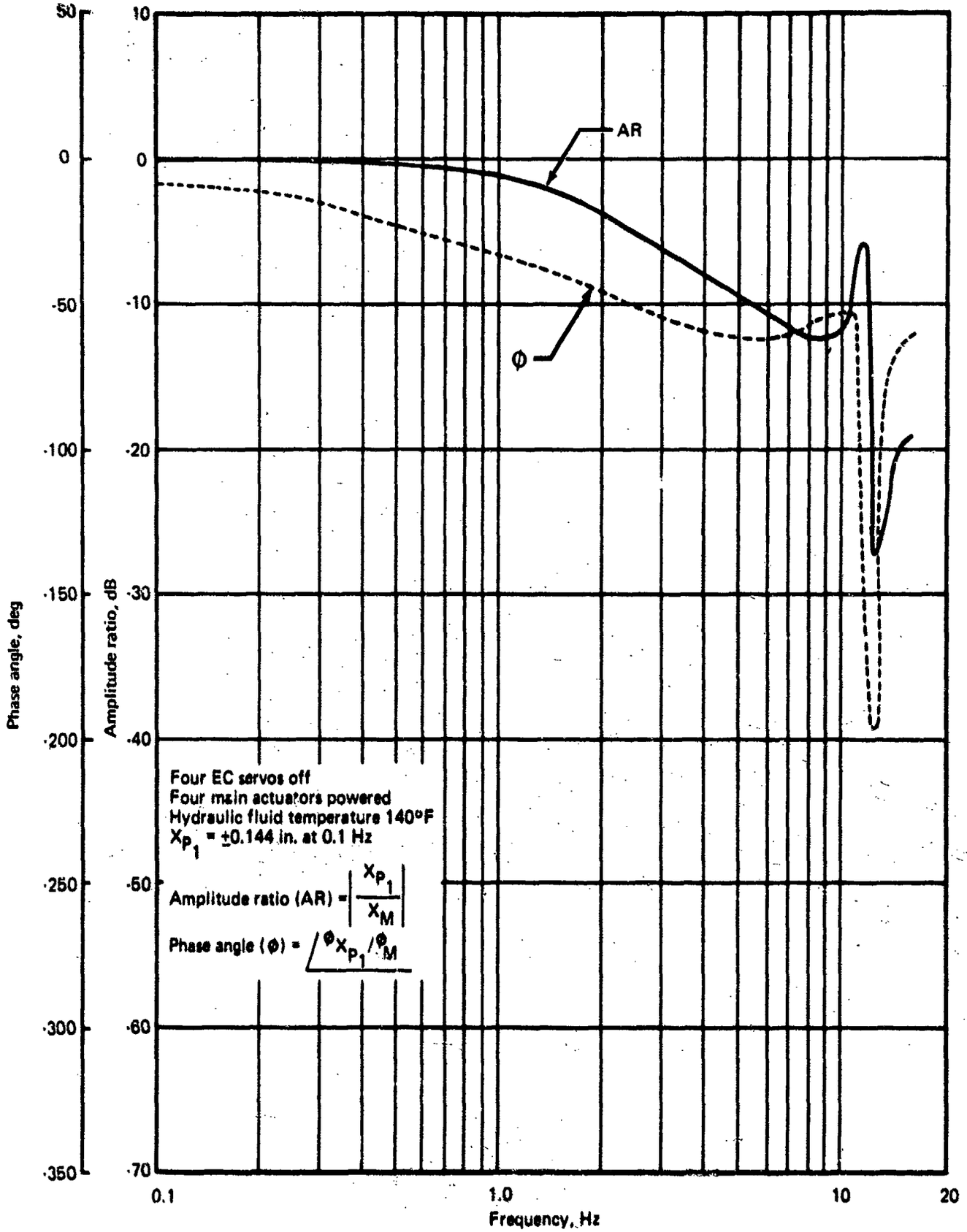

FIGURE 48.–CLOSED-LOOP FREQUENCY RESPONSE– MECHANICAL COMMAND, ELEVATORS REMOVED

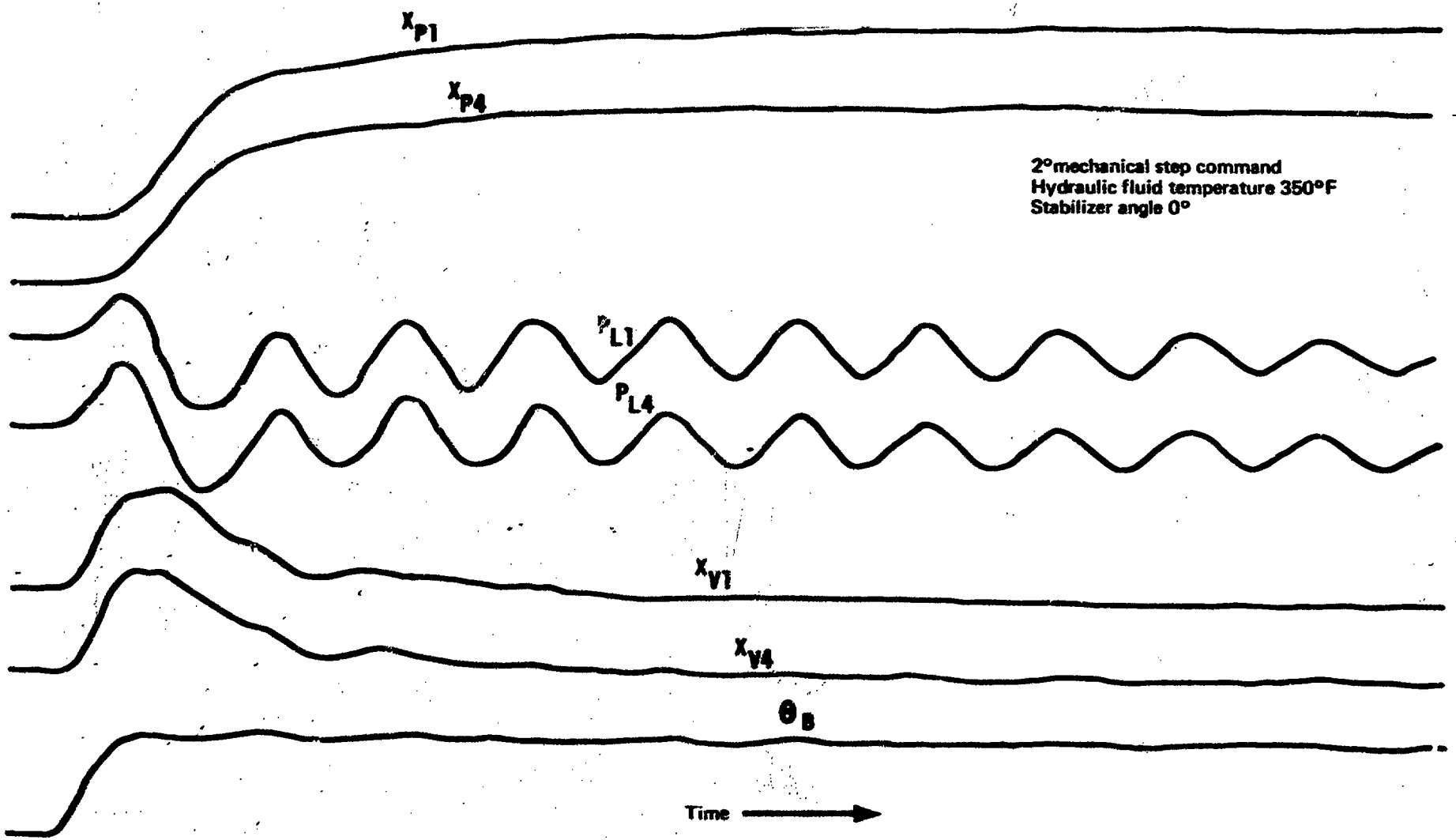

FIGURE 49.–STEP RESPONSE TEST–ELEVATORS REMOVED, $\zeta = 0.022$

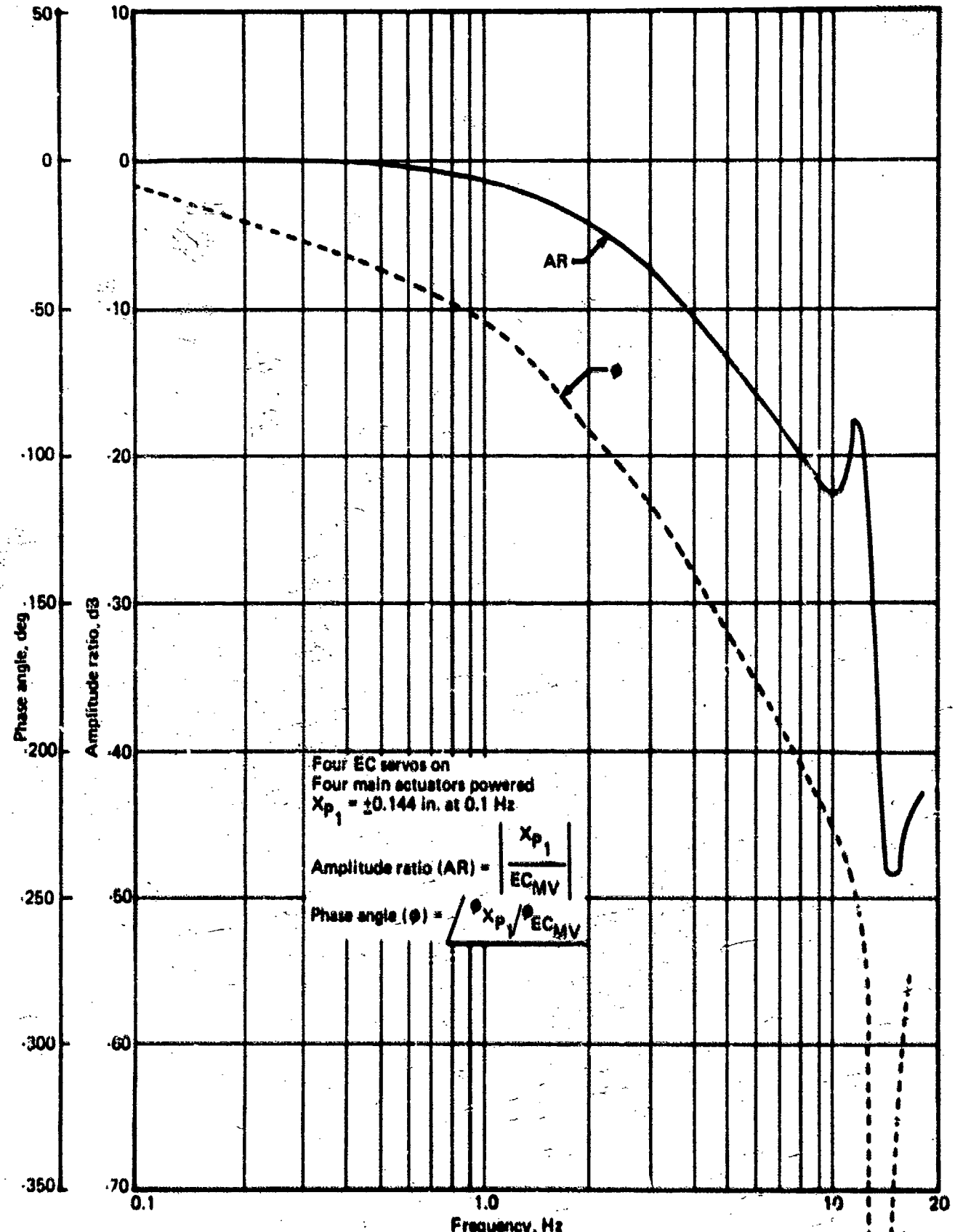

FIGURE 50.–CLOSED-LOOP FREQUENCY RESPONSE–ELECTRICAL COMMAND, ELEVATORS REMOVED, HYDRAULIC FLUID TEMPERATURE 350° F

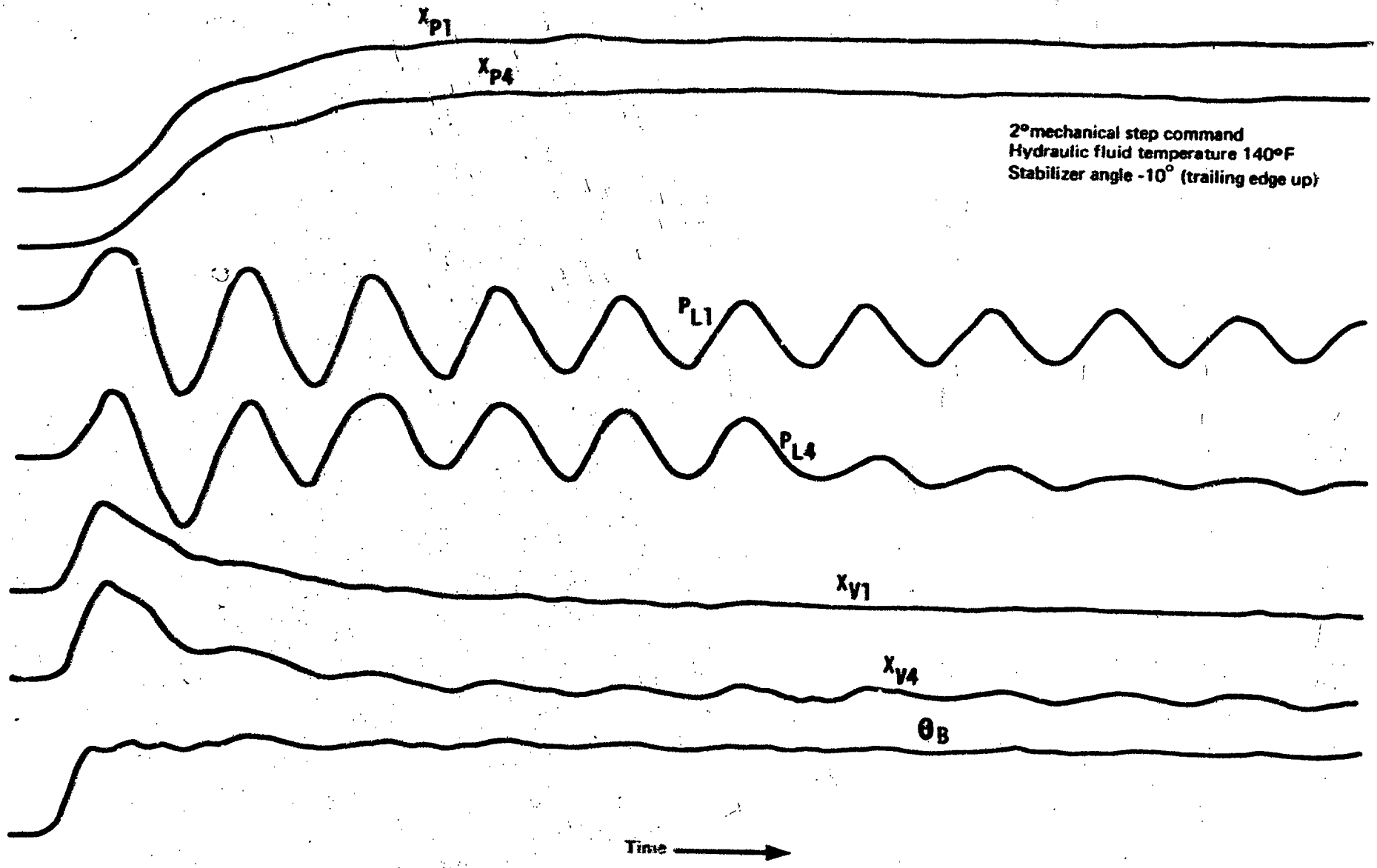

FIGURE 51.–STEP RESPONSE TEST–ELEVATORS REMOVED, $\zeta = 0.016$

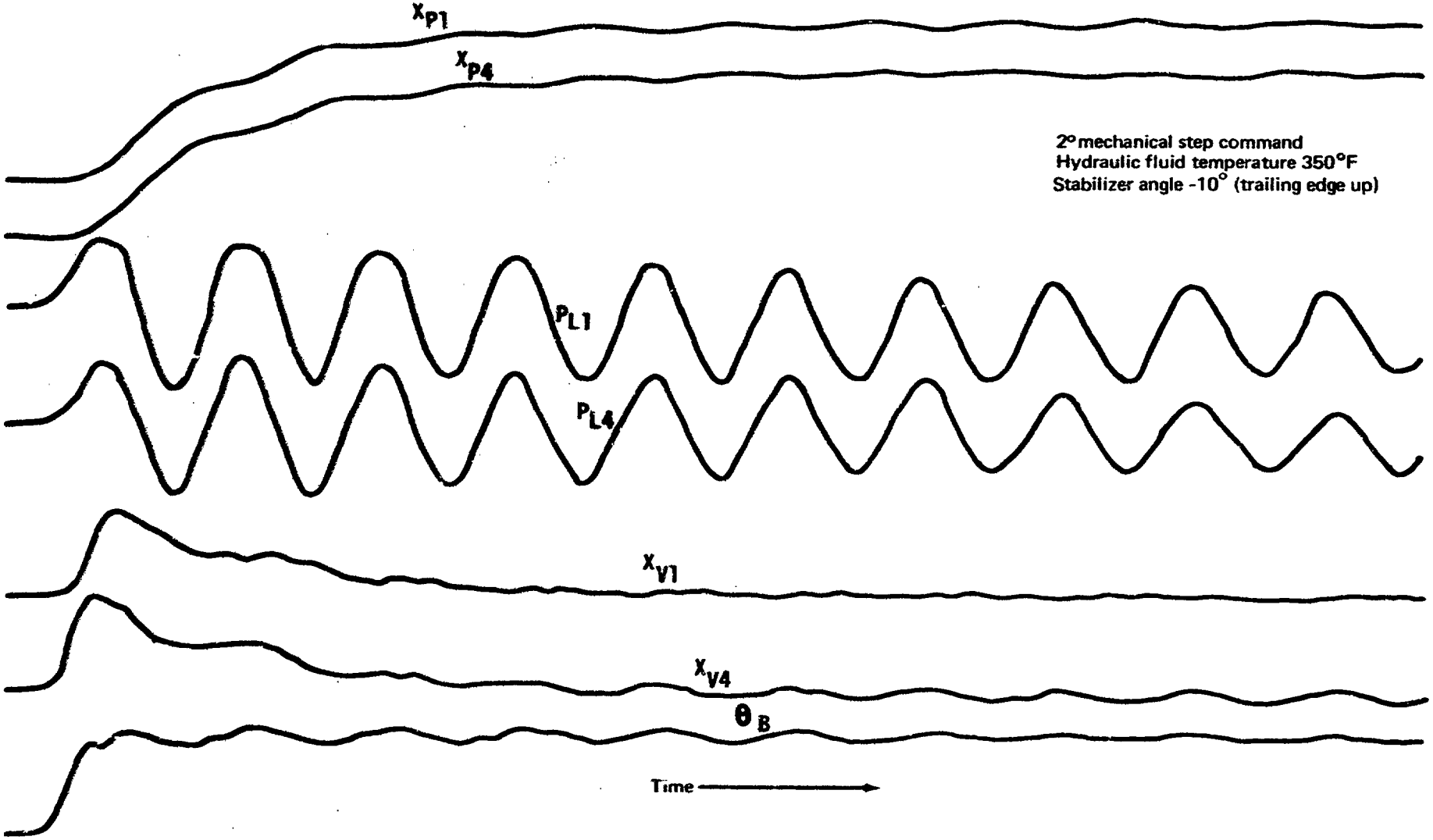

FIGURE 52.–STEP RESPONSE TEST–ELEVATORS REMOVED, $\zeta = 0.017$

TABLE 8.–STEP RESPONSE TEST–MECHANICAL COMMAND, ELEVATORS REMOVED

Initial stabilizer position, δ, deg	System temperature, °F	Damped natural frequency (f_D = Hz)	Damping ratio, ζ	Command, deg, TE up
0	140	12.5	0.025	-2
0	350	11.7	0.022	-2
-10 (TE up)	140	11.7	0.016	-2
-10 (TE up)	350	11.2	0.017	-2

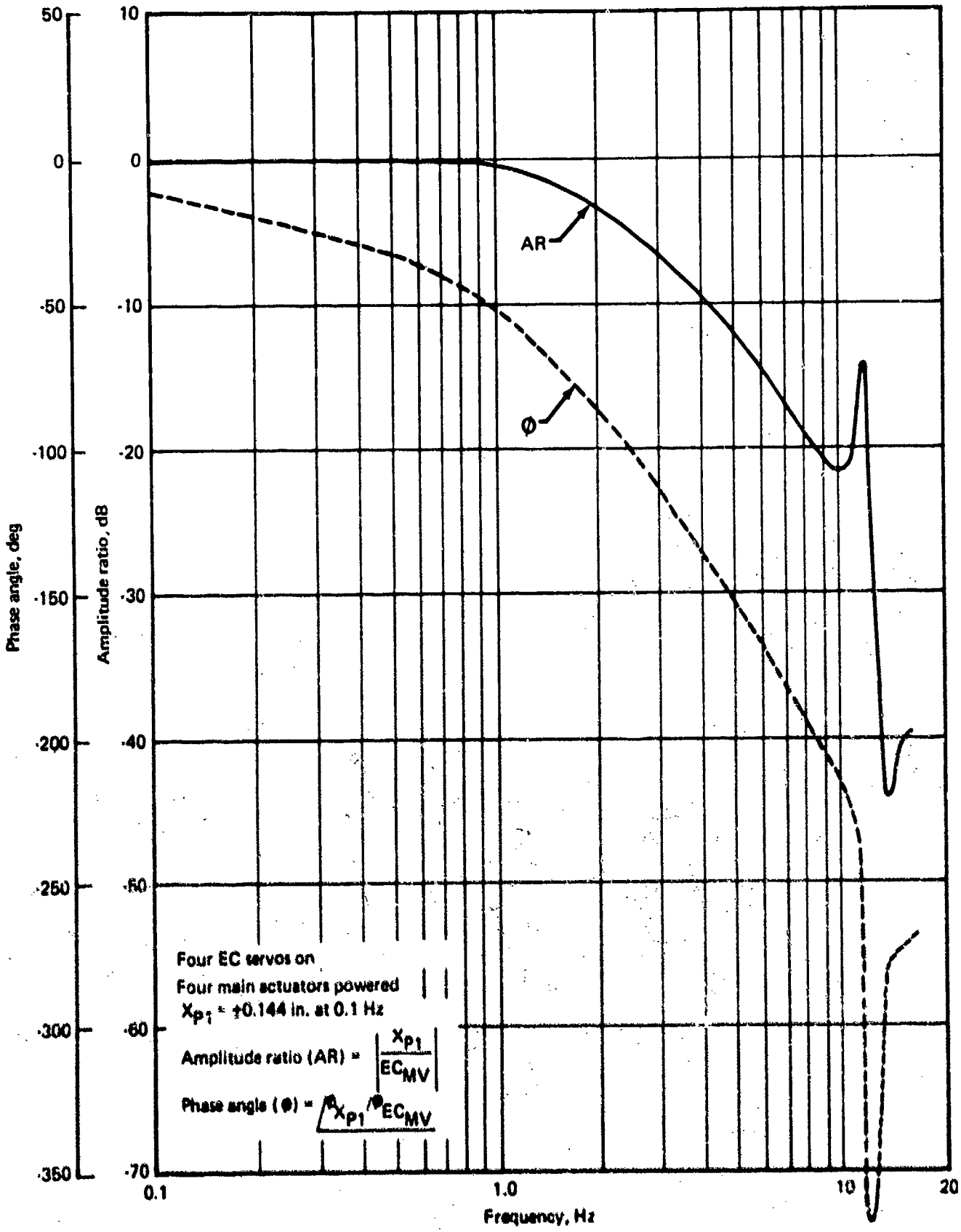

FIGURE 53.–CLOSED-LOOP FREQUENCY RESPONSE–ELECTRICAL COMMAND, ELEVATORS REMOVED, HYDRAULIC FLUID TEMPERATURE 140°F

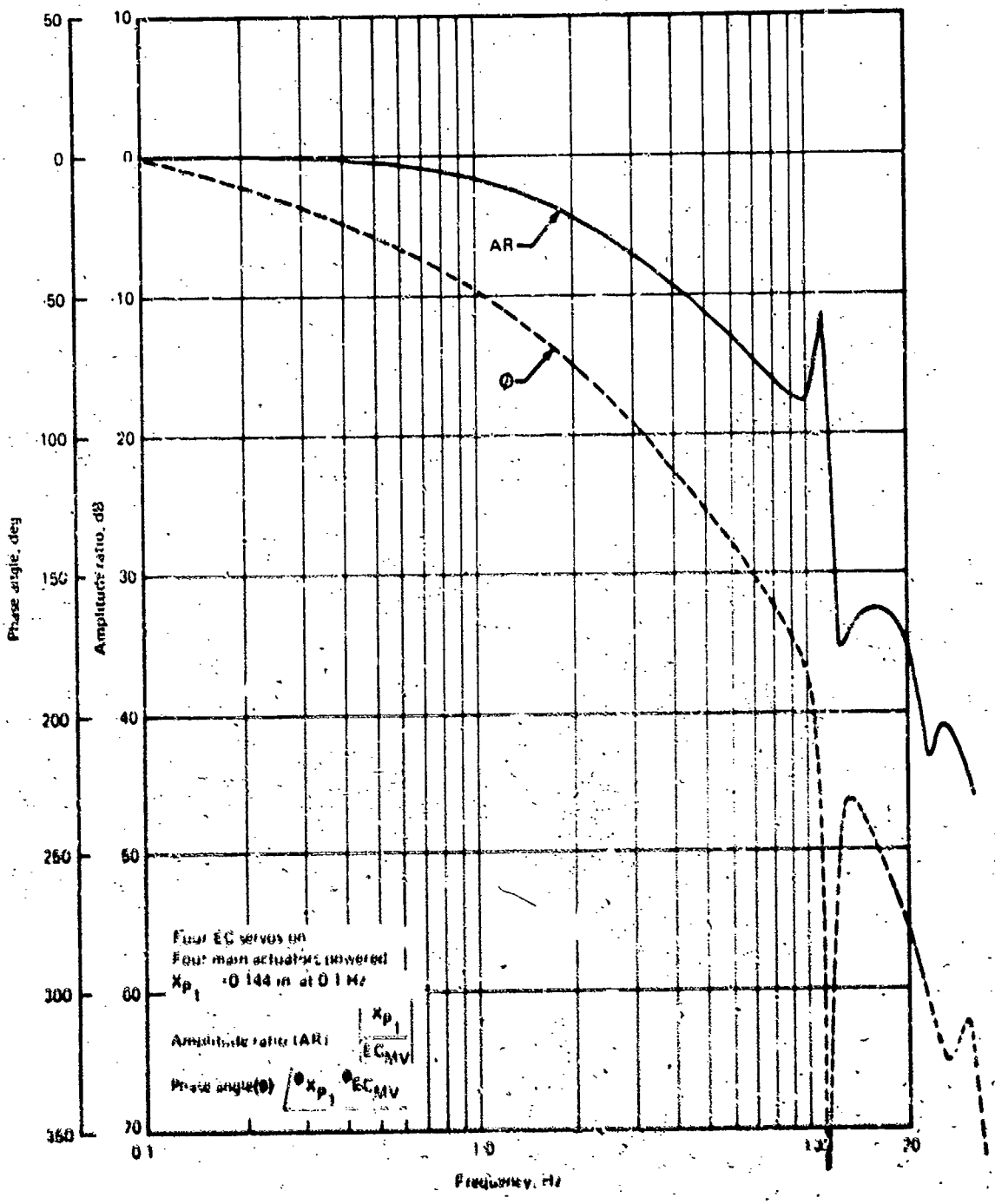

FIGURE 54.–CLOSED-LOOP FREQUENCY RESPONSE–ELECTRICAL COMMAND, ELEVATORS REMOVED, HYDRAULIC FLUID TEMFERATURE 140°F, EC LOOP GAIN 60 RAD/SEC

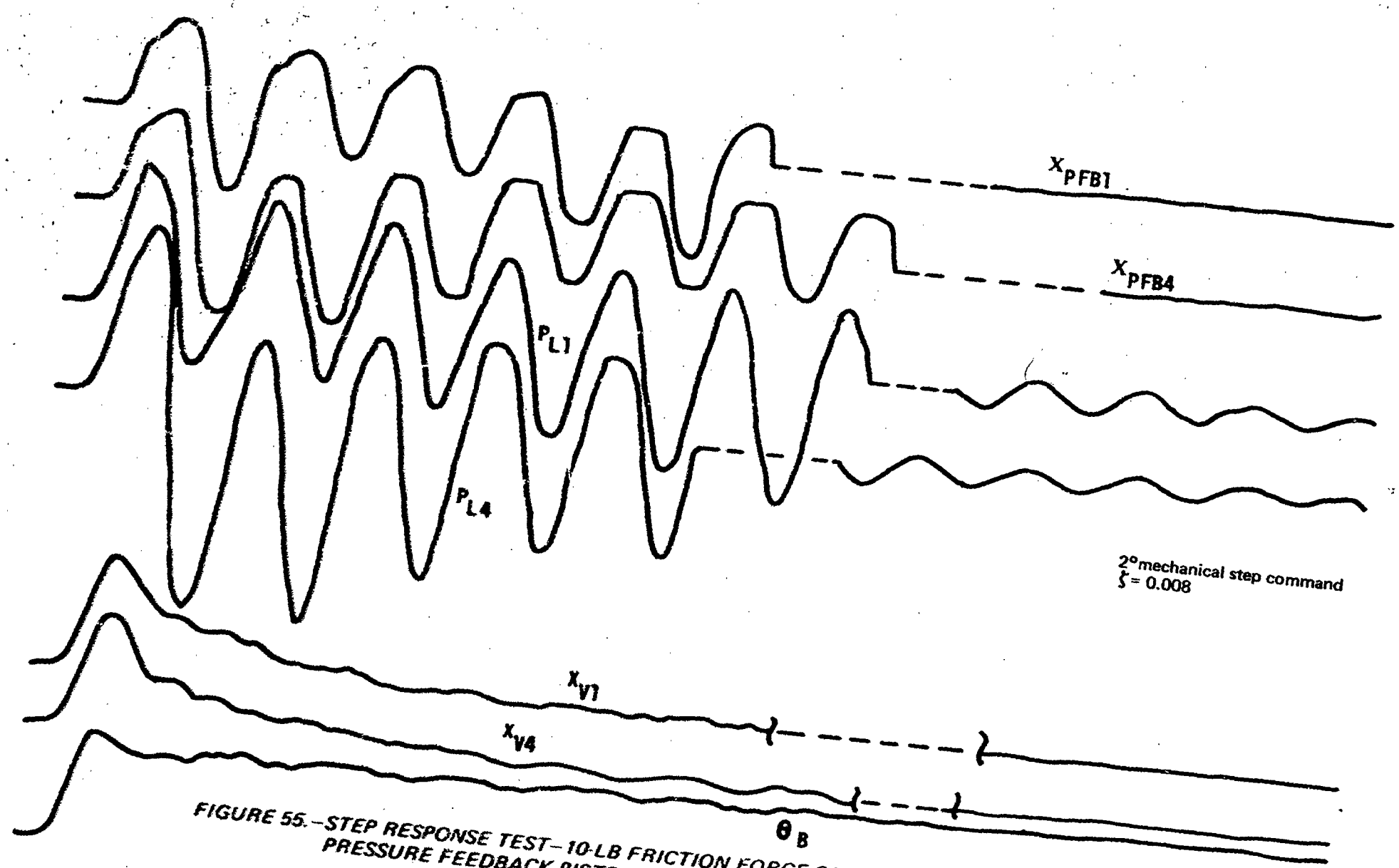

FIGURE 55.–STEP RESPONSE TEST–10-LB FRICTION FORCE ON ACTUATOR 1 AND 4 PRESSURE FEEDBACK PISTONS

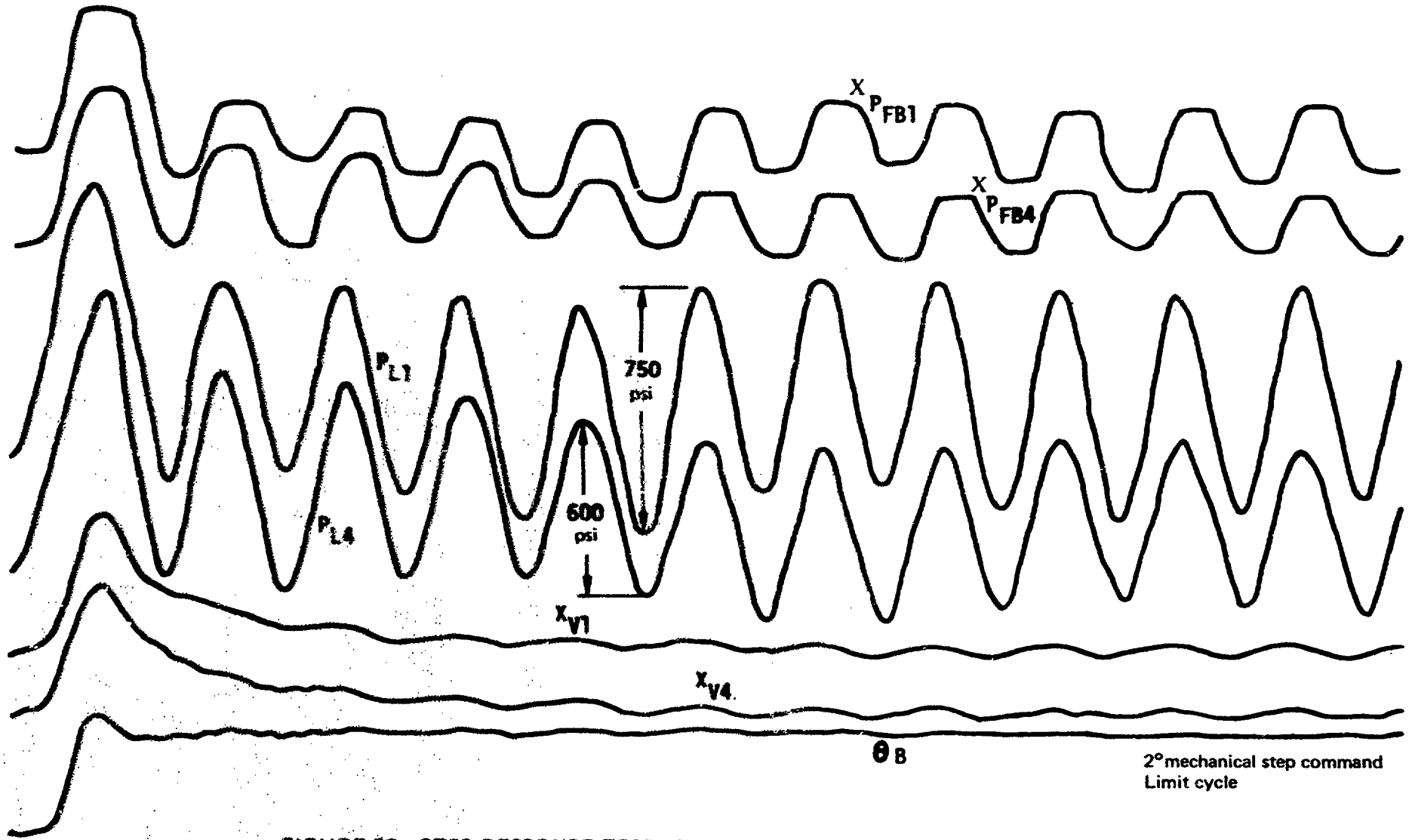

FIGURE 56.–STEP RESPONSE TEST–20-LB FRICTION FORCE ON ACTUATOR 1 AND 4 PPESSURE FEEDBACK PISTONS

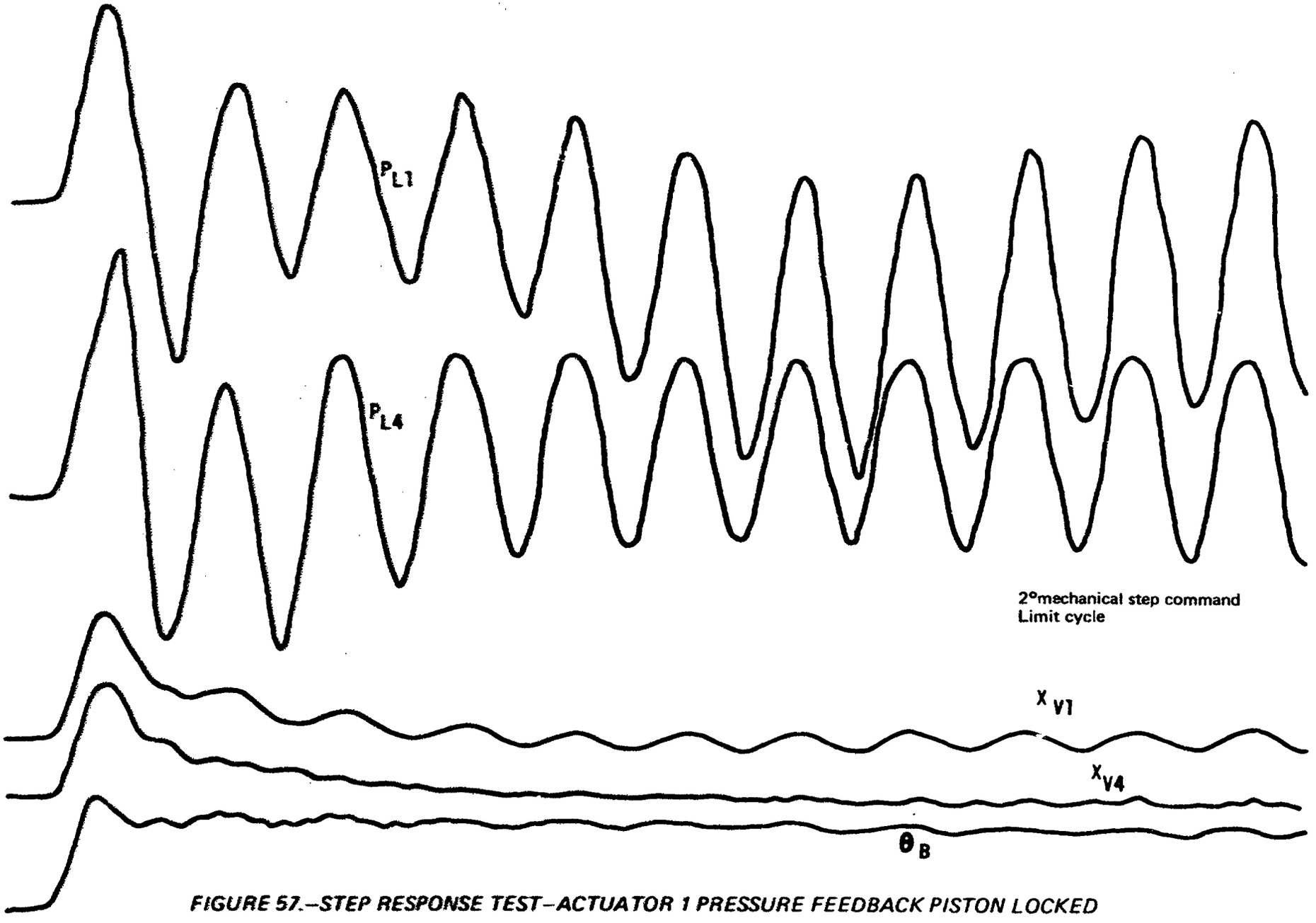

FIGURE 57.–STEP RESPONSE TEST–ACTUATOR 1 PRESSURE FEEDBACK PISTON LOCKED

pressure feedback friction devices installed. The decrease in the stability of the system when the friction force is increased on the pressure feedback pistons is caused by the hysteresis of the pressure feedback piston as shown in figures 42 and 43. Within the deadband of the hysteresis, there is no pressure feedback to the main servovalve. As a result the effective pressure gain of the actuator, the static stiffness is increased by a factor of 20 and the margin of stability is reduced accordingly. The system also limit cycled when one pressure feedback was locked out as shown in figure 57.

5.2.4 Conclusions

Stability tests using mechanical and electrical commands have demonstrated that the control system dynamic response characteristics compare favorably with those predicted by theoretical analysis. The differences between the test results and the analytical predictions were due to characteristics of the test structure external to the actuators. The test structure did not duplicate the SST mathematical model representing the stabilizer and elevators. It was also demonstrated that pressure feedback piston friction or a locked pressure feedback piston can cause a limit cycle in the system. The system cannot tolerate a hysteresis characteristic in the pressure feedback loop, since within the hysteresis loop pressure feedback is zero, resulting in a large increase in the effective pressure gain and a consequent decrease in stability margin. Friction effects are insidious since they are not controllable or predictable. Artificially controlling actuator stability by pressure feedback requires special care in the design of such a device.

Although the system did not meet the SST requirement for stability with two pressure feedbacks jammed, increasing the pressure feedback gain on all actuators would have provided the required stability. However, raising the gain lowers the static stiffness of the system and this could have had a detrimental effect on flutter stiffness.

5.3 FORCE SYNCHRONIZATION TESTS

One of the fundamental design considerations of a multiple actuator installation is to find a means of keeping the actuators tracking or force synchronized. By minimizing the tracking error or equalizing force sharing, the structural design is improved from the standpoint of lower weight and greater fatigue life. The design objective for this installation was to control the fabrication and installation tolerances of the actuator, external linkage, and mounting structure so that each actuator could be installed without any rigging adjustments and yet maintain force synchronization within 20% of the rated force. The force synchronization requirement was that the force, F, developed by any one actuator would not differ from the average force, F_A, of all four actuators by more than ±20% of the rated force, F_R, of a single actuator. Rated force is that force developed by an individual actuator at 4000 psid. That is, $(F - F_A)/A = 0.20\ F_R/A = 800$ psi maximum. Statically the force developed by an actuator depends on the position and pressure gain of the main servovalve. Due to the random nature of installation and control element tolerances, the actuators of a multiple parallel actuator installation seldom have equal servovalve displacements. Differential deflections due to the nonuniformity of the actuator mounting structure also affect the main servovalve position, which results in further force missynchronization.

The overall tolerance limit requires lowering the effective pressure gain of the actuator to meet force synchronization requirements. Thus, low static stiffness will enhance force synchronization between actuators for a given cumulative tolerance band.

The four EC servo actuators also have differences in their positions even though they are mechanically connected. These differences, due to assembly and installation tolerances and compliance of the EC synchronization shaft, result in additional differences between the main control valves and consequently additional force difference between the main actuators.

5.3.1 Test Objective

The objective of this test was to evaluate the sensitivity of force synchronization between actuators as a function of stabilizer position for various normal and abnormal operating conditions.

5.3.2 Test Description

Prior to testing, the system was adjusted to have force synchronization within 7.5% on all actuators. The system was mechanically and electrically commanded to the stabilizer trailing edge full-up position at a rate of 0.5°/sec to measure the force synchronization between actuators for the following conditions:

- Simulated maximum installation tolerances achieved by adjusting individual input linkages so that static force synchronization was 20%
- Locked pressure feedback piston that increases the pressure gain and static stiffness of that actuator
- Simulated aerodynamic load applied to the system
- Loss of hydraulic power to one or more actuators

5.3.3 Test Results

Experience obtained during the test program showed that the force synchronization could be reduced to 7.5% by adjusting the mechanical input links. As the test program continued, little change was observed in the force synchronization as conditions were changed or if actuators were removed and replaced in the same location.

In the no-load test using a mechanical command, there was very good force synchronization between actuators as shown in figure 58 and table 9. The differential pressure across the main actuator piston on two of the actuators oscillated at 1.6 Hz with an amplitude of ±250 psi. It is believed that this oscillation is a basic characteristic of the actuator that was aggravated by stiction of the stabilizer load hinge pins. It was also observed that the EC servo equalizer valve on actuator 1 bypassed as the main actuators extended against a simulated air load on the stabilizer. This occurred even though the differential pressure across each of the four EC servo actuators was zero when the actuators were in an initial static condition.

The remaining tests were performed using electric command signals, and the results of these tests are summarized in table 9 and shown in figures 59 through 62.

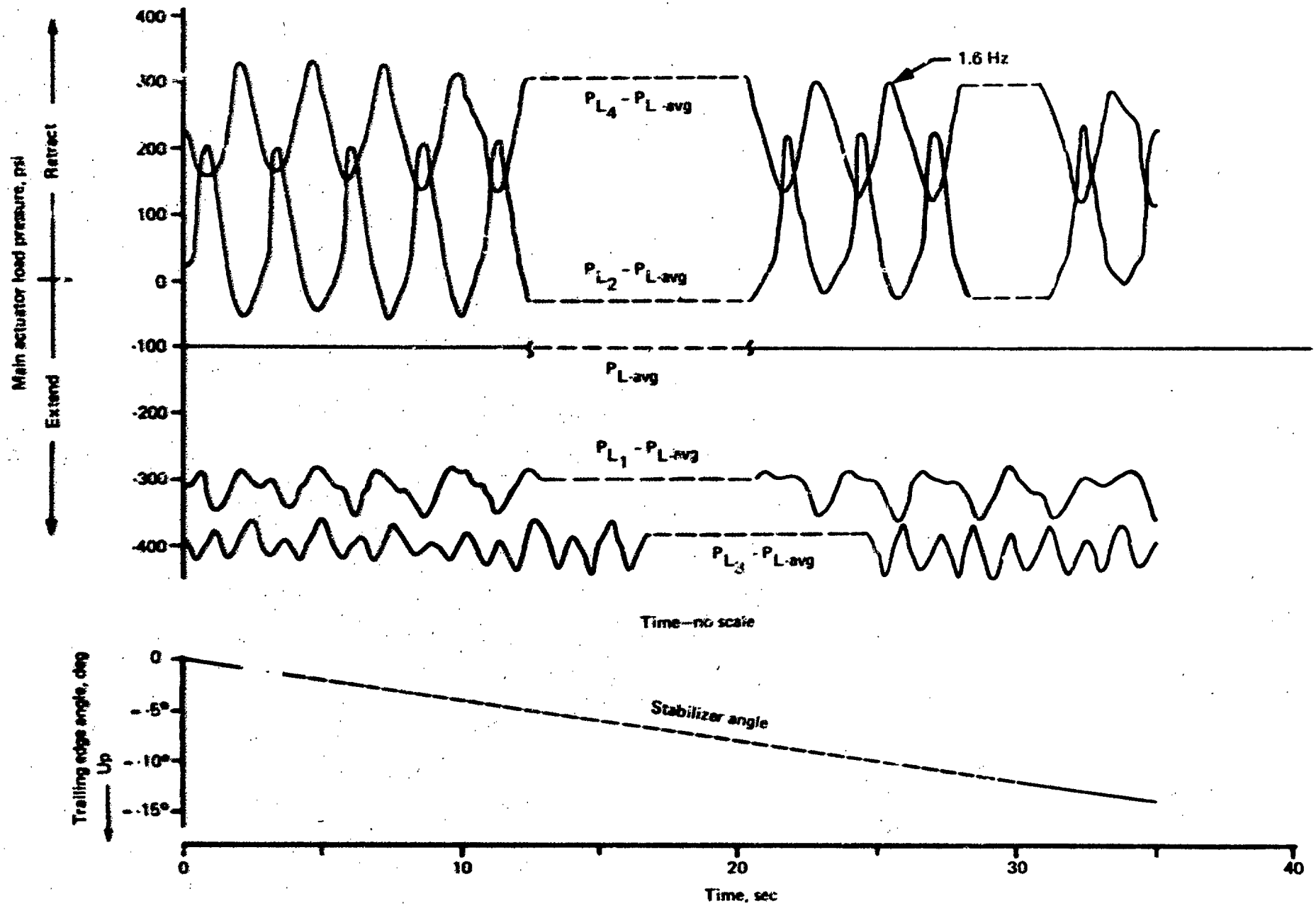

FIGURE 58.–FORCE SYNCHRONIZATION TEST–MECHANICAL COMMAND, NO LOAD

TABLE 9.–FORCE SYNCHRONIZATION

Condition	Actuators, powered	[a](F – F_A)A psi		ΔP variation in any one servo		Remarks
		Maximum static	Maximum dynamic	Magnitude, psi	Frequency, Hz	
Mechanical command (no load)	1,2,3,4	390	440	±350	1.6	EC servo bypass valve 1 relieved
	1,3,4	332	350	±45	0.3	–
	1,4	124	224	±80	0.5	–
Electrical command (no load)	1,2,3,4	[b]250	1260	±125	1.25	EC servo bypass valves 1 and 4 relieved
	1,3,4	300	1350	±65	1.6	–
	1,4	224	675	±50	1.0	–
Electrical command (no load)	1,2,3,4	[c] 750	1440	±25	1.0	EC servo bypass valves 1 and 4 relieved
	1,3,4	682	1200	–	–	–
	1,4	448	200	–	–	–
Electrical command (system loaded)	1,2,3,4	336	720	±20	Random change	EC servo bypass valve 1 relieved
	1,3,4	100	660	±20	Random change	–
	1,4	50	150	–	–	–
Electrical command (no load)	1,2,3,4	840 Servo 1	2200 Servo 1	±850 Servo 1	12.5 Limit cycle	Servo 1 pressure feedback piston locked; EC servo bypass valves 1 and 4 relieved.
	1,2,3,4	3860 Servo 1 4120 Servo 4	3740 Servo 1 4360 Servo 4	±150 Servos 1,4	1.0	Servo 1 and 4 pressure feedback pistons locked; EC servo bypass valves 1 and 4 relieved.

[a]Design objective = 800 psi, maximum; A = area of main actuator piston.

[b]Initial static condition $(F_0 \cdot F_A)/A$ = 250 psi.

[c]Initial static condition $(F_0 \cdot F_A)/A$ = 750 psi.

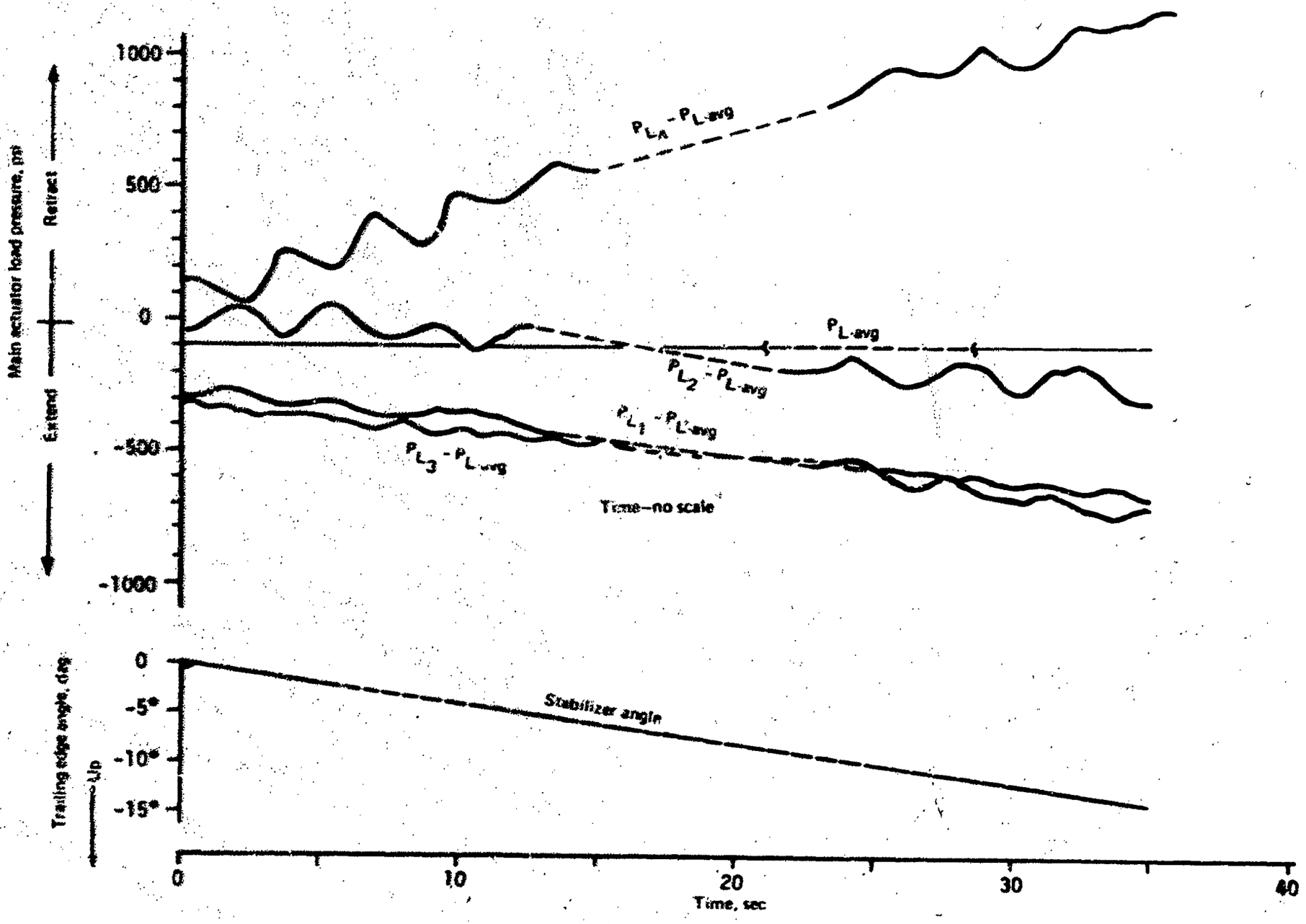

FIGURE 59.–FORCE SYNCHRONIZATION TEST–ELECTRICAL COMMAND, NO LOAD, INITIAL STATIC CONDITION: $(F - F_A)/A = 250$ PSI

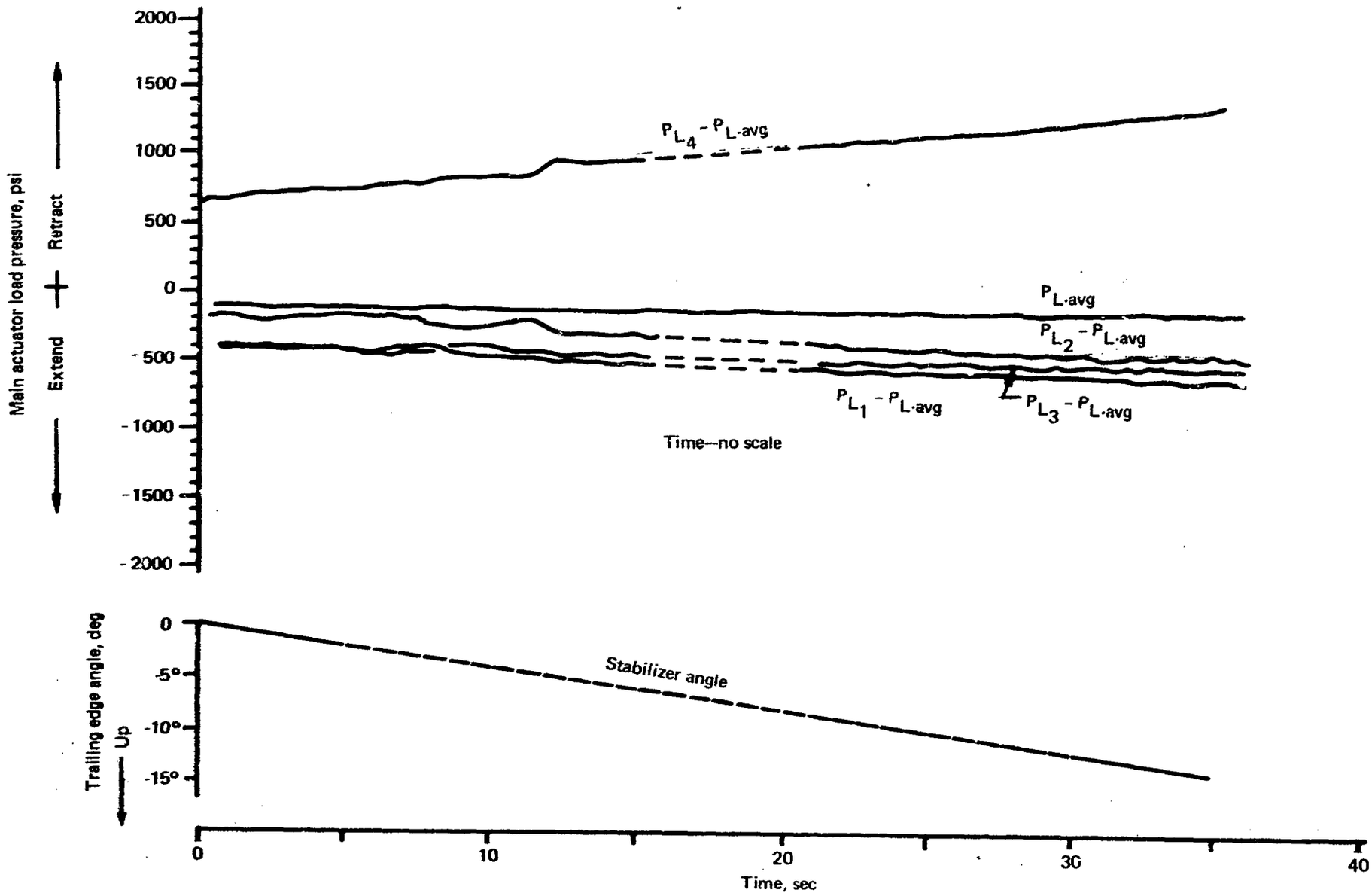

FIGURE 60.—FORCE SYNCHRONIZATION TEST—ELECTRICAL COMMAND, NO LOAD, INITIAL STATIC CONDITION: $(F - F_A)/A = 750$ PSI

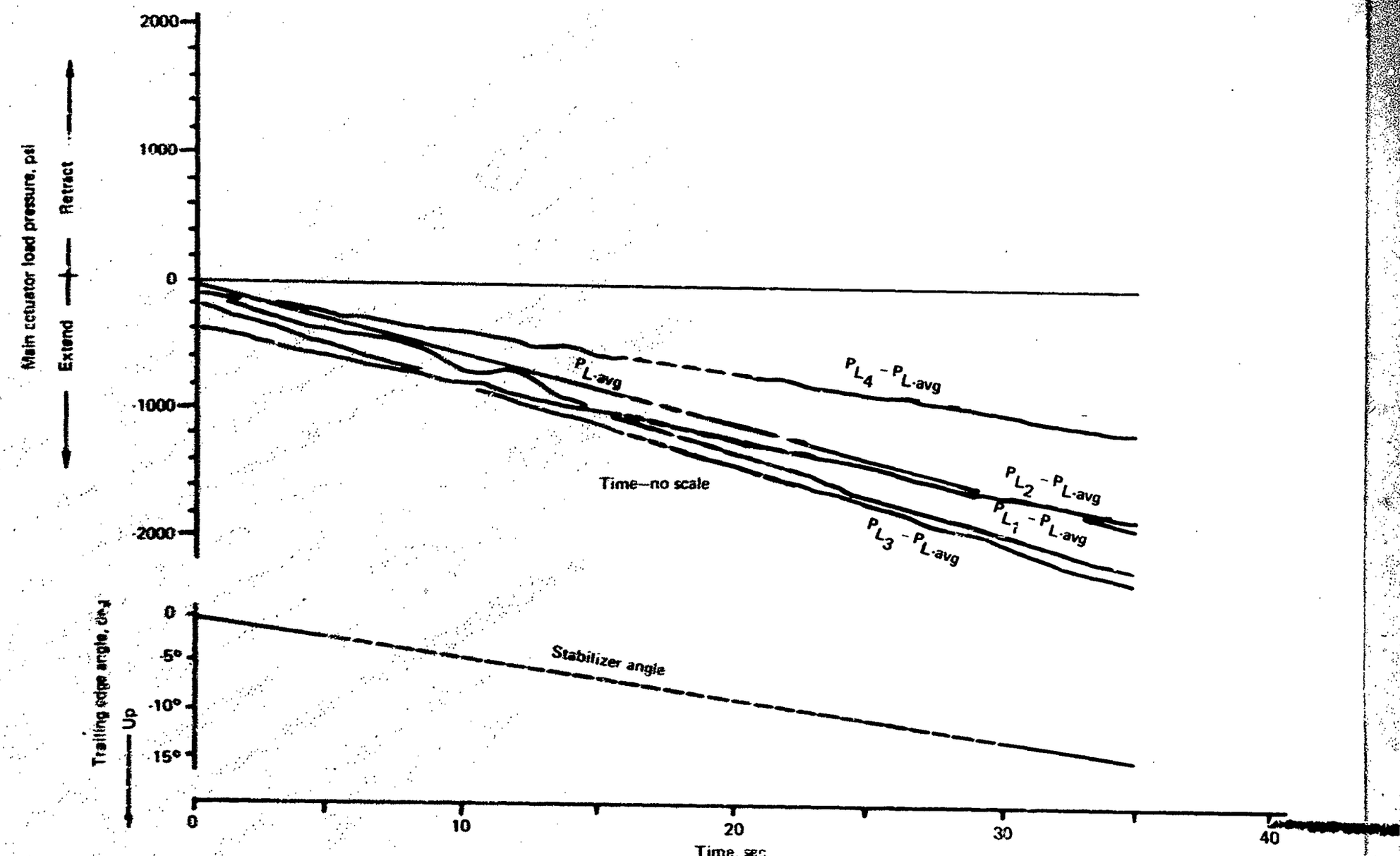

FIGURE 61.--FORCE SYNCHRONIZATION TEST--ELECTRICAL COMMAND, SYSTEM LOADED, INITIAL STATIC CONDITION: $(F - F_A)/A$ = 336 PSI

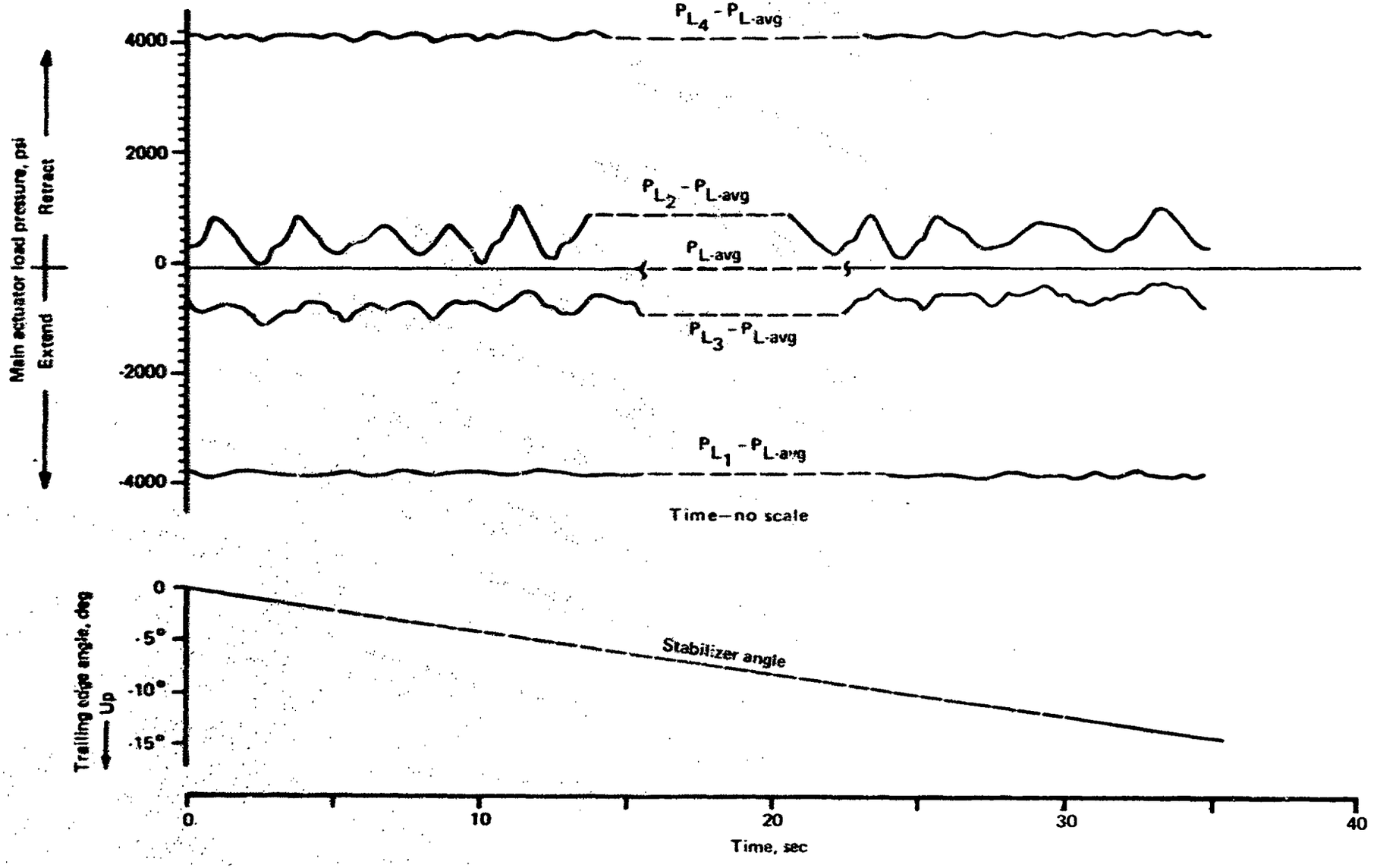

FIGURE 62.–FORCE SYNCHRONIZATION TEST–ELECTRICAL COMMAND, NO LOAD, ACTUATOR 1 AND 4 PRESSURE FEEDBACK PISTONS LOCKED

In most of the tests conducted using electric command signals, the force synchronization between the main actuators deteriorated as a function of increased actuator extension. This occurred despite the fact that the EC actuators were carefully aligned in the static condition.

Locking the pressure feedback piston increased the effective pressure gain of the actuator causing a serious degradation in force synchronization (table 9).

5.3.4 Conclusions

Force synchronization tests using mechanical commands demonstrated that the system would maintain force synchronization during normal and abnormal operation, except for the conditions with the pressure feedback locked out. Pressure feedback was required on the SST because of the destabilizing structural feedback. The locked pressure feedback is a failure case and was detected by the main actuator relief/bypass valve operation.

The tracking problem between EC channels is probably caused by differential deflections in the actuator mounting structure and synchronization shaft assembly tolerances. To understand this problem completely would require additional investigation. These deflections have a direct effect on EC synchronization, since the synchronization shaft is mounted on the same structure as the actuators. Assembly and installation tolerances that can be offset in a static condition also begin to affect EC synchronization as the system moves and the geometry of the synchronization linkage changes.

Force synchronization tests using electric commands were inconclusive. Main actuator 4 consistently developed a large force difference. The maximum mechanical differences of the EC servo positions cannot cause this force fight. Additional investigation would be required to isolate the external input causing this problem.

5.4 STIFFNESS TESTS

In the design of any actuation system, the designer must be aware of and control the system stiffness at all frequencies to meet the many design constraints imposed by performance, stability, and flutter requirements.

These requirements put demands on the actuation system that are sometimes contradictory and not necessarily compatible. The system must have high stiffness for flutter suppression and have the proper relationship between low-frequency and high-frequency stiffness for stability. The system must have low stiffness for actuator synchronization, but also have sufficient stiffness at low frequencies to minimize actuator hysteresis and static position error under load for good performance. Figure 63 is a curve depicting the asymptotic approximation of the actuation system stiffness frequency response for a typical stable system and the nomenclature that will be used throughout this report. The stiffness transfer function as well as the mathematical expression for the break frequencies are developed in appendix A.

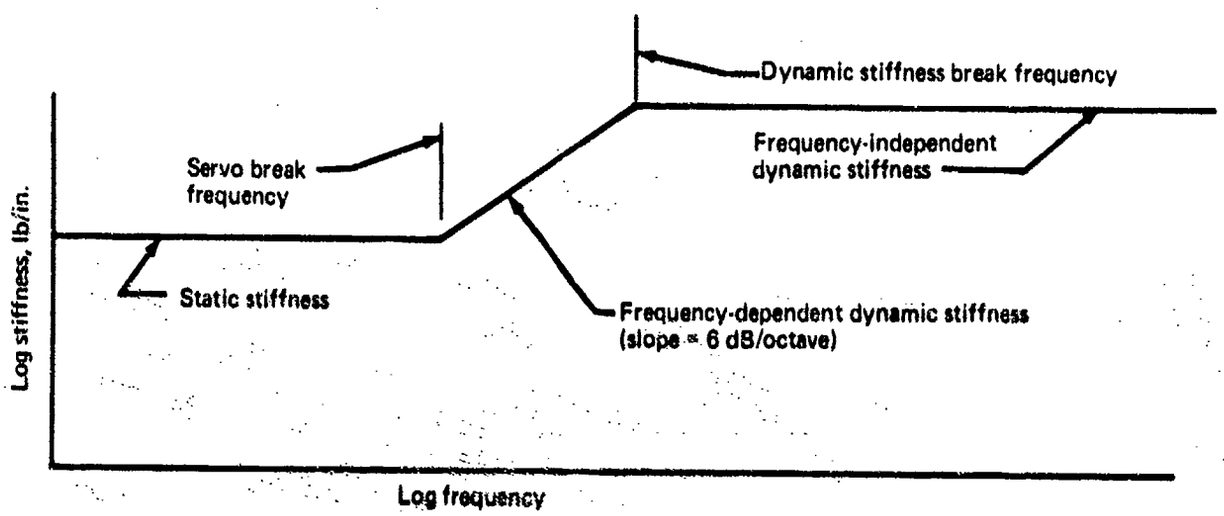

FIGURE 63.–SYSTEM STIFFNESS FREQUENCY RESPONSE

The most important design constraint from the SST point of view was the flutter stiffness requirement. Most flight control surfaces will flutter unless they are either constrained by their actuation system or are mass balanced. In cases where actuator redundancy is provided for other reasons, the lightest weight method of flutter suppression is often restraint by the actuation system. Providing a minimum stiffness through the actuation system can put a severe constraint on system design, particularly if the flutter frequencies of concern are lower than the dynamic stiffness break frequency.

In the SST design, the frequency at which the horizontal stabilizer tended to flutter (2.4 Hz) was closely associated with the first vertical body bending frequency of 2 Hz. To ensure a flutter-free surface with two hydraulic systems failed, each of the actuators had to have a minimum frequency-dependent dynamic stiffness of 115,000 lb/in. at 2.4 Hz.

It has been common to consider the flutter stiffness at the "normal actuator condition." This is the condition where the actuation system position command is satisfied and the actuator is stationary with its servovalve nearly closed holding any load less than stall. There are other transient and abnormal operating conditions that must be considered in addition to the normal condition to enable construction of mathematical models for flutter analyses. These are:

- Stall, in which the actuator is stalled against a load, the servovalve open, and load pressure equal to supply pressure
- Blowback, in which the actuator is driven backward away from its commanded position, the servovalve fully opened, the load pressure above supply pressure, and the bypass valve open between cylinders
- Under command, in which the actuator is in transit to a newly commanded position, the servovalve open to drive the actuator at commanded rate, and the load pressure less than supply pressure

5.4.1 "Normal Actuator" Dynamic Stiffness Test

The "normal actuator" dynamic stiffness tests described in this section were concerned with identifying not only the frequency-independent dynamic stiffness but also the frequency-dependent stiffness of the system in the "normal actuator condition." Frequency-independent dynamic stiffness is defined as the stiffness that the system presents to a load at frequencies so high that no flow passes through the main actuator control valve.

Changes in actuator configuration, such as pressure feedback changes, open-loop gain changes, or different main control valve positions will only change the frequency-dependent stiffness. The frequency-independent dynamic stiffness will be the same for all actuator configurations but will change with temperature, since it is a function of fluid bulk modulus which does vary with temperature.

5.4.1.1 Test Objectives

The objective of this test was to measure the pin-to-pin system stiffness, using a single actuator, as a function of frequency at two different operating temperatures to show compliance with design goals and to gain confidence in the analytical methods shown in section 4.6.

5.4.1.2 Test Description

One actuator was selected for the test. It was disconnected from the mechanical input bus shaft (opening the position feedback loop) and the EC synchronization shaft. The input arm was rigidly attached to the actuator body in a position that put the main valve near null. All the tests were run open-loop in this manner. The test actuator piston rod was displaced sinusoidally by commanding the other three actuators over the desired frequency range. The data plotted were the peak-to-peak actuator force divided by the peak-to-peak actuator pin-to-pin displacement. Actuator force was either measured with strain gages or was calculated from actuator differential pressure.

The 150° F tests were run with and without the pressure feedback locked out. The frequency-independent dynamic stiffness of the system was low enough at 340° F that sufficient data to define the open-loop stiffness frequency response was obtained without locking out the pressure feedback.

5.4.1.3 Test Results

Figure 64 presents the open-loop system stiffness frequency response at 150° F with the pressure feedback locked out. Locking out the pressure feedback moved the dynamic stiffness break frequency from 7.5 to 0.38 Hz, allowing good data acquisition. In testing the system with normal pressure feedback, the dynamic stiffness break frequency occurred close to the system natural frequency W_{CL} = 12 Hz, allowing good data acquisition. In testing the the stiffness break difficult to identify. In addition, the driver actuators had a sharp amplitude attenuation at frequencies above the system natural frequency. Good data at these high frequencies were difficult to obtain. Raising the effective pressure gain by blocking out the pressure feedback lowered the dynamic stiffness break frequency, giving good separation between the stiffness break frequency and the system natural frequency. The "best-fit" frequency-independent dynamic stiffness was 500,000 lb/in. The calculated value was 503,000 lb/in. The dynamic stiffness is influenced by the hydraulic fluid bulk modulus, which cannot be calculated exactly due to air inclusion and local temperature variation:

$$\frac{1}{K_{A(\infty)}} = \frac{1}{K_{rod}} + \frac{1}{K_{housing}} + \frac{1}{K_{oil}}$$

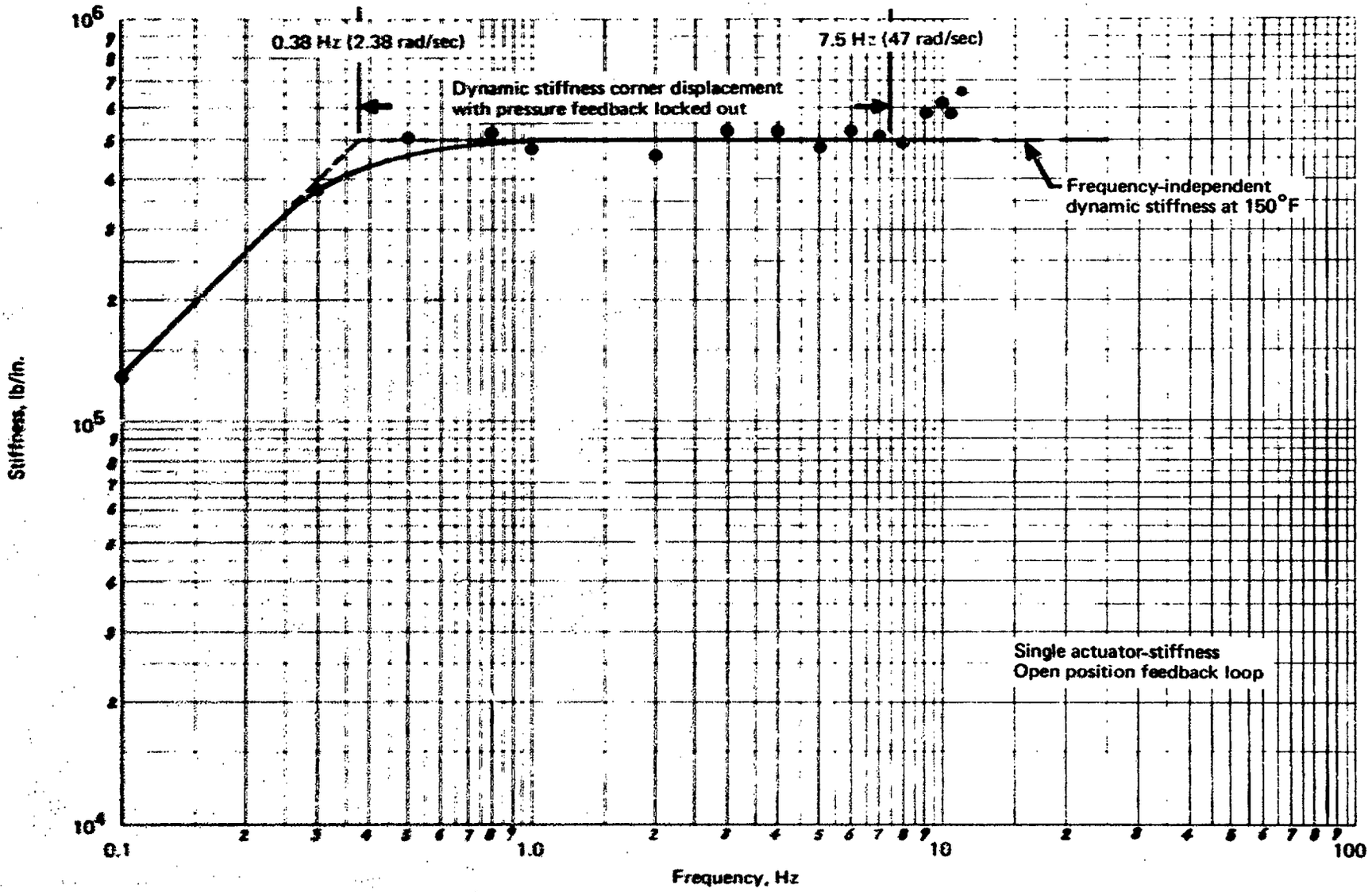

FIGURE 64.–"NORMAL ACTUATOR" SYSTEM STIFFNESS FREQUENCY RESPONSE– PRESSURE FEEDBACK REMOVED, 150° F

and

$$K_{oil} = \frac{4\beta A^2}{V}$$

where

$K_A(\infty)$ = actuator frequency-independent dynamic stiffness

K_{rod} = actuator rod stiffness (1,290,000 lb/in)

$K_{housing}$ = actuator housing stiffness (2,880,000 lb/in)

β = effective oil bulk modulus (240,000 psi at 150° F)

A = actuator area = 21.8 sq in.

V = actuator volume = 400.2 cu in. (active plus 20 cu. in. dead)

Then

$$K_{oil} = \frac{4(240{,}000)(21.8)^2}{400.2} = 1{,}140{,}000 \text{ lb/in.}$$

$$\frac{1}{K_A(\infty)} = \frac{1}{1{,}290{,}000} + \frac{1}{2{,}880{,}000} + \frac{1}{1{,}140{,}000}$$

$$K(\infty) = 503{,}000 \text{ lb/in.}$$

This test also allowed calculation of the main servovalve pressure gain with pressure feedback locked out. Using the measured dynamic stiffness break frequency, the pressure gain was calculated to be 820,000 psi/in. using equation (2), appendix A.

The system open-loop stiffness frequency response was constructed by using the frequency-independent dynamic stiffness from the test above and test data taken with the pressure feedback operating normally and is presented in figure 65. Very little data scatter occurs at low frequencies, giving extremely good agreement with the theoretical slope of 6 dB per octave. In addition, the dynamic stiffness break frequency obtained with these data and the frequency-independent dynamic stiffness data agree almost exactly with the theoretical break frequency calculated by using the design value of 36,500 psi/in. for the main servovalve with pressure feedback.

Figure 66 shows data taken at 350° F. There is no change in the frequency-dependent stiffness with temperature. The measured frequency-independent dynamic stiffness was approximately 350,000 lb/in., which is the same as the value calculated below.

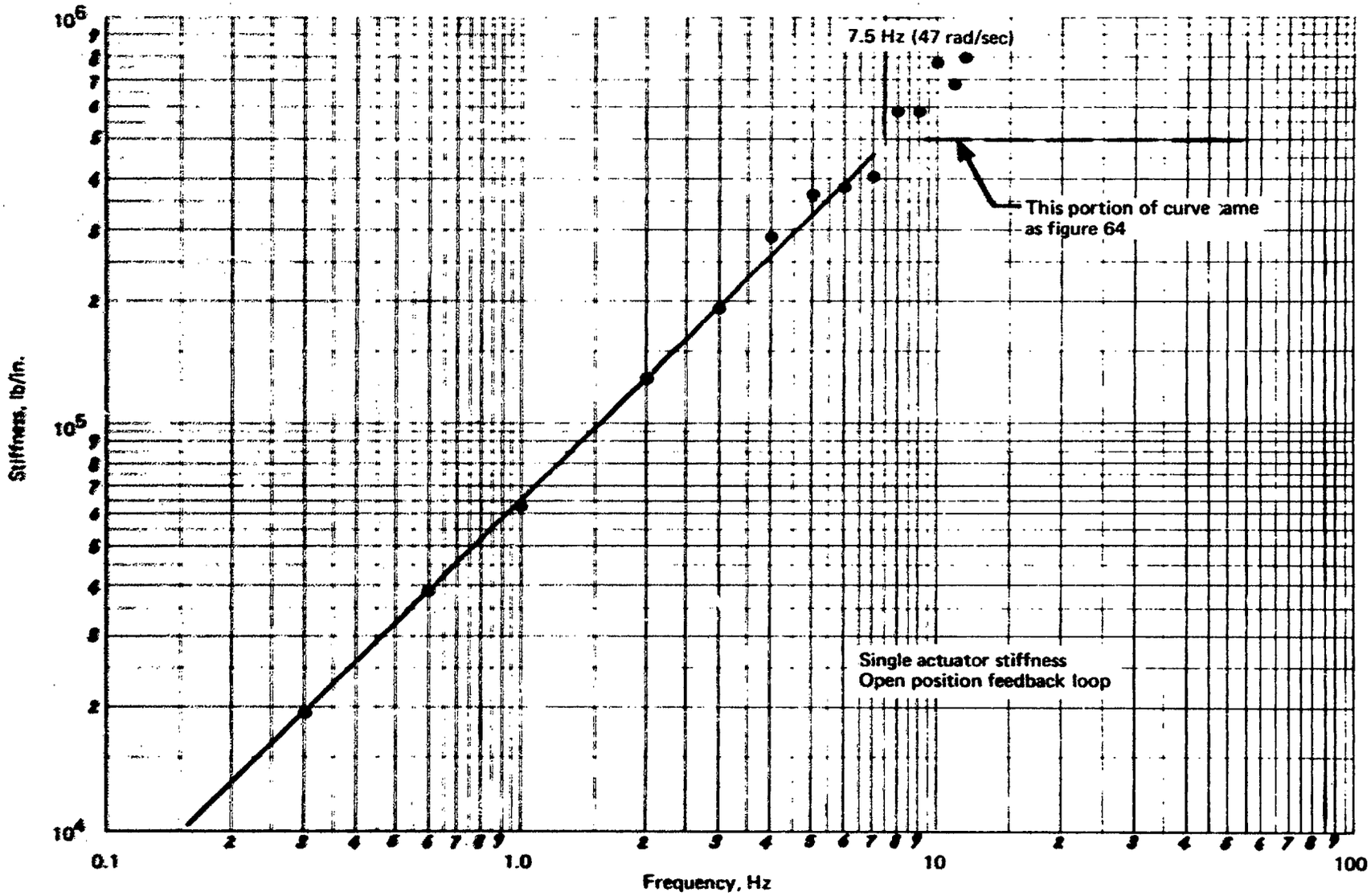

FIGURE 65.—"NORMAL ACTUATOR" SYSTEM STIFFNESS FREQUENCY RESPONSE—150° F

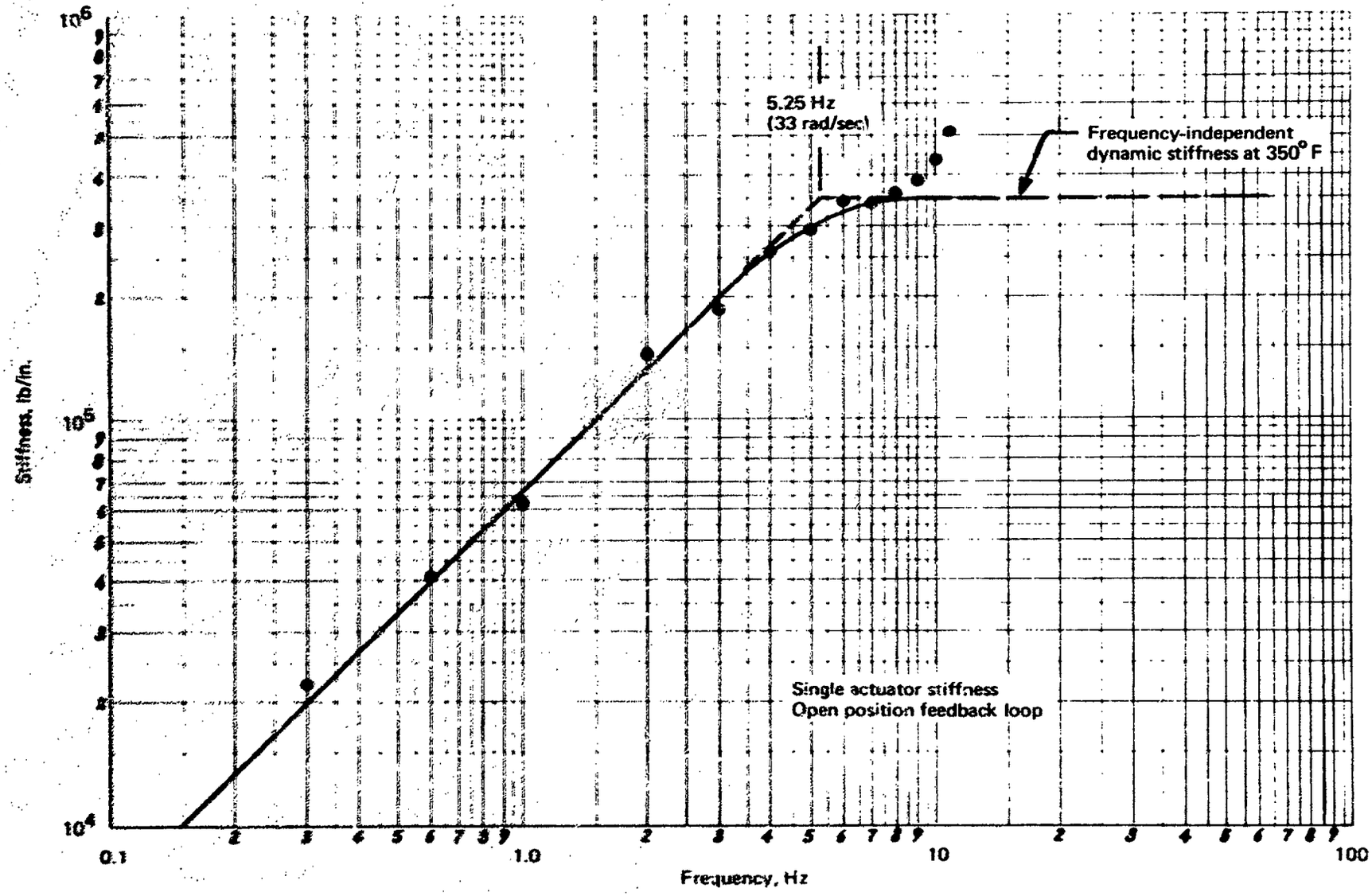

FIGURE 66.–"NORMAL ACTUATOR" SYSTEM STIFFNESS FREQUENCY RESPONSE–350° F

Using the terms previously defined:

$$\beta = 120{,}000 \text{ psi at } 350^{\circ} \text{ F}$$

$$\frac{1}{K_A(\infty)} = \frac{1}{1{,}290{,}000} + \frac{1}{2{,}880{,}000} + \frac{1}{570{,}000}$$

$$K_A(\infty) = 350{,}000 \text{ lb/in.}$$

5.4.1.4 Conclusions

The "normal actuator" dynamic stiffness tests produced excellent data, which allowed complete identification of the open-loop stiffness transfer function for an actuator in the normal configuration. Open-loop stiffness frequency response can be used in conjunction with static stiffness measurements for construction of the closed-loop frequency-dependent stiffness curve as is demonstrated in section 5.4.7.

The test data agree extremely well with analytical predictions and give confidence in the analytical solutions for the stiffness of actuators in the normal stiffness configuration.

5.4.2 "Stalled Actuator" Dynamic Stiffness Tests

The SST horizontal stabilizer design was such that the surface hinge moments were large enough to stall the actuators in some cases. Since the actuation system was required to provide the necessary stiffness to prevent surface flutter, the system stiffness with stalled actuators was of interest. SST analysis had shown that a significant decrease in stiffness at the flutter frequency would occur under stalled conditions.

When an actuation system is commanded to move to a position that requires more force than the actuator can develop, the actuator stalls against the load. Since the position command is not satisfied, the main servovalve is open. Normally, when the servovalve is open, the actuator is connected to the hydraulic system. The SST actuator design included an inlet check valve that prevents backflow from the actuator to the supply line. For the SST actuator, the system stiffness for the stalled case results from a fluid spring consisting of the checked-off high-pressure side of the actuator and the low-pressure side connected to the return portion of the hydraulic system through the open servovalve.

To provide fluid for internal leakage, the inlet check valve must be slightly open. Opening the check valve opens the high-pressure side of the actuator to the supply side of the hydraulic system, further reducing the system stiffness that is frequency dependent. As the actuator wears, internal leakage generally increases.

5.4.2.1 Test Objectives

The stall stiffness tests determined the open-loop stiffness frequency response characteristics with one actuator in the stall condition. The effects of increased actuator leakage resulting from actuator wear and operating temperatures were also assessed.

5.4.2.2 Test Description

These "stalled actuator" stiffness tests were conducted in the same manner as the "normal actuator" dynamic stiffness tests (see sec. 5.4.1), except that:

- No tests were run with the pressure feedback locked out.
- Tests were run with a bypass circuit between the main actuator cylinders opened to simulate various leakages from 0 to 6 gpm at 150°and 350° F fluid temperatures.
- The stalled actuator was commanded hard-over to fully open the servovalve, and the three drive actuators were used to restrain the stalled actuator while superimposing the sinusoidal drive force.
- The stalled actuator was supplied by a separate hydraulic system to preclude hydraulic power system transients from affecting the stiffness data. Also, because the servovalve was open and the hydraulic plumbing affected the system stiffness, the stalled actuator was connected to the hydraulic supply by plumbing that simulated the SST hydraulic power distribution system. A schematic of the plumbing is shown in figure 67.

5.4.2.3 Test Results

As shown on figure 68, the frequency-dependent stiffness under "stalled actuator" conditions decreased when compared with the "normal actuator" stiffness tests. This decrease in stiffness results from additional compressible flow due to opening of the low-pressure side of the actuator to the large additional volume of the return portion of the hydraulic system.

The increase in leakage through the inlet check valve seemed to have little effect. Inspection of the data showed that no matter what the leakage value, the inlet check valve was closed for most of the sine wave loading cycle.

Figure 69 shows the data taken at high temperature. Except for the change in frequency-independent dynamic stiffness, no change in stall stiffness was observed below the dynamic stiffness break frequency.

The direction of the stall load application made no appreciable difference in the "stalled actuator" stiffness. Data for stall in each direction are shown in figure 70. Any differences which might have been expected due to actuator manifold differences in the extend and retract directions are lost in data scatter.

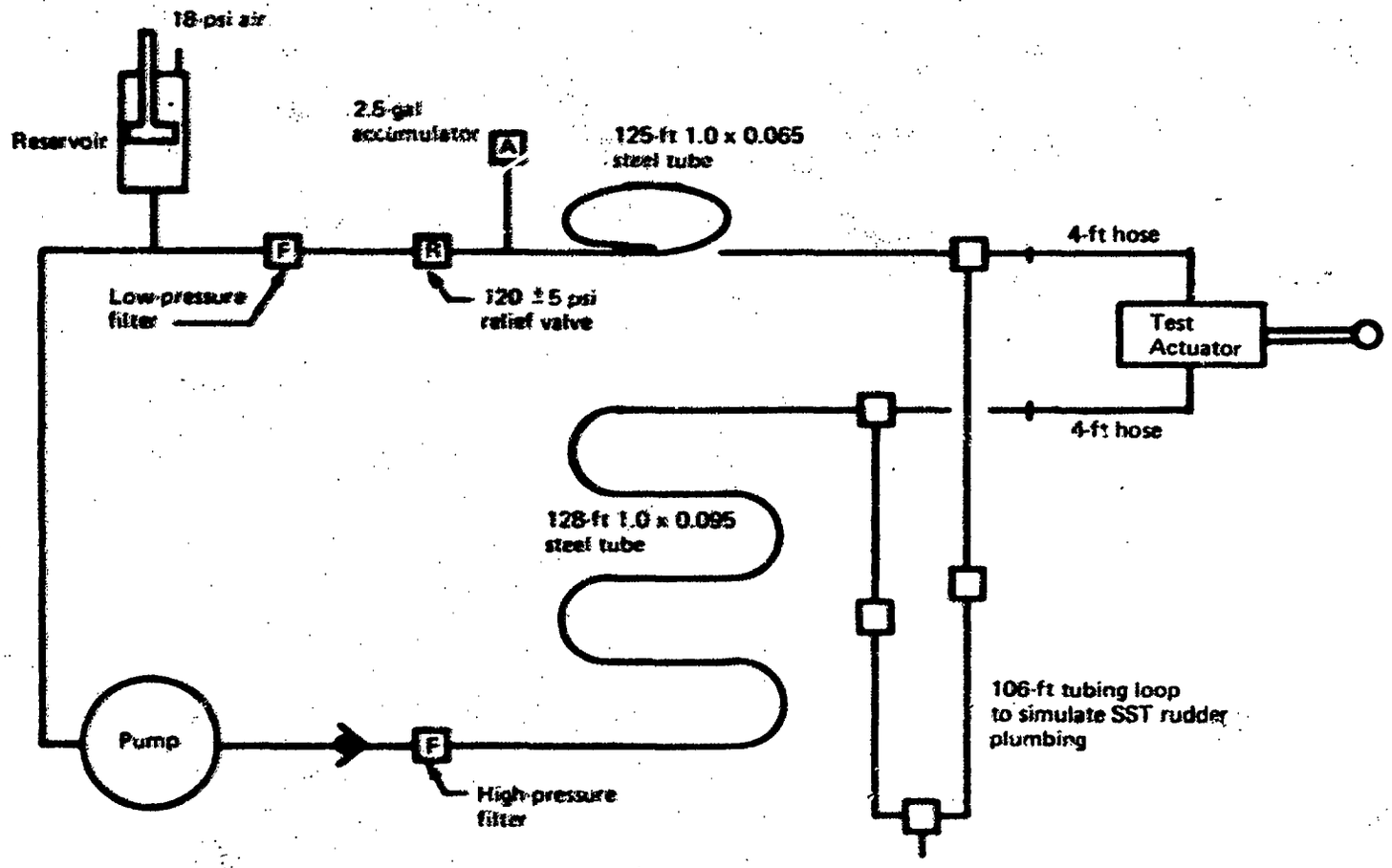

FIGURE 67.–SIMULATED AIRPLANE TUBING

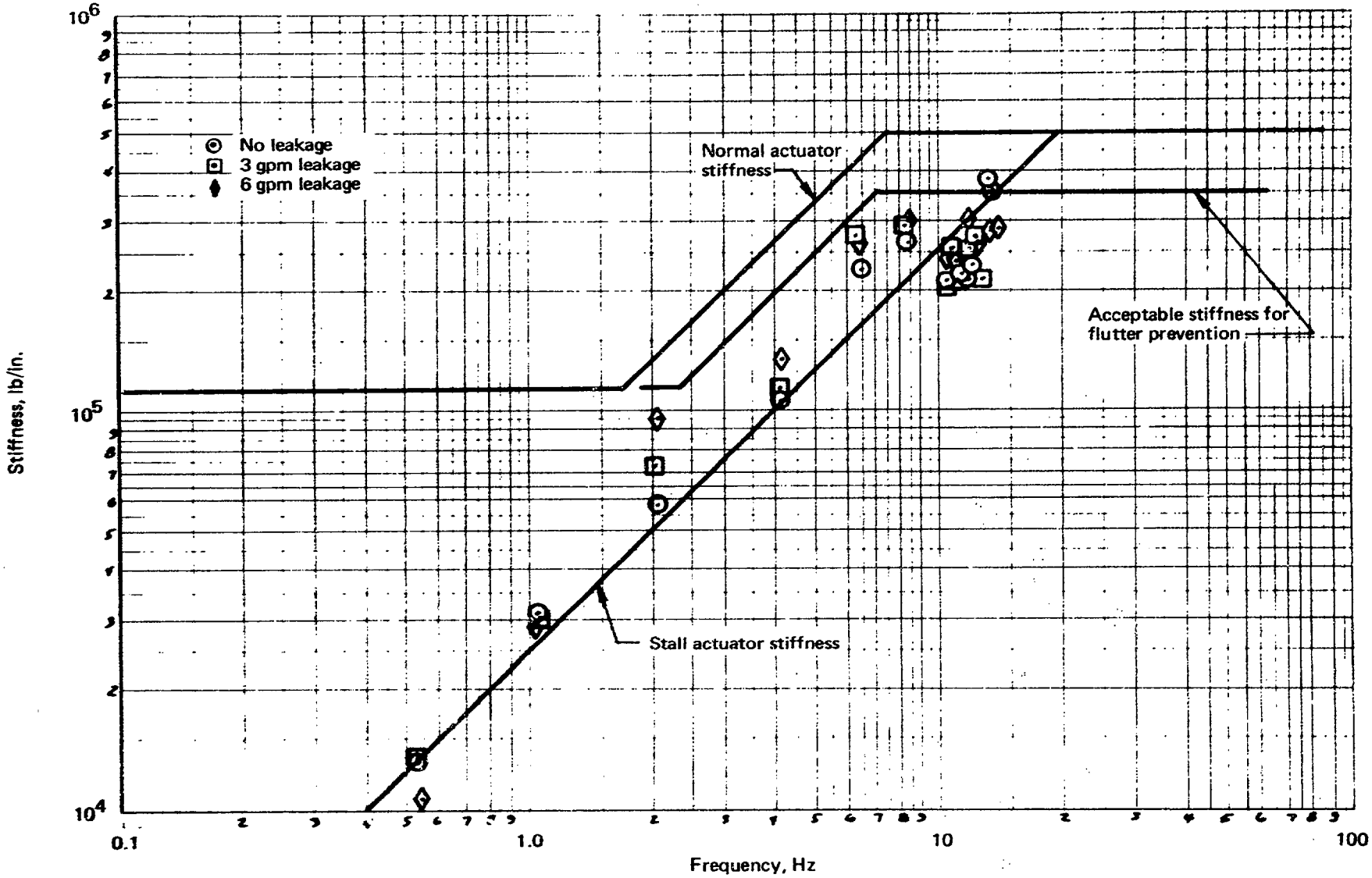

FIGURE 68.—"STALLED ACTUATOR" SYSTEM STIFFNESS FREQUENCY RESPONSE—150° F

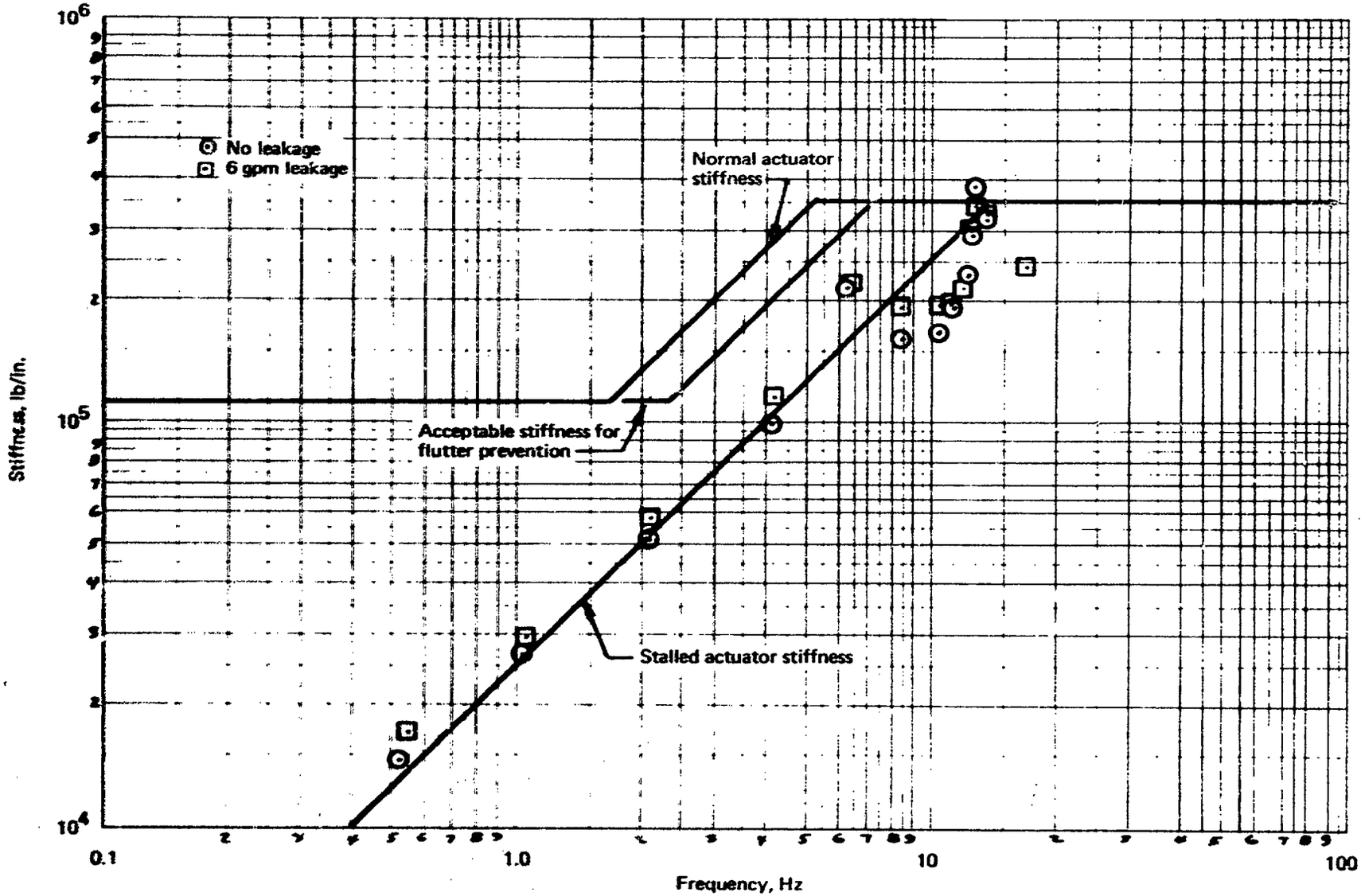

FIGURE 69.–"STALLED ACTUATOR" SYSTEM STIFFNESS FREQUENCY RESPONSE–350° F

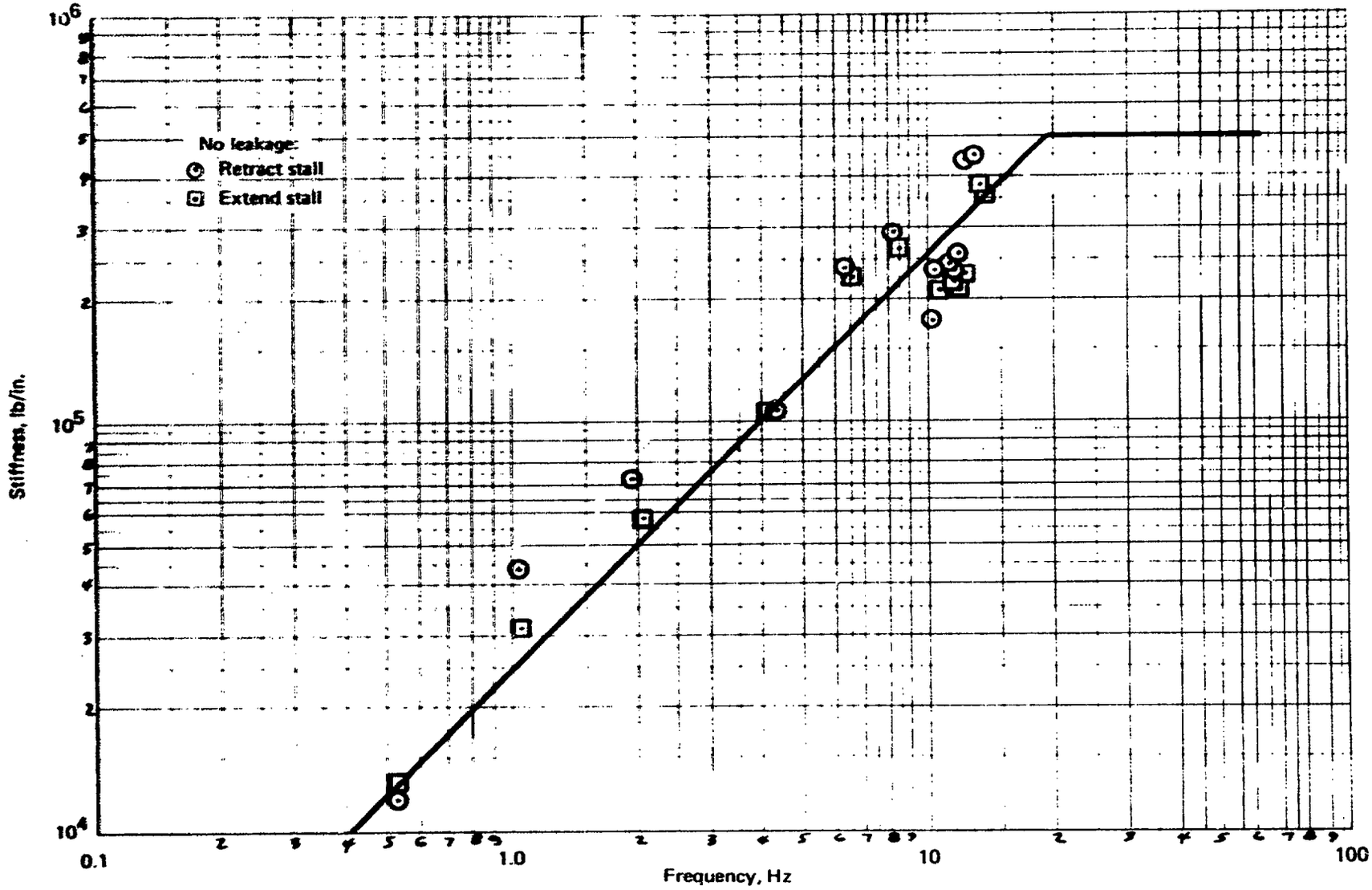

FIGURE 70.—"STALLED ACTUATOR" SYSTEM STIFFNESS FREQUENCY RESPONSE— ACTUATOR STALLED IN EACH DIRECTION, 150° F

Linear analysis of the open-loop stiffness transfer function predicts the stiffness behaving as a first-order high-pass filter. All of the stall stiffness test data show good agreement with this prediction, as indicated by comparison with the 6 db per octave line up to the dynamic stiffness break frequency.

Deviations around 7 Hz are caused by hydraulic line dynamics in the side of the actuator connected to the return line. The data scatter observed around 12 Hz was caused by peaking at the system natural frequency.

5.4.2.4 Conclusions

When an actuator is stalled, the frequency-dependent stiffness is reduced. If the surface actuators are designed to stall to limit airplane or surface loads, and if the actuation system must provide flutter stiffness, then the actuation system design must account for the degradation in flutter stiffness if the flutter frequency is less than the dynamic stiffness break frequency. The transient nature of the stall condition, as well as the reduced stiffness, should be considered in all flutter studies.

5.4.3 "Actuator Blowback" Dynamic Stiffness Tests

There existed, for the SST, a certain probability that a combination of airplane maneuvers, failed actuators, and gust conditions could produce forces that would exceed the capability of the actuators to resist. If this condition occurred, the actuators would be driven backward away from their commanded position, resulting in a decrease in actuation system flutter stiffness.

As explained in section 5.6, multiple surface actuators require overpressure protection to allow the remaining actuators to function after a failure in one actuator. In multiple-actuator installations, it is desirable to maintain as much performance as possible after a failure or shutdown of hydraulic supply systems. The failed or dead actuator is usually off-loaded by a bypass valve that interconnects the two ends of an actuator cylinder when hydraulic pressure is off. In the SST, one valve, the main actuator relief/bypass valve described in section 3.2.2.1, provided both overpressure protection and bypass functions.

The pressure setting for the relief function of the valve plus the pressure drop through the open valve at maximum flow determines the maximum load that can be applied to any actuator. The lower this maximum load limit, the lighter the actuator and its reaction structure can be. The nominal cracking pressure for the relief function of the SST main actuator relief/bypass valve was 4350 psi (supply pressure plus 200 psi). The design pressure drop through the valve and manifold at the maximum design flow rate (75 gpm) was 550 psi.

During actuator blowback the inlet check valve closes and the relief/bypass valve opens, allowing flow from one side of the actuator to the other. Since the actuator is not satisfying its position command, the main servovalve is also open. The opening of both the relief/bypass valve and the servovalve essentially opens both sides of the actuator to return and reduces the system stiffness at all frequencies below the dynamic stiffness corner. The actuator configuration during blowback is shown in figure 71.

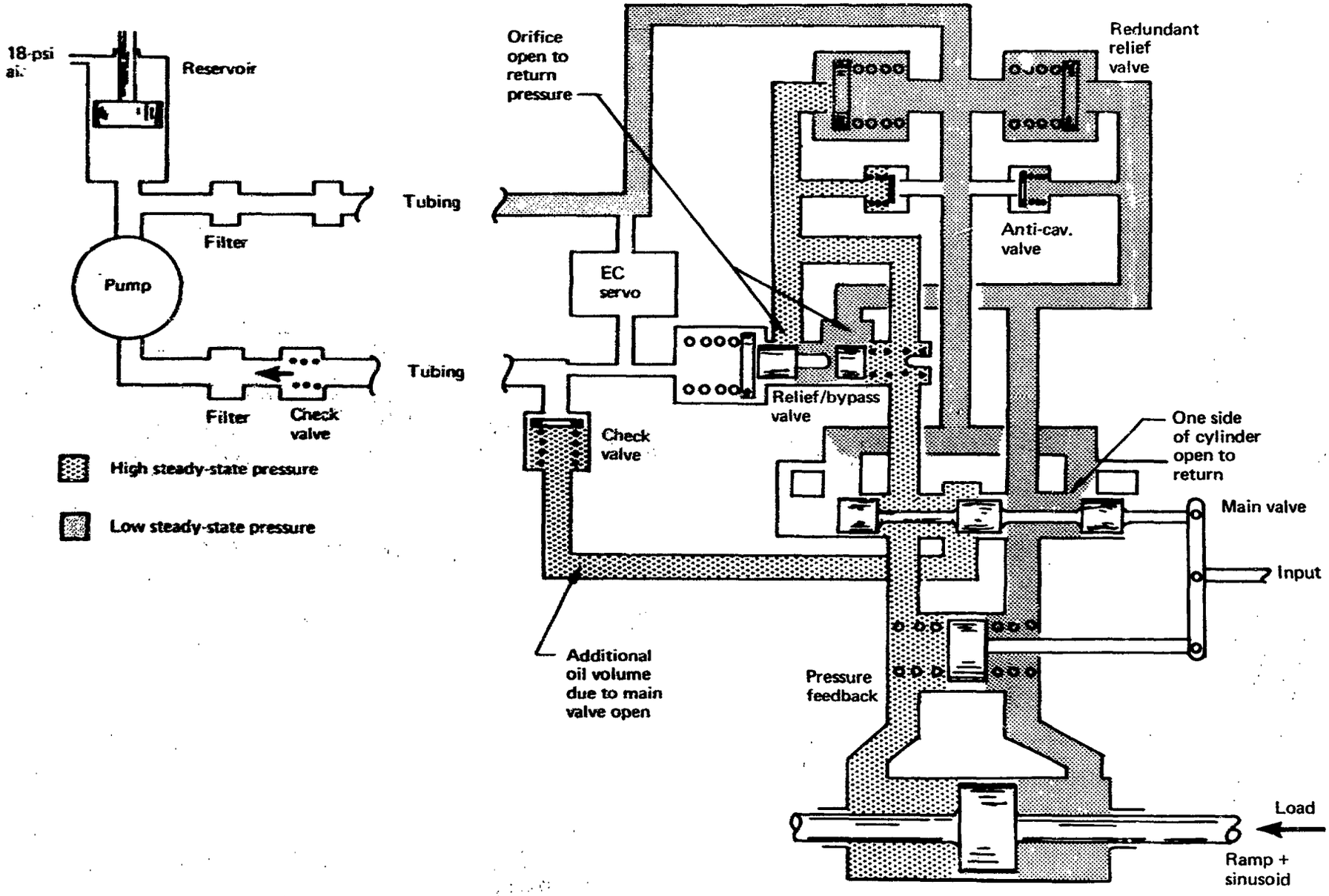

FIGURE 71.–ACTUATOR CONFIGURATION DURING BLOWBACK

At the termination of the SST program, transfer functions were being developed that would describe the system stiffness frequency response with the actuator in the blowback condition. These transfer functions were to be used in combination with airplane, surface, and gust simulations to determine whether the blowback condition caused stiffness degradation below the minimum stiffness required to prevent surface flutter.

5.4.3.1 Test Objective

The objective of the test was to determine the blowback dynamic stiffness frequency response of the system at various backdriving rates.

5.4.3.2 Test Description

These blowback tests were conducted in the same manner as the "normal actuator" system dynamic stiffness tests (sec. 5.4.1), except that:

- No tests were run with the pressure feedback locked out.
- No tests were run at 350°F.
- The backdriven actuator was commanded hard-over to fully open the main servovalve in one direction, and the three drive actuators were used to backdrive (blow back) the actuator in the opposite direction at a steady rate while simultaneously applying the sinusoidal drive force.
- The backdriven actuator was supplied by a separate hydraulic system to preclude pumping system transients from affecting the stiffness data. Also, because the servovalve was open and the hydraulic plumbing affected the system stiffness, the test actuator was connected to the hydraulic supply by plumbing that simulated the SST hydraulic power distribution system. A schematic of the plumbing is shown in figure 67.

5.4.3.3 Test Results

Figure 72 shows the system stiffness frequency response for various blowback rates compared to a normal actuator stiffness. The system stiffness rapidly decreased as the blowback rate increased. The stiffness seems to reach a minimum at about 5°/sec backdriving rate. This limit may be due to the restriction to flow in the actuator manifold passages.

5.4.3.4 Conclusions

At slow backdriving rates, the main actuator relief/bypass valve opening was small and had little effect on system stiffness. The main servovalve opening was the predominant factor and resulted in stiffness frequency response approximately the same as that for the stall case where the bypass valve was closed. However, the system stiffness decreased drastically as the blowback rate increased because larger flows were bypassed. When bypass flows reached an equivalent of 5°/sec blowback rate, the relief/bypass valve had opened sufficiently to provide complete interconnection of the two sides of the actuator. The stiffness at these relatively high rates of 5°/sec was very low and would not have provided the necessary flutter restraint for the SST.

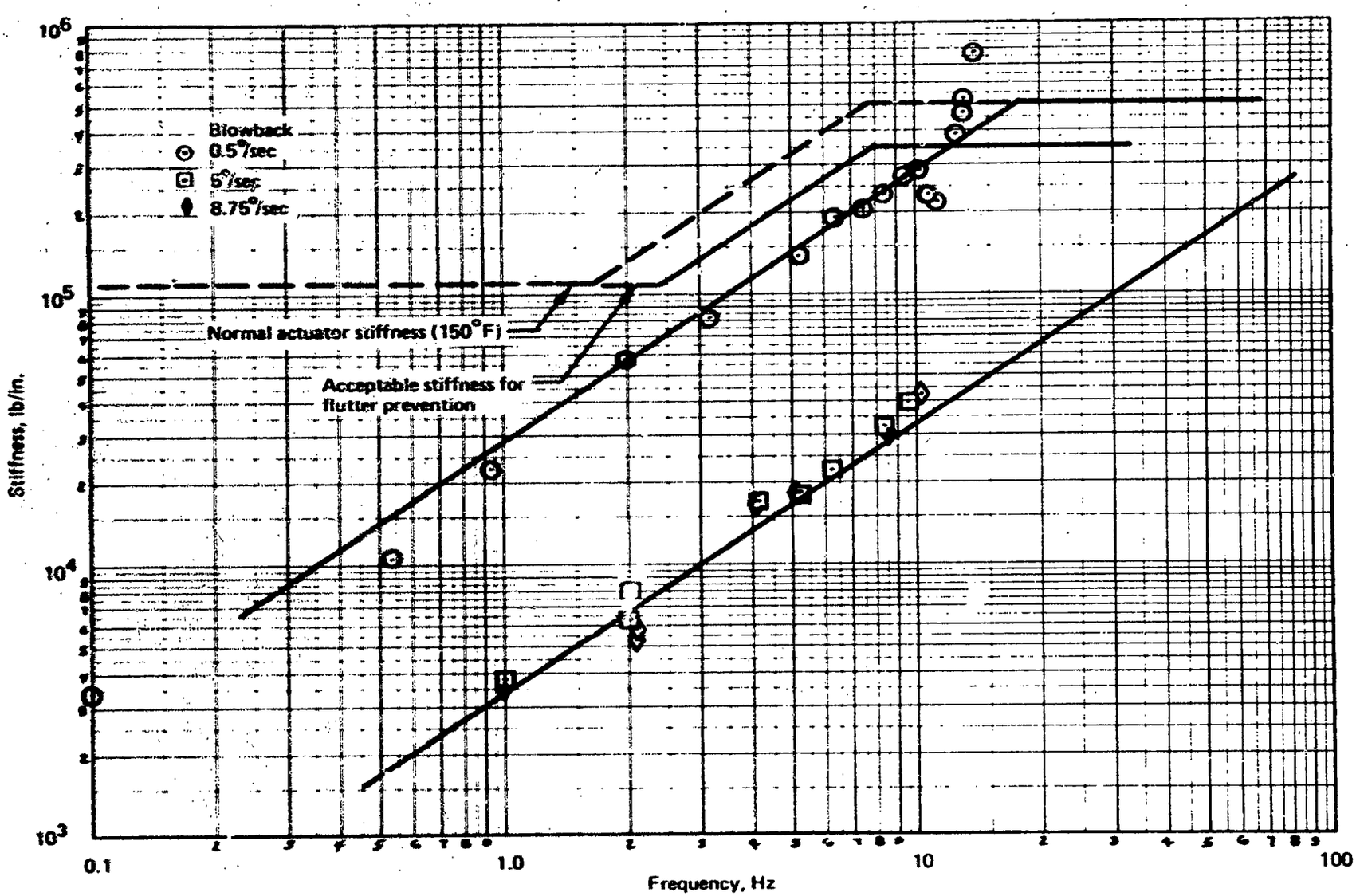

FIGURE 72 – "ACTUATOR BLOWBACK" SYSTEM STIFFNESS FREQUENCY RESPONSE

System stiffness is the lowest at the highest blowback rates where the actuator would be in the blowback condition for the shortest period of time. Any use of blowback stiffness for flutter analyses should consider the limited time that the actuator spends in the blowback condition.

5.4.4 "Actuator Under-Command" Dynamic Stiffness Tests

When the actuator is responding to changes in commanded position, the main servovalve opens in proportion to the position error and connects each end of the actuator to the hydraulic system pressure and return lines. With the resulting increase in fluid volume, the system frequency-dependent stiffness will modulate as a function of the valve position.

The modulation of system stiffness may be of concern when considering the stiffness required to prevent surface flutter. At one extreme, the main servovalve is open and the "actuator under-command" stiffness approaches the "stalled actuator" stall stiffness. At the other extreme, the main servovalve is nearly closed and the "actuator under-command" stiffness approaches the "normal actuator" stiffness.

5.4.4.1 Test Objectives

The "actuator under-command" dynamic stiffness tests determined the frequency-dependent stiffness of the system as a function of actuator load pressure and surface rate.

5.4.4.2 Test Description

These under-command tests were conducted in the same manner as the normal dynamic stiffness tests (sec. 5.4.1) except that:

- No tests were run with the pressure feedback locked out.
- No tests were run at 350° F.
- The under-command actuator was commanded to move and the three drive actuators were used to restrain the motion while simultaneously applying sinusoidal drive force. A bypass circuit between the main actuator cylinders was opened to allow flow through the inlet check valve and the servovalve to simulate the actuator piston rate. The under-command actuator commands and bypass flows were adjusted to simulate various loads (up to 2500 psi) and rates (up to 10 /sec of stabilizer).
- The under-command actuator was supplied by a separate hydraulic system to preclude power system transients from affecting the stiffness data. Also, because the servovalve was open and the hydraulic plumbing affected the system stiffness, the under-command actuator was connected to the hydraulic supply by plumbing that simulated the SST hydraulic power distribution system. A schematic of the plumbing is shown in figure 67.

5.4.4.3 Test Results

The system stiffness frequency response variation with load at constant flow (simulated surface rate) is shown in figure 73. The data showing the stiffness variation with flow at constant load are shown in figure 74. Test points above the dynamic stiffness break frequency were difficult to obtain, since the loading actuators had poor response at high frequencies. Enough data points were obtained, however, to confirm analyses that showed the frequency-independent dynamic stiffness unchanged from the values obtained in the normal actuator stiffness tests.

The test data were influenced by the simulated load flow and had to be corrected before use. The introduction of the bypass circuit to simulate piston rate introduces a leak across the piston that reduces stiffness. To get under-command system stiffness, the effect of the leak was calculated and the test data adjusted to remove that portion of the stiffness reduction.

Figure 75 was developed using data from this test as well as from the "stalled actuator" stiffness and "normal actuator" stiffness tests. Frequency-dependent dynamic stiffness is obtainable for combinations of surface rate and load once the "normal actuator" frequency-dependent stiffness is known. This allows construction of asymptotic approximations of system stiffness frequency response for any under-command condition. A stiffness frequency response is constructed by drawing a line with a slope of 6 dB per octave through a frequency-dependent stiffness value obtained from the ratio of under-command and normal frequency-dependent stiffness. The dynamic stiffness break frequency is the intersection of the 6 dB per octave line and the frequency-independent stiffness of the actuator at the temperature of interest.

A portion of figure 75 has been extrapolated by using general trends. A more complete study of under-command system stiffness would include tests to give better definition at high load pressures.

5.4.4.4 Conclusions

"Actuator under-command" frequency-dependent stiffness is much lower than "normal actuator" frequency-dependent stiffness for much of the under-command spectrum. The frequency-independent stiffness does not change. The combination of high surface rates and high loads gives the least system stiffness. Stiffness is the lowest at the highest under-command rates where the actuator would be in the under-command condition for the shortest period of time. If under-command stiffness data are used for flutter analyses, the transient nature of the reduction in stiffness resulting from this condition must be considered.

5.4.5 Static Stiffness

Two design constraints fix the upper limit of the actuation system static stiffness. These are system stability and actuator synchronization. High static stiffness is required to minimize actuator hysteresis caused by friction and to reduce static position error under load. Appendix A shows how static stiffness affects the frequency-dependent dynamic stiffness

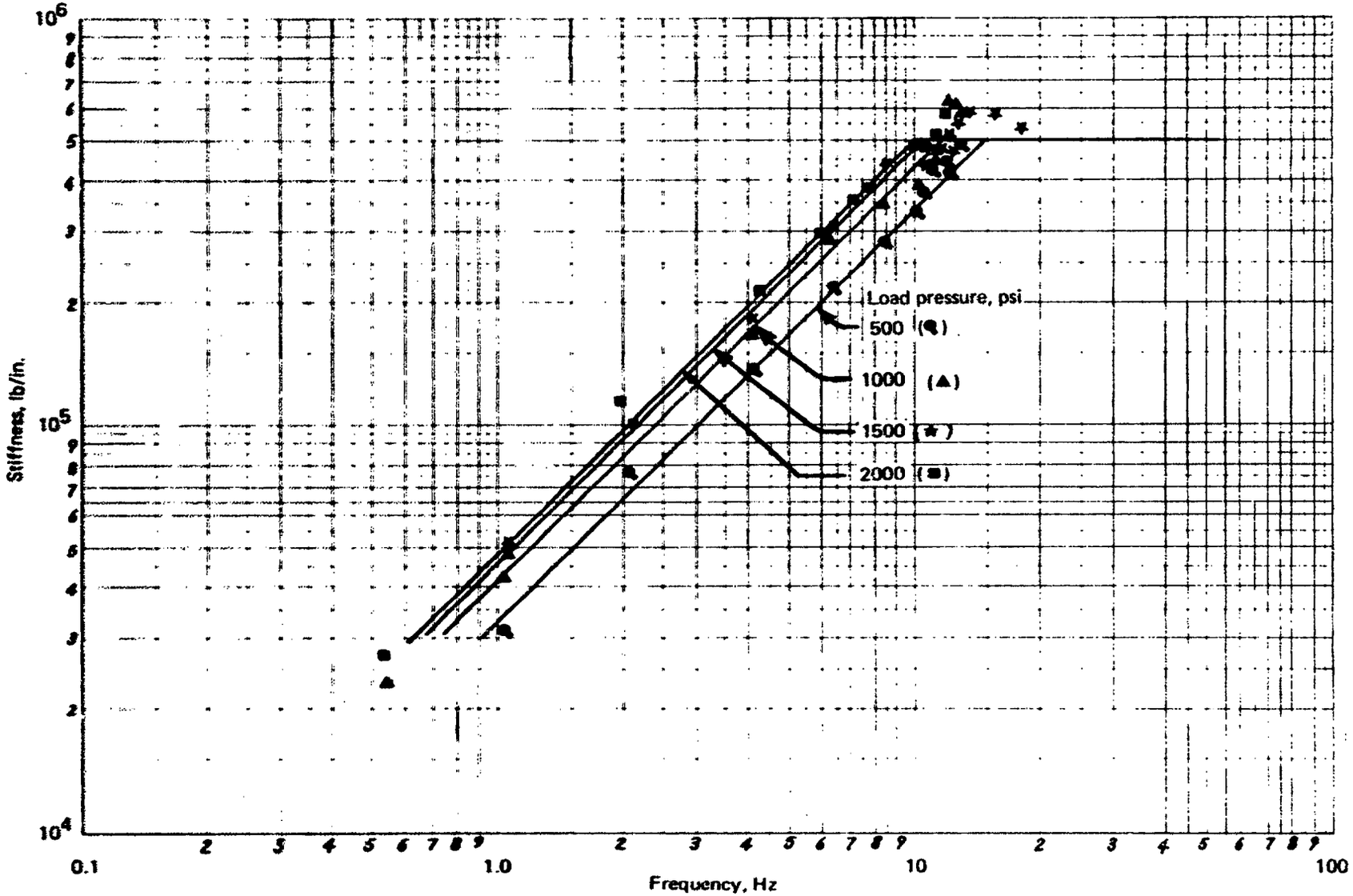

FIGURE 73.–"ACTUATOR UNDER-COMMAND" SYSTEM STIFFNESS FREQUENCY RESPONSE–150° F–3°/SEC

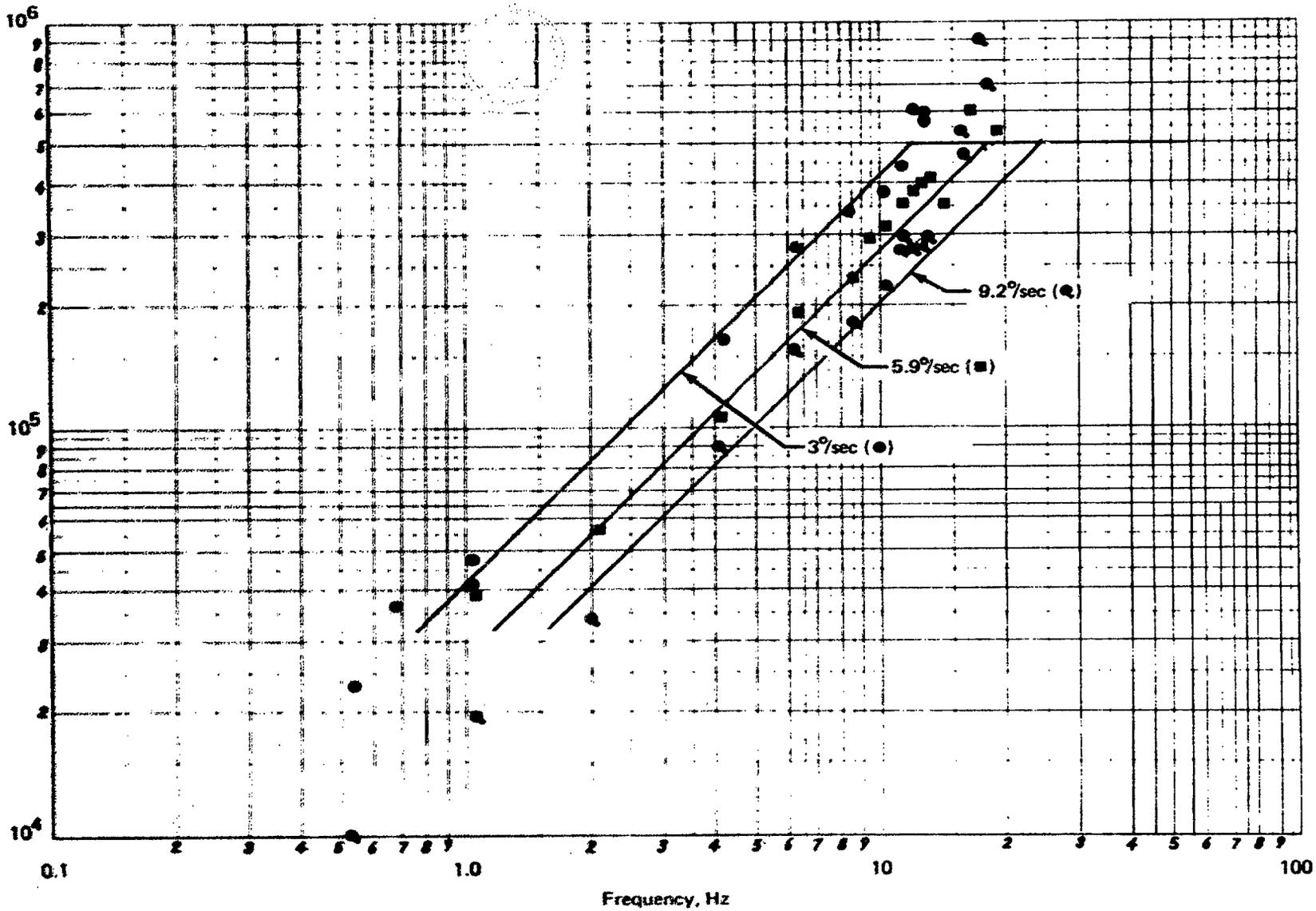

FIGURE 74.—"ACTUATOR UNDER-COMMAND" SYSTEM STIFFNESS FREQUENCY RESPONSE—150° F—1000-PSI LOAD PRESSURE

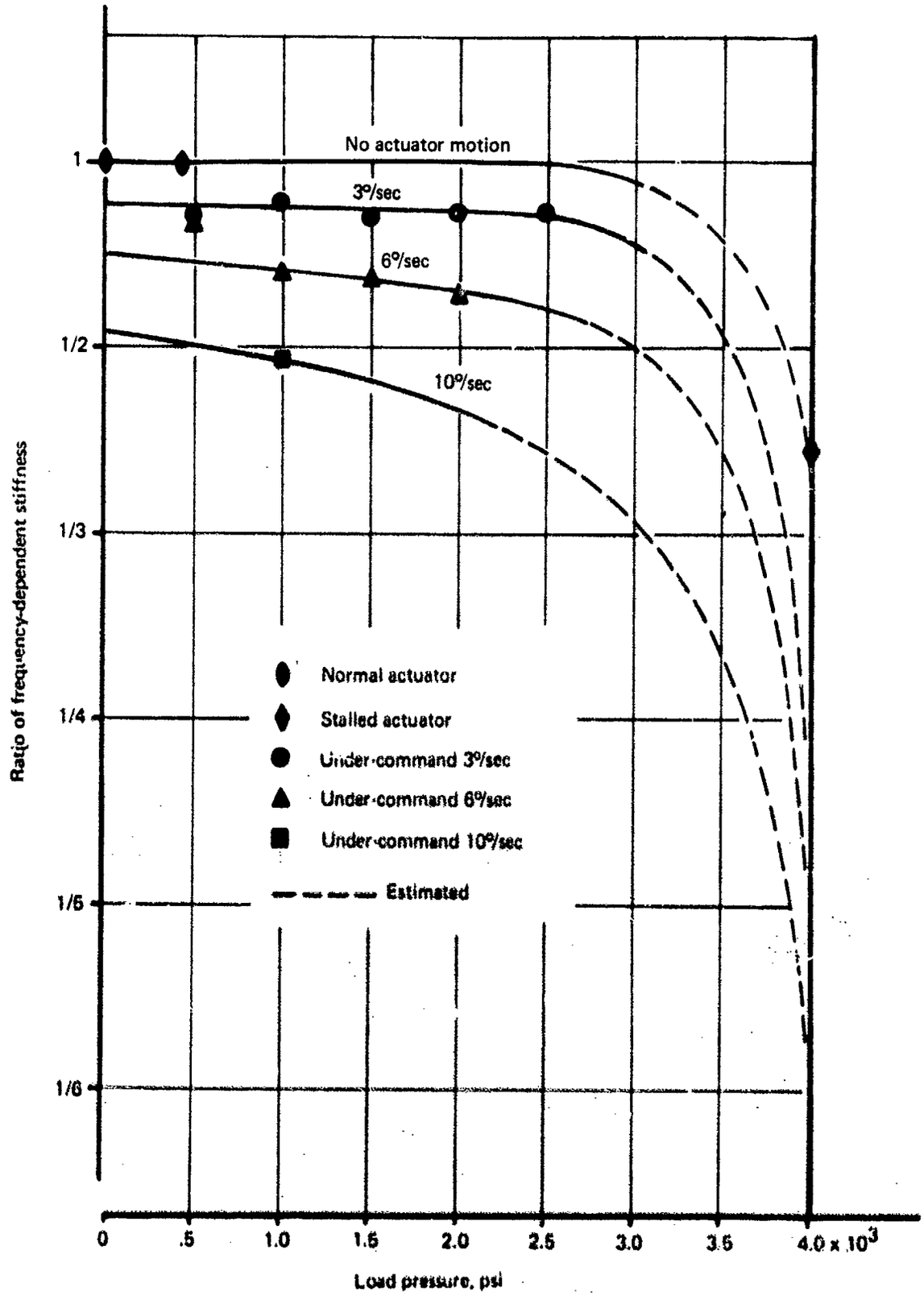

FIGURE 75.–SYSTEM FREQUENCY-DEPENDENT STIFFNESS RATIO– "ACTUATOR UNDER-COMMAND" AND "STALL" CONDITIONS COMPARED TO "NORMAL ACTUATOR"

and the dynamic stiffness break frequency. In the SST, static stiffness higher than the upper limit for stability and synchronization was desired to maintain adequate flutter stiffness in the frequency-dependent stiffness range.

As shown in the analyses in section 4.0, the actuation system static stiffness upper limit to ensure stability at high temperatures was 350,000 lb/in. Static stiffness of 124,000 lb/in. was the upper limit to maintain force synchronization within 800 psi of the average load pressure considering maximum actuator installation tolerances.

The minimum static stiffness requirements for flutter stiffness were set at 110,000 lb/in. This value was also an acceptable minimum for hysteresis. The actuator stroke was increased to compensate for the static position error under load based on 110,000 lb/in.

Early startup tests showed that the actuation system static stiffness with no structural feedback or pressure feedback was 2,260,000 lb/in. This extremely high value results directly from the pressure gain of the high-performance main actuator servovalve. Analyses of the horizontal stabilizer actuation system also disclosed that a strong destabilizing structural feedback existed where structural deflections, resulting from actuator loads, cause the actuator stiffness to increase. Figure 76 shows how these structural deflections are reflected into the actuator valve.

Reduction of effective valve pressure gain by means of differential pressure feedback was necessary, both to reduce this extremely high system static stiffness to meet the system stability and actuator synchronization requirements, and to negate the destabilizing structural feedback. The pressure feedback is described in section 3.2.2.1 and shown in figure 13. The pressure feedback gain was designed to reduce the system static stiffness to 110,000 lb/in. with no structural effects by reducing the effective valve pressure gain from 820,000 to 38,000 psi/in. of valve.

With this as a basis, analysis predicted the actuation system static stiffness to increase from 110,000 lb/in. to approximately 225,000 lb/in. when the destabilizing structural feedback was introduced. (See table 3 for actual values.)

5.4.5.1 Test Objective

This series of static stiffness tests determined the system stiffness with no structural influence, the structural deflections under load, and the static stiffness of installed actuators.

5.4.5.2 Test Description

Deflections and forces required to determine static stiffness were obtained by applying a load to one actuator or to the entire actuation system and measuring the actuator pin-to-pin displacement and the differential pressure resisting the load. Some force measurements were made with load cells for comparison. Stiffness was calculated by multiplying the differential pressure by actuator area and then dividing by the pin-to-pin displacement. Where more than one actuator was being used, individual stiffnesses were calculated and then summed to get system stiffness. Surface rotation measurements were also used to calculate system stiffness and to check symmetry.

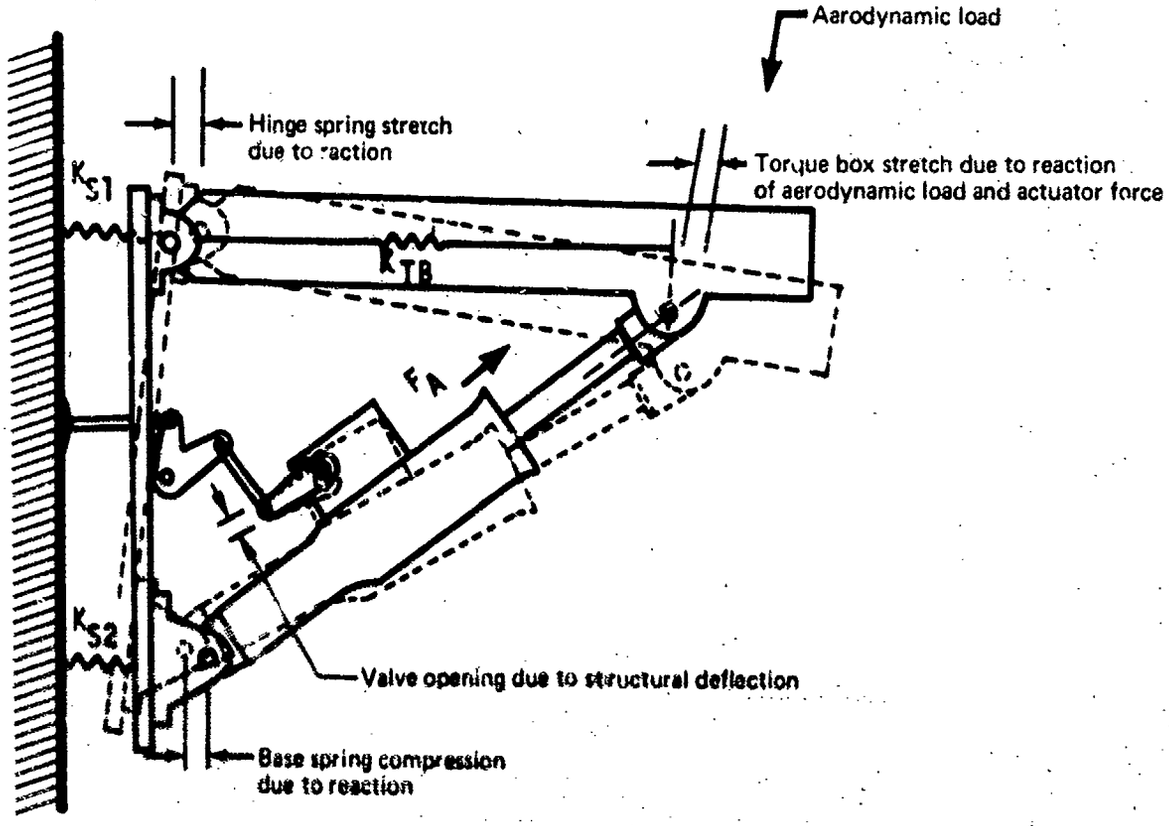

FIGURE 76.–STRUCTURAL FEEDBACK

The tests were conducted in two ways. Loads applied to a single actuator were either from adjacent actuators or from the simulated aeroloading system described in section 3.4. When more than one actuator was under test, all loading was done with the simulated aeroload system.

In some single actuator tests, it was desirable to eliminate the unpredictable structural influences to obtain test data for the isolated actuator. The actuator was isolated from structure by disconnecting the normal position feedback path and substituting an electronic analog of this feedback through the EC servo.

When the aeroload system was used, the loads were applied at two positions on the load beam, one near the end of the beam and one near the actuator rod attachment (load positions 4 and 1). The shift in loading positions was to determine the effect on system static stiffness of changes in pressure distribution on the control surface.

5.4.5.3 Test Results

The single actuator system static stiffness with no destabilizing structural influences was measured as 105,000 lb/in., agreeing very closely with the predicted value of 110,000 lb/in. The difference is directly attributable to the manufacturing tolerances of the pressure feedback device, since its gain controls the effective pressure gain of the installed main servovalve and the force gain of the actuator.

Unexpected stiffness differences were obtained which depended on how the load was applied to the test actuator. The single actuator system stiffness, measured by loading it with the other actuators, was 110,000 lb/in. A higher stiffness had been expected. The reason for the low stiffness, even though the actuator was mounted in structure, is that the loading actuators share the structure and load it in the opposite direction so that the only structural deflections reflected to the test actuator occur in the extremely stiff structure between actuators. Since the destabilizing structural feedback gain is inversely proportional to the structural stiffness, the more stiff the structure becomes, the less its influence.

By loading a single actuator with the aeroload system, the stiffness increased to 234,000 lb/in. This increase is due to the destabilizing structural feedback. By loading the actuator in this manner, all of the backup structure is supporting the single actuator alone; the structure is not shared by the other actuators as in the above case. Although the actuator is reacted by structure, with approximately four times the structural stiffness that is reacting the actuator in the normal quadruple configuration, it is a lower reaction stiffness than that which resulted from loading with the other three actuators. Again, this lower stiffness resulted in a higher destabilizing structural feedback gain and consequently a higher static stiffness.

Figure 77 summarizes the single actuator system static stiffness values discussed above and shows the loading geometry for the load system case.

When all the actuators were loaded by the aeroload system at a forward position (No. 1), the structure was shared by all actuators and consequently the stiffness that reacts each actuator was less, thereby increasing the structural feedback gain. From the tabulation of stiffness values in figure 78 the effect of the decreased actuator reaction structural

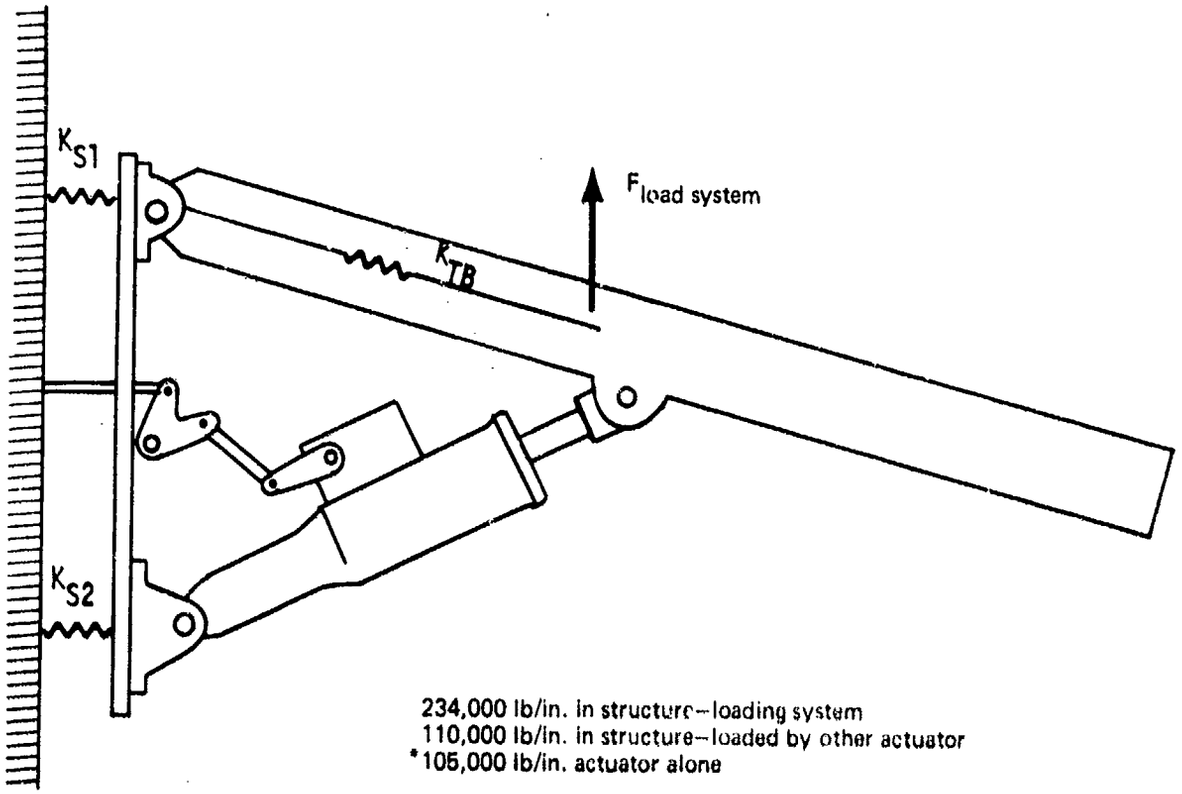

234,000 lb/in. in structure–loading system
110,000 lb/in. in structure–loaded by other actuator
*105,000 lb/in. actuator alone

*This number from above test geometry
Other values from other test data

FIGURE 77.–SYSTEM STATIC STIFFNESS–SINGLE ACTUATOR

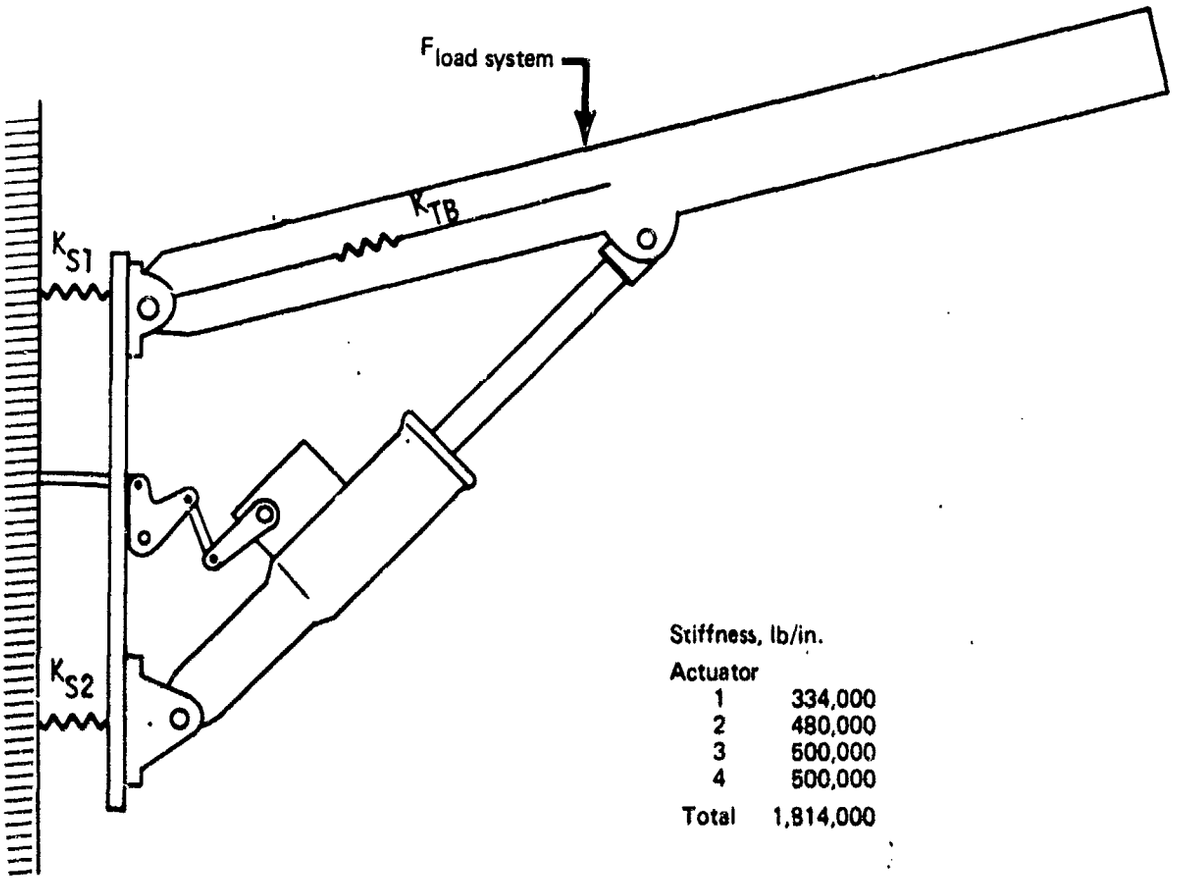

Stiffness, lb/in.	
Actuator	
1	334,000
2	480,000
3	500,000
4	500,000
Total	1,814,000

FIGURE 78.–SYSTEM STATIC STIFFNESS–FORWARD CENTER OF PRESSURE, TRAILING EDGE UP

stiffness can be seen as an increase in single actuator system static stiffness from 234,000 lb/in. to an average of 453,000 lb/in. The large differences in individual actuator stiffness are attributed to the nonuniform load distribution at this forward load position.

When the stabilizer was loaded at an aft position (No. 4) to simulate a center-of-pressure shift with Mach number increase, the measured stiffnesses were very consistent, as shown in figure 79. The aft location loaded the actuators more uniformly and resulted in a decrease in static stiffness.

Geometric effects in both actuator and structure caused by moving the stabilizer to the trailing-edge-down position caused changes in structural spring distribution which in turn caused stiffness changes as shown in figure 80. Although the measured stiffnesses are lower than for the trailing-edge-up position (fig. 79), the values are again consistently uniform due to the aft loading.

Loading the stabilizer with the aeroload system was difficult in the zero stabilizer position due to load system geometry. The values in figure 81 were obtained with relatively small hinge moment values. The differences in stiffness are more obvious at these low load levels, since the structure does not deflect enough to evenly distribute the loads and deflections. The lack of structural symmetry is shown by the large differences in stiffness between the pairs of actuators on each side of the airplane. Figure 82 shows the surface deflections with load that result from this asymmetric structure. Figures 83 and 84 show the deflections of the backup structure and stabilizer under load and again illustrate the structural asymmetry.

5.4.5.4 Conclusions

Static stiffness that depends on deflection of a complex structure and distribution of that deflection among parallel actuators is difficult to predict. Asymmetric structure causes stiffness changes that greatly emphasize the asymmetry if structural feedback is used to influence static stiffness. Obviously, the destabilizing feedback that resulted from this particular installation is undesirable, but it serves to illustrate the effect asymmetric structure can have on actuator static stiffness regardless of feedback polarity. The differences in load position error, caused by different static stiffnesses on each side of the airplane, are undesirable for a slab stabilizer because of the rolling moment introduced. Airplane structure probably would be more symmetric than the test structure, and therefore this surface position difference would be reduced.

The measured static stiffness in an installation of this type is dependent on the method of measurement. The high static stiffness values that were found in testing were influenced by the point loading system. In actuality, the air load would be distributed more uniformly over the surface, and local deflections at the actuators would change, modifying the static stiffness. It is predicted from the trend of test results that the static stiffness for an aerodynamically loaded surface would probably be lower than the values obtained from the point loading test.

The static stiffness upper limit to ensure a stable system was 350,000 lb/in. The static stiffness value for the stability analysis would be derived from the distributed loading caused by surface inertia. The spreading of the load in this manner probably kept the true static stiffness for stability less than the upper limit. The value of the inertial static stiffness is difficult to measure and was not obtained in this test program.

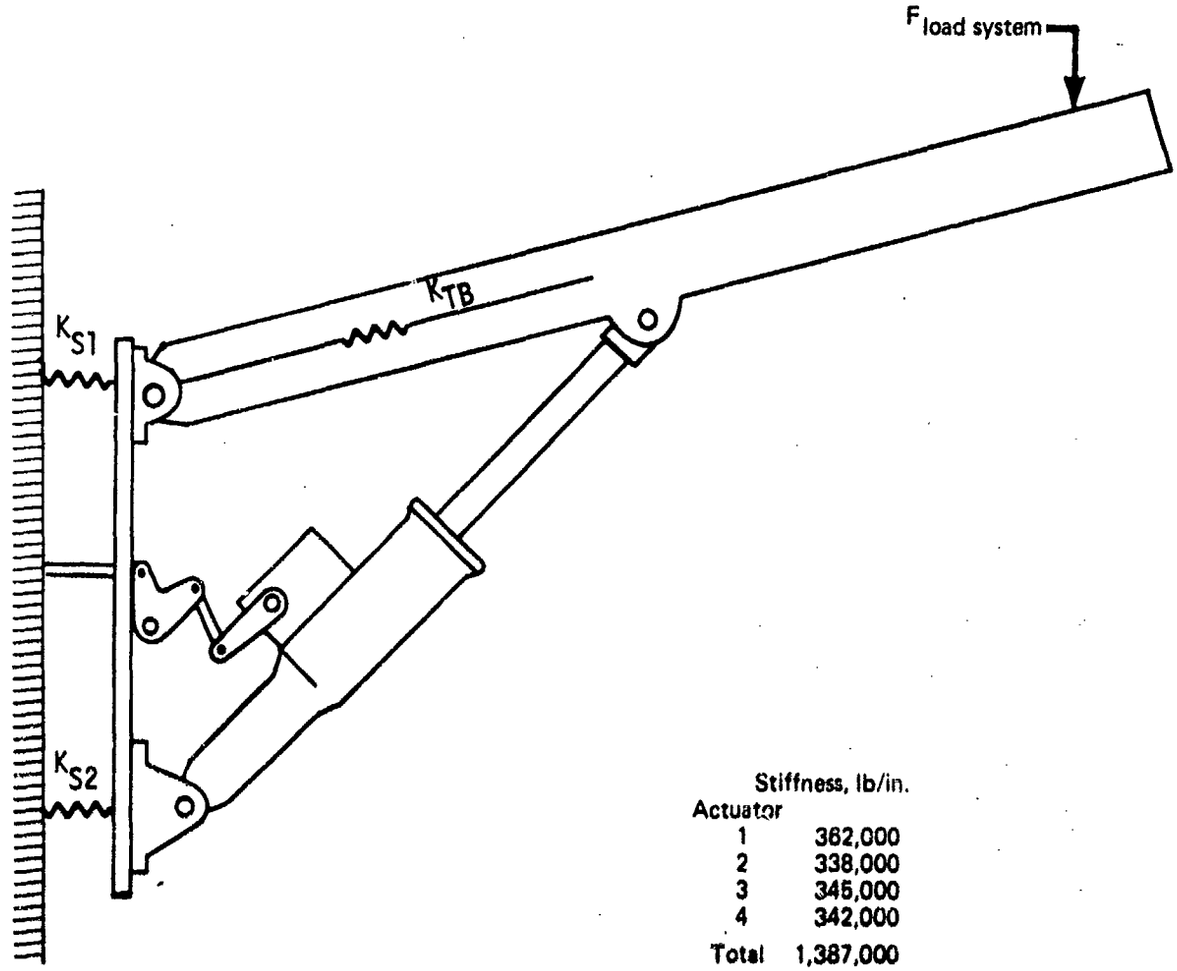

Actuator	Stiffness, lb/in.
1	362,000
2	338,000
3	345,000
4	342,000
Total	1,387,000

FIGURE 79.–SYSTEM STATIC STIFFNESS–AFT CENTER OF PRESSURE, TRAILING EDGE UP

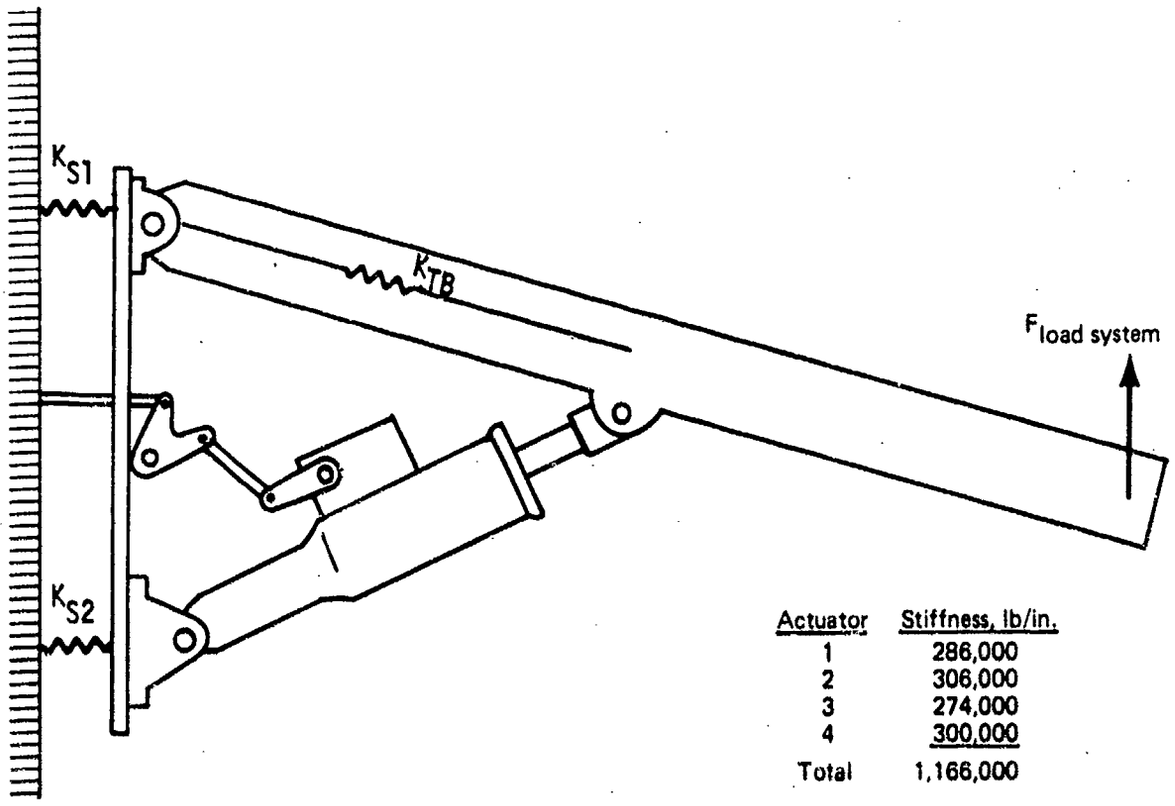

Actuator	Stiffness, lb/in.
1	286,000
2	306,000
3	274,000
4	300,000
Total	1,166,000

FIGURE 80.–SYSTEM STATIC STIFFNESS–AFT CENTER OF PRESSURE, TRAILING EDGE DOWN

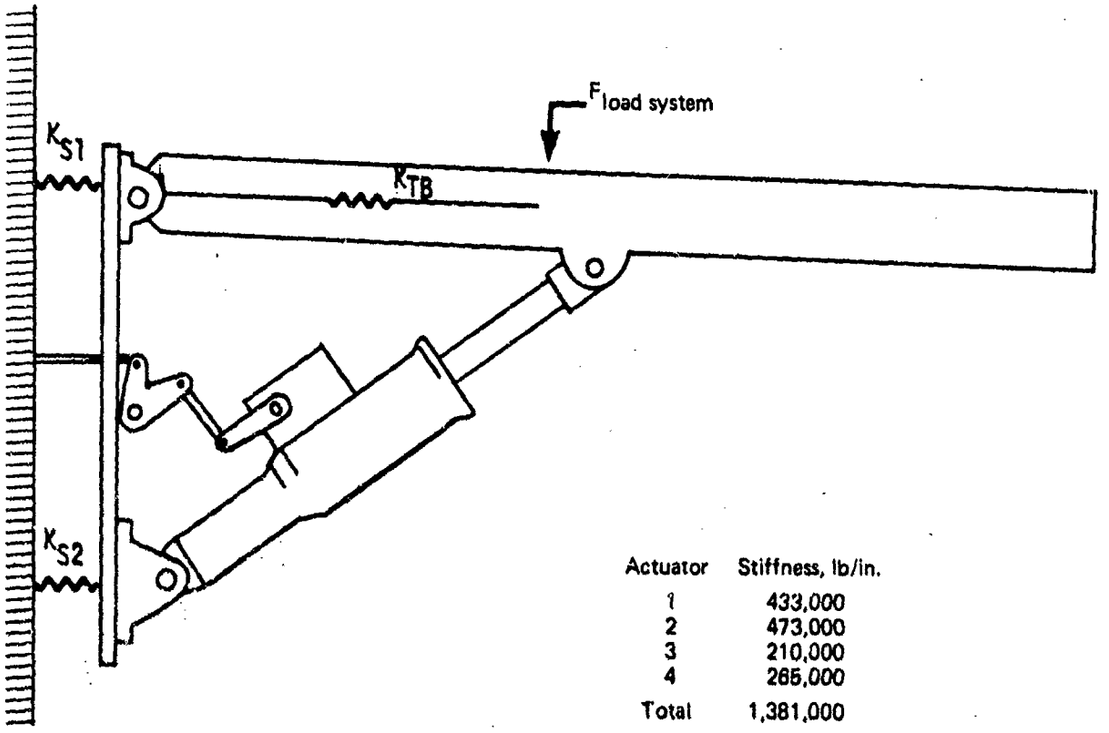

Actuator	Stiffness, lb/in.
1	433,000
2	473,000
3	210,000
4	265,000
Total	1,381,000

FIGURE 81.–SYSTEM STATIC STIFFNESS–FORWARD CENTER OF PRESSURE, ZERO STABILIZER

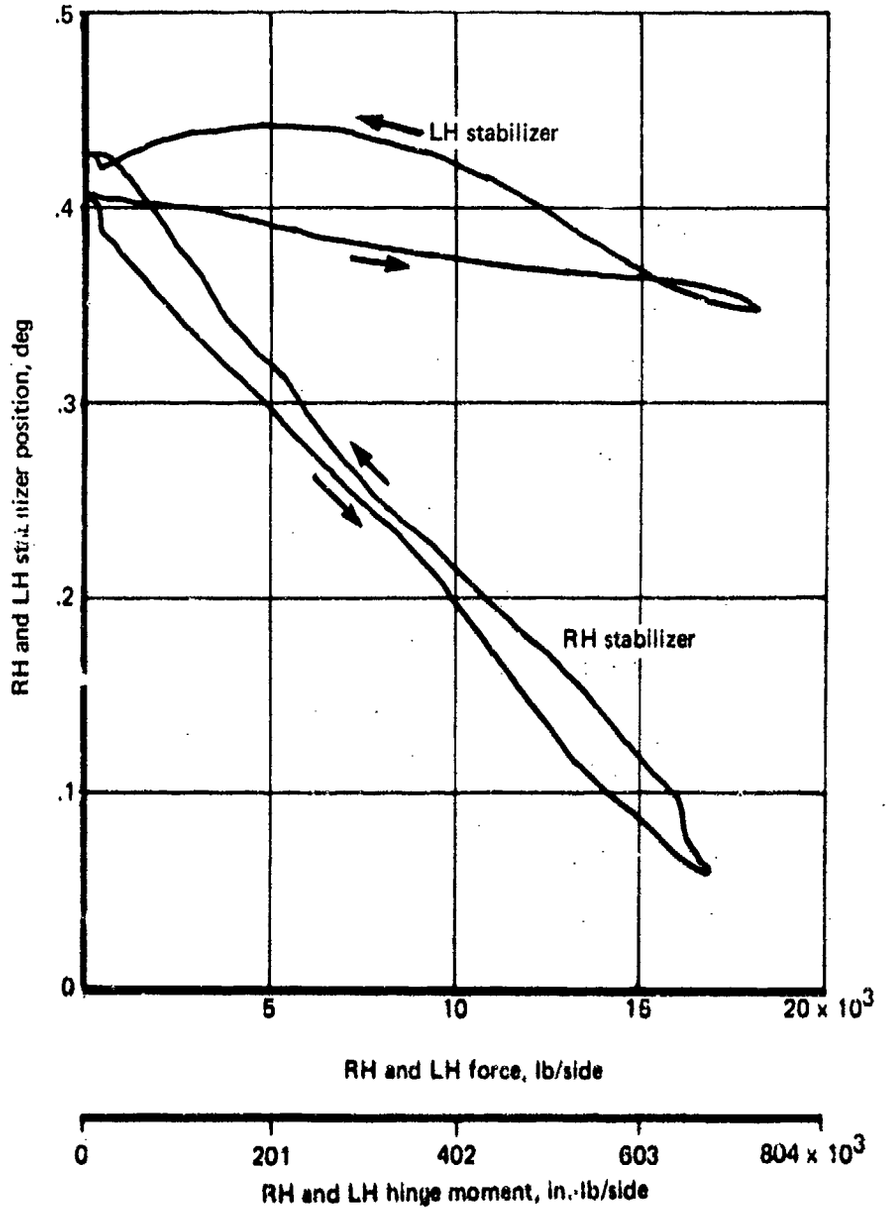

FIGURE 82.–ASYMMETRIC SURFACE MOTION UNDER LOAD

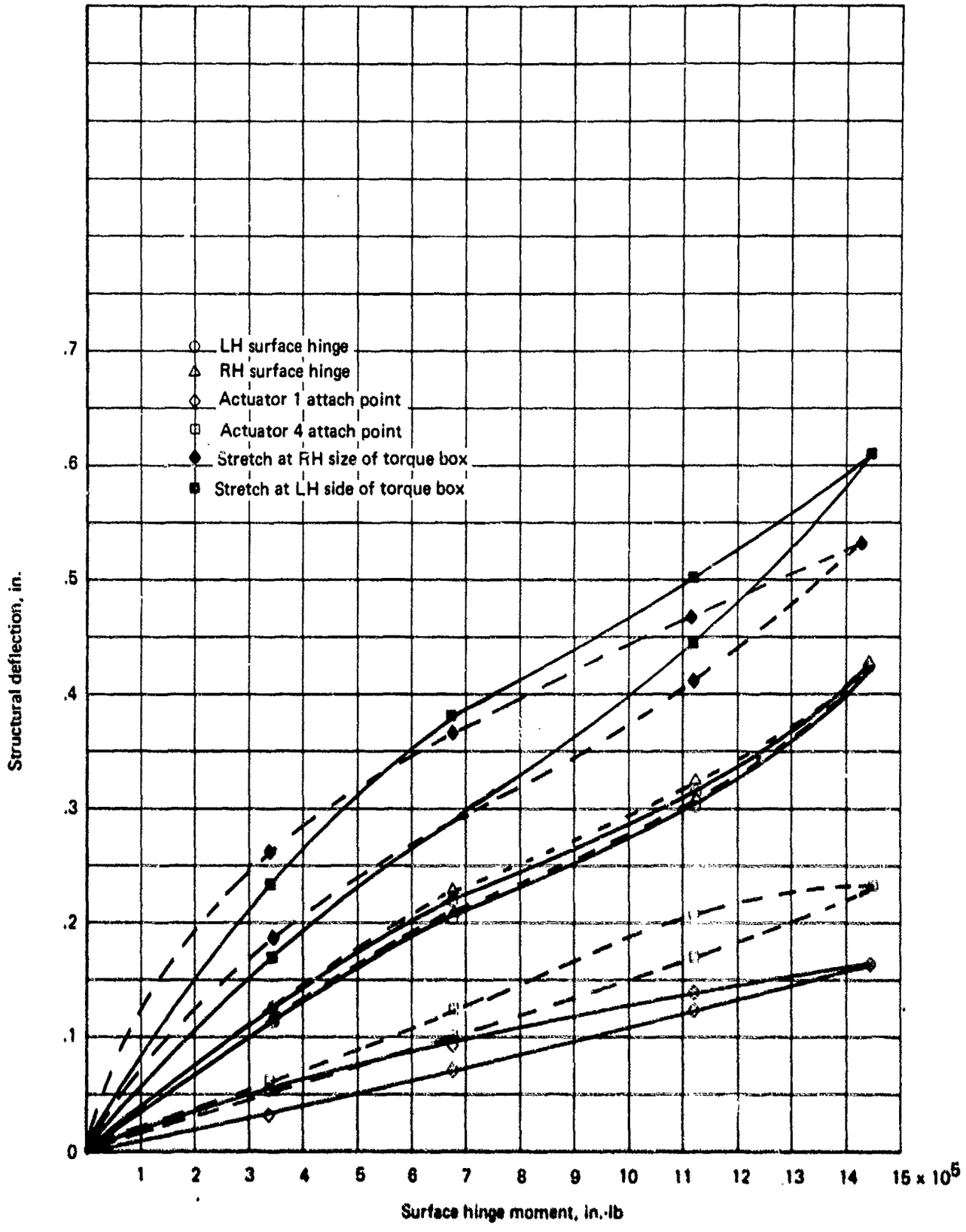

FIGURE 83.--HORIZONTAL STRUCTURAL DEFLECTION

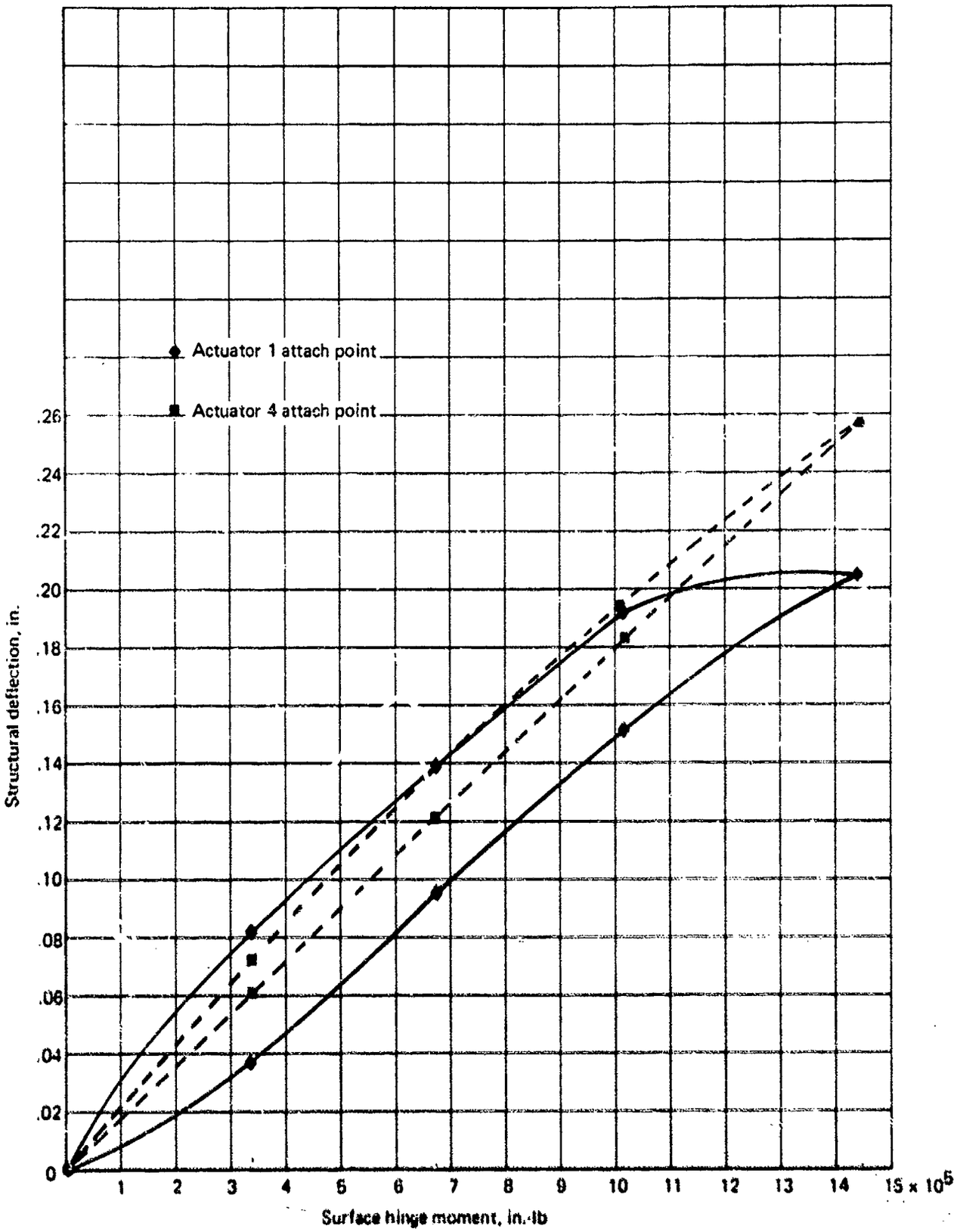

FIGURE 84.–VERTICAL STRUCTURAL DEFLECTION

The static stiffness limit of 124,000 lb/in. for actuator synchronization was exceeded by the installed actuators with structural feedback. The effect of the increased stiffness on actuator force synchronization was not obtained because the actuators were individually adjusted to be within the force synchronization tolerance on installation to compensate for structural and actuator dimensions that were out of tolerance.

The flutter stiffness, the hysteresis, and the actuator static position error under load all tend to be improved by static stiffness being higher than design values.

The most dependable method of ensuring static stiffnes values for actuation systems and structure of this complexity would be to eliminate all structural influences and design the actuator and its installation to give the static stiffness value desired. This can be achieved by providing internal pressure feedback or by providing a separate reaction structural member and appropriately located linkage to produce a controlled structural feedback.

5.4.6 Electrical Stiffness Compensation Test

If the static stiffness is too low to satisfy the static position error due to load, it can be increased over a limited frequency range by a compensated position feedback path operating in parallel with the normal mechanical feedback path. For an uncompensated system, the static stiffness of an actuation system must be less than its dynamic stiffness to maintain stability. However, as shown in appendix A, use of electrical compensation can increase static stiffness above dynamic stiffness and still maintain stability.

The test system was readily adaptable to testing of this concept, since the actuators contained electrical position sensing devices and electric command servos.

5.4.6.1 Test Objective

The objective of the test was to demonstrate that the static stiffness could be increased by a limited amount, with no change in the frequency-dependent dynamic stiffness or the stability margin of the system.

5.4.6.2 Test Description

The uncompensated static stiffness of a single actuator was determined by driving it with the other three actuators. The single actuator static stiffness was increased by a factor of two with the electrical compensation shown in figure 85.

The compensated stiffness transfer function is discussed in appendix A. The compensation was designed as follows:

- Set the numerator to cancel the EC servo break frequency.
- Set the denominator and gain such that the single actuator static stiffness is doubled, but with minimum change of the frequency-dependent dynamic stiffness and actuator stability.

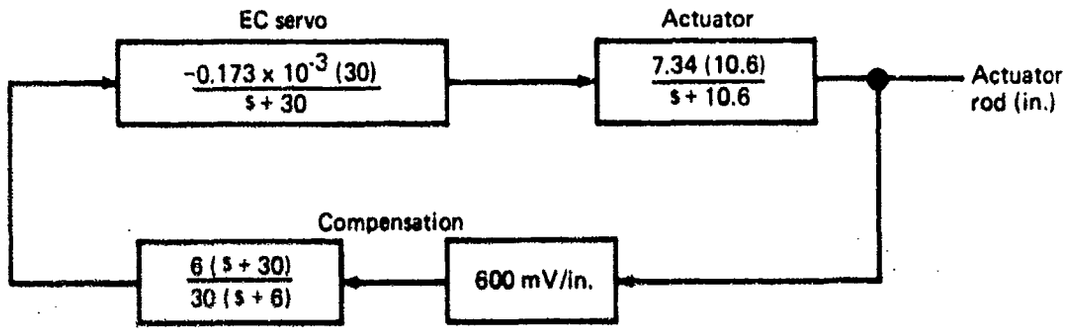

FIGURE 85.–ELECTRICAL STIFFNESS COMPENSATION

Compensation networks were applied to all four actuators. Stability tests, hysteresis tests, and force synchronization tests were conducted with the compensated system.

5.4.6.3 Test Results

The system static stiffness using a single, uncompensated actuator with no structural influences was measured to be 105,000 lb/in. The uncompensated stiffness frequency response associated with this actuation configuration is shown in figure 86. With electrical compensation, the single actuator system static stiffness was 200,000 lb/in. The stiffness frequency response of the compensated actuator shown in figure 87 verified that the frequency-dependent dynamic stiffness was virtually unchanged.

Stability, force synchronization, and static performance were measured with all four actuators operating with compensation. The closed-loop damping ratio was unchanged with compensation, and no perceptible difference in force synchronization could be detected. The repeatability improved from 0.07° to 0.012°, primarily due to the increase in steady-state feedback gain (fig. 88). Test results are summarized in table 10.

5.4.6.4 Conclusions

Electrical compensation feedback can be used to increase the static stiffness of an actuation system by a predictable increment, if the static stiffness of the uncompensated system is known. The static load error and repeatability of the system can be improved with no change in system stability margin.

5.4.7 Stiffness Summary

Sections 5.4.1 through 5.4.6 have been concerned with actuation system stiffness. It has been explained that the designer must be concerned with actuation system stiffness at all frequencies. The design constraints are based on closed-loop requirements. By using the open-loop frequency response test data plus the static stiffness test data, closed-loop stiffness frequency response can be constructed. In the electric stiffness compensation testing, a single actuator system closed-loop frequency response was measured. The asymptotic approximation of closed-loop stiffness constructed from open-loop test data and the stiffness frequency response test data are compared in figure 89.

The static stiffness of the system has been shown to be a function of both the installed actuator effective pressure gain and the stiffness of the mounting structure. Figure A-6d in appendix A shows the effect on the stiffness frequency response of changing the pressure feedback gain. Increase in static stiffness due to structural feedback has the same effect.

The stiffness tests show an increase in the average single actuator system static stiffness from 105,000 lb/in. to 290,000 lb/in. with the surface trailing edge down and 345,000 lb/in. with the surface trailing edge up. These results were obtained by point loads on the surface. The true value of static stiffness for flutter restraint or system stability was estimated to be lower than these values. For flutter stiffness requirements, the structural deflection would come from a distributed air load. For stability, the structural deflections would come from the surface inertia. Both flutter and stability static stiffness would be lower than that

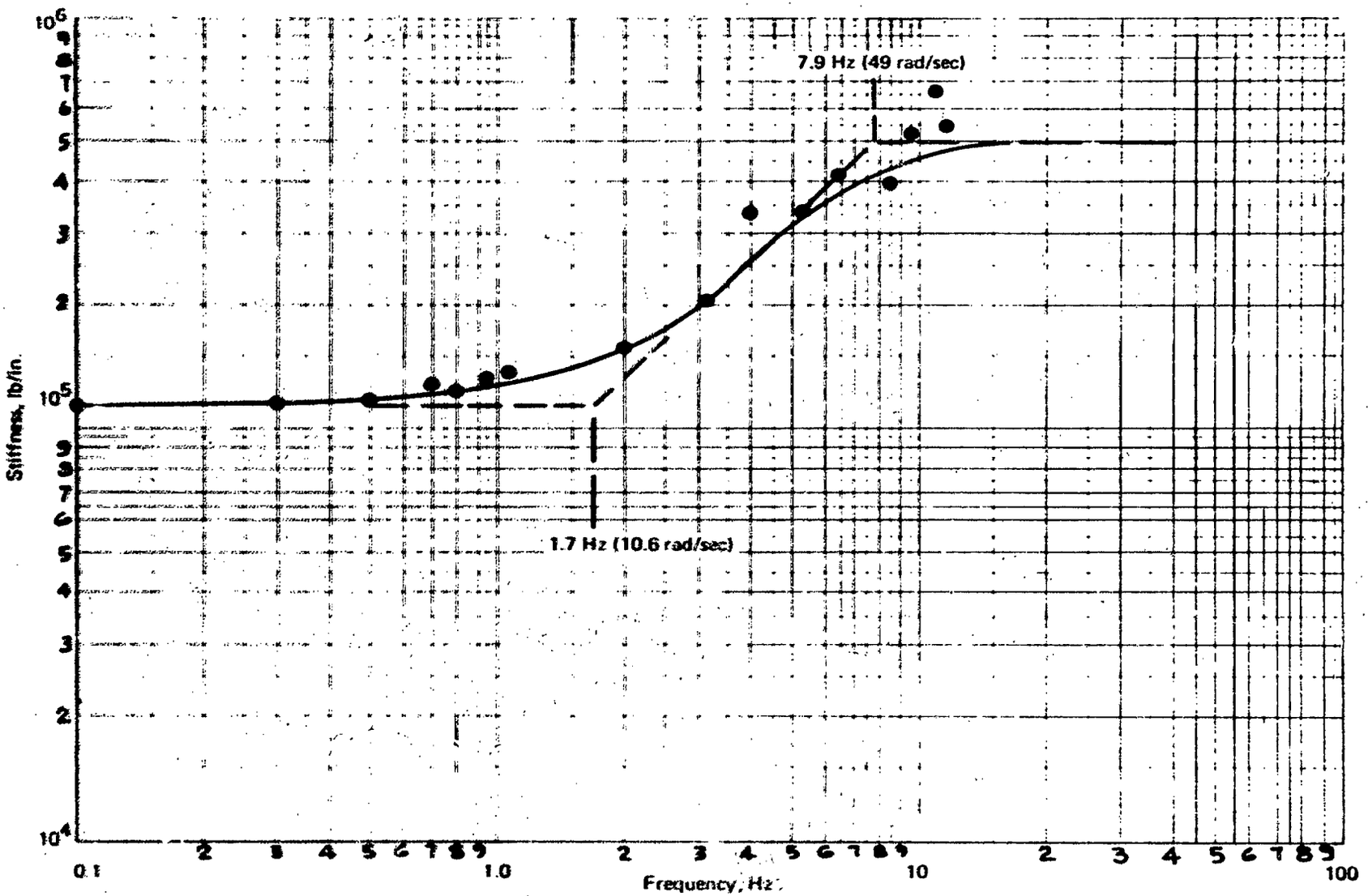

FIGURE 86.–SYSTEM STIFFNESS FREQUENCY RESPONSE–SINGLE ACTUATOR (CLOSED LOOP)

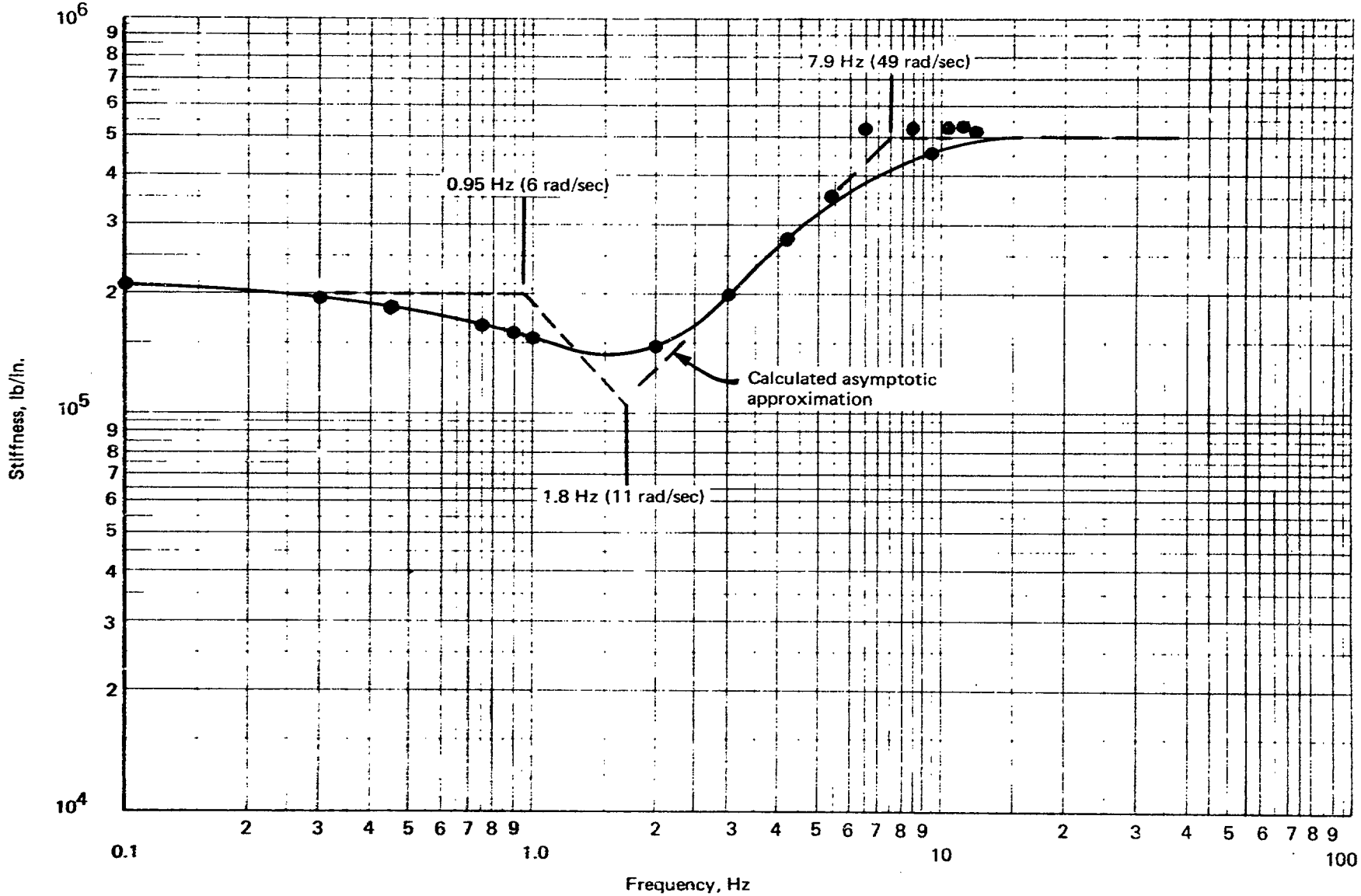

FIGURE 87.—SYSTEM STIFFNESS FREQUENCY RESPONSE—SINGLE ACTUATOR (CLOSED LOOP) WITH ELECTRICAL STIFFNESS COMPENSATION

TABLE 10.–SUMMARY OF COMPENSATION RESULTS

	Without compensation	With compensation
Single-actuator stiffness	105,000 lb/in.	200,000 lb/in.
Hysteresis	0.07°	0.012°
Force synchronization	No change	No change
Basic stability	No change	No change

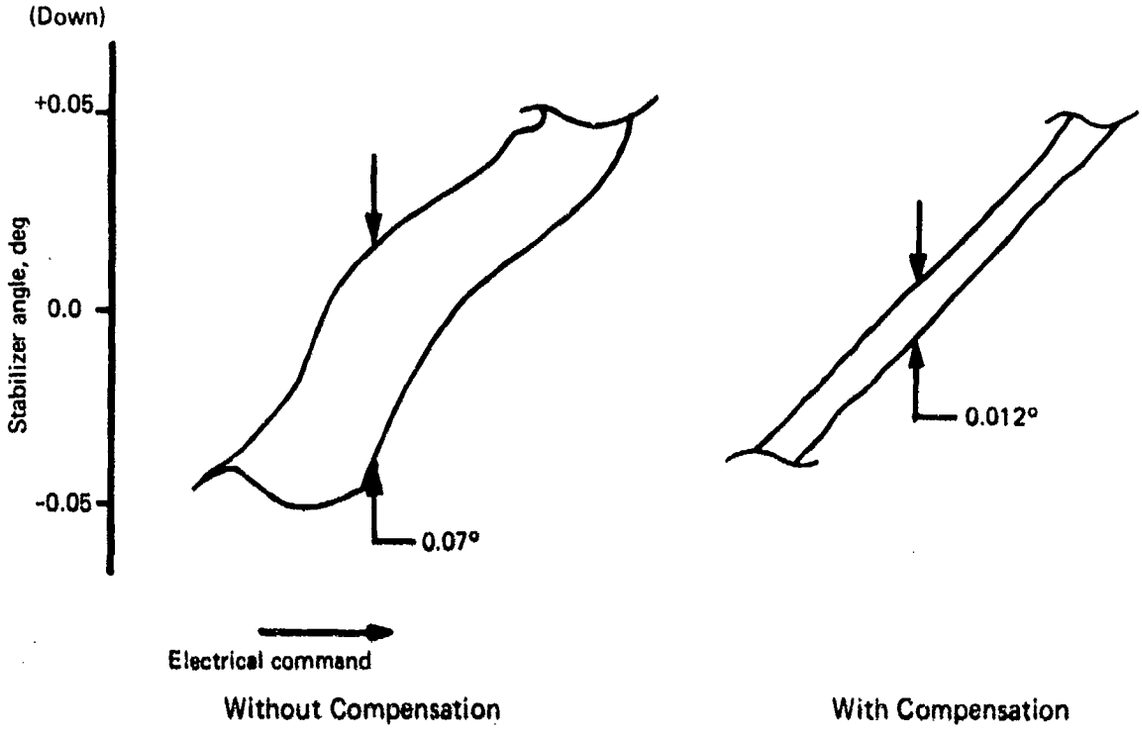

FIGURE 88.–EFFECTS OF SYSTEM STIFFNESS COMPENSATION ON HYSTERESIS

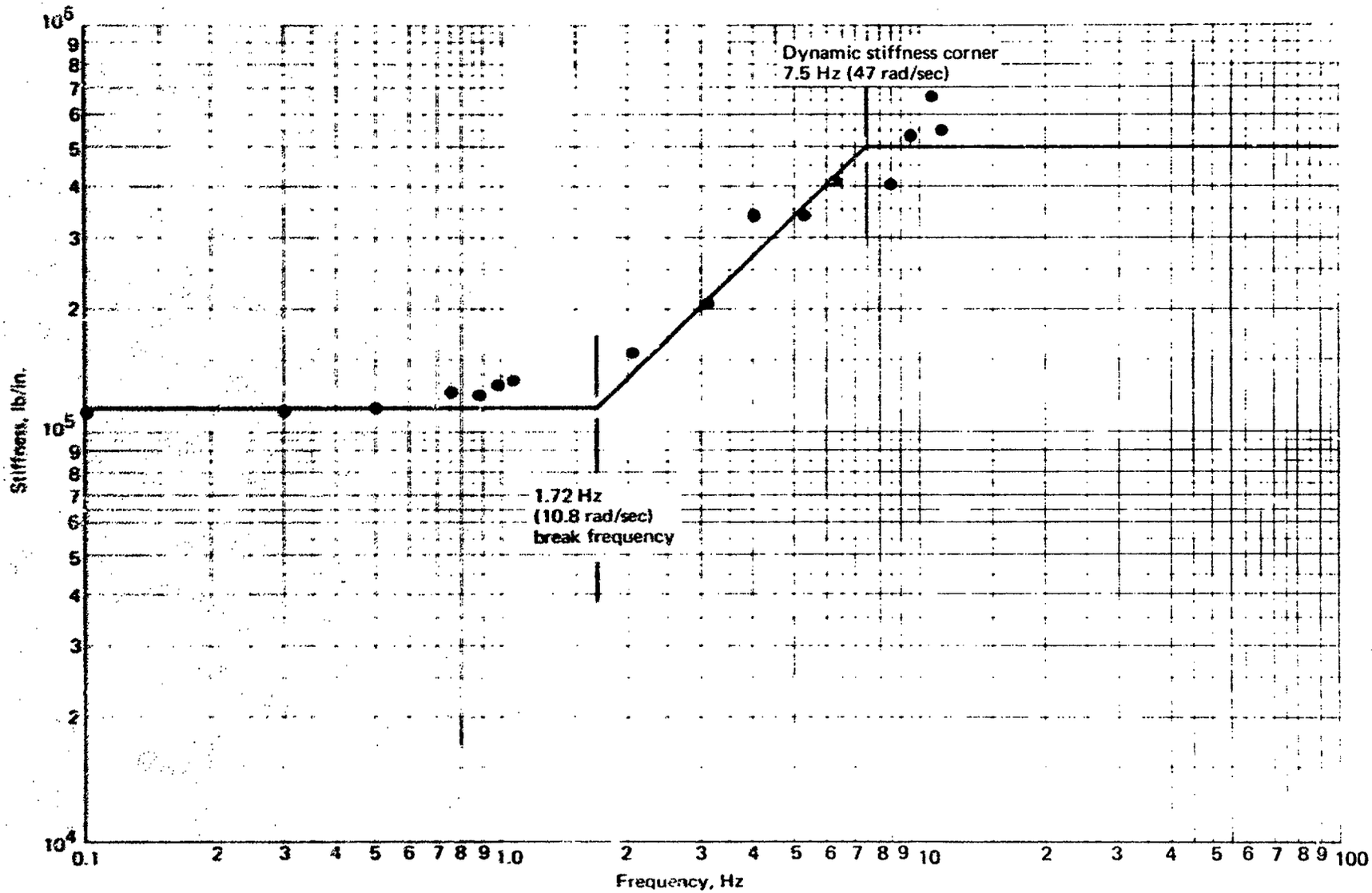

FIGURE 89.–CLOSED-LOOP SYSTEM STIFFNESS FREQUENCY RESPONSE–150° F

measured by point loading. Based on computer studies, a value of 250,000 lb/in. was chosen as a normal single actuator system static stiffness to illustrate the change in stiffness with operating condition. The stiffness frequency response using 250,000 lb/in. is labeled "normal installed actuator–closed loop" on figure 90.

Shown for comparison is a curve labeled "acceptable for flutter restraint." This stiffness would have resulted in a 1-kn flutter margin for the SST horizontal stabilizer for the symmetric flutter case. Since flutter stiffness requirements depend on the structural backup spring as well as the actuator stiffness, the curve should only be considered as typical.

System stiffness frequency responses for stall conditions, for limits of blowback conditions, and for typical under-command conditions are shown in figure 90. The under-command condition with reasonable rates and load pressures shows small stiffness degradation. The stall condition and slow backdrive conditions are less stiff. The reduction in stiffness with fast backdriving leaves almost no stiffness for flutter restraint.

The degradation in stiffness resulting from under-command and stall conditions could probably be reduced to acceptable levels by actuator and/or structural changes to increase stiffness. This is also true of the slow blowback case. A system that is subject to rapid backdriving must have a method of flutter restraint not dependent on actuation system stiffness if the duration of the backdriving condition will allow flutter to develop. Since the slow backdriving does not significantly reduce stiffness, it is possible to restrain flutter by sizing the bypass valve to prevent rapid backdriving. This arrangement would require that loads caused by actuator failures be relieved by another valve controlled by failure detection and switching logic.

Electric stiffness compensation has been proven to be a valid method of increasing the low frequency stiffness and static performance without affecting actuator stability or high-frequency performance.

A system that depends on structural feedback through a complex structure to control static stiffness is undesirable and should be avoided. If the structural feedback is destabilizing (increases static stiffness), it magnifies any structural asymmetry. The best methods of static stiffness control are through pressure feedback or reaction linkage that can be controlled.

5.5 BOTTOMING LOADS TEST

The load imposed on an actuator and surrounding structure upon impact against integral end stops is:

$$F_i = \frac{\omega_i (K_s J)^{1/2}}{R}$$

where

F_i = force of impact (lb)

ω_i = impact velocity (rad/sec)

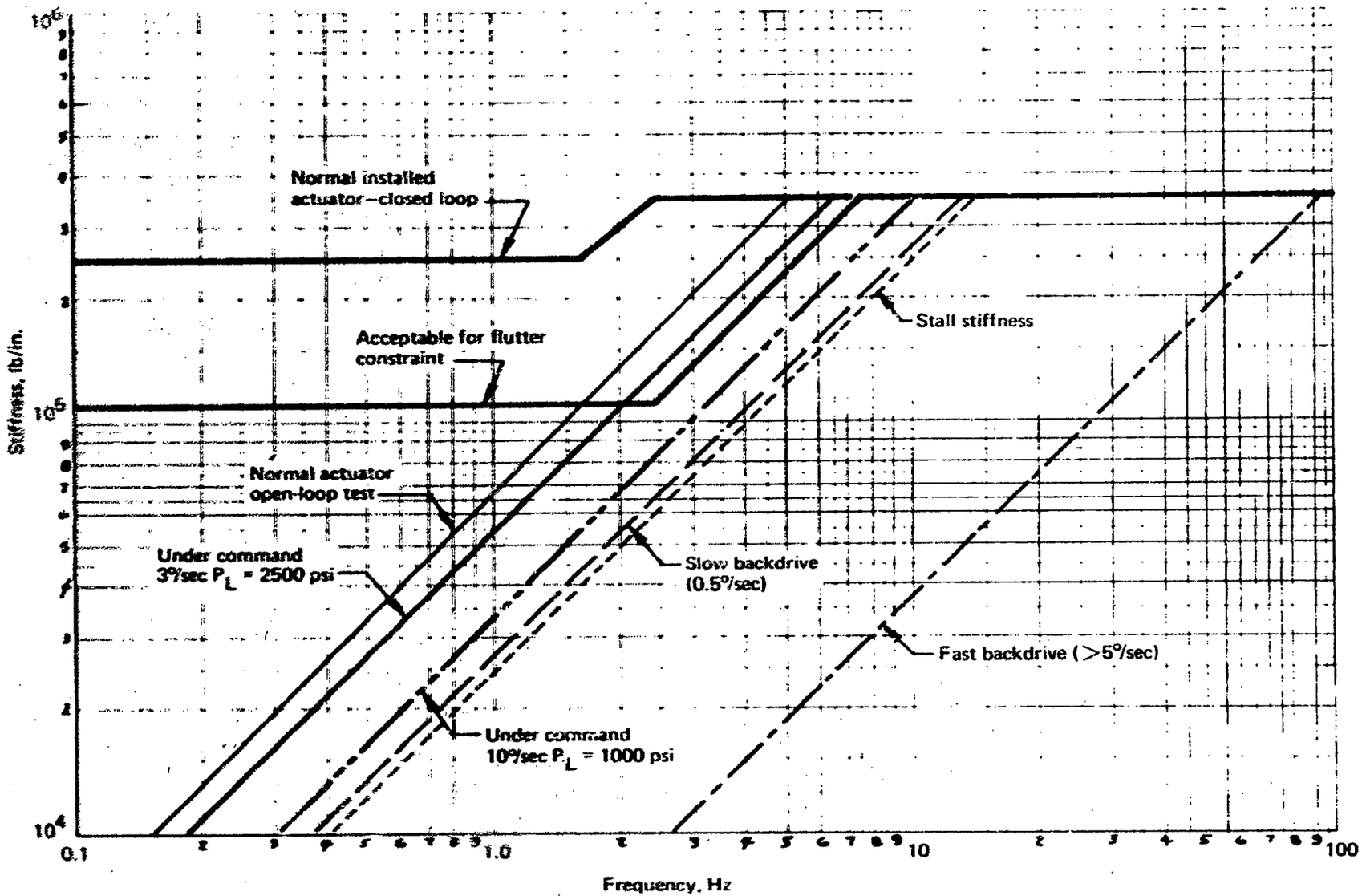

FIGURE 9.–COMPOSITE SYSTEM STIFFNESS FREQUENCY RESPONSE

K_s = structural spring rate (in.-lb/rad)

J = control surface rotational inertia (lb-in.-sec^2)

R = actuator moment arm at impact (in.)

Because of the geared elevator geometry, the inertia of the SST horizontal stabilizer varied with surface angle as shown in figure 91. It is largest in the trailing-edge-up condition (maximum negative surface angle), where the actuator moment arm is the smallest. Because of these geometry factors and the inexact structural spring values, the actuator design had end snubbing in the extend end only.

Early in the test program, the simulated elevator structure failed and the elevators were removed. The rotational inertia of the horizontal stabilizer with no elevators decreased as shown in figure 91. All data in the bottoming loads testing were taken without the elevators installed and have been extrapolated to the elevator-installed configuration to verify the design.

5.5.1 Test Objective

The bottoming loads tests were performed to verify the design of the end snubbing and to determine the loads imposed on the actuator and surrounding structure by impact at maximum design surface rate.

5.5.2 Test Description

The surface was driven at the maximum rate possible against the end stops in both directions. The actuator load pressures, the forces in one actuator attachment, piston rate, and surface rate were measured.

5.5.3 Test Results

Figure 92 shows data for the actuator being driven against the down stops. The maximum surface rate achievable was 23.4°/sec. When the actuator impacted against the stops, the load developed was 12,000 lb. When this value is adjusted to reflect the 29°/sec design velocity and for the elevator effects, the impact force would be 25,300 lb.

Figure 93 shows the actuator being driven against the up stops. The maximum surface rate developed was 23°/sec. When the actuator entered the snubbing region, the surface rate was slowed to 3°/sec. When the piston hit the end stops at this low rate, the force developed was very small (less than 3000 lb). A force level this low made extrapolation of data for adjustment to high rates and elimination of snubbing difficult. Therefore, the impact force from the other end of the stroke was adjusted to the higher values. After adjustment for differences in moment arm, increased inertia, and the 29°/sec design surface rate, the non-snubbed impact force for the trailing-edge-up direction was 40,000 lb.

It should be noted that the acceleration forces for both cases were higher than the impact forces. In the trailing-edge-up direction, the acceleration force was 50,000 lb, which was greater than the value that was calculated by assuming no snubbing and including elevator effects.

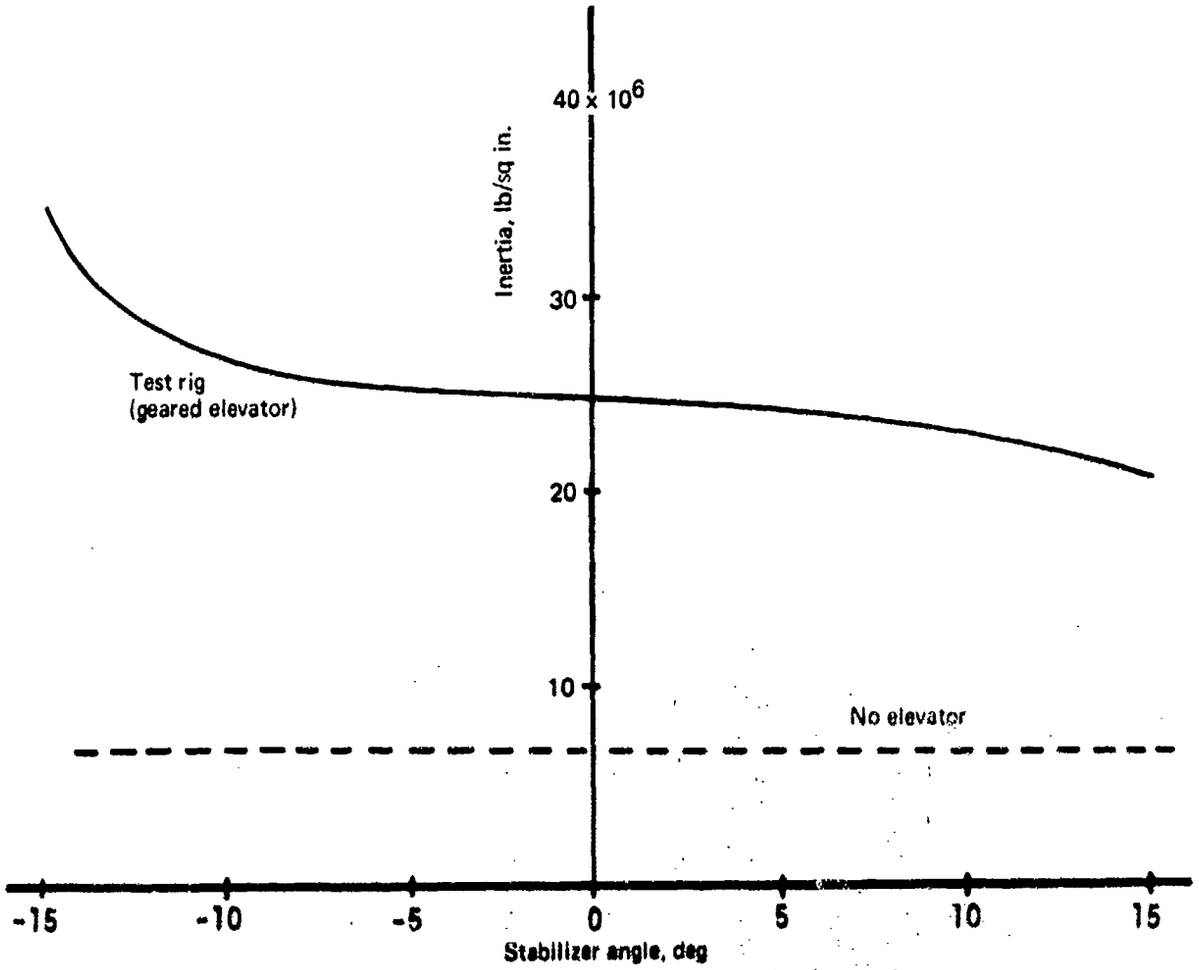

FIGURE 91.–HORIZONTAL STABILIZER ROTATIONAL INERTIA ABOUT HINGE LINE (PER SIDE)

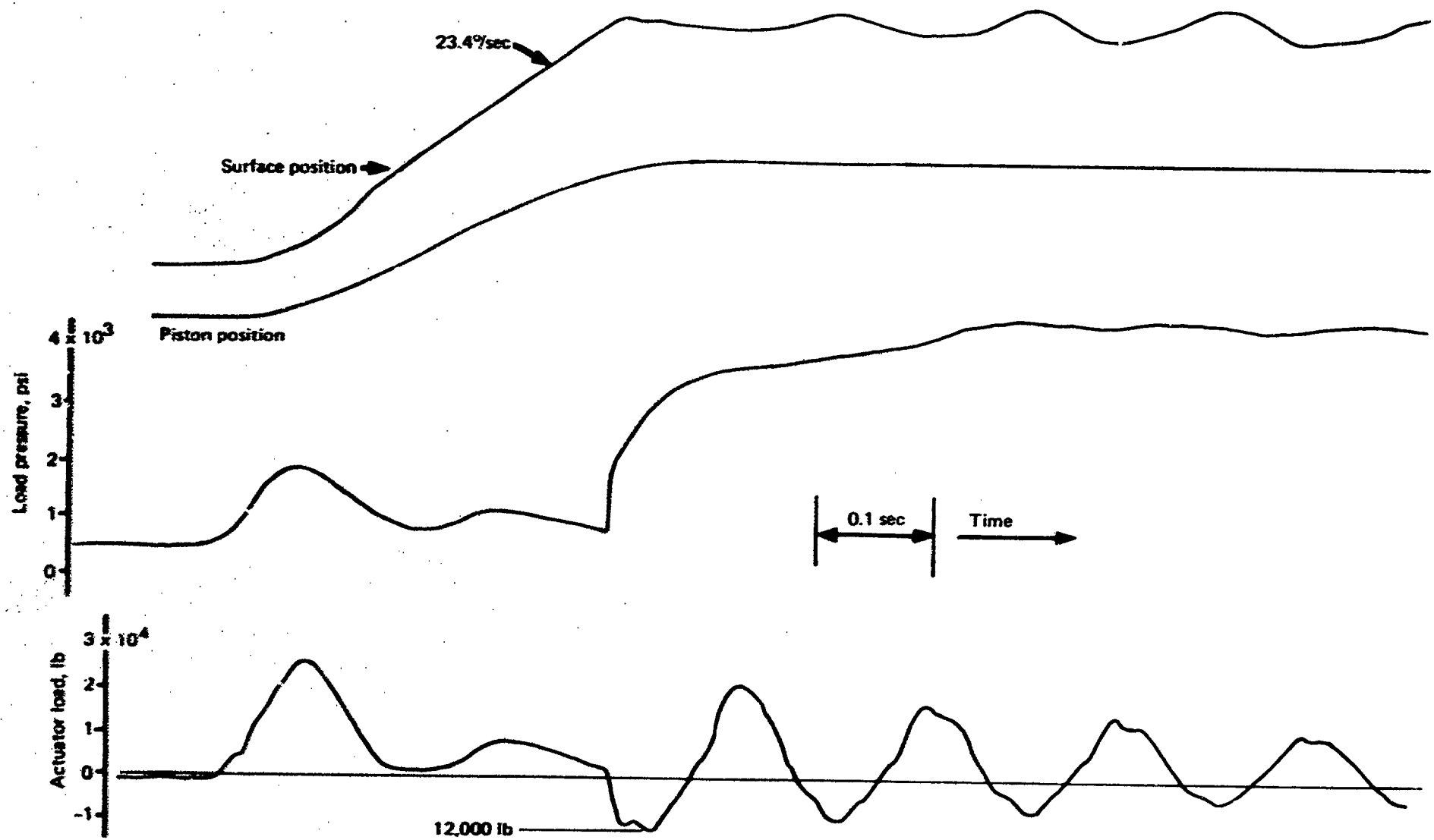

FIGURE 92.–ACTUATOR BOTTOMING–DOWN STOPS, NO SNUBBING

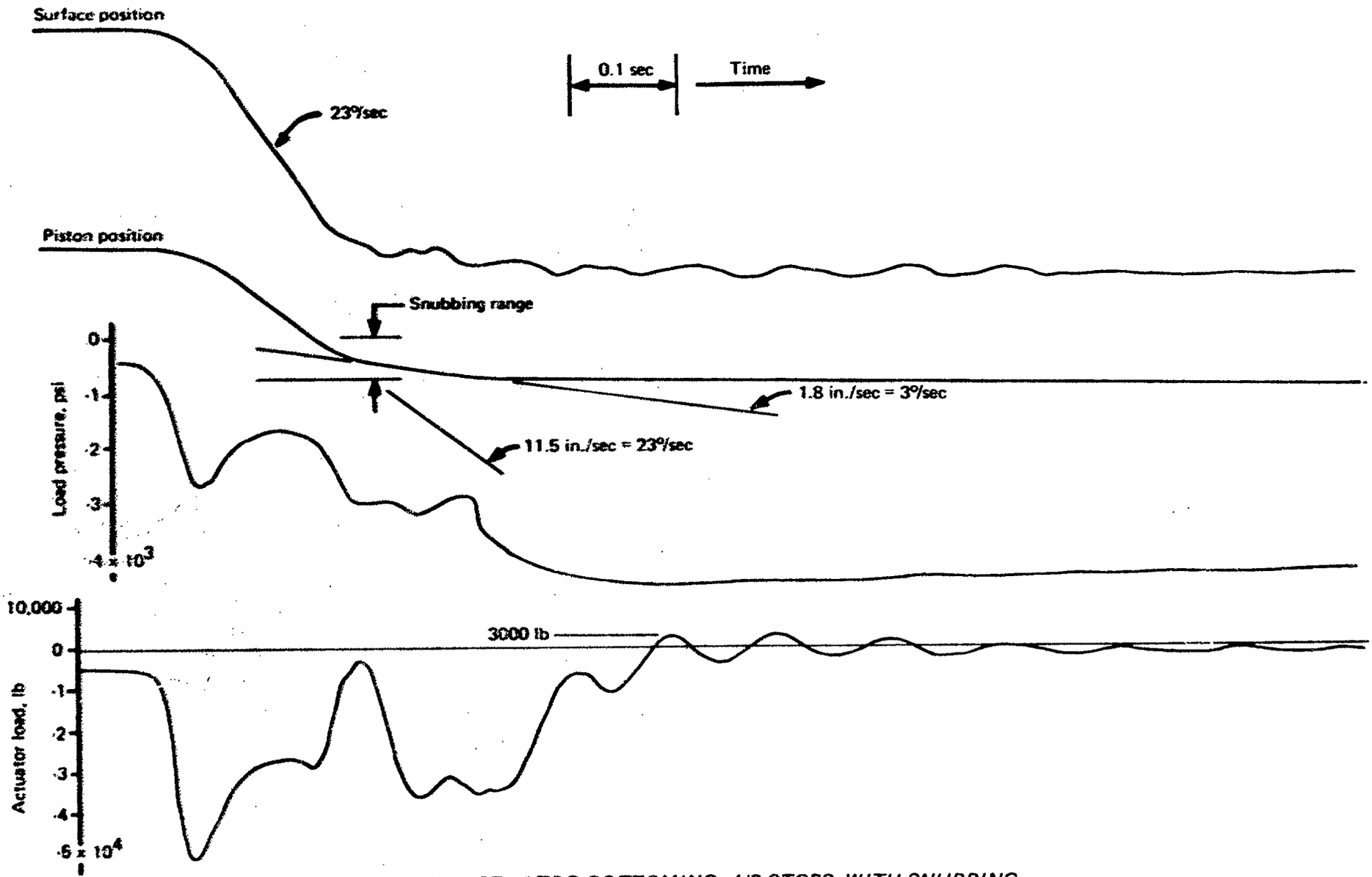

FIGURE 93.–ACTUATOR BOTTOMING– UP STOPS, WITH SNUBBING

5.5.4 Conclusions

Snubbing was very effective in this actuator design. However, actuators capable of exerting large forces can also withstand high loads due to impact. The SST horizontal stabilizer actuators were designed to exert forces of 87,000 lb each. In no case did the impact loads without snubbing approach this value. Unless fatigue loading would shorten the life of the actuator, snubbing cannot be justified.

5.6 MAIN ACTUATOR FAILURE DETECTION AND EFFECTS TESTS

In a parallel installation of flight control actuators, some provision must be made to offset the effects of single actuator malfunction so that the remaining actuators can continue to function at levels adequate for safe flight. In the case of the SST longitudinal control system, certain malfunctions and failures within an actuator can be counteracted by providing a pressure-operated relief/bypass valve on each actuator. Operation of this valve is described in section 3.2.2.1.

The primary purpose of this relief/bypass valve is to act as an overpressure relief valve for the main servo actuator in both the pressurized and unpressurized conditions (see fig. 94). For example, if a control link to a main control valve becomes jammed or disconnected, the actuator would try to go hard-over and would resist movement of the other actuators when they attempt to backdrive the malfunctioning actuator against its hardover command. This condition is prevented by bypassing the cylinder-to-cylinder flow whenever load pressure exceeds supply pressure.

By incorporating an electrical transducer to sense the position of the relief/bypass valve slide, a remote failure indication of abnormal operation of the main actuator is provided to the flight crew. A "failure" is indicated when either cylinder pressure equals the supply pressure. The indicator system was also mechanized to indicate valve motion when hydraulic power was supplied to the actuators. This function was to be used during preflight operations to indicate that the relief/bypass valve was not jammed.

5.6.1 Test Objectives

The objectives of these tests were to verify the hydraulic function of the main actuator relief/bypass valve, to determine the electrical signal characteristics to enable design of the failure detection circuitry, to establish the failure detection and indication sensitivity of the relief/bypass valve to various misrigging or failure conditions, to evaluate the detection method as an effective means of signaling a failed or misrigged condition, and to determine if the relief/bypass valve is stable in a variety of bypass conditions.

5.6.2 Test Description

The relief/bypass valve failure detection and indication sensitivity was tested by misrigging one actuator by different amounts with respect to the other three actuators. The system was commanded at several different rates to determine what conditions of loading, misrigging, and rate of motion would result in failure detection signals.

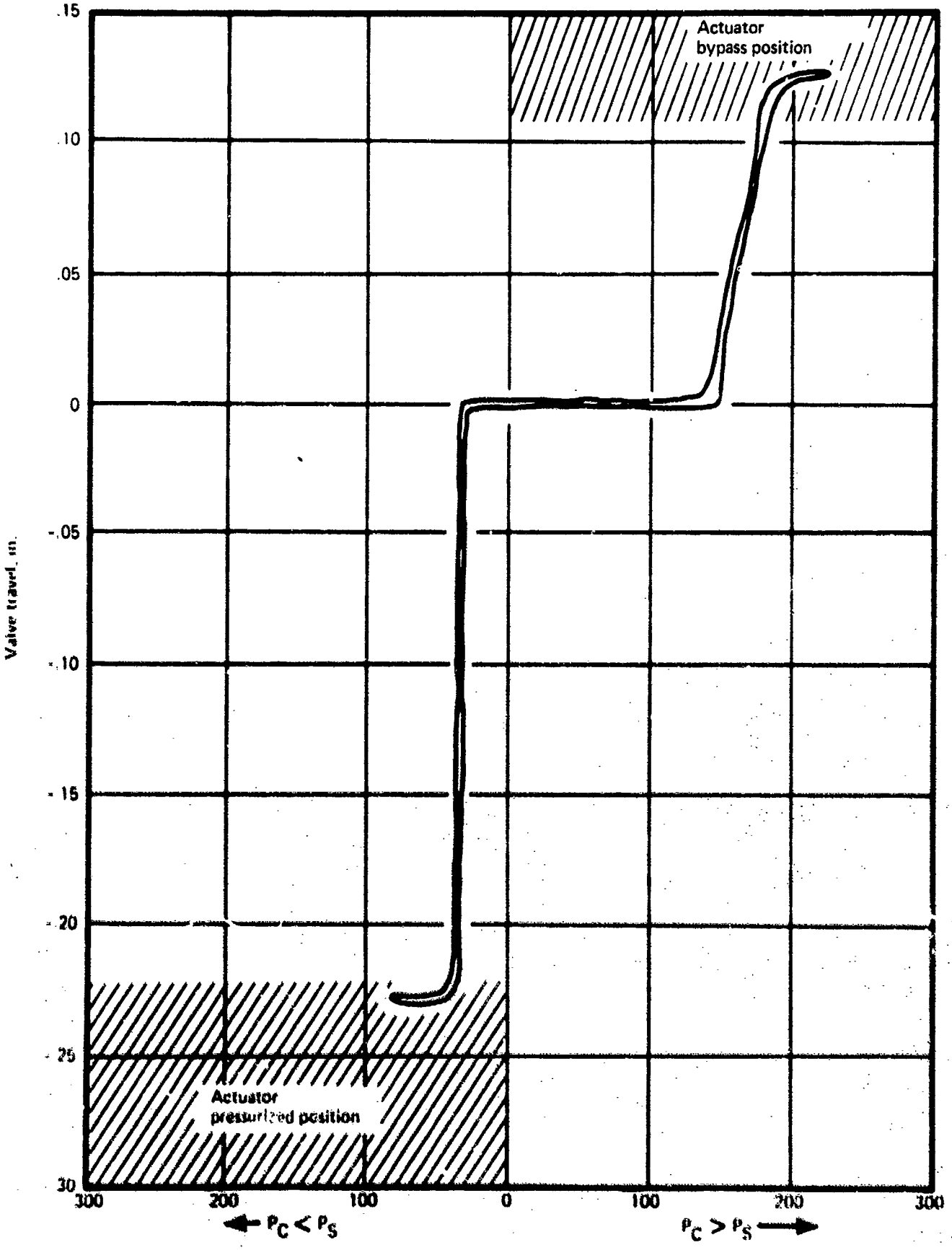

FIGURE 94.–MAIN ACTUATOR RELIEF/BYPASS VALVE

In combination with the detection tests, hydraulic power to one of the three actuators that was not misrigged was turned off to ascertain the effect on the failure detection scheme of a second failure in the system.

The stability of the relief/bypass valve was evaluated by sinusoidally backdriving an actuator that had been commanded to a hardover position, with and without hydraulic power to the actuator.

5.6.3 Test Results

Figures 95 and 96 show the time histories that verify relief/bypass valve operation for an actuator failed hard-over, unpressurized and pressurized, respectively.

As shown in figure 97, between 2° and 3.5° of equivalent misrigging caused the relief/bypass valve to signal a system malfunction. At 2° misrig, detection was evident only in the extend direction, but at 3.5° misrig there was continuous detection for all rates, extend or retract.

In addition, when an actuator had been misrigged in any amount greater than the equivalent of 2° of stabilizer travel and was backdriven at a rate greater than 2.28°/sec of stabilizer travel, the bypass valve would go into a limit cycle (see fig. 98). The frequency of the limit cycle was audible at approximately 580 Hz and was modulated at 30 Hz. The valve functioned properly when an actuator was backdriven against a hardover command at a rate equivalent to 0.4°/sec of stabilizer travel (see fig. 96).

5.6.4 Conclusions

These tests have shown that the relief/bypass valve operation is affected by the magnitude of force sharing between the actuators as represented by misrigging (see fig. 97). It was pointed out in section 5.3 that the fatigue life of the common mounting structure of the actuators establishes the limit on the degree of force synchronization between them. On the SST this limit was established at 800 psi maximum, and is equivalent to misrigging one actuator approximately 1/4° of stabilizer travel with respect to the other three. These tests have shown that one actuator could be misrigged nearly eight times greater than the established limit without relief/bypass valve operation. Since this is considerably greater than the 1/4° misrig limit, these tests show that the relief/bypass valve would function properly during normal operation for the rates tested.

Also, for the SST a certain probability existed that a combination of airplane maneuvers and gust conditions could produce actuator forces that would exceed the capability of the actuators. Under these conditions relatively little misrigging (1/4°) of one actuator can cause a failure indication. Although the system is within tolerance, this transient condition would result in nuisance failure warnings to the flight crew during this flight condition. Therefore, the failure detection circuitry would have to provide a time delay to prevent transient condition indications.

Stability of the bypass valve is also sensitive to rate of command of the actuators. When the command rate was increased to 2.0°/sec, the valve became unstable.

Mechanical command
No hydraulic power on actuator 3
Actuator 3 main valve fixed in hardover retract position

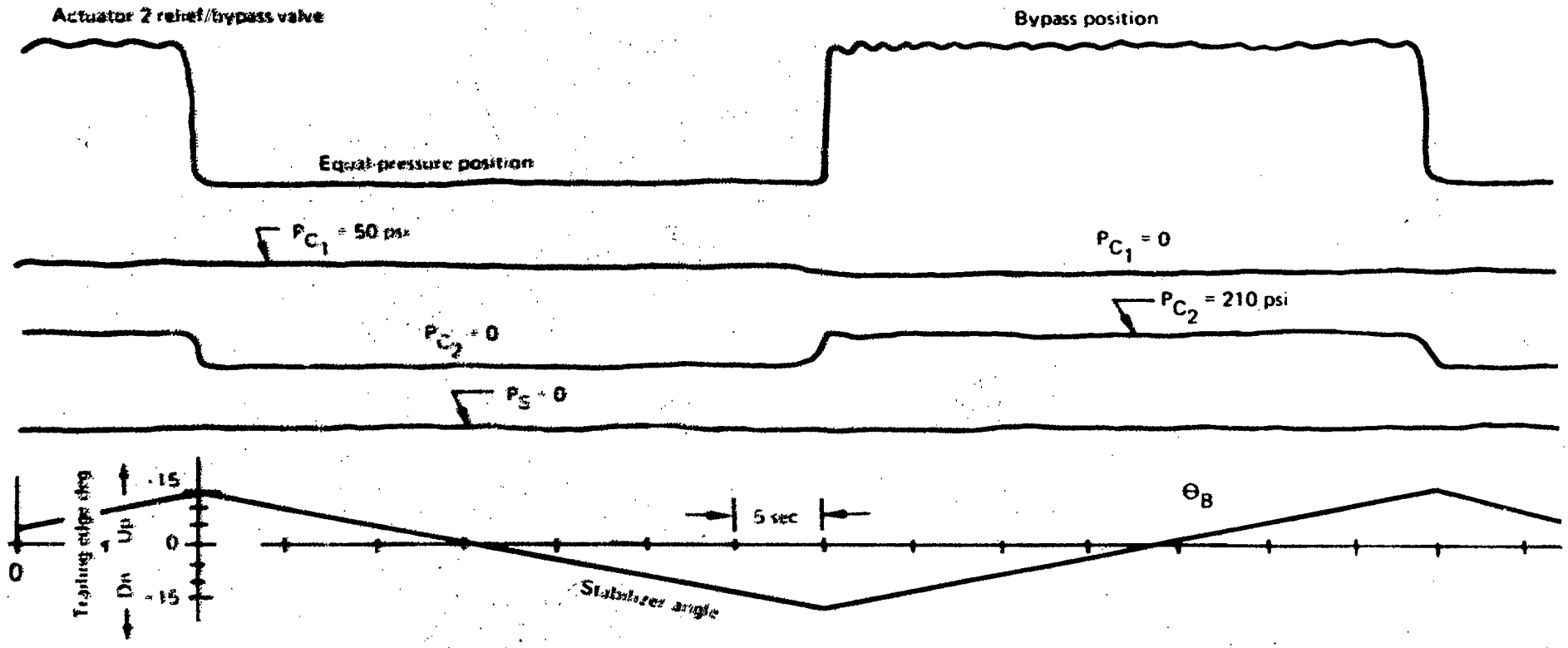

FIGURE 95.–FAILURE DETECTION AND EFFECTS TEST

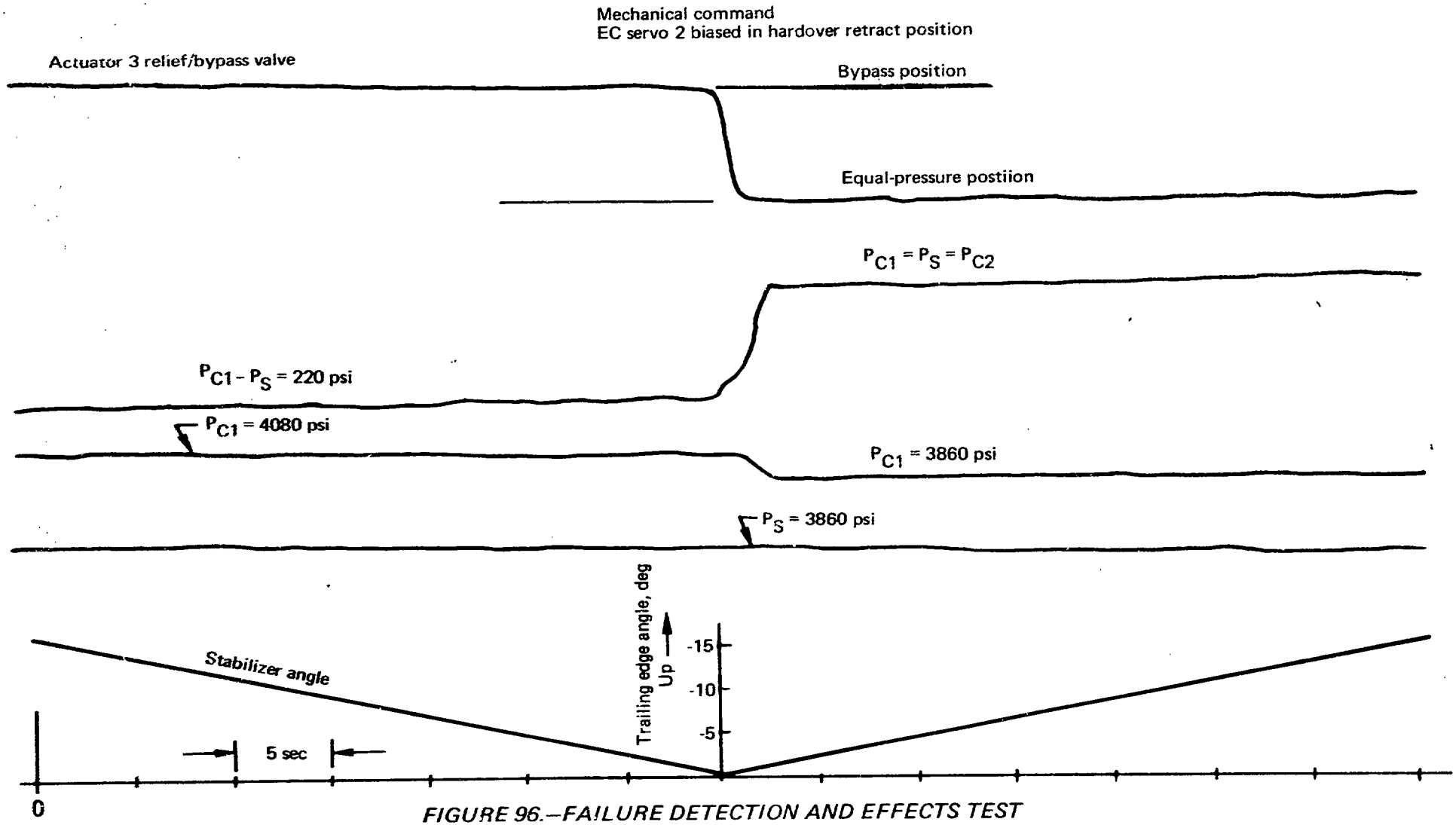

FIGURE 96.—FAILURE DETECTION AND EFFECTS TEST

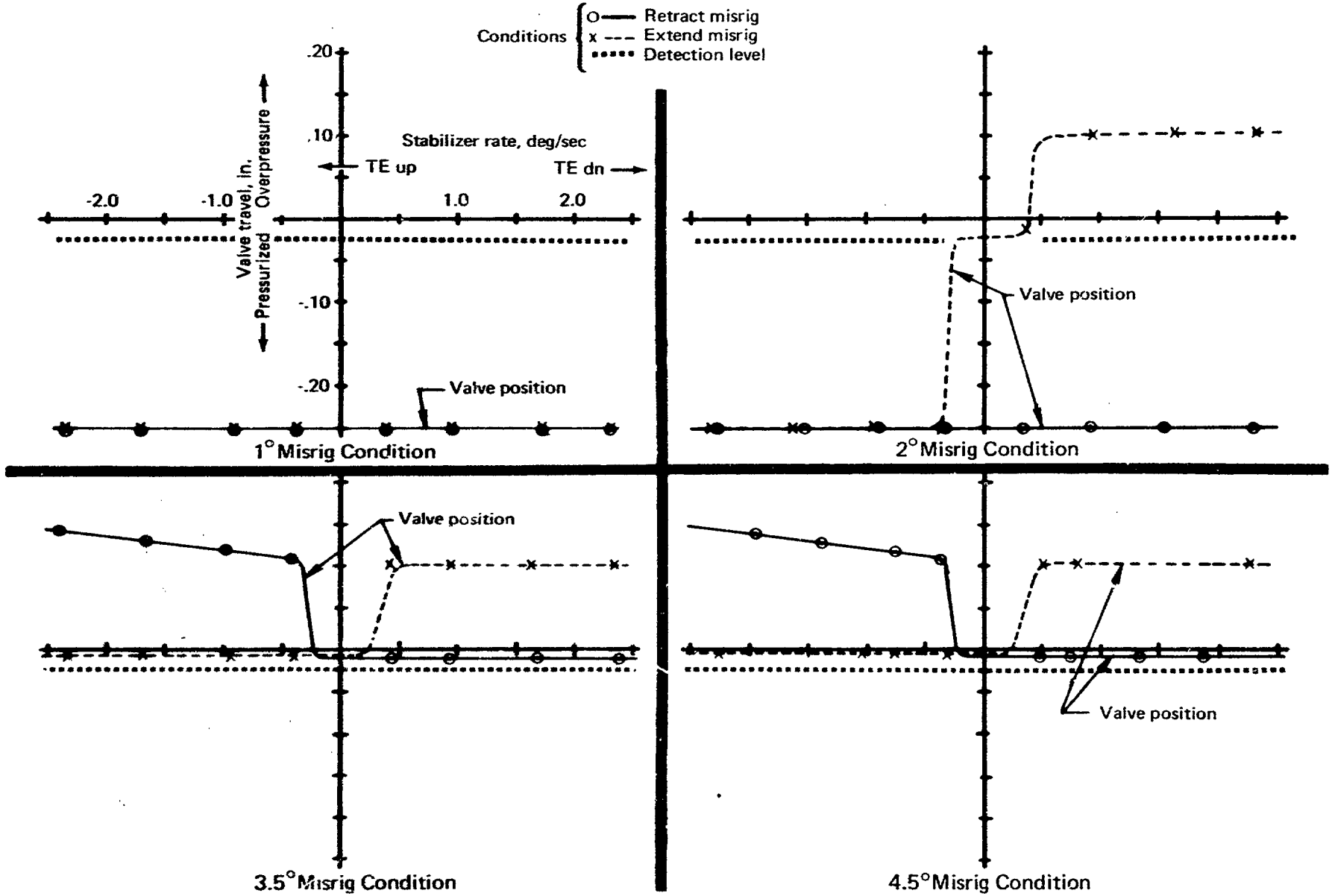

FIGURE 97.—MAIN ACTUATOR BYPASS VALVE—MALFUNCTION DETECTION

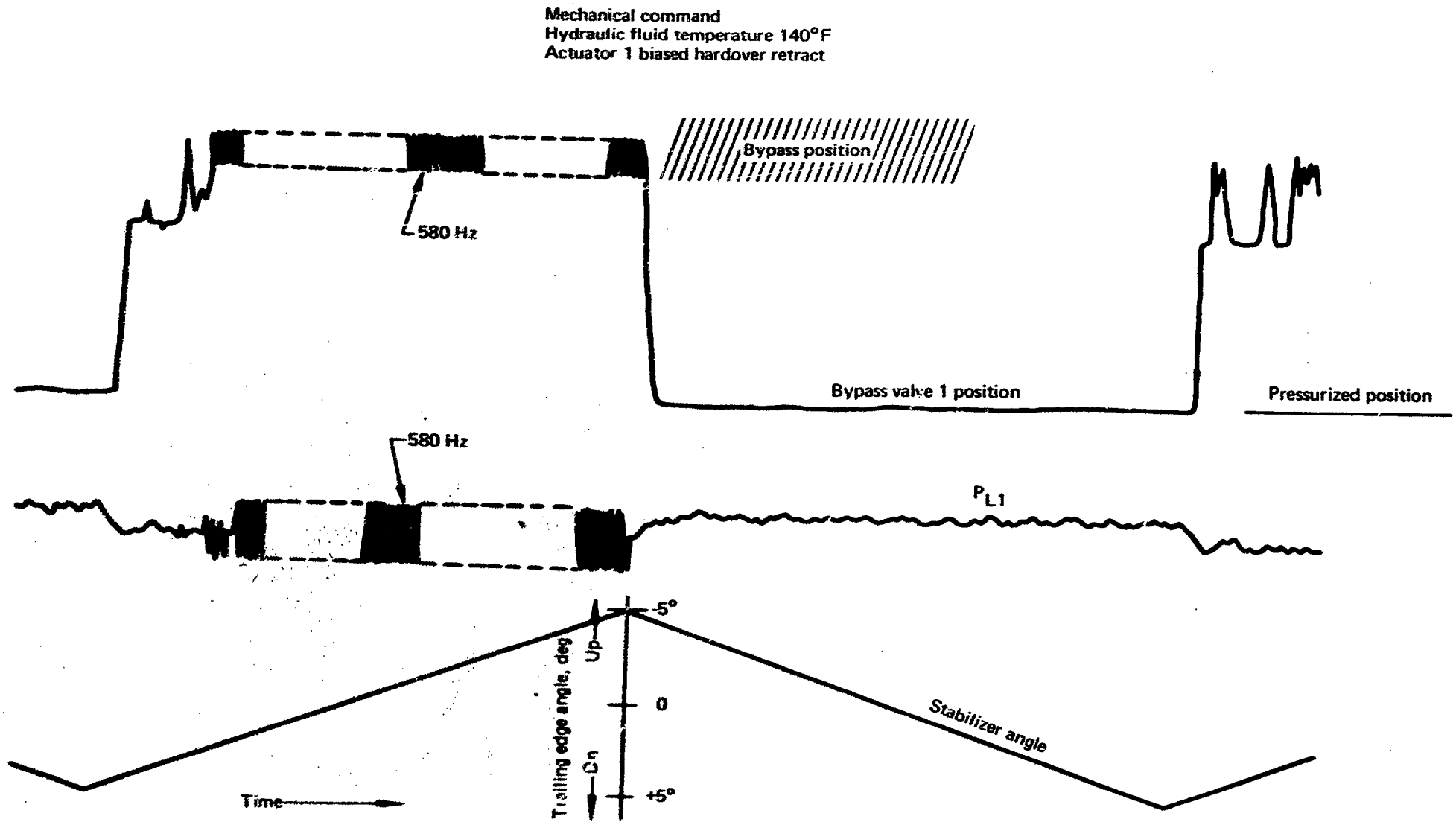

FIGURE 95.–FAILURE DETECTION AND EFFECTS TEST

A review of the design of the relief/bypass valve points out that the valve instability is not caused by either steady-state flow-induced forces or the hydraulic reaction transient forces. Both of these forces on the valve are in a direction that stabilizes it, and both are directly proportional to the area gradient of the valve and the pressure drop through it. Since the area gradient and pressure drop are both large, the steady-state and transient forces would not cause instability. The instability of the valve is believed to be due to non-linearities that are attributed to the hysteresis of the centering springs and stiction in the valve itself. However, this was not investigated during these tests.

5.7 EC SERVO FAILURE DETECTION TEST

Fail-operational capability is achieved by coupling the four EC servos to the EC servo synchronization shaft and by limiting the force of each EC servo by the EC servo equalizer. With this force voting, all four actuators receive similar commands and minimum surface transients when one or two EC servos are failed or shut off.

Because of this fail-operational capability, reliance upon the failure detection system is not required for safety. The failure detection system must annunciate failures to the crew for action, but it can be designed with thresholds and time delays significantly above the system operating levels thereby eliminating "nuisance" and false indications.

However, under certain conditions opening up thresholds and time delays allows passive or oscillatory failures to go undetected. Although an undetected failure does not affect airplane performance, a second failure may cause critical degradation in airplane performance. It is important in the failure detection system design to analyze the electronic system to determine combinations of component failures that can be critical. The companion document to this volume, D6-60271, describes such an analysis used to establish failure mode criticality on the SST lateral-directional control system.

The failure detection system designed for the SST longitudinal control system, as described in section 3.1.2 and shown on figure 99, consisted of the static failure detection (SFD) and the dynamic failure detection (DFD) systems. Although the trip levels were not confirmed by a thorough failure mode criticality analysis, the SFD was set to indicate a failure in a channel if that channel differed from the other channels by more than ±5° of stabilizer. The DFD was set to indicate at ±2° difference. Both the SFD and DFD had a 1-sec time delay.

5.7.1 Test Objectives

The objectives of this test were to verify the detection capability of the SFD and DFD and to determine the failure transients at the control surface for the following simulated EC servo failure conditions:

- Hard-over (3° step command to one channel)
- Passive (open servovalve coil in one channel with ±3° at 0.02-Hz triangle wave command to the other three channels)

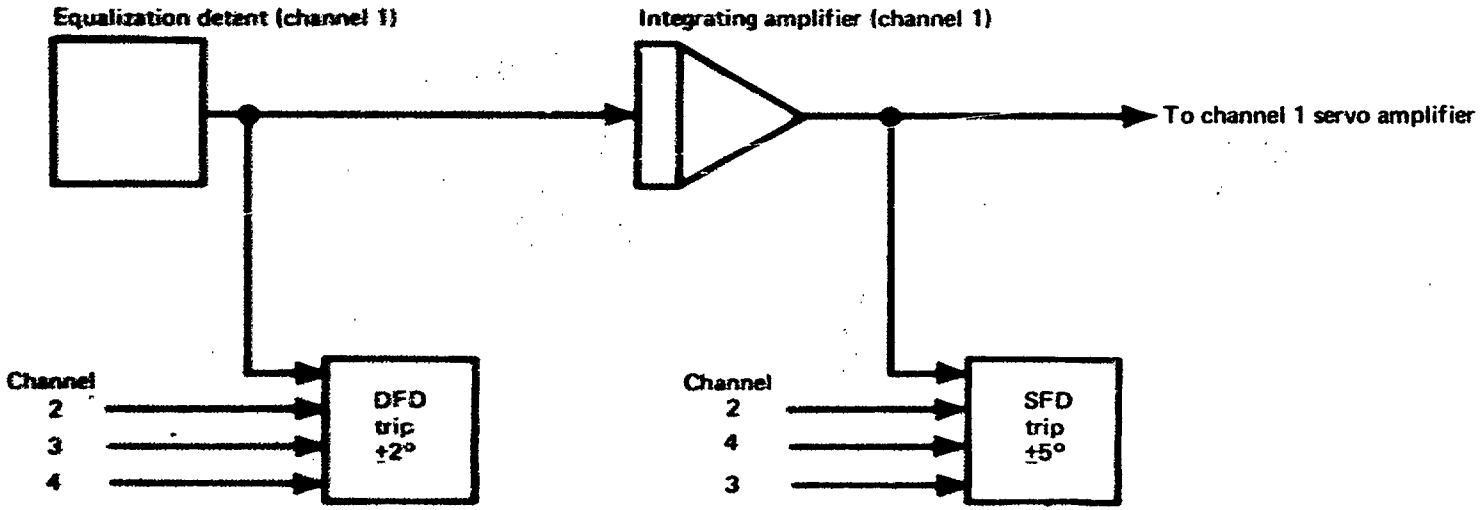

DFD = dynamic failure detection
SFD = static failure detection

FIGURE 99.—EC SERVO FAILURE DETECTION

- Slow-over (0.1°/sec ramp command to one channel)
- Oscillatory (±3° at 0.02-Hz triangular wave command to one channel)

5.7.2 Test Description

All failures were introduced to EC servo channel 1 since it was one of the outboard channels and resulted in maximum stabilizer deflections. The failures imposed were chosen to trip the failure detection system if working properly.

5.7.3 Test Results

The test results are shown on figure 100. The hardover, passive, and oscillatory failures were properly detected by the DFD after the 1-sec time delay. In the slowover case, the equalization detent tended to remain near its center position, offset only enough to provide a small input command for offloading the failure. After 50 sec, the equalization integrator reached a correction level of 5° and the SFD indicated a failure.

For all failures, the stabilizer transients were within 0.1° of the command by the three unfailed channels. This transient is considered negligible and would permit essentially unchanged controllability while the crew evaluated the failure indication.

5.7.4 Conclusion

The SST fail-operational concept ensures minimum stabilizer failure transients (0.1°) for any single EC servo failure in four-, three-, or two-channel operation. The test results indicate that the failure detection system as designed could be used with confidence without "nuisance trip" problems. A failure-mode criticality analysis to determine the criticality of any undetected single failure or combinations of failures must be performed to ensure adequacy of the detection system as well as formulating preflight and/or system test requirements.

5.8 HIGH HYDRAULIC FLOW RATE TEST

Large hydraulic actuators, such as those used to actuate large flight control surfaces, require high hydraulic flow rates when moved rapidly. Traditional hydraulic design practice has been to limit the fluid velocity in tubing to 15 to 30 ft/sec. The result of this limitation is small pressure surges and low pressure drop. For an airplane such as the SST, weight optimization studies determined that a significant weight saving was available if small-diameter tubing and high flow rates were used. Fluid velocities of approximately 60 ft/sec were used in the design under test. The pressure loss in the line for maximum design velocity of the actuator was 3000 psi, approximately one-half in the supply and one-half in the return lines. If the surge pressure analysis had been done using lumped parameters, lossless line, and linear equations, the expected surge pressure would have been 2250 psi and peak pressures 6400 psi. The design limit was 1450 psi surge pressure or 5600 psi peak pressure. A digital computer program (HYTRAN) was used to make a more exact analysis, including branch lines, leakage flows, shaped valve ports, distributed fluid and line parameters, and pump characteristics. This computer analysis was used to design the lightest weight system that would meet performance requirements with acceptable surge pressures.

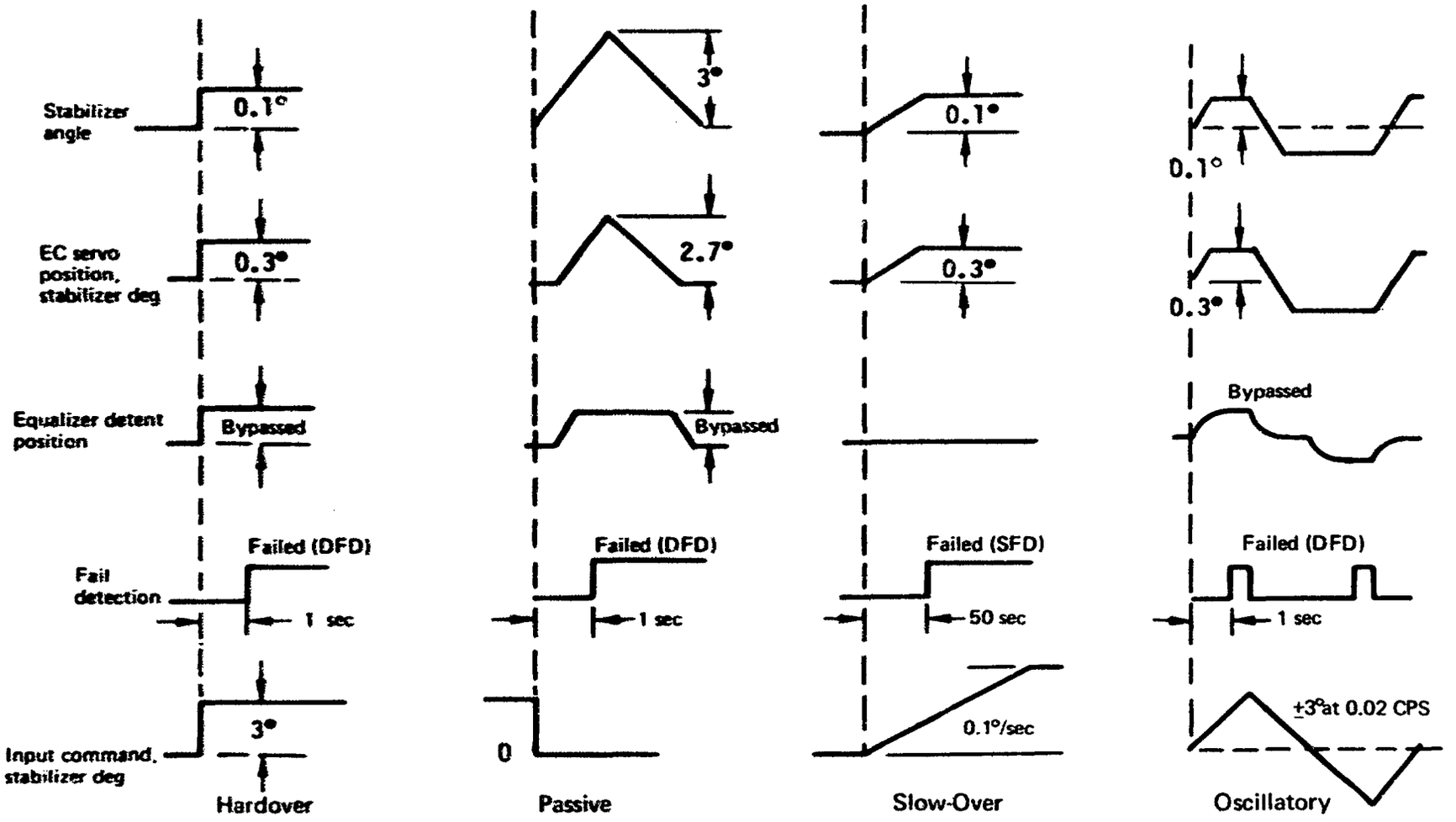

FIGURE 100.–EC SERVO FAILURE DETECTION TEST RESULTS–ALL EQUALIZATION "ON"

5.8.1 Test Objectives

Test objectives were to determine the dynamic characteristics of transient pressure in the hydraulic supply and return lines to show compliance with design goals and to compare the results to analytical predictions to gain confidence in analytical methods for future system design.

5.8.2 Test Description

The SST horizontal stabilizer hydraulic plumbing was approximated by using lines of appropriate length and diameter to connect one actuator to the high-temperature hydraulic system. This simulation is shown schematically in figure 67. Another actuator, connected to the other hydraulic system, was used to help drive the surface in order to get higher flow rates. The surface was signalled in a manner that developed steady-state maximum flow and then the valve was closed rapidly to develop maximum surge pressure. Tests were run with various oil temperatures up to 340° F.

5.8.3 Test Results

The test results were in good agreement with analytical predictions. Peak pressure levels due to pressure surges were less than design allowables. Figure 101 shows the comparison between analytical and test results for the 340° F case, the only one analyzed by computer (HYTRAN). The analytical results for the pressure line gave conservative answers for the two most important design questions. The peak pressure and the number of cycles of pressure peaks were both lower than predicted, but the surge pressure was much less conservative than a simple lumped-parameter calculation would give. The damping ratio of the pressure peak is difficult to calculate analytically. The first pressure peak (1400 psi) was not clearly defined in the computer results due to a more rapid pressure recovery predicted by the analysis. The magnitude of the first pressure peak can be calculated accurately by lumped-parameter methods by using the speed of sound in the hydraulic lines that would give the same frequency of pressure oscillations predicted by the computer analysis. The calculated value using this method for the first pressure peak was 1380 psi. Had the pump response been faster and the line losses less, the peak pressure would still have been less than design allowable (see fig. 102).

The computer simulation of the return side of the system was not as good as the simulation of the supply side. The predicted peak return pressure was 20% less than the actual value. However, the difference would be acceptable in return line design since return lines were designed for half supply pressure for other operating conditions. The computer program did not predict the pressure surges caused by the collapse of the cavitation bubble created by rapid closure of the valve. Additional computer subroutines are now available which could predict this pressure activity.

A comparison of pressure line transients resulting from rapid valve operation at 90° and 340° F is shown in figure 103. The higher peak pressure reached at 95° F was due to the higher bulk modulus of the fluid at this temperature. The first pressure peak started from a lower pressure because of the greater line losses at lower temperature. The damping as indicated by the larger number of pressure cycles after valve closure was less at low temperatures due to decreased actuator and system leakage.

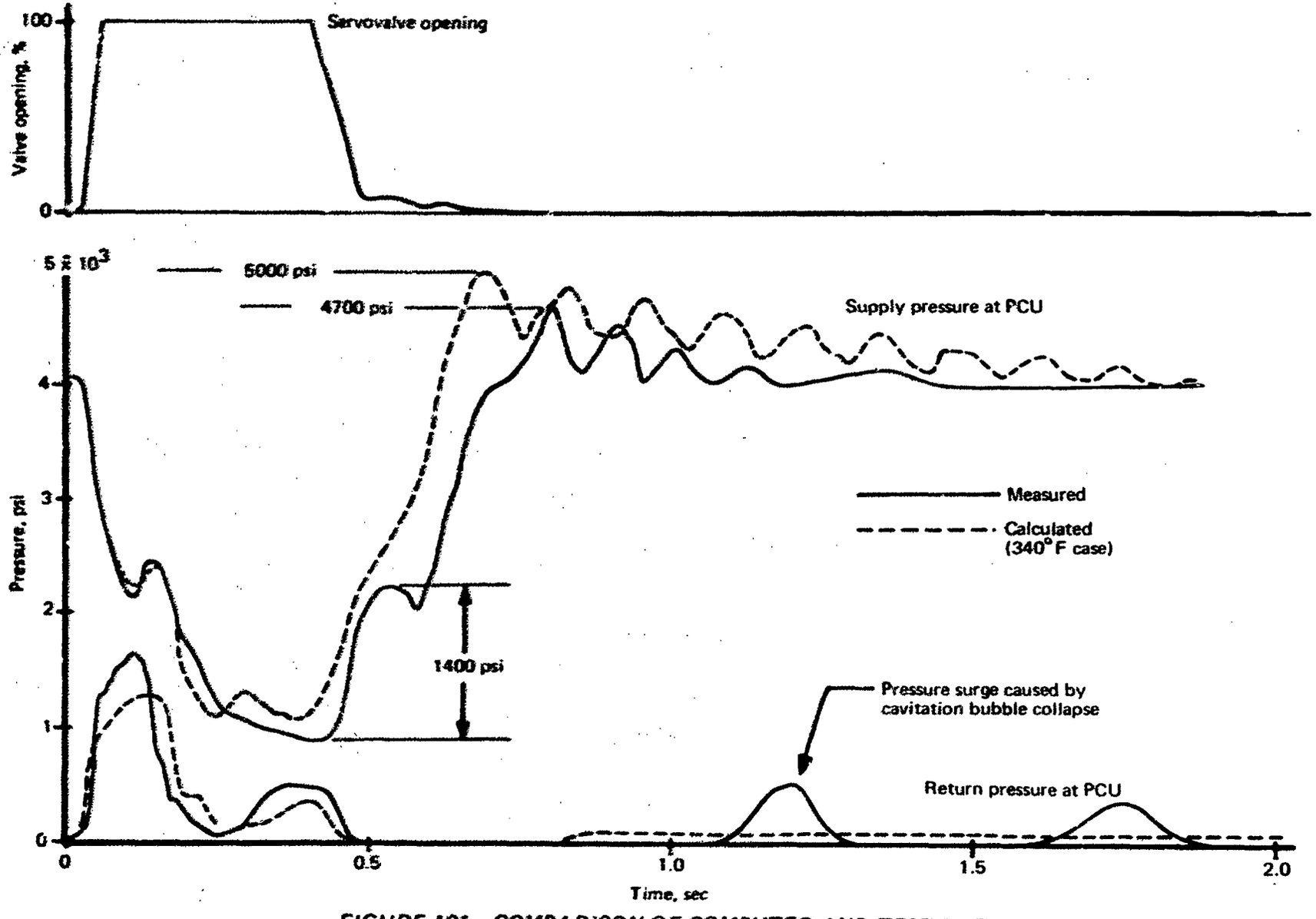

FIGURE 101.–COMPARISON OF COMPUTER AND TEST DATA

1 Lumped parameter calculation of surge pressure peak using

$$P_T = (\rho\beta)^{1/2} v$$

where

ρ = Mass density of fluid, 3×10^{-5} lb-sec^2/in.^{4}

β = Effective bulk modulus, 120,000 psi

v = Fluid velocity, 720 in./sec

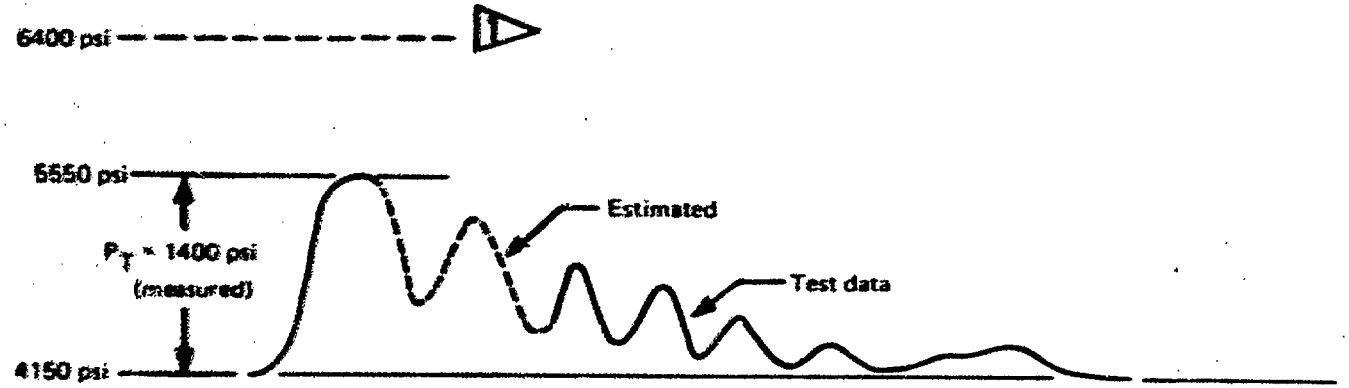

FIGURE 102.–SUPPLY LINE SURGE PRESSURE ADJUSTED TO 4150 PSI BASELINE PRESSURE

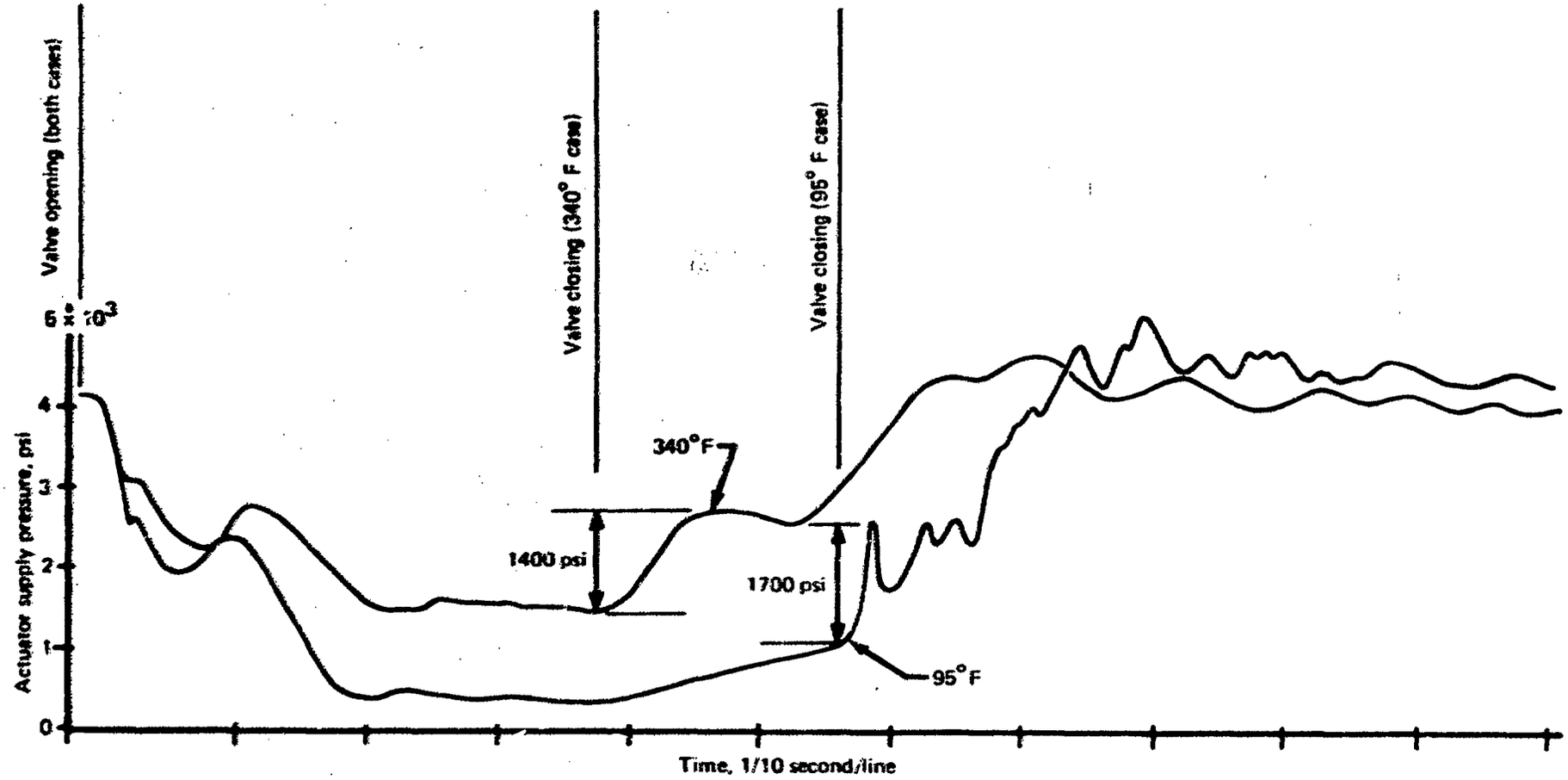

FIGURE 103.–SUPPLY LINE SURGE PRESSURE

The return line pressure transients are compared for 95° and 340° F in figure 104. The peak pressure in each case was about the same. The peak was caused by rapid connection of actuator cylinder pressure of 2000 psi to a column of fluid at rest. For the system tested, the return lines were of relatively small diameter, and there was no volume of fluid near the actuator to reduce the pressure by fluid compression. Since the cylinder pressure changes very little with temperature and the system resistance to fluid acceleration is changed little by temperature, the same peak pressure value was expected. In systems with large return lines, the return line pressure surge is much less and even lower pressures will occur if return line accumulators are used.

5.8.4 Conclusions

Design of hydraulic control systems with a major portion of the pressure drop in the hydraulic lines is an acceptable way to reduce system weight. The pressure line surges that would be expected with high fluid velocities occur, but with lower initial pressure due to flow losses in the tubing the peak pressure is reduced. The return line is subjected to high pressures upon rapid opening of the actuator valve unless return line capacitance is provided. This effect must be considered in the design.

The HYTRAN analysis method used to predict transient behavior was in good agreement with test data for the pressure side of the system and could be used with confidence as a design tool even though minor discrepancies would be present for the return side data.

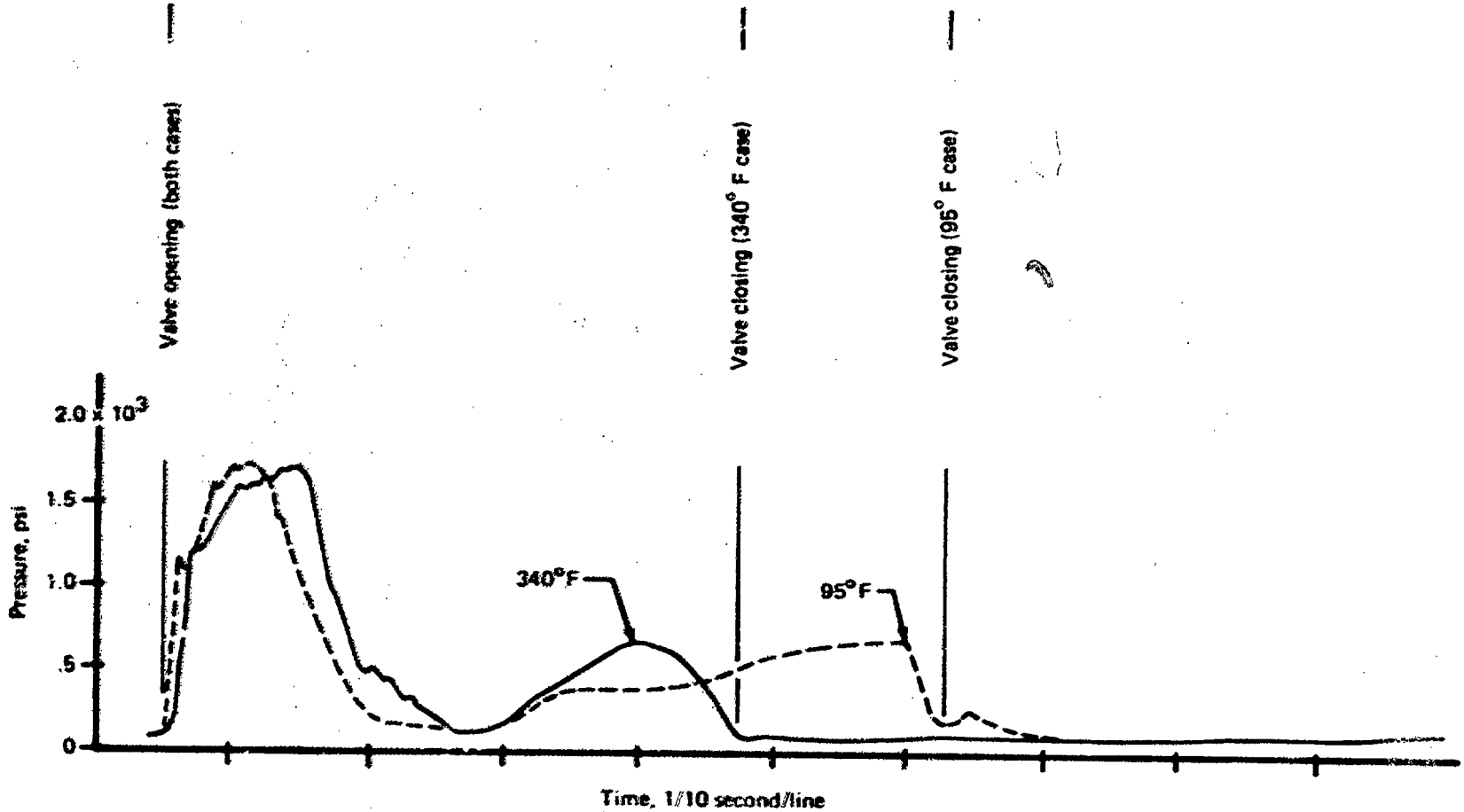

FIGURE 104.—RETURN LINE SURGE PRESSURE

APPENDIX A
LINEAR ANALYSIS EQUATIONS OF STABILIZER ACTUATION SYSTEM

INTRODUCTION

This appendix contains equations and transfer functions which define the dynamic performance of an actuation system without air loads but including structure and surface structure. First, the stiffness transfer function is developed to define both static and dynamic stiffnesses. The open-loop transfer function of the actuator is then developed to define stability margin and relate it to the stiffness transfer function. The closed-loop transfer function is developed to show the relationship of the overall dynamic performance to stiffness, and finally, a scheme for electrical stiffness compensation is discussed.

Actuator installations of the type analyzed herein are characterized as follows:

- Load damping (structural damping) is very low (ζ_L = 0.01 to 0.02) and cannot be reliably predicted until the structure is built; it is usually considered to be zero in the stability analysis.
- Viscous damping forces and friction in actuators of this size are not great enough to introduce significant damping of large inertias, and are neglected in the analysis.

LINEAR MODEL

The horizontal stabilizer actuator system has four identical actuators driving a common load. However, the system's dynamic performance can be described by analyzing one actuator driving 1/4 of the load (inertia).

A linear model of a single actuator can be constructed by assuming small perturbations about a steady-state operating point in a pressure region where the relief and bypass valves are not operating.

A simplified schematic of the actuator from which a linear model was developed is shown in figure A-1. All motions and forces are designated positive which cause a positive, or trailing-edge-down stabilizer. All structure is originally considered rigid, so that a fixed relationship exists between actuator retraction or extension and actuator rotation. The load ("stabilizer") is represented by a second-order system equivalent to the first-mode natural frequency of the surface.

A block diagram of the model is shown in figure A-2. The EC servo is depicted as "no-load," since its load poles are approximately 200 cps (1200 rad/sec) and have no effect at the frequencies of interest. The model can be reduced to the simplified block diagram in figure A-3 by the following assumptions:

- Replace the EC servo with a first-order transfer function.
- Neglect viscous damping between the cylinder and piston.

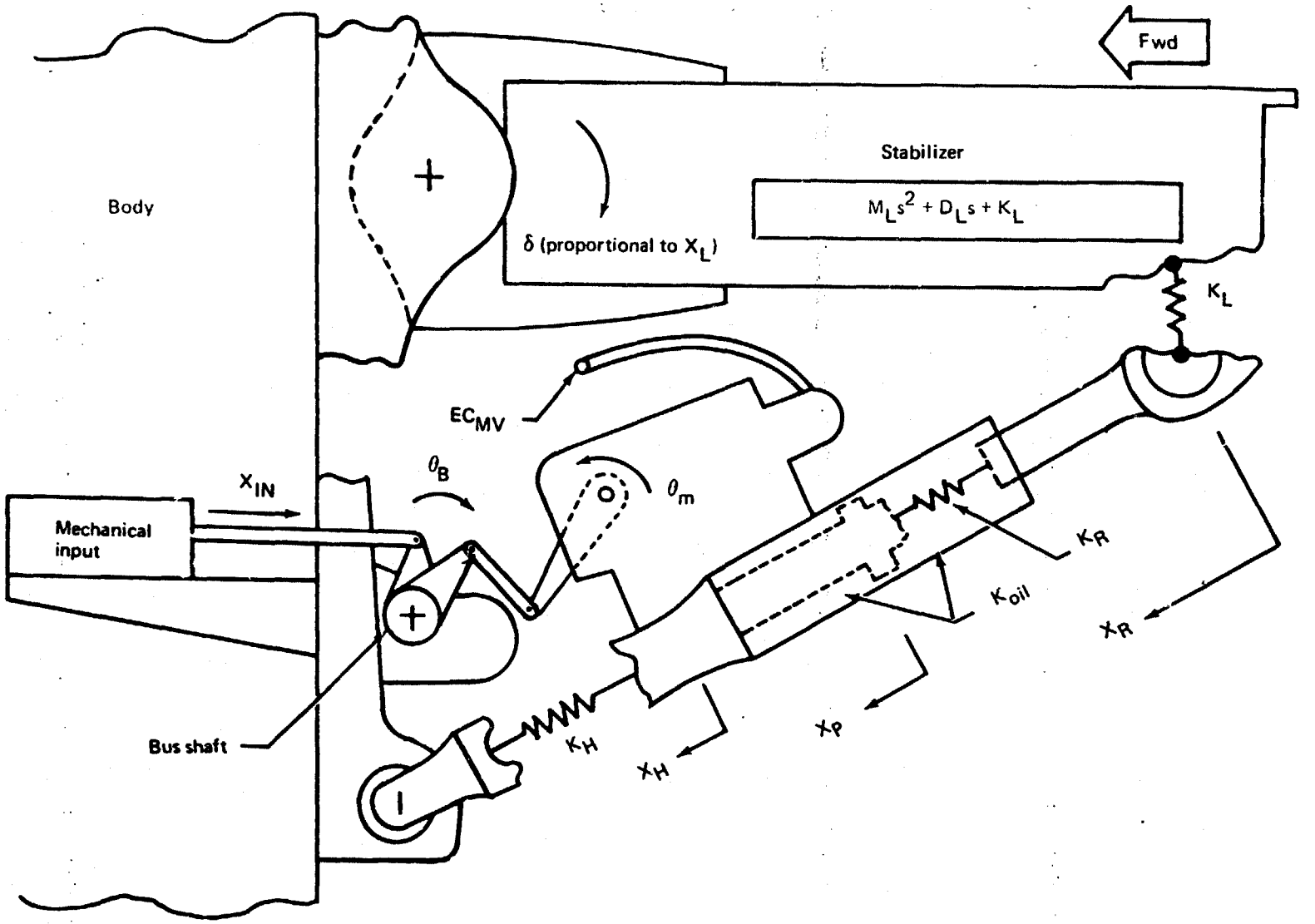

FIGURE A-1.—LINEAR ACTUATOR MODEL

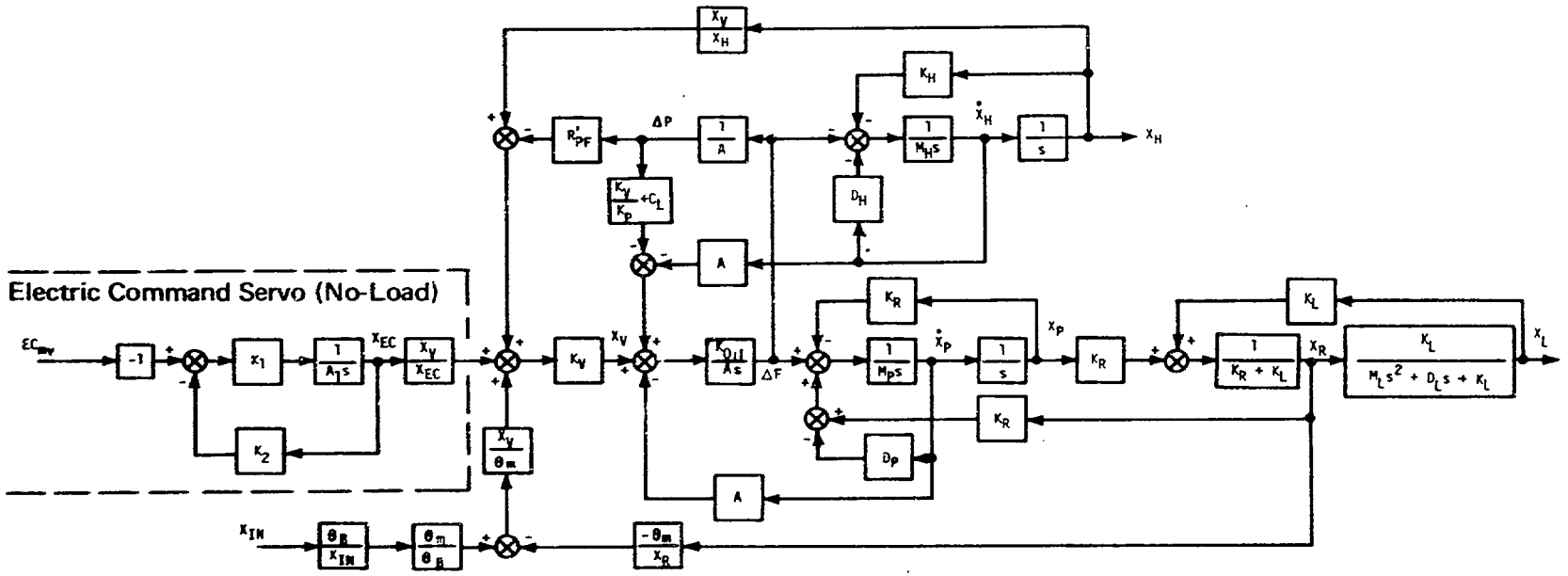

FIGURE A-2.—BLOCK DIAGRAM OF LINEAR ACTUATOR MODEL

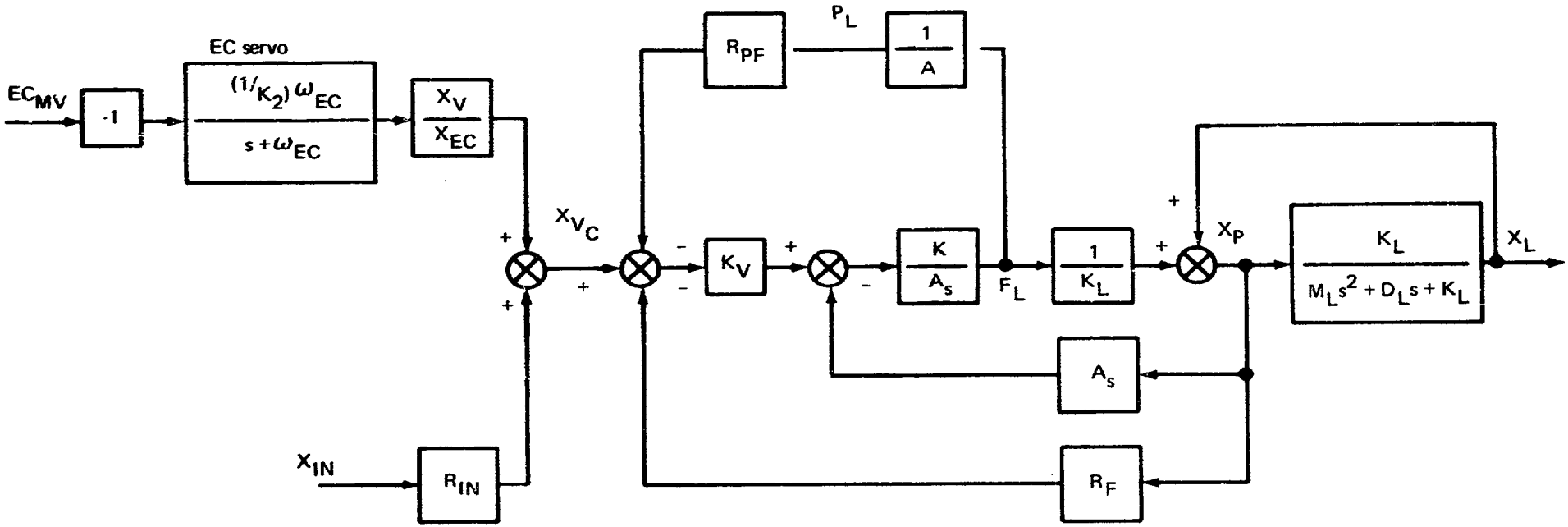

FIGURE A-3.—SIMPLIFIED BLOCK DIAGRAM

- Neglect housing and piston masses (natural frequencies are in excess of 300 cps).
- Combine the oil, housing, and rod springs into a single spring constant K (equivalent to pin-to-pin, frequency-independent dynamic stiffness).
- The rod spring constant exceeds the load spring constant by a large ratio; therefore, redefine $X_P \equiv X_R$ and $F_L \equiv \Delta F$.
- Since the effect of actuator pressure feedback (R'_{PF}) is identical to the effects of leakage, housing feedback, and the inverse of pressure gain, all these terms are combined as a single pressure feedback term R_{PF}.
- Combine the input ratios and feedback ratios as R_{IN} and R_F, respectively.

Since the EC servo is not a part of the feedback loop, it has no effect on the actuator dynamics, and will not be included until electrical stiffness compensation is discussed.

Equations of the block diagram (fig. A-3) are summarized in the following matrix equation, with valve command as the input:

$$\begin{bmatrix} \left(\frac{As}{K} + \frac{K_V R_{PF}}{A}\right) & (As + K_V R_F) & 0 \\ -1 & K_L & -K_L \\ 0 & -K_L & (M_L s^2 + D_L s + K_L) \end{bmatrix} \begin{bmatrix} F_L \\ X_P \\ X_L \end{bmatrix} = \begin{bmatrix} K_V X_{V_C} \\ 0 \\ 0 \end{bmatrix} \quad (1)$$

STIFFNESS

An actuation system is viewed as two devices: (1) as a servo system to force the surface to its commanded position, and (2) as a large stiffness to the flutter modes. The latter view of the system is discussed first to illustrate the definition of stiffness.

The stiffness transfer function is derived by assuming no input commands ($X_{V_C} = 0$) and applying a sinusoidal force to the load. Neglecting the mass and damping of the piston

and recognizing that the applied force is equal to the negative of the load force, the stiffness transfer function is:

$$\frac{-F_L(s)}{X_p(s)} = \frac{K\left(s + \frac{K_V R_F}{A}\right)}{\left(s + \frac{K K_V R_{PF}}{A^2}\right)} = \frac{K(s + \omega_S)}{(s + \omega_D)} = K_A(s) \qquad (2)$$

The quantity $(K_V R_F)/A$ is the position feedback loop gain and, for a first-order system, is identical to the no-load servo break frequency, ω_S. The quantity $(K K_V R_{PF})/A^2$ is the pressure feedback loop gain, and will be referred to as the dynamic stiffness break frequency, ω_D.

Static stiffness and frequency-independent dynamic stiffness are defined as the value of the transfer function expressed in equation (2) at $s = 0$ and $s = \infty$, respectively:

$$\left[\frac{-F_L}{X_p}\right]_{s=0} = \frac{A R_F}{R_{PF}} \equiv K_A(0) = \text{static stiffness} \qquad (3)$$

$$\left[\frac{-F_L}{X_p}\right]_{s=\infty} = K \equiv K_A(\infty) = \text{frequency-independent dynamic stiffness} \qquad (4)$$

A straight-line approximation for the stiffness transfer function is shown in figure A-4, with the actual transfer function superimposed.

STABILITY

The actuator stability will be determined from the open-loop position transfer function by applying the Nyquist stability criteria. From equation (1):

$$R_F G(s) = \frac{X_p(s)}{X_{V_C}(s)} = \frac{K_V M_L R_F \left(s^2 + \frac{D_L}{M_L}s + \frac{K_L}{M_L}\right)}{\frac{A M_L (K + K_L)}{K} s\left[s^2 + \left(\frac{D_L}{M_L} + \frac{K K_L K_V R_{PF}}{A^2(K + K_L)}\right)s + \frac{K K_L}{M_L(K + K_L)}\left(1 + \frac{K_V R_{PF} D_L}{A^2}\right)\right]} \qquad (5)$$

or:

$$R_F G(s) = \frac{K_V R_F}{A} \frac{\omega_O^2 (s^2 + 2\zeta_L \omega_L s + \omega_L^2)}{\omega_L^2 s(s^2 + 2\zeta_{OD} \omega_{OD} s + \omega_{OD}^2)} \qquad (6)$$

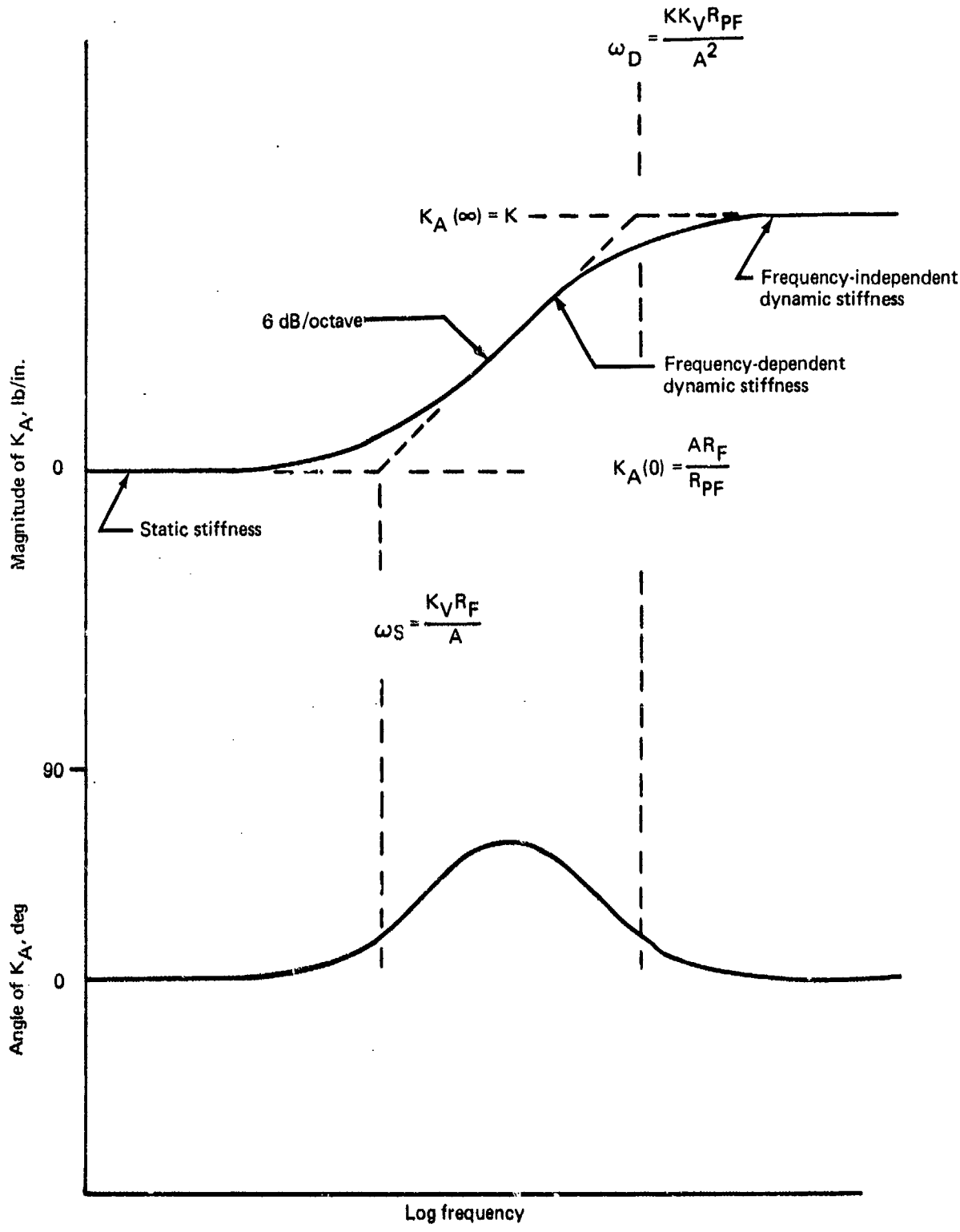

FIGURE A-4.–ACTUATION SYSTEM STIFFNESS FREQUENCY RESPONSE

where:

$$\omega_{OD}^2 = \omega_O^2 \left(1 + \frac{K_V R_{PF}}{A^2} D_L\right) \tag{7}$$

$$\omega_O^2 = \frac{K K_L}{M_L(K + K_L)} = \frac{K_{TOT}}{M_L}$$

$$2\zeta_{OD}\,\omega_{OD} = \frac{D_L}{M_L} + 2\zeta_O\,\omega_O \tag{8}$$

$$2\zeta_O\,\omega_O = \omega_O^2\left(\frac{K_V R_{PF}}{A^2} M_L\right)$$

$$\omega_L^2 = \frac{K_L}{M_L} \tag{9}$$

$$2\zeta_L\,\omega_L = \frac{D_L}{M_L} \tag{10}$$

Since the load damping is assumed to be negligible, the equations are simplified by setting $D_L = 0$:

$$R_F\,G(s) = \frac{K_V R_F}{A} \frac{\omega_O^2 (s^2 + \omega_L^2)}{\omega_L^2 s\left(s^2 + 2\zeta_O\,\omega_O\,s + \omega_O^2\right)} \tag{11}$$

The open-loop transfer function (eq. 11) can be represented as shown in figure A-5 and represents a condensation of figure A-3.

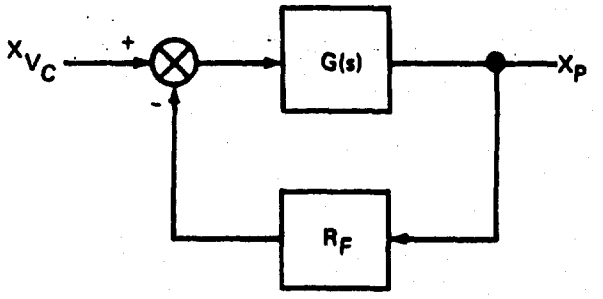

FIGURE A-5 CLOSED-LOOP TRANSFER FUNCTION

The closed-loop transfer function is:

$$\frac{X_P(s)}{X_{V_C}(s)} = \frac{G(s)}{1 + R_F\, G(s)} \tag{12}$$

The Nyquist criterion for stability requires that the quantity $1 + R_F\, G(s)$ must not be zero:

$$\begin{aligned} R_F\, G(j\omega) \; &< 1.0 \; \angle 180^\circ \\ \text{or } |R_F\, G(j\omega)| &< 1.0, \text{ at } 180^\circ \end{aligned} \tag{13}$$

For complicated transfer functions, it is usually necessary to compute the Nyquist plot to determine the frequency at which a phase shift of 180° occurs. However, evaluating equation (11) at $s = j\omega_O$ yields:

$$R_F\, G(j\omega_O) = \frac{K_V\, R_F}{A} \frac{\omega_O{}^2 (-\omega_O{}^2 + \omega_L{}^2)}{\omega_L{}^2 (j\omega_O)(-\omega_O{}^2 + 2\,\zeta_O\, \omega_O{}^2 + \omega_O{}^2)} \tag{14}$$

$$= \frac{K_V\, R_F}{A} \frac{-\omega_O{}^2 + \omega_L{}^2}{2\,\zeta_O\, \omega_O\, \omega_L{}^2}$$

Combining equations (7), (8), (9), and (14):

$$R_F\, G(j\omega_O) = \frac{-A\, R_F}{K\, R_{PF}} = \frac{A\, R_F}{K\, R_{PF}} \angle 180^\circ \tag{15}$$

or

$$|R_F\, G(j\omega_O)| = \frac{A\, R_F}{K\, R_{PF}} = \frac{K_A(0)}{K_A(\infty)} \equiv \text{stiffness ratio} \leq 1 \tag{16}$$

Equation (16) states that the system is stable if, and only if, the static stiffness is less than the frequency-independent dynamic stiffness. The stability criterion defined in equation (16) does not specify damping ratio, except that it will be in excess of zero. Furthermore, the criterion is independent of the load mass or load spring (M_L and K_L).

The Bode plot in figure A-6 illustrates the frequency response of the open-loop system and the gain and phase margins of the system. The level of 0 dB is equivalent to a loop gain of 1.0, and occurs at a frequency of $(K_V\, R_F)/A$, the open-loop gain (eq. 14).

RELATIONSHIP OF OPEN-LOOP DAMPING RATIO AND STIFFNESS RATIO

The open-loop damping ratio cannot be obtained from examination of the stiffness ratio, even though a stiffness ratio less than 1.0 implies a system with positive damping.

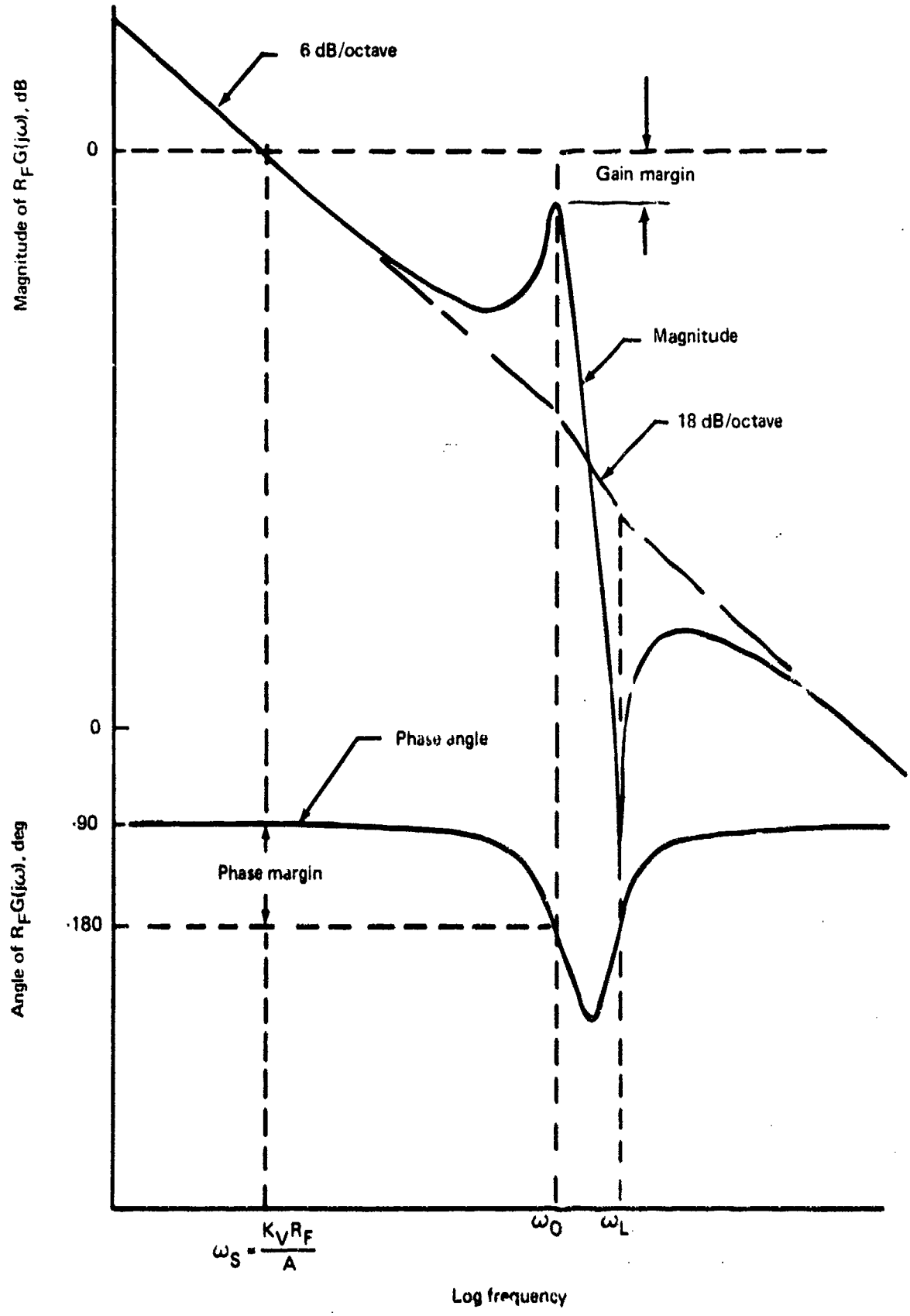

FIGURE A-6.—OPEN-LOOP FREQUENCY RESPONSE

However, their relationship can be illustrated by varying system parameters and observing the changes in the stiffness frequency response and the open-loop frequency response.

The relative effects of the actuator spring, K, and the load spring, K_L, cannot be shown exactly since they combine to form the total spring, K_{TOT}. However, K_L is estimated to be less than one-half of K for the SST horizontal stabilizer actuation system, and approximate effects can be illustrated.

From equations (7) and (8), open-loop damping ratio and natural frequency can be expressed as:

$$\omega_O = \sqrt{\frac{K_{TOT}}{M_L}} = \sqrt{\frac{K\,K_L}{M_L(K + K_L)}} \tag{17}$$

$$\zeta_O = \frac{K_V\,R_{PF}}{2\,A^2}\,\omega_O\,M_L = \frac{K_V\,R_{PF}\,K_{TOT}}{2\,A^2\,\omega_O} = \frac{K_V\,R_{PF}}{2\,A^2}\sqrt{M_L\,K_{TOT}} \tag{18}$$

Assuming piston area, load mass, and load spring to be constants, the following discussion, together with the graphic illustrations in figure A-7, describes the sensitivity of damping ratio to variations in the remaining parameters.

a) Actuator spring (fig. A-7a)

Assume the actuator spring, K, is increased by a factor (x), by either a decrease of temperature (oil bulk modulus increase) or a decrease of oil volume. The actuator spring, gain margin, and dynamic stiffness break frequency, ω_D, increase proportionately. Since the actuator spring is combined with the load spring, an increase of the actuator spring (decreased temperature) causes only a small increase of the open-loop natural frequency and damping ratio, as follows:

$$\left.\begin{aligned}
K_{A_x}(0) &= K_A(0) \\
K_{A_x}(\infty) &= x\,K_A(\infty) \\
\omega_{S_x} &= \omega_S \\
\omega_{D_x} &= \frac{(x\,K)\,K_V\,R_{PF}}{A^2} = x\,\omega_D \\
\omega_{O_x} &= \sqrt{\frac{(x\,K)\,K_L}{(x\,K) + K_L} \cdot \frac{1}{M_L}} \approx \omega_O \\
\zeta_{O_x} &= \frac{K_V\,R_{PF}}{2\,A^2}\sqrt{\frac{(x\,K)\,K_L\,M_L}{(x\,K) + K_L}} \approx \zeta_O
\end{aligned}\right\} \tag{19}$$

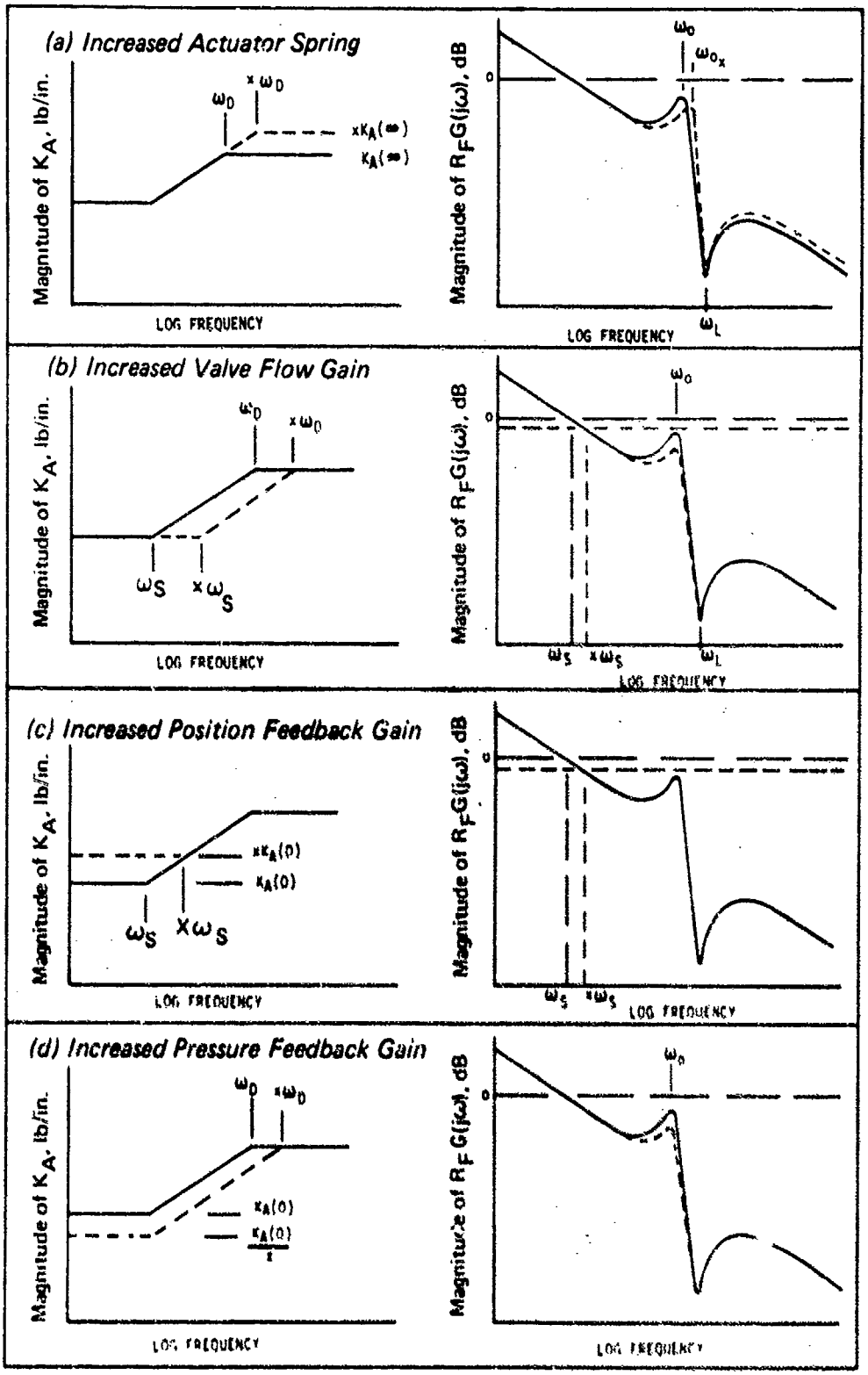

FIGURE A-7. - EFFECT OF ACTUATOR PARAMETERS ON STIFFNESS AND STABILITY

b) Valve flow gain (fig. A-7b)

As the valve flow gain, K_V, is increased by a factor (x), the servo and dynamic stiffness break frequencies, ω_S and ω_D, increase proportionately, and the frequency-dependent stiffness decreases proportionately. The open-loop damping ratio increases proportionately to flow gain, but the gain margin is unchanged:

$$\left.\begin{aligned} K_{A_x}(0) &= K_A(0) \\ K_{A_x}(\infty) &= K_A(\infty) \\ \omega_{S_x} &= \frac{(x\,K_V)\,R_F}{A} = x\,\omega_S \\ \omega_{D_x} &= \frac{K\,(x\,K_V)\,R_{PF}}{A^2} = x\,\omega_D \\ \omega_{O_x} &= \omega_O \\ \zeta_{O_x} &= \frac{(x\,K_V)\,R_{PF}}{2\,A^2}\sqrt{M_L\,K_{TOT}} = x\,\zeta_O \end{aligned}\right\} \quad (20)$$

c) Position feedback gain (fig. A-7c)

If the position feedback gain, R_F, is increased by a factor (x), the servo break frequency, ω_S, and the low-frequency stiffness (static stiffness), increase proportionately. The open-loop natural frequency and damping ratio are unchanged, but the gain margin decreases as a result of the open-loop gain increase:

$$\left.\begin{aligned} K_{A_x}(0) &= x\,K_A(0) \\ K_{A_x}(\infty) &= K_A(\infty) \\ \omega_{S_x} &= \frac{K_V\,(x\,R_F)}{A} = x\,\omega_S \\ \omega_{O_x} &= \omega_O \\ \zeta_{O_x} &= \zeta_O \end{aligned}\right\} \quad (21)$$

d) Pressure feedback gain (fig. A-7d)

If the pressure feedback gain, R_{PF}, is increased by a factor (x), the static stiffness and frequency-dependent stiffness decrease proportionately and the dynamic stiffness break frequency increases proportionately. The open-loop damping ratio and

dynamic stiffness break frequency increase proportionately to (x), resulting in an increased gain margin:

$$\left.\begin{aligned} K_{A_x}(0) &= \frac{A\,R_F}{(x\,R_{PF})} = \frac{K_A(0)}{x} \\ K_{A_x}(\infty) &= K_A(\infty) \\ \omega_{S_x} &= \omega_S \\ \omega_{D_x} &= \frac{K\,K_V\,(x\,R_{PF})}{A^2} = x\,\omega_D \\ \omega_{O_x} &= \omega_O \\ \zeta_{O_x} &= \frac{K_V\,(x\,R_{PF})}{2\,A^2}\sqrt{M_L\,K_{TOT}} = x\,\zeta_O \end{aligned}\right\} \qquad (22)$$

As shown in equation (2) and noted above, the load constants do not affect the stiffness ratio. However, they do affect the open-loop natural frequency and damping ratio, as shown in equations (7) and (8). The effects on open-loop response of variations in the load mass and load spring are illustrated in figure A-8 and are discussed below:

a) Load mass and load spring (fig. A-8a)

Assume an increase in the load mass and spring by the factor (x). The load natural frequency is unchanged, the open-loop natural frequency decreases slightly, the damping ratio increases approximately by the proportion (x), but the gain margin is unchanged.

$$\left.\begin{aligned} \omega_{L_x} &= \sqrt{\frac{(x\,K_L)}{(x\,M_L)}} = \omega_L \\ \omega_{O_x} &= \sqrt{\frac{K\,(x\,K_L)}{K + (x\,K_L)} \cdot \frac{1}{(x\,M_L)}} \approx \omega_O \\ \zeta_{O_x} &= \frac{K_V\,R_{PF}}{2\,A^2}\sqrt{\frac{(x\,M_L)\,K(x\,K_L)}{K + (x\,K_L)}} \approx x\,\zeta_O \end{aligned}\right\} \qquad (23)$$

b) Load spring (fig. A-8b)

If the load spring is increased by the factor (x), the load natural frequency increases. Based on the assumption of the load spring's relative magnitude, the open-loop natural frequency and damping ratio increase approximately by the square root of (x), and the gain margin is unchanged.

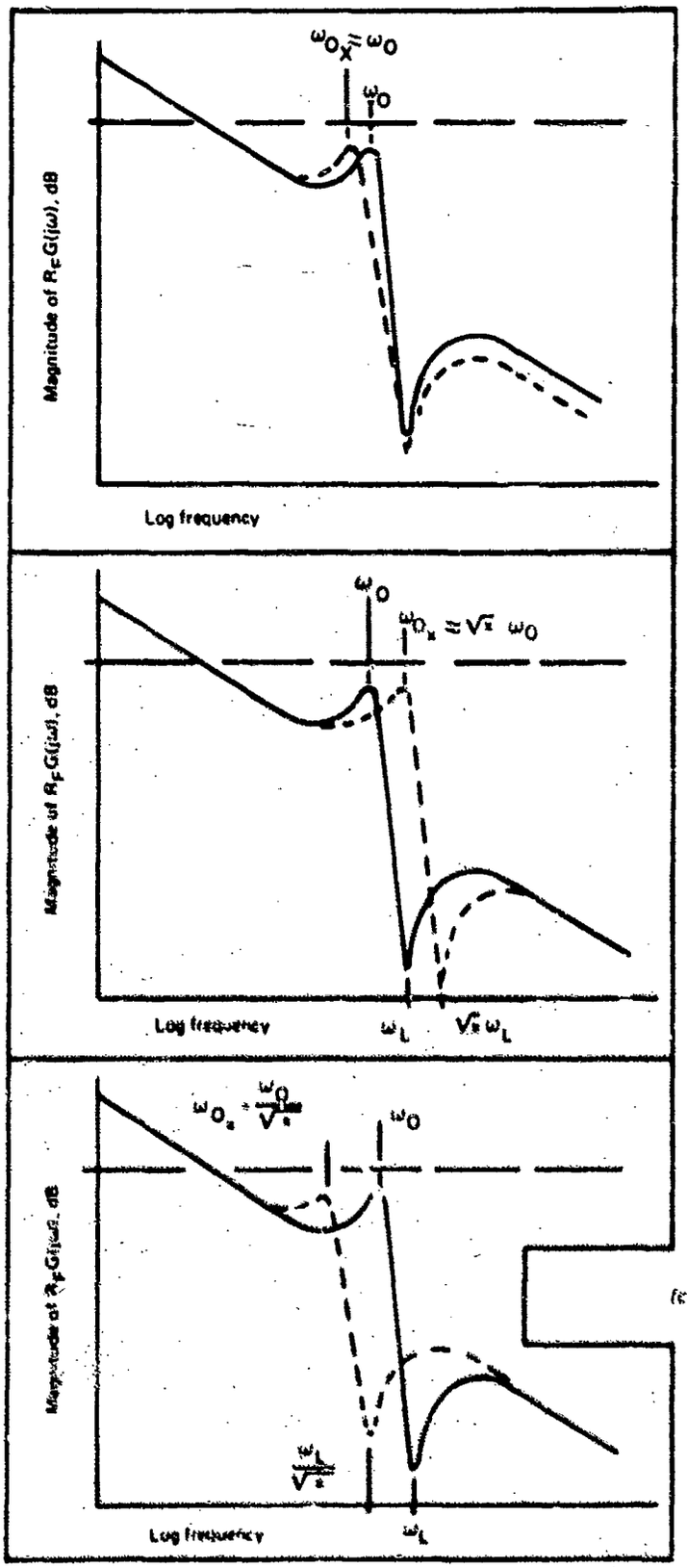

(a) Increased Load Mass and Load Spring

(b) Increased Load Spring

(c) Increased Load Mass

FIGURE A-8.–EFFECTS OF LOAD VARIATION

$$\left.\begin{aligned} \omega_{L_x} &= \sqrt{\frac{(x\,K_L)}{M_L}} = \sqrt{x}\;\omega_L \\ \omega_{O_x} &= \sqrt{\frac{K\,(x\,K_L)}{K+(x\,K_L)} \times \frac{1}{M_L}} \approx \sqrt{x}\;\omega_O \\ \zeta_{O_x} &= \frac{K_V\,R_{PF}}{2\,A^2}\sqrt{\frac{M_L\,K(x\,K_L)}{K+(x\,K_L)}} \approx \sqrt{x}\,\zeta_O \end{aligned}\right\} \quad (24)$$

c) Load mass (fig. A-8c)

If the load mass is increased by the factor (x), the load natural frequency and open-loop natural frequency decrease inversely as the square root of the proportion (x), and the damping ratio increases proportionately. The gain margin is unchanged:

$$\left.\begin{aligned} \omega_{L_x} &= \sqrt{\frac{K_L}{(x\,M_L)}} = \frac{1}{\sqrt{x}}\,\omega_L \\ \omega_{O_x} &= \sqrt{\frac{K_{TOT}}{(x\,M_L)}} = \frac{1}{\sqrt{x}}\,\omega_O \\ \zeta_{O_x} &= \frac{K_V\,R_{PF}}{2\,A^2}\sqrt{(x\,M_L)\,K_{TOT}} = \sqrt{x}\,\zeta_O \end{aligned}\right\} \quad (25)$$

CLOSED-LOOP CHARACTERISTICS

The closed-loop transfer function must be used to determine the dynamic performance in terms of transient response and frequency response. The open-loop transfer function is useful to determine the stability margin of a system without regard to dynamic performance. The closed-loop transfer function can be written from equation (1), or directly from equations (11) and (12). With $D_L = 0$:

$$\frac{X_P(s)}{X_{V_C}(s)} = \left(\frac{1}{R_F}\right)\left(\frac{K_V\,R_F}{A}\right)\frac{\omega_O^2\,(s^2+\omega_L^2)}{\omega_L^2\left[s^3+\left(2\,\zeta_O\,\omega_O+\omega_S\,\frac{\omega_O^2}{\omega_L^2}\right)s^2+\omega_O^2\,s+\omega_S\,\omega_O^2\right]} \quad (26)$$

or, in terms of "closed-loop parameters":

$$\frac{X_P(s)}{X_{V_C}(s)} = \frac{\omega_C}{R_F}\left(\frac{\omega_O^2}{\omega_L^2}\right)\frac{(s^2+\omega_L^2)}{(s+\omega_C)(s^2+2\,\zeta_{CL}\,\omega_{CL}\,s+\omega_{CL}^2)} \quad (27)$$

Substituting $s = j\omega$ in equation (27), the closed-loop frequency response of figure A-9 results. Expanding the denominator in equation (27):

$$s^3 + (2\zeta_{CL}\omega_{CL} + \omega_C)s^2 + (\omega_{CL}^2 + 2\zeta_{CL}\omega_{CL}\omega_C)s + \omega_C\omega_{CL}^2 \qquad (28)$$

Comparing the coefficients in the denominator of equation (26) with the coefficients of equation (28):

$$\left.\begin{aligned} 2\zeta_O\omega_O + \omega_S\frac{\omega_O^2}{\omega_L^2} &= 2\zeta_{CL}\omega_{CL} + \omega_C \\ \omega_O^2 &= \omega_{CL}^2 + 2\zeta_{CL}\omega_{CL}\omega_C \\ \omega_S\omega_O^2 &= \omega_C\omega_{CL}^2 \end{aligned}\right\} \qquad (29)$$

From the first and third of equations (29), the closed-loop damping ratio is:

$$\zeta_{CL} = \frac{\omega_O}{\omega_{CL}}\zeta_O + \left[\left(\frac{\omega_O}{\omega_L}\right)^2 - \left(\frac{\omega_O}{\omega_{CL}}\right)^2\right]\frac{\omega_S}{2\omega_{CL}} \qquad (30)$$

The relationships can be simplified since the open-loop poles and zeros are close together, and they are also more than five times the magnitude of ω_S, the inverse of the closed-loop time constant. Therefore:

$$\omega_{CL} \approx \omega_O \qquad (31)$$

Using equation (31) in equation (30):

$$\zeta_{CL} \approx \zeta_O - \tfrac{1}{2}\omega_S\omega_O\left(\frac{\omega_L^2 - \omega_O^2}{\omega_O^2\omega_L^2}\right) \qquad (32)$$

From equations (3), (4), (7), (9), and (32),

$$\zeta_{CL} \approx \zeta_O\left[1 - \frac{A R_F}{K R_{PF}}\right] = \zeta_O\left[1 - \frac{K_A(0)}{K_A(\infty)}\right] \qquad (33)$$

Equation (33) shows that the system is stable for stiffness ratios less than 1.0, and relates the open-loop and closed-loop damping ratios. Since pressure feedback gain is a part of the open-loop damping ratio, the effects of pressure feedback are apparent if equation (33) is rewritten, so that if R_{PF} only is varied, the ratio ζ_O/R_{PF} will be constant:

$$\zeta_{CL} \approx \left(\frac{\zeta_O}{R_{PF}}\right)\left[R_{PF} - \frac{A R_F}{K}\right] \qquad (34)$$

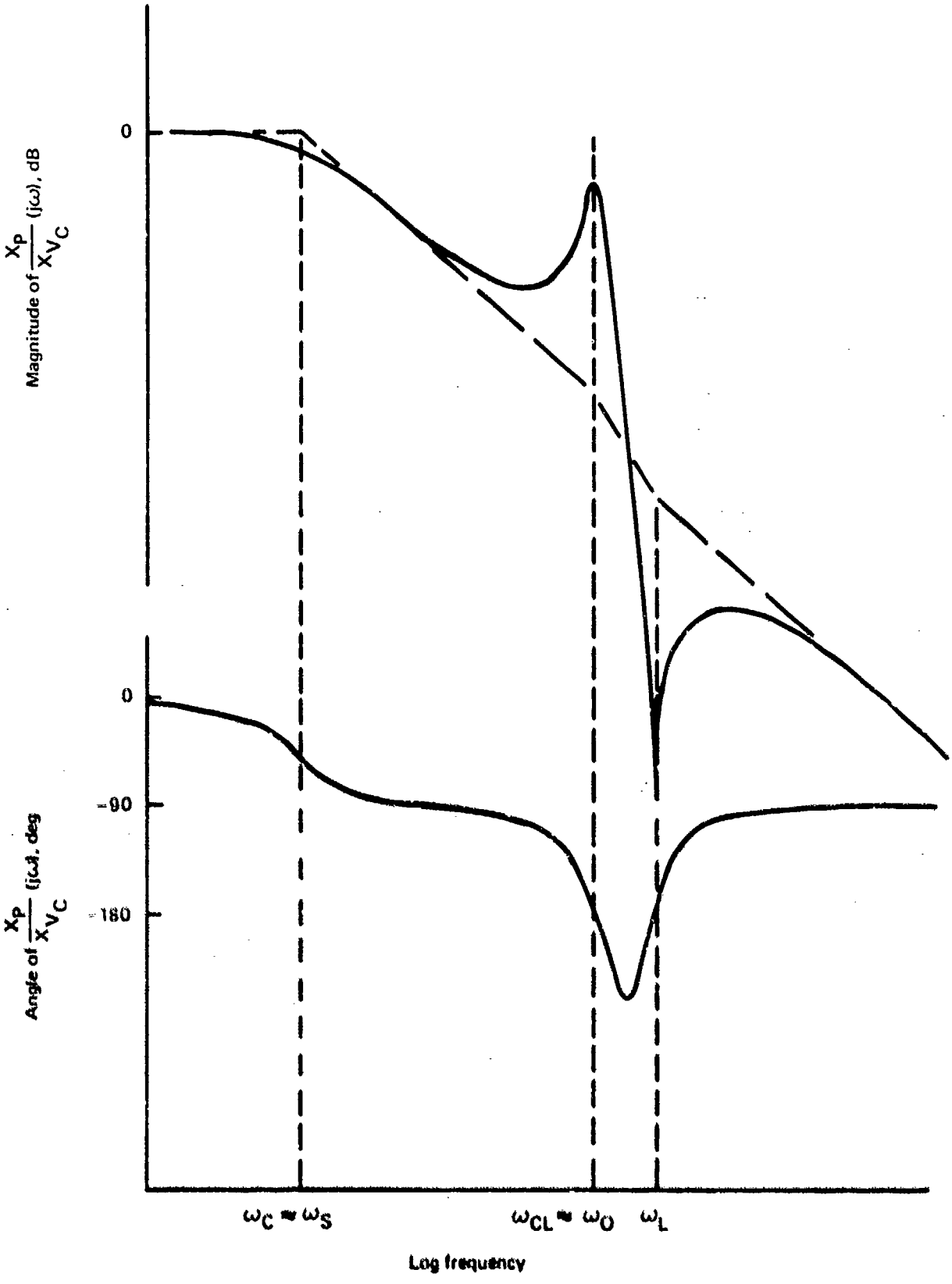

FIGURE A-9.–CLOSED-LOOP FREQUENCY RESPONSE

The complete equation is shown by substituting for ζ_O from equation (18):

$$\left.\begin{aligned} \zeta_{CL} &\approx \frac{K_V R_{PF}}{2A^2}\omega_O M_L - \frac{K_V R_F \omega_O}{2A}\left(\frac{M_L}{K}\right) \\ \zeta_{CL} &\approx \frac{K_V R_{PF}}{2A^2}\sqrt{M_L K_{TOT}}\left[1 - \frac{A R_F}{K R_{PF}}\right] \\ \zeta_{CL} &\approx \frac{K_V R_{PF}}{2A^2}\sqrt{M_L K_{TOT}}\left[1 - \frac{K_A(0)}{K_A(\infty)}\right] \end{aligned}\right\} \quad (35)$$

Equation (35) verifies the relationship between stiffness ratio and system stability, since the damping ratio becomes negative whenever the stiffness ratio exceeds 1.0.

STRUCTURAL FEEDBACK

If the structure is flexible, the structural deflections, which are a function of load, are fed back as added inputs to the valve, as illustrated in the simplified diagram of figure A-10. Since the valve receives an input as a function of load pressure, the structural feedback is effectively a pressure feedback term. The structural feedback is destabilizing if the effective pressure gain of the actuator is raised.

The magnitude of the structural feedback cannot be determined easily when it is transmitted through a complex structure. A structural model of the total structure and actuator must be developed and analyzed. Only then can the stability margin of the system be predicted.

ELECTRICAL STIFFNESS COMPENSATION

An actuation system that has adequate stability margin frequently has a static stiffness that is inadequate to satisfy the static load requirements. That is, under high aerodynamic loads, the actuator does not deflect the surface nearly as far as commanded. The nonlinear effects of repeatability (hysterisis) are also inversely proportional to the static stiffness.

The stiffness can be increased in a given frequency range by filtering either the position feedback or the pressure feedback. Neither method was practical for the test program since both feedbacks were mechanical, so the stiffness was "compensated" electrically by introducing a parallel position path through the EC servo, as in figure A-11.

Using equation (2), and letting $G_2(s)$ represent the EC servo:

$$K_A(s) = \frac{-F_L(s)}{X_p(s)} = \frac{K\left[s + \frac{K_V}{A}\left(R_F + G_2(s)\,H_2(s)\right)\right]}{s + \frac{K K_V R_{PF}}{A^2}} \quad (36)$$

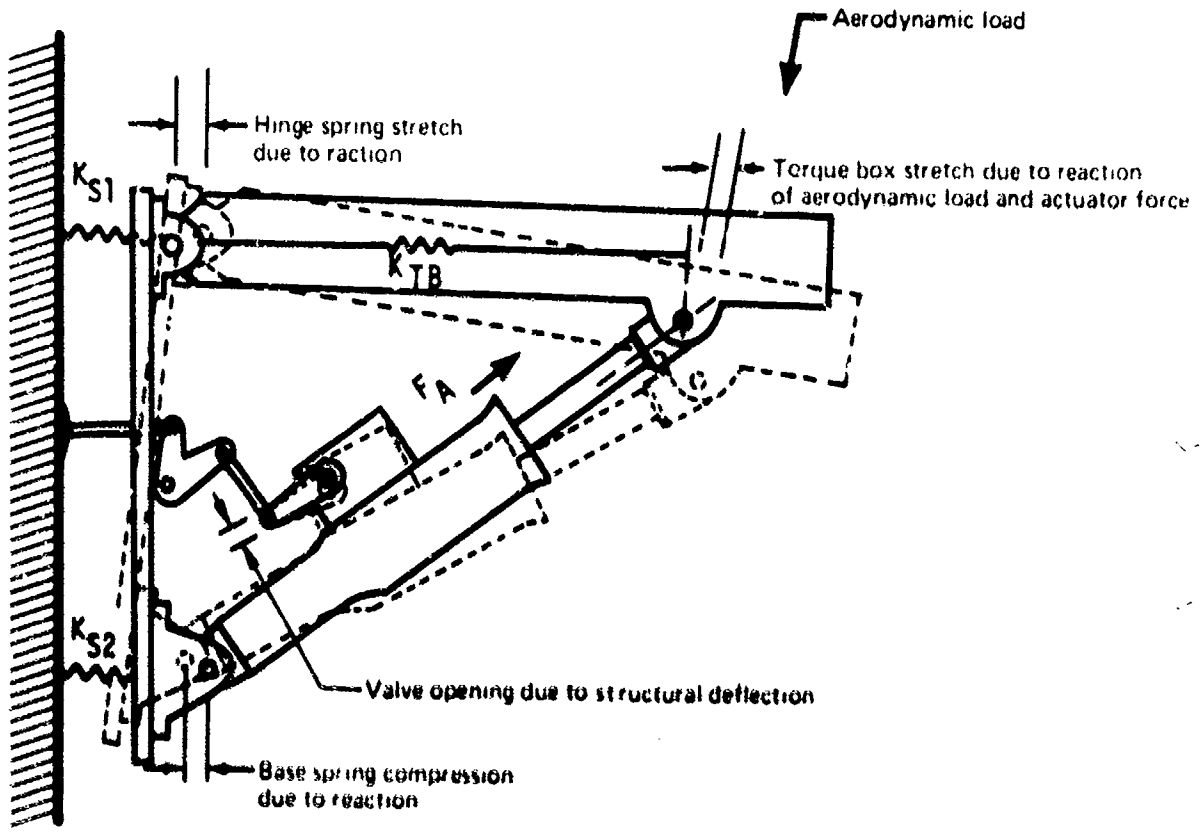

FIGURE A-10.– STRUCTURAL FEEDBACK

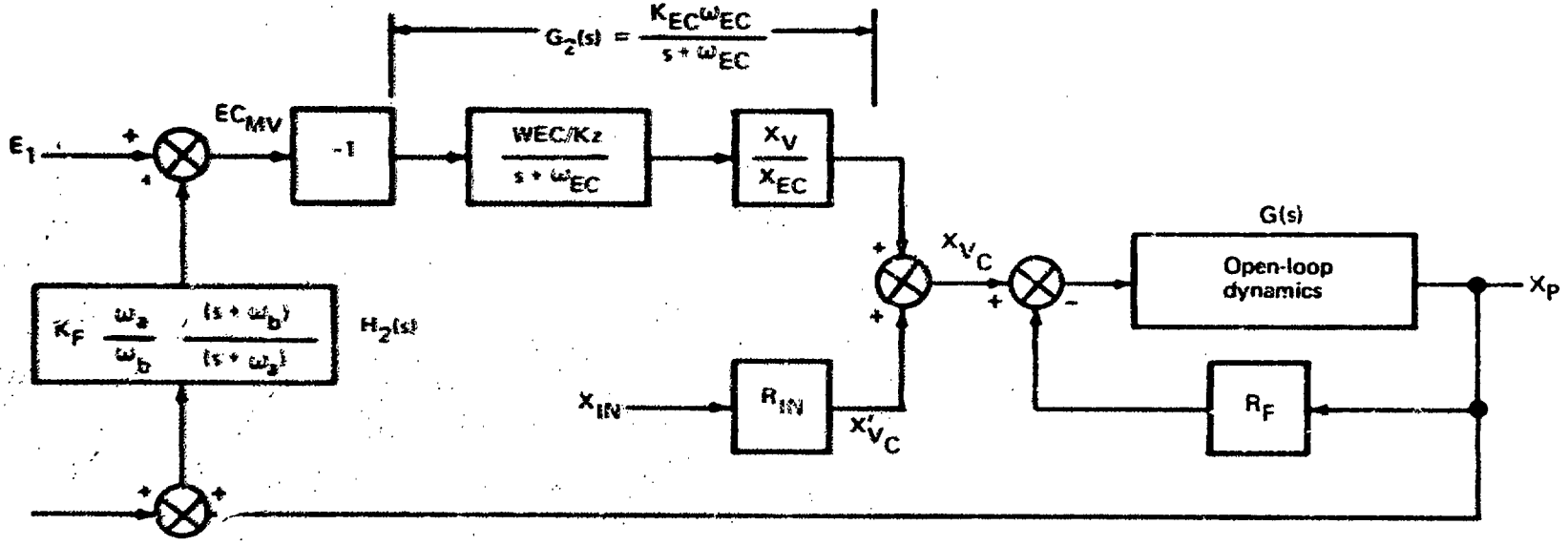

FIGURE A-11.–ELECTRICAL STIFFNESS COMPENSATION LOOP

Let

$$H_2(s) = K_F \left(\frac{\omega_a}{\omega_b}\right) \frac{(s+\omega_b)}{(s+\omega_a)} \tag{37}$$

where $\omega_b = \omega_{EC}$, to cancel the EC servo break frequency, or:

$$G_2(s)\, H_2(s) = K_{EC}\, K_F\, \frac{\omega_a}{(s+\omega_a)} \tag{38}$$

Substituting in equation (36):

$$K_A(s)\, \frac{-F_L(s)}{X_p(s)} = \frac{K\left[s^2 + \left(\omega_a + \frac{K_V R_F}{A}\right)s + \left(\frac{K_{EC}\, K_F\, K_V}{A} + \frac{K_V R_F}{A}\right)\omega_a\right]}{\left(s + \frac{K\, K_V\, R_{PF}}{A^2}\right)\left(s+\omega_a\right)} \tag{39}$$

Setting $s = 0$:

$$K_A(0) = \left[\frac{-F_L}{X_p}\right]_{s=0} = \frac{A\, R_F}{R_{PF}}\left[1 + \frac{K_{EC}\, K_F}{R_F}\right] \tag{40}$$

and for $s = \infty$:

$$K_A(\infty) = \left[\frac{-F_L}{X_p}\right]_{s=\infty} = K \tag{41}$$

Compared to the uncompensated case, the above stiffness equations show (fig. A-12) that:

- A new break frequency is added at $s = -\omega_a$
- The single servo break frequency is replaced by a new pair of break frequencies.
- The low-frequency stiffness (static stiffness) is increased by the factor $(A\, K_{EC}\, K_F)/R_{PF}$

A closed-loop transfer function can be written as shown in figure A-13 by simplifying figure A-11.

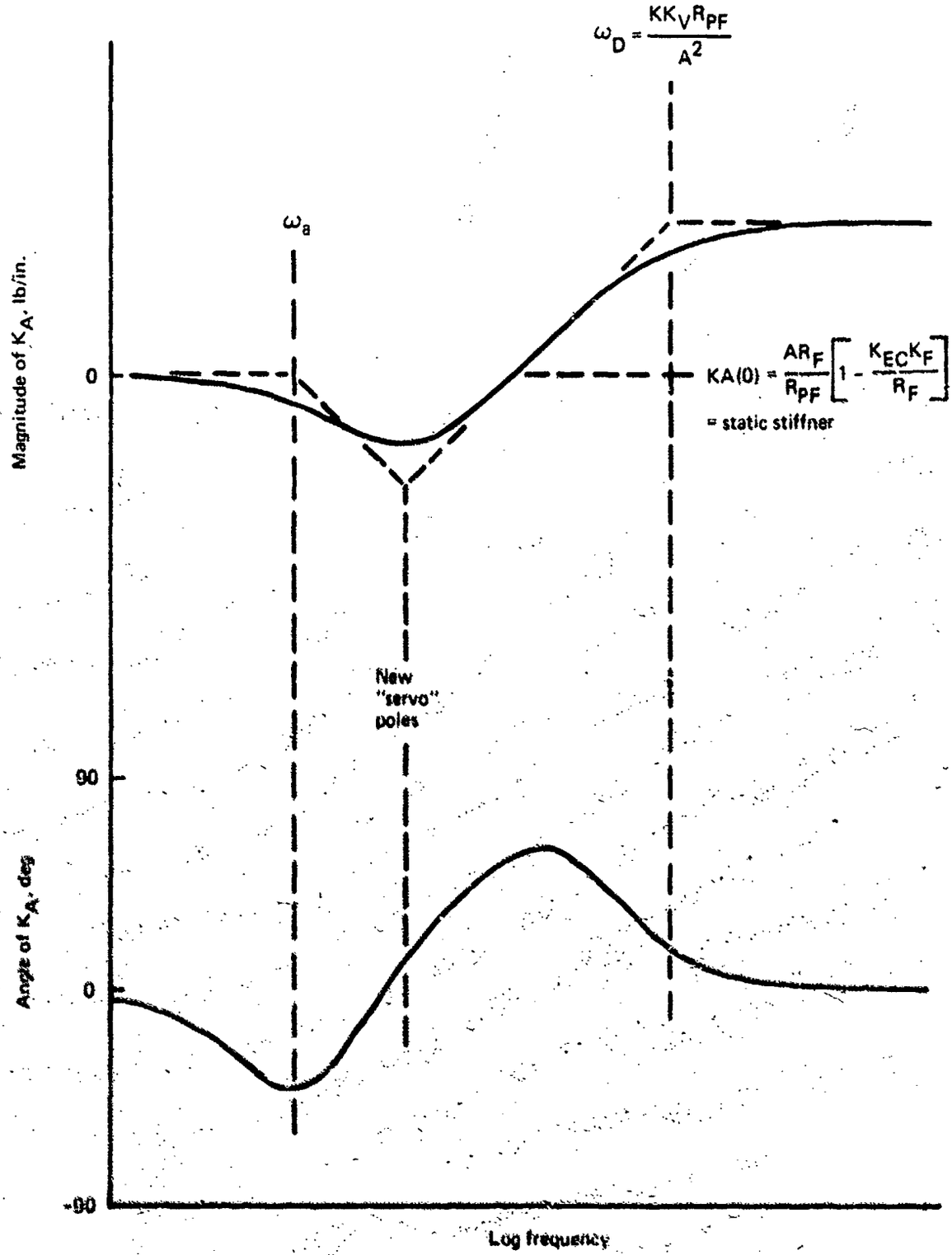

FIGURE A-12.–STIFFNESS FREQUENCY RESPONSE WITH ELECTRICAL COMPENSATION

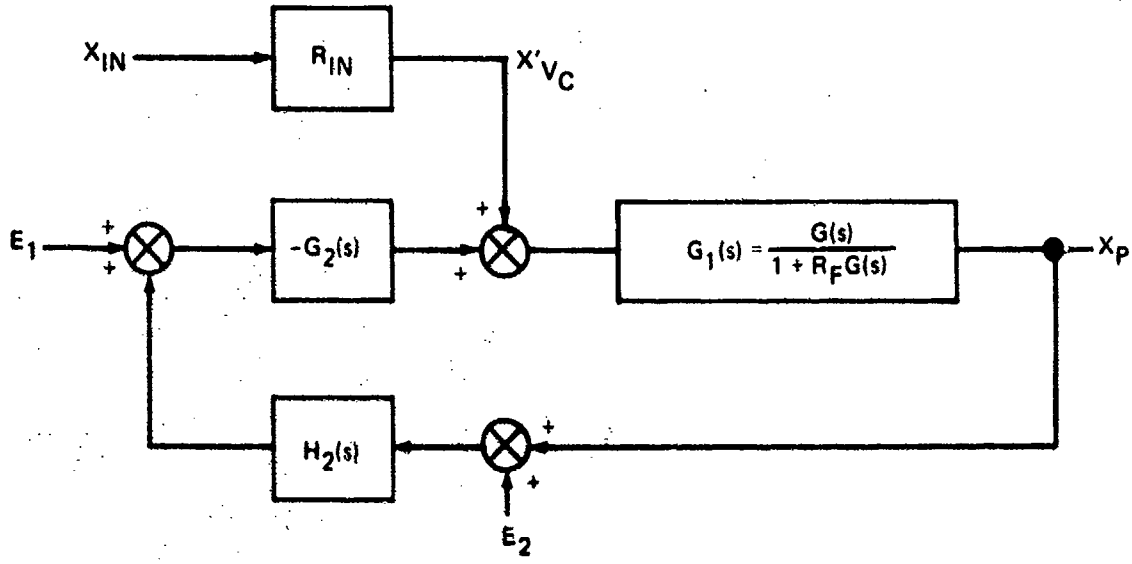

FIGURE A-13.–CLOSED-LOOP TRANSFER FUNCTION

The closed-loop transfer function through the mechanical input is:

$$\frac{X_p(s)}{R_{IN}\, X_{IN}(s)} = \frac{X_p(s)}{X'_{V_C}(s)} = \frac{G_1(s)}{1 + G_1(s)\, G_2(s)\, H_2(s)} \tag{42}$$

For stability, the quantity $1 + G_1(s)\, G_2(s)\, H_2(s)$ must not be zero or

$$|G_1(j\omega)\, G_2(j\omega)\, H_2(j\omega)| \leq 1.0 \tag{43}$$

The frequency where a phase shift of -180° occurs is not as easy to define as previously. It is approximately equal to ω_O, however.

The open-loop transfer function for the compensated system is:

$$G_1(s)\, G_2(s)\, H_2(s) = \frac{K_{LC}\, K_F\, \omega_C\, \omega_a}{R_F} \left(\frac{\omega_O}{\omega_L}\right)^2 \frac{(s^2 + \omega_L^2)}{(s + \omega_C)(s + \omega_a)(s^2 + 2\zeta_{CL}\, \omega_{CL}\, s + \omega_{CL}^2)} \tag{44}$$

Comparing the compensated system with the uncompensated system of equations (11) and (12), the compensated system has the following differences.

- The closed-loop poles become the new open-loop poles.
- The single pole at $s = 0$ has been replaced by a pole at the closed-loop servo break frequency.
- A new pole has been added at $s = -\omega_a$, adding an additional 90° of phase lag at the system natural frequency.

- The open-loop gain is changed from $(K_V R_F)/A$ to $(K_{EC} K_F)/R_F$.

The transfer function has become more complicated compared to the uncompensated system. The results of compensation can be demonstrated more easily by writ , the transfer function with both the normal and compensation feedback loops open:

$$G_1(s)\,G_2(s)\,H_2(s) = \left[R_F + K_{EC}\,K_F\,\frac{\omega_a}{(s+\omega_a)}\right]\left[\frac{K_V}{A}\left(\frac{\omega_O}{\omega_L}\right)^2\,\frac{(s^2+\omega_L{}^2)}{(s^2+2\zeta_O\,\omega_O\,s+\omega_O{}^2)}\right] \quad (45)$$

It is valid to assume that the compensation pole, ω_a, will be chosen at a frequency lower than one-tenth of the system natural frequency, ω_O, if the static stiffness only is to be increased. Further, the damping ratio, ζ_O, is very low, and the additional 90° of phase lag has a small effect on the open-loop frequency response near the system natural frequency. Therefore, at $s = j\omega_O$:

$$G_1(s)\,G_2(s)\,H_2(s) \approx \left[R_F + K_{EC}\,K_F\,\frac{\omega_a}{\omega_O}\right]\frac{A}{K\,R_{PF}} = \frac{K_A(0)}{K_A(\infty)}\left[1 + \frac{K_{EC}\,K_F\,\omega_a}{R_F\,\omega_O}\right] \quad (46)$$

Comparing equation (46) with equation (16), the new condition for stability is not stiffness ratio, but has been modified by the quantity in parentheses.

The closed-loop transfer function of equation (43) becomes fourth order with compensation. Based on previous assumptions that the system natural frequency is considerably higher than ω_C or ω_a, the closed-loop natural frequency ω_{CL} will be approximately the same with or without compensation. The transfer function through the mechanical path is:

$$\frac{X_p(s)}{X'_{V_C}(s)} \approx \frac{1}{R_F}\,\frac{\omega\,(s+\omega_a)}{\left[s^2 + (\omega+\omega_a)\,s + \omega\omega_a\left(1+\frac{K_{EC}\,K_F}{R_F}\right)\right]}\,\frac{\omega_O{}^2\,(s^2+\omega_L{}^2)}{\omega_L{}^2\,(s^2+2\zeta_{CL}\,\omega_{CL}\,s+\omega_{CL}{}^2)} \quad (47)$$

Compared with the normal closed-loop transfer function of equation (27), the compensated system has a new zero at $s = -\omega_a$, and the single servo break frequency has been replaced by a pair of poles. The pair of poles may be either real or complex depending on the choice of K_{EC} and ω_a. The zero in the numerator will cause over-shoot and may be undesirable in an actual system. It can be eliminated in an actual system design by proper prefiltering. For the sample configuration shown in figure A-11, the transfer function for an input at E_1 also has the zero, but using the E_2 input eliminates the zero.

APPENDIX B
STRUCTURAL MATRIX FOR DIGITAL PROGRAM

MATRIX

1	1	0	1.1465014E+06	1	2	0	).	1	3	0	2.7136159E-01	1	4	0	-7.9644054E+03
1	5	0	-2.9386767E+01	1	6	0	-1.4870862E+03	1	7	0	-1.3936655E+04	1	8	0	-1.5829917E+05
1	9	0	-2.1012246E+05	1	10	0	-1.0247003E+05	1	11	0	-2.1464336E+04	1	12	0	0.
1	13	0	1.4133170E-01	1	14	0	-1.3808157E+03	1	15	0	-1.0887172E+01	1	16	0	1.7542609E+03
1	17	0	3.2556618E+03	1	18	0	1.0333269E+04	1	19	0	3.4198248E+03	1	20	0	2.4564256E+03
1	21	0	8.3863516E+03	1	22	0	).	1	23	0	1.5984109E-01	1	24	0	5.0041729E+05
1	25	0	-7.0168423E+00	1	26	0	3.7267163E+02	1	27	0	1.4692125E+03	1	28	0	2.5245028E+03
1	29	0	5.7624473E+03	1	30	0	+.7856437E+03	1	31	0	4.0502715E+03	1	32	0	3.9421728E+03
1	37	0	-1.0255263E+05	1	38	0	-2.7531243E+05	1	39	0	-4.1900058E+04	1	40	0	-2.9802640E+05
1	43	0	-3.4191780E+01	1	50	0	).	1	51	0	-1.5727716E+05	1	52	0	-1.2250774E+05
2	1	0	0.	2	2	0	7.5190000E+05	2	3	0	0.	2	4	0	-7.5190000E+05
3	1	0	2.7196169E-01	3	2	0	).	3	3	0	4.7263179E+03	3	4	0	1.1016952E+01
3	5	0	-1.0717738E+04	3	6	0	>.0975595E+03	3	7	0	4.1086537E-01	3	8	0	-4.0171414E-01
3	9	0	-6.4733639E-02	3	10	0	-3.6307211E-02	3	11	0	-6.2513656E-02	3	12	0	0.
3	13	0	-1.9255636E-01	3	14	0	2.9722576E+00	3	15	0	1.4833149E+01	3	16	0	-1.4731518E+01
3	17	0	7.4343966E-03	3	18	0	7.8042035E-05	3	19	0	4.2159359E-02	3	20	0	1.4051456E-02
3	21	0	3.6993299E-03	3	22	0	).	3	23	0	-2.1771984E-01	3	24	0	1.1647211E+00
3	25	0	9.5600462E+00	3	26	0	-1.7275203E-04	3	27	0	-9.3391193E+00	3	28	0	2.4543816E-02
3	29	0	2.1795487E-02	3	30	0	3.5322769E-03	3	31	0	5.4087532E-03	3	32	0	3.8015267E-03
3	37	0	1.9256836E+00	3	38	0	-3.3674875E-01	3	39	0	6.4596405E-01	3	40	0	-7.5237859E-01
3	43	0	-1.1179685E+02	3	50	0	).	3	51	0	1.5721847E+01	3	52	0	3.2360030E-01
4	1	0	-7.9044054E+03	4	2	0	-7.5190000E+05	4	3	0	1.1016952E+01	4	4	0	1.4173267E+06
4	5	0	-1.1984379E+03	4	6	0	1.3968403E+04	4	7	0	-1.1939832E+04	4	8	0	1.1675581E+04
4	9	0	1.8814466E+03	4	10	0	1.0465282E+03	4	11	0	1.8170366E+03	4	12	0	0.
4	13	0	5.7252508E+00	4	14	0	-3.6386908E+04	4	15	0	-4.4103139E+02	4	16	0	3.0779849E+03
4	17	0	-2.1507633E+02	4	18	0	-2.2682455E+00	4	19	0	-1.2253281E+03	4	20	0	-4.0839724E+02
4	21	0	-1.0751883E+02	4	22	0	).	4	23	0	6.4734328E+00	4	24	0	-3.3651929E+04
4	25	0	-2.8424749E+02	4	26	0	3.0289373E+00	4	27	0	1.8456344E+02	4	28	0	-7.1335131E+02
4	29	0	-6.3347292E+02	4	30	0	-2.4798557E+02	4	31	0	-1.5722235E+02	4	32	0	-1.1148912E+02
4	37	0	-5.5968852E+04	4	38	0	2.4319607E+04	4	39	0	-1.8775144E+04	4	40	0	2.1867438E+04
4	43	0	-1.3850857E+03	4	50	0	).	4	51	0	-4.5694618E+05	4	52	0	-3.4405251E+05
5	1	0	-2.9386767E+01	5	2	0	).	5	3	0	-1.0717733E+04	5	4	0	-1.1984379E+03
5	5	0	4.6506837E+04	5	6	0	-+.3516581E+04	5	7	0	-4.4389553E+01	5	8	0	4.3407132E+01
5	9	0	6.9947872E+03	5	10	0	3.9307521E+00	5	11	0	6.7555432E+00	5	12	0	0.
5	13	0	2.8806640E+01	5	14	0	-3.2116672E+02	5	15	0	-1.2825813E+04	5	16	0	1.5918112E+03
5	17	0	-8.0332226E-01	5	18	0	-3.4328163E-03	5	19	0	-4.5554399E+00	5	20	0	-1.5183273E+02
5	21	0	-3.9373837E-01	5	22	0	).	5	23	0	2.3525674E+01	5	24	0	-1.2585377E+02
5	25	0	6.4496180E+03	5	26	0	1.9666693E-02	5	27	0	1.0091307E+03	5	28	0	-2.6520766E+00
5	29	0	-2.3551071E+00	5	30	0	-3.2195351E-01	5	31	0	-5.8444231E-01	5	32	0	-4.1773226E-01
5	37	0	-2.0387936E+02	5	38	0	3.0414722E+01	5	39	0	-6.9801679E+01	5	40	0	5.1299121E+01
5	43	0	1.2180187E+04	5	50	0	).	5	51	0	-1.6583211E+03	5	52	0	-3.4966567E+01
6	1	0	-1.4870862E+03	6	2	0	).	6	3	0	6.0972559E+03	6	4	0	1.3963458E+04
6	5	0	-+.3516581E+04	6	6	0	3.0585635E+05	6	7	0	-1.8014258E+05	6	8	0	1.6927816E+02
6	9	0	5.2705592E+03	6	10	0	3.3969343E+03	6	11	0	5.4284344E+03	6	12	0	0.
6	13	0	3.4543915E+01	6	14	0	1.0280537E+03	6	15	0	-2.6011133E+03	6	16	0	-1.6136129E+05
6	17	0	2.3669339E+03	6	18	0	-+.1398891E+03	6	19	0	4.0213852E+03	6	20	0	2.2671169E+03
6	21	0	5.3410493E+03	6	22	0	).	6	23	0	3.9056152E+01	6	24	0	-1.3363173E+03
6	25	0	-1.7150377E+03	6	26	0	-1.9525872E+03	6	27	0	3.2343171E+04	6	28	0	1.8291474E+04
6	29	0	1.3511630E+04	6	30	0	>.5675463E+03	6	31	0	3.9239006E+03	6	32	0	5.1135479E+03
6	37	0	-9.0341843E+03	6	38	0	+.9160792E+02	6	39	0	-3.1461637E+03	6	40	0	-9.8872212E+02

Row — Column — Power of s

6	43	0	-2.5312531E+04	6	50	0	0.	6	51	0	4.6182234E+03	6	52	0	7.7515200E+03
7	1	0	-1.3930655E+04	7	2	0	0.	7	3	0	4.1080397E-01	7	4	0	-1.1933832E+04
7	5	0	-4.4389558E+01	7	6	0	-1.9310259E+05	7	7	0	5.4871926E+05	7	8	0	-2.4897199E+05
7	9	0	-1.0722509E+04	7	10	0	+.2437263E+03	7	11	0	8.9843833E+03	7	12	0	0.
7	13	0	2.1348561E-01	7	14	0	3.9478762E+02	7	15	0	-1.6449387E+01	7	16	0	1.3733754E+04
7	17	0	-1.6515301E+05	7	18	0	-2.1613509E+04	7	19	0	-2.8749500E+03	7	20	0	-2.1130052E+01
7	21	0	5.0706694E+03	7	22	0	0.	7	23	0	2.4133414E-01	7	24	0	1.1263371E+03
7	25	0	-1.0599142E+01	7	26	0	2.5773093E+03	7	27	0	1.7101352E+04	7	28	0	2.3435836E+04
7	29	0	1.5173522E+04	7	30	0	7.2740272E+03	7	31	0	3.8675025E+03	7	32	0	4.3073147E+03
7	37	0	-3.1083622E+04	7	38	0	-5.6808345E+02	7	39	0	-7.5766318E+03	7	40	0	-5.8895219E+03
7	43	0	-5.1647669E+01	7	50	0	0.	7	51	0	4.0180423E+04	7	52	0	1.3944312E+04
8	1	0	-1.5829917E+05	8	2	0	0.	8	3	0	-4.0171434E-01	8	4	0	1.1675591E+04
8	5	0	4.3407132E+01	8	6	0	1.6927815E+02	8	7	0	-2.4897199E+05	8	8	0	1.1933948E+06
8	9	0	-3.8628876E+05	8	10	0	-2.4202897E+04	8	11	0	9.4580835E+03	8	12	0	0.
8	13	0	-2.0876076E-01	8	14	0	3.6031021E+03	8	15	0	1.6081419E+01	8	16	0	1.4342315E+03
8	17	0	-1.5473696E+04	8	18	0	-2.1301712E+05	8	19	0	-3.4065857E+04	8	20	0	-4.7825684E+03
8	21	0	5.1224404E+03	8	22	0	0.	8	23	0	-2.3604185E-01	8	24	0	-1.2718167E+03
8	25	0	1.0364563E+01	8	26	0	3.3733827E+02	8	27	0	3.4099545E+03	8	28	0	5.5312999E+03
8	29	0	1.8401884E+04	8	30	0	7.8326563E+03	8	31	0	4.8269025E+03	8	32	0	4.8012554E+03
8	37	0	-2.8322005E+05	8	38	0	-1.1306834E+04	8	39	0	-4.2048454E+04	8	40	0	-3.6503794E+04
8	43	0	5.0504607E+01	8	50	0	0.	8	51	0	2.4176371E+05	8	52	0	3.4265719E+04
9	1	0	-2.1012246E+05	9	2	0	0.	9	3	0	-6.4733639E-02	9	4	0	1.8314466E+03
9	5	0	6.9947872E+00	9	6	0	3.2705592E+03	9	7	0	-1.0722539E+04	9	8	0	-3.8628076E+05
9	9	0	1.2333956E+06	9	10	0	-3.9479866E+05	9	11	0	-1.0256686E+04	9	12	0	0.
9	13	0	-3.3648488E-02	9	14	0	3.6485167E+02	9	15	0	2.5914198E+00	9	16	0	2.5226249E+03
9	17	0	-7.1333045E+02	9	18	0	-3.4670303E+04	9	19	0	-1.8716133E+05	9	20	0	-2.7728470E+04
9	21	0	-4.7406729E+02	9	22	0	0.	9	23	0	-3.8036664E-02	9	24	0	-2.2662133E+02
9	25	0	1.6701844E+00	9	26	0	3.8214673E+02	9	27	0	2.1671031E+03	9	28	0	4.1522256E+03
9	29	0	1.6388485E+04	9	30	0	1.6261794E+04	9	31	0	9.2430935E+03	9	32	0	8.6489199E+03
9	37	0	-2.4329404E+04	9	38	0	-1.0693744E+04	9	39	0	-6.4027523E+03	9	40	0	-5.9755722E+03
9	43	0	8.1385088E+00	9	50	0	0.	9	51	0	1.6252035E+04	9	52	0	3.6705273E+02
10	1	0	-1.6247003E+05	10	2	0	0.	10	3	0	-3.6067210E-02	10	4	0	1.0465282E+03
10	5	0	3.8907523E+00	10	6	0	3.3969343E+03	10	7	0	4.2437263E+03	10	8	0	-2.4202897E+04
10	9	0	-3.9479866E+05	10	10	0	1.1622563E+06	10	11	0	-3.6133672E+05	10	12	0	0.
10	13	0	-1.3712049E-02	10	14	0	2.8971189E+01	10	15	0	1.4414409E+03	10	16	0	1.4599439E+03
10	17	0	4.9754158E+02	10	18	0	-5.4685685E+03	10	19	0	-2.7921069E+04	10	20	0	-1.4896890E+05
10	21	0	-2.7606158E+04	10	22	0	0.	10	23	0	-2.1157350E-02	10	24	0	-3.6522933E+01
10	25	0	9.2901657E-01	10	26	0	1.9687914E+02	10	27	0	1.0141630E+03	10	28	0	1.7277576E+03
10	29	0	4.4238614E+03	10	30	0	7.2619129E+03	10	31	0	1.4208198E+04	10	32	0	1.2142843E+04
10	37	0	-4.1679483E+02	10	38	0	-+.8424725E+03	10	39	0	2.6229699E+03	10	40	0	-1.3509177E+04
10	41	0	0.	10	42	0	0.	10	43	0	0.	10	44	0	0.
10	49	0	.52692665+10	10	50	0	0.	10	51	0	-1.2126639E+04	10	52	0	-1.6536414E+05
11	1	0	-2.1464988E+04	11	2	0	0.	11	3	0	-6.2519656E-02	11	4	0	1.8170964E+03
11	5	0	6.7555492E+00	11	6	0	3.4284044E+03	11	7	0	8.9843833E+03	11	8	0	9.4080865E+03
11	9	0	-1.8256686E+04	11	10	0	-3.6133672E+05	11	11	0	1.0976949E+06	11	12	0	0.
11	13	0	-3.2489985E-02	11	14	0	2.4654813E+02	11	15	0	2.5027873E+00	11	16	0	2.8362643E+03
11	17	0	1.7498108E+03	11	18	0	1.7262289E+03	11	19	0	-3.5315671E+03	11	20	0	-3.4227058E+04
11	21	0	-2.3407995E+05	11	22	0	0.	11	23	0	-3.6735722E-02	11	24	0	-3.3304162E+01
11	25	0	1.6130682E+00	11	26	0	+.4326239E+02	11	27	0	1.7423222E+03	11	28	0	2.4272835E+03
11	29	0	4.4720312E+03	11	30	0	7.1544847E+03	11	31	0	1.2416835E+04	11	32	0	1.7603115E+04
11	37	0	1.2535955E+01	11	38	0	-1.4298754E+03	11	39	0	3.7754136E+03	11	40	0	-4.7307625E+04
11	43	0	7.8601451E+00	11	50	0	0.	11	51	0	-1.7235J2E+04	11	52	0	-5.1527565E+05
12	1	0	0.	12	10	0	0.	12	11	0	0.	12	12	0	3.3175385E+05
12	13	0	0.	12	14	0	-3.3175385E+05	12	15	0	0.	12	16	0	0.
13	1	0	1.4133170E-01	13	2	0	0.	13	3	0	-1.9259J36E-01	13	4	0	5.7252500E+00
13	5	0	2.0886640E+01	13	6	0	3.4543915E+01	13	7	0	2.1346551E-01	13	8	0	-2.0876376E-01
13	9	0	-3.3648488E-02	13	10	0	-1.8712343E-02	13	11	0	-3.2481305E-02	13	12	0	0.

13	13	0	8.2036422E+03	13	14	0	1.5446081E+00	13	15	0	-1.6584771E+04	13	16	0	8.3810816E+03
13	17	0	3.8634704E-03	13	18	0	+.0556498E-05	13	19	0	2.1900011E-02	13	20	0	7.3021910E-03
13	21	0	1.9224495E-03	13	22	0	0.	13	23	0	-1.3650933E+00	13	24	0	6.0527649E-01
13	25	0	8.1931322E+01	13	26	0	-3.9774952E-05	13	27	0	-8.0063757E+01	13	28	0	1.2754866E-02
13	29	0	1.1326571E-02	13	30	0	+.4340114E-03	13	31	0	2.8107957E-03	13	32	0	1.9755585E-03
13	37	0	1.0007297E+00	13	38	0	-+.3433745E-01	13	39	0	3.3570179E-01	13	40	0	-3.9099238E-01
13	43	0	-5.8098035E+01	13	50	0	0.	13	51	0	8.1702518E+00	13	52	0	1.6816700E-01
14	1	0	-1.3808157E+03	14	2	0	0.	14	3	0	2.9722576E+00	14	4	0	-8.6386908E+04
14	5	0	-3.2116672E+02	14	6	0	1.0280537E+03	14	7	0	8.9478702E+02	14	8	0	5.6031021E+03
14	9	0	3.6485167E+02	14	10	0	2.0871183E+01	14	11	0	2.4654813E+02	14	12	0	-9.3175385E+05
14	13	0	1.5446081E+00	14	14	0	1.5783533E+06	14	15	0	-1.1898544E+02	14	16	0	4.9872070E+02
14	17	0	-5.5564474E+02	14	18	0	+.0522419E+02	14	19	0	-1.7393511E+02	14	20	0	-1.8692439E+02
14	21	0	-6.1617181E+02	14	22	0	0.	14	23	0	1.7464592E+00	14	24	0	-2.4793115E+05
14	25	0	-7.6686769E+01	14	26	0	-2.0384704E+01	14	27	0	9.8314477E+01	14	28	0	7.2693555E+01
14	29	0	-8.0211656E+01	14	30	0	-5.3773624E+01	14	31	0	-1.0108234E+02	14	32	0	-1.2396880E+02
14	37	0	-2.5455258E+04	14	38	0	3.2938705E+03	14	39	0	-8.4316316E+02	14	40	0	4.5945861E+03
14	43	0	-3.7368050E+02	14	50	0	0.	14	51	0	-2.8244925E+05	14	52	0	-3.9511942E+03
15	1	0	-1.0887172E+01	15	2	0	0.	15	3	0	1.4833149E+01	15	4	0	-4.4103190E+02
15	5	0	-1.2826810E+04	15	6	0	-2.6610133E+03	15	7	0	-1.6445387E+01	15	8	0	1.6001419E+01
15	9	0	2.5314198E+00	15	10	0	1.4414403E+00	15	11	0	2.5027873E+00	15	12	0	0.
15	13	0	-1.6584771E+04	15	14	0	-1.1898544E+02	15	15	0	8.0524509E+04	15	16	0	-3.0263866E+04
15	17	0	-2.9761381E-01	15	18	0	-3.1241792E-03	15	19	0	-1.6877117E+00	15	20	0	-5.6250797E-01
15	21	0	-1.4809160E-01	15	22	0	0.	15	23	0	1.4373531E+02	15	24	0	-4.6626122E+01
15	25	0	-2.8759611E+04	15	26	0	5.9156128E-03	15	27	0	6.1675326E+03	15	28	0	-9.8253797E-01
15	29	0	-8.7251707E-01	15	30	0	-3.4156415E-01	15	31	0	-2.1652344E-01	15	32	0	-1.5218274E-01
15	37	0	-7.7088976E+01	15	38	0	3.3496731E+01	15	39	0	-2.5860037E+01	15	40	0	3.6119224E+01
15	41	0	0.	15	42	0	0.	15	43	0	0.	15	44	0	0.
15	45	0	0.	15	46	0	0.	15	47	0	0.	15	48	0	0.
15	49	0	4.4754523E+03	15	50	0	0.	15	51	0	-6.2937709E+02	15	52	0	-1.2954369E+01
16	1	0	1.7542609E+03	16	2	0	0.	16	3	0	-1.4731518E+01	16	4	0	3.0779849E+03
16	5	0	1.5918112E+03	16	6	0	-1.6190129E+05	16	7	0	1.3733754E+04	16	8	0	1.4342315E+03
16	9	0	2.5226249E+03	16	10	0	1.5499493E+03	16	11	0	2.8362643E+03	16	12	0	0.
16	13	0	8.3810816E+03	16	14	0	+.9872070E+02	16	15	0	-3.0263866E+04	16	16	0	4.2446874E+05
16	17	0	-1.5220509E+05	16	18	0	5.1601203E+02	16	19	0	6.5025209E+03	16	20	0	3.0422694E+03
16	21	0	5.1629826E+03	16	22	0	0.	16	23	0	-1.4192183E+02	16	24	0	-4.1834018E+02
16	25	0	6.2316109E+03	16	26	0	-1.3019682E+04	16	27	0	-1.2473438E+05	16	28	0	-1.3511452E+04
16	29	0	2.3473833E+03	16	30	0	+.4727709E+03	16	31	0	3.3005817E+03	16	32	0	5.6639597E+03
16	37	0	-1.8074437E+03	16	38	0	3.7552610E+02	16	39	0	-8.6866322E+02	16	40	0	7.1974864E+02
16	43	0	-4.4059229E+03	16	50	0	0.	16	51	0	1.2927690E+03	16	52	0	4.4844198E+03
17	1	0	3.2556618E+03	17	2	0	0.	17	3	0	7.4343966E-03	17	4	0	-2.1607633E+02
17	5	0	-6.0332226E-01	17	6	0	2.3669333E+03	17	7	0	-1.6515301E+05	17	8	0	-1.5473696E+04
17	9	0	-7.1333045E+02	17	10	0	+.3754153E+02	17	11	0	1.7498108E+03	17	12	0	0.
17	13	0	3.8634704E-03	17	14	0	-5.5664474E+02	17	15	0	-2.9761381E-01	17	16	0	-1.5220509E+05
17	17	0	6.8389544E+05	17	18	0	-2.1438460E+05	17	19	0	-5.3079435E+03	17	20	0	3.4736003E+03
17	21	0	6.2461605E+03	17	22	0	0.	17	23	0	4.3683529E-03	17	24	0	1.9569667E+02
17	25	0	-1.9181374E-01	17	26	0	-5.2281717E+02	17	27	0	-1.7561689E+04	17	28	0	-1.0762622E+05
17	29	0	-2.4013225E+04	17	30	0	-7.2323913E+03	17	31	0	-5.2265349E+02	17	32	0	3.6178712E+03
17	37	0	7.7983209E+02	17	38	0	1.1033663E+03	17	39	0	2.3344233E+02	17	40	0	1.6438931E+03
17	43	0	-9.3467302E-01	17	50	0	0.	17	51	0	1.1034106E+03	17	52	0	3.3780202E+03
18	1	0	1.0333269E+04	18	2	0	0.	18	3	0	7.8042035E-05	18	4	0	-2.2682455E+00
18	5	0	-8.4328168E-03	18	6	0	-+.1898891E+03	18	7	0	-2.1613508E+04	18	8	0	-2.1301712E+05
18	9	0	-3.4670300E+04	18	10	0	-5.4685685E+03	18	11	0	1.7262288E+03	18	12	0	0.
18	13	0	4.0556498E-05	18	14	0	+.0522419E+02	18	15	0	-3.1241792E-03	18	16	0	5.1601200E+02
18	17	0	-2.1438460E+05	18	18	0	1.0634764E+06	18	19	0	-4.2895818E+05	18	20	0	-1.3512115E+04
18	21	0	2.4203710E+04	18	22	0	0.	18	23	0	4.5856466E-05	18	24	0	5.0653121E+02
18	25	0	-2.0135507E-03	18	26	0	1.2740986E+03	18	27	0	-3.0118379E+03	18	28	0	-2.1875264E+04
18	29	0	-1.5053735E+05	18	30	0	-2.4829343E+04	18	31	0	-2.5930691E+03	18	32	0	1.3968666E+04

18	37	0	5.2590302E+01	18	38	0	5.1090384E+03	18	39	0	2.5279672E+03	18	40	0	9.1929410E+03
18	43	0	-9.8116618E-03	18	50	0	0.	18	51	0	-1.0022570E+03	18	52	0	7.7500304E+03
19	1	0	3.4198248E+03	19	2	0	0.	19	3	0	4.2159059E-02	19	4	0	-1.2253281E+03
19	5	0	-4.5554889E+00	19	6	0	9.8218062E+03	19	7	0	-2.8749500E+03	19	8	0	-3.4065857E+04
19	9	0	-1.8716103E+05	19	10	0	-2.7921063E+04	19	11	0	-3.5315671E+03	19	12	0	0.
19	13	0	2.1909811E-02	19	14	0	-1.7393511E+02	19	15	0	-1.6877117E+08	19	16	0	6.5025269E+03
19	17	0	-5.3079435E+03	19	18	0	-4.2535818E+05	19	19	0	1.2400778E+06	19	20	0	-4.3306600E+05
19	21	0	1.1266E31E+04	19	22	0	0.	19	23	0	2.4772105E-02	19	24	0	2.8569724E+02
19	25	0	-1.0877395E+08	19	26	0	1.7267101E+03	19	27	0	3.0747197E+03	19	28	0	-4.8355725E+05
19	29	0	-2.6113385E+04	19	30	0	-1.1906341E+05	19	31	0	-2.2061127E+04	19	32	0	2.3968709E+03
19	37	0	1.8552635E+04	19	38	0	1.7147353E+03	19	39	0	2.1015864E+03	19	40	0	6.2575697E+03
19	43	0	-5.3303542E+00	19	50	0	0.	19	51	0	-5.8575784E+03	19	52	0	9.2522078E+03
20	1	0	2.4564256E+03	20	2	0	0.	20	3	0	1.4051456E-02	20	4	0	-4.0839724E+02
20	5	0	-1.5163273E+00	20	6	0	2.0671109E+03	20	7	0	-2.1136052E+01	20	8	0	-4.7825684E+03
20	9	0	-2.7728470E+04	20	10	0	-1.4896890E+05	20	11	0	-3.4227058E+04	20	12	0	0.
20	13	0	7.3821918E-03	20	14	0	-1.8592433E+02	20	15	0	-5.6250797E-01	20	16	0	3.0422694E+03
20	17	0	3.4736803E+03	20	18	0	-1.3512115E+04	20	19	0	-4.3306600E+05	20	20	0	1.1932209E+06
20	21	0	-4.0563156E+05	20	22	0	0.	20	23	0	8.2564493E-03	20	24	0	-4.0275167E+01
20	25	0	-3.6253948E-01	20	26	0	9.5866290E+02	20	27	0	2.4945826E+03	20	28	0	1.7146863E+03
20	29	0	-3.7964116E+03	20	30	0	-2.0171562E+04	20	31	0	-1.1057034E+05	20	32	0	-2.2033501E+04
20	37	0	5.3402658E+03	20	38	0	-5.3730615E+02	20	39	0	1.8536735E+03	20	40	0	2.0262427E+03
20	43	0	-1.7665881E+00	20	50	0	0.	20	51	0	-4.7495481E+03	20	52	0	1.0025598E+04
21	1	0	5.3863516E+03	21	2	0	0.	21	3	0	3.6993299E-03	21	4	0	-1.0751883E+02
21	5	0	-3.9973037E-01	21	6	0	5.3410493E+03	21	7	0	5.0705634E+03	21	8	0	5.1224404E+03
21	9	0	-4.7486729E+02	21	10	0	-2.7606163E+04	21	11	0	-2.3407935E+05	21	12	0	0.
21	13	0	1.9224495E-03	21	14	0	-5.1617181E+02	21	15	0	-1.4809150E-01	21	16	0	5.1629826E+03
21	17	0	6.2461685E+03	21	18	0	2.4203713E+04	21	19	0	1.1268631E+04	21	20	0	-4.0563156E+05
21	21	0	7.8375196E+05	21	22	0	0.	21	23	0	2.1736772E-03	21	24	0	-5.3711664E+02
21	25	0	-9.5465850E-02	21	26	0	1.7417755E+03	21	27	0	6.5871508E+03	21	28	0	1.0714361E+04
21	29	0	1.5527222E+04	21	30	0	1.0493571E+04	21	31	0	-2.0416376E+04	21	32	0	-1.5887058E+05
21	37	0	1.6932991E+04	21	38	0	-7.3663155E+02	21	39	0	7.1659700E+03	21	40	0	2.9680225E+03
21	43	0	-4.6589885E-01	21	50	0	0.	21	51	0	-1.8407094E+04	21	52	0	1.3529964E+04
22	21	0	0.	22	22	0	1.4395765E+06	22	23	0	0.	22	24	0	-1.4395765E+06
23	1	0	1.5988189E-01	23	2	0	0.	23	3	0	-2.1771384E-01	23	4	0	6.4734328E+00
23	5	0	2.3525674E+01	23	6	0	5.8856152E+01	23	7	0	2.4138414E-01	23	8	0	-2.3604185E-01
23	9	0	-3.8836664E-02	23	10	0	-2.1157360E-02	23	11	0	-3.6735722E-02	23	12	0	0.
23	13	0	-1.8558585E+03	23	14	0	1.7464592E+00	23	15	0	1.4373531E+02	23	16	0	-1.4192283E+02
23	17	0	4.3563529E-03	23	18	0	4.5856460E-05	23	19	0	2.4772105E-02	23	20	0	8.2564493E-03
23	21	0	2.1736772E-03	23	22	0	0.	23	23	0	2.2278426E+04	23	24	0	6.8437465E-01
23	25	0	-3.7096535E+04	23	26	0	-2.0150684E-04	23	27	0	1.4818111E+04	23	28	0	1.4421618E+02
23	29	0	1.2506739E-02	23	30	0	5.0134523E-03	23	31	0	3.1781146E-03	23	32	0	2.2337257E-03
23	37	0	1.1315061E+00	23	38	0	-4.9166248E-01	23	39	0	3.7957157E-01	23	40	0	-4.4208709E-01
23	43	0	-6.5590349E-01	23	50	0	0.	23	51	0	9.2379432E+00	23	52	0	1.9014325E-01
24	1	0	5.6041729E+03	24	2	0	0.	24	3	0	1.1647211E+00	24	4	0	-3.3851929E+04
24	5	0	-1.2585371E+02	24	6	0	-1.3363173E+03	24	7	0	1.1263371E+03	24	8	0	-1.2718187E+03
24	9	0	-2.2562133E+02	24	10	0	-3.4522933E+01	24	11	0	-3.3984162E+01	24	12	0	0.
24	13	0	6.0527649E-01	24	14	0	-2.4793115E+05	24	15	0	-4.6626122E+01	24	16	0	-4.1834018E+02
24	17	0	1.9569667E+02	24	18	0	5.0653121E+02	24	19	0	2.8569724E+02	24	20	0	-4.0275167E+01
24	21	0	-5.3711664E+02	24	22	0	-1.4395765E+06	24	23	0	6.8437465E-01	24	24	0	1.8218645E+06
24	25	0	-3.0050792E+01	24	26	0	1.3250866E+01	24	27	0	2.5498958E+01	24	28	0	6.8550610E+01
24	29	0	1.6103418E+02	24	30	0	5.1756645E+01	24	31	0	-2.3407641E+01	24	32	0	2.2756289E+02
24	37	0	2.6661360E+03	24	38	0	-5.9257461E+03	24	39	0	1.8197642E+04	24	40	0	-1.4450892E+04
24	43	0	-1.4643198E+02	24	50	0	0.	24	51	0	-1.2866747E+05	24	52	0	3.9418662E+03
25	1	0	-7.0166423E+00	25	2	0	0.	25	3	0	9.5630402E+00	25	4	0	-2.8424749E+02
25	5	0	6.4496180E+03	25	6	0	-1.2715377E+03	25	7	0	-1.0593142E+01	25	8	0	1.0364503E+01
25	9	0	1.6701844E+00	25	10	0	3.2901657E-01	25	11	0	1.6133602E+03	25	12	0	0.
25	13	0	8.1931322E+01	25	14	0	-7.6634763E+01	25	15	0	-2.8759611E+04	25	16	0	6.2318109E+03

25	17	0	-1.9181374E-01	25	18	0	-2.0135507E-03	25	19	0	-1.0877395E+03	25	20	0	-3.6253948E-01
25	21	0	-9.5445850E-02	25	22	0	0.	25	23	0	-3.7090535E+04	25	24	0	-3.0050792E+01
25	25	0	8.7369102E+04	25	26	0	+.4571505E-03	25	27	0	-3.5307J01E+04	25	28	0	-6.3325113E-01
25	29	0	-5.6234206E-01	25	30	0	-2.2013993E-01	25	31	0	-1.3955J55E-01	25	32	0	-9.6082612E-02
25	37	0	-4.9584269E+01	25	38	0	2.1588823E+01	25	39	0	-1.6666336E+01	25	40	0	1.9412066E+01
25	43	0	2.8844536E+03	25	50	0	0.	25	51	0	-4.0563700E+02	25	52	0	-8.3491622E+00
26	1	0	3.7267163E+02	26	2	0	0.	26	3	0	-1.7275209E-04	26	4	0	5.02u9373E+00
26	5	0	1.8566693E-02	26	6	0	-1.3625872E+03	26	7	0	2.5773093E+03	26	8	0	3.3733827E+02
26	9	0	3.8214679E+02	26	10	0	1.9o87914E+02	26	11	0	4.4926230E+02	26	12	0	0.
26	13	0	-8.9774952E-05	26	14	0	-2.0384704E+01	26	15	0	6.9159128E-03	26	16	0	-1.3019642E+04
26	17	0	-6.2281717E-02	26	18	0	1.2740985E+03	26	19	0	1.7267101E+03	26	20	0	9.5865290E+02
26	21	0	1.7417755E+03	26	22	0	0.	26	23	0	-1.015o884E-04	26	24	0	1.3250866E+01
26	25	0	4.4571505E-03	26	26	0	1.4646952E+05	26	27	0	-2.5619960E+05	26	28	0	6.0778789E+04
26	29	0	2.9963371E+04	26	30	0	1.3741043E+04	26	31	0	4.8403276E+03	26	32	0	5.1111421E+03
26	37	0	-8.6011536E+00	26	38	0	1.2519711E+02	26	39	0	-4.4891841E+01	26	40	0	1.5908138E+02
26	43	0	2.1718874E-02	26	50	0	0.	26	51	0	1.9057141E+02	26	52	0	6.6414866E+02
27	1	0	1.4692125E+03	27	2	0	0.	27	3	0	-9.3391193E+00	27	4	0	1.8456344E+02
27	5	0	1.0091367E+03	27	6	0	3.2343171E+04	27	7	0	1.7101352E+04	27	8	0	3.4099545E+03
27	9	0	2.1671091E+03	27	10	0	1.0101681E+03	27	11	0	1.7423222E+03	27	12	0	0.
27	13	0	-8.0063757E+01	27	14	0	9.8314477E+01	27	15	0	6.1e7532oE+03	27	16	0	-1.2478438E+05
27	17	0	-1.7561689E+04	27	18	0	-3.0118373E+03	27	19	0	3.0747137E+03	27	20	0	2.4945826E+03
27	21	0	6.5871508E+03	27	22	0	0.	27	23	0	1.4819111E+04	27	24	0	2.5098966E+01
27	25	0	-3.5307061E+04	27	26	0	-2.5619960E+05	27	27	0	8.5091350E+05	27	28	0	-5.3193099E+05
27	29	0	-2.5315262E+04	27	30	0	9.4052317E+03	27	31	0	1.8073204E+04	27	32	0	2.1790196E+04
27	37	0	1.1263737E+02	27	38	0	+.5227727E+02	27	39	0	-1.2527J75E+02	27	40	0	5.662896lE+02
27	43	0	-2.8191665E+03	27	50	0	0.	27	51	0	1.0670344E+03	27	52	0	2.4241755E+03
28	1	0	2.5245028E+03	28	2	0	0.	28	3	0	2.4543810E-02	28	4	0	-7.1335131E+02
28	5	0	-2.6520766E+00	28	6	0	1.8251474E+04	28	7	0	2.3435836E+04	28	8	0	5.5312999E+03
28	9	0	+.1522256E+03	28	10	0	1.7277575E+03	28	11	0	2.4272835E+03	28	12	0	0.
28	13	0	1.2754906E-02	28	14	0	7.2693555E+01	28	15	0	-9.3253737E-01	28	16	0	-1.3511452E+04
28	17	0	-1.0762622E+05	28	18	0	-2.1875264E+04	28	19	0	-4.8355725E+03	28	20	0	1.7146863E+03
28	21	0	1.0714751E+04	28	22	0	0.	28	23	0	1.4421618E-02	28	24	0	6.8550616E+01
28	25	0	-5.3325113E-01	28	26	0	5.0778783E+04	28	27	0	-5.3193J99E+05	28	28	0	1.1353997E+06
28	29	0	-5.7916737E+05	28	30	0	-5.3035547E+04	28	31	0	-4.1377004E+02	28	32	0	5.0640854E+04
28	37	0	1.4218749E+03	28	38	0	1.3235o63E+02	28	39	0	0.2925621E+02	28	40	0	1.0598376E+03
28	43	0	-3.0857161E+00	28	50	0	0.	28	51	0	-1.0786054E+01	28	52	0	2.8035936E+03
29	1	0	5.7o24473E+03	29	2	0	0.	29	3	0	2.1795437E-02	29	4	0	-6.3347292E+02
29	5	0	-2.3551071E+00	29	6	0	1.3511E33E+04	29	7	0	1.5173522E+04	29	8	0	1.8401804E+04
29	9	0	1.0300405E+04	29	10	0	+.4238614E+03	29	11	0	4.4726312E+03	29	12	0	0.
29	13	0	1.1326571E-02	29	14	0	-3.3211659E+01	29	15	0	-8.7251707E-01	29	16	0	2.3473833E+03
29	17	0	-2.4013225E+04	29	18	0	-1.5053735E+05	29	19	0	-2.6113335E+04	29	20	0	-3.7964116E+03
29	21	0	1.5527322E+04	29	22	0	0.	29	23	0	1.2806739E-02	29	24	0	1.6303418E+02
29	25	0	-5.6234206E-01	29	26	0	1.3463371E+04	29	27	0	-2.5315262E+04	29	28	0	-5.7916737E+05
29	29	0	1.4846546E+06	29	30	0	-7.1957905E+05	29	31	0	-8.7636553E+04	29	32	0	5.0854058E+04
29	37	0	4.7370975E+03	29	38	0	1.0144335E+03	29	39	0	9.8093109E+02	29	40	0	2.4564373E+03
29	43	0	-2.7401893E+00	29	50	0	0.	29	51	0	-2.6306534E+03	29	52	0	4.7661403E+03
30	1	0	4.8856437E+03	30	2	0	0.	30	3	0	9.5322709E-03	30	4	0	-2.4798557E+02
30	5	0	-9.2195350E-01	30	6	0	5.5575463E+03	30	7	0	7.2744272E+03	30	8	0	7.8326503E+03
30	9	0	1.6261794E+04	30	10	0	7.2619123E+03	30	11	0	7.1544847E+03	30	12	0	0.
30	13	0	4.4340114E-03	30	14	0	-3.377362+E+01	30	15	0	-3.4156416E-01	30	16	0	4.4727709E+03
30	17	0	-7.2323913E+03	30	18	0	-2.4629349E+04	30	19	0	-1.1906341E+05	30	20	0	-2.0171562E+04
30	21	0	1.0493570E+04	30	22	0	0.	30	23	0	5.0134528E-03	30	24	0	5.1756646E+01
30	25	0	-2.2013998E-01	30	26	0	1.3741045E+04	30	27	0	9.4052317E+03	30	28	0	-6.3005547E+04
30	29	0	-7.1957866E+05	30	30	0	1.5694488E+06	30	31	0	-6.9850499E+05	30	32	0	-2.2805297E+04
30	37	0	4.1112217E+03	30	38	0	5.5286278+E+02	30	39	0	9.9984802E+02	30	40	0	1.9664532E+03
30	43	0	-1.0727016E+00	30	50	0	0.	30	51	0	-2.8663575E+03	30	52	0	5.6296663E+03
31	1	0	4.0502715E+03	31	2	0	0.	31	3	0	5.4087592E-03	31	4	0	-1.5720235E+02

31	5	0	-5.6444230E-01	31	6	0	5.9235033E+03	31	7	0	3.8675025E+03	31	8	0	4.8269025E+03
31	9	0	9.2438905E+03	31	10	0	1.4208199E+04	31	11	0	1.2416835E+04	31	12	0	0.
31	13	0	2.8187967E-03	31	14	0	-1.6108294E+02	31	15	0	-2.1652344E-01	31	16	0	3.3005807E+03
31	17	0	-5.2265349E+02	31	18	0	-2.5936691E+03	31	19	0	-2.2061127E+04	31	20	0	-1.1857004E+05
31	21	0	-2.6416376E+04	31	22	0	0.	31	23	0	3.1781146E-03	31	24	0	-2.3407644E+01
31	25	0	-1.3955855E-01	31	26	0	4.8403276E+03	31	27	0	1.8073204E+04	31	28	0	-4.1377004E+02
31	29	0	-8.7636583E+04	31	30	0	-5.9356493E+05	31	31	0	1.5470512E+06	31	32	0	-6.9595085E+05
31	33	0	4.3712103E+03	31	34	0	2.8902363E+02	31	39	0	1.2529025E+03	31	40	0	1.6380617E+03
31	41	0	-6.8880412E-01	31	50	0	0.	31	51	0	-3.6251917E+03	31	52	0	7.8502283E+03
32	1	0	3.9421728E+03	32	2	0	0.	32	3	0	3.8015267E-03	32	4	0	-1.1048912E+02
32	5	0	-4.1377322E-01	32	6	0	5.1135473E+03	32	7	0	4.3073147E+03	32	8	0	4.8012554E+03
32	9	0	8.6469199E+03	32	10	0	1.2142883E+04	32	11	0	1.7003115E+04	32	12	0	0.
32	13	0	1.9755585E-03	32	14	0	-1.2396883E+02	32	15	0	-1.5218274E-01	32	16	0	5.6639597E+03
32	17	0	3.0178712E+03	32	18	0	1.3368665E+04	32	19	0	2.3963709E+03	32	20	0	-2.2033501E+04
32	21	0	-1.5487058E+05	32	22	0	0.	32	23	0	2.2337267E-03	32	24	0	2.2756289E+03
32	25	0	-9.8382612E-02	32	26	0	5.1111421E+03	32	27	0	2.1790196E+04	32	28	0	5.0640854E+04
32	29	0	5.0854858E+04	32	30	0	-2.2805287E+04	32	31	0	-6.9595985E+05	32	32	0	6.7933829E+05
32	37	0	5.9976975E+03	32	38	0	3.3338213E+01	32	39	0	1.6806541E+03	32	40	0	1.6676991E+03
32	41	0	-4.7793851E-01	32	50	0	0.	32	51	0	-5.7151910E+03	32	52	0	5.4649053E+03
33	33	0	3.7459088E+06	33	34	0	-1.0185131E+04	33	35	0	-3.4015535E+05	33	36	0	5.2083988E+04
33	41	0	5.7254286E+02	33	42	0	1.9671233E+02	33	43	0	-2.4159868E+02	33	44	0	-7.2400456E+02
33	45	0	-3.5387912E+04	33	46	0	-5.7557443E+04	33	47	0	-1.3741204E+04	33	48	0	-2.3705573E+04
33	49	0	-3.5319093E+04	33	50	0	5.0090757E+04	33	51	0	-1.0612307E+05	33	52	0	-1.2519205E+05
34	33	0	-1.0185131E+04	34	34	0	4.7727963E+05	34	35	0	5.5332535E+04	34	36	0	-1.4497458E+05
34	41	0	-6.2363888E+02	34	42	0	-5.8172827E+02	34	43	0	-1.8416781E+03	34	44	0	-3.3242284E+03
34	45	0	-3.4851376E+04	34	46	0	-5.2960955E+04	34	47	0	-2.5354862E+04	34	48	0	-4.2513071E+04
34	49	0	4.4754824E+03	34	50	0	-1.5378573E+04	34	51	0	2.2629752E+04	34	52	0	-1.2517892E+05
35	33	0	-3.4315535E+05	35	34	0	5.5332535E+04	35	35	0	3.7450300E+06	35	36	0	8.6713548E+03
35	41	0	-2.8514892E+04	35	42	0	-5.5351635E+02	35	43	0	-2.2896542E+04	35	44	0	-1.0948661E+04
35	45	0	-1.8481618E+04	35	46	0	-3.1306600E+04	35	47	0	-4.3031474E+04	35	48	0	-7.1083006E+04
35	49	0	-2.3452827E+04	35	50	0	1.6418981E+04	35	51	0	-1.5700507E+05	35	52	0	-1.1438102E+05
36	33	0	5.2283988E+04	36	34	0	-1.4497653E+05	36	35	0	8.6713548E+03	36	36	0	4.5972976E+05
36	41	0	9.2422967E+03	36	42	0	5.6912741E+02	36	43	0	1.1389653E+04	36	44	0	7.5899489E+03
36	45	0	-2.4393905E+04	36	46	0	-4.1491795E+04	36	47	0	-4.8872460E+04	36	48	0	-8.6915652E+04
36	49	0	8.2817431E+02	36	50	0	-7.8335647E+03	36	51	0	4.0967739E+04	36	52	0	-8.5262510E+04
37	1	0	-1.6255263E+05	37	2	0	0.	37	3	0	1.9250836E+00	37	4	0	-5.5968852E+04
37	5	0	-2.6887936E+02	37	6	0	-3.0341843E+03	37	7	0	-3.1083622E+04	37	8	0	-2.8322005E+05
37	9	0	-2.4529484E+04	37	10	0	-4.1579953E+02	37	11	0	1.2685355E+04	37	12	0	0.
37	13	0	1.6887297E+08	37	14	0	-2.5455254E+04	37	15	0	-7.7038976E+01	37	16	0	-1.8074437E+03
37	17	0	7.7383289E+02	37	18	0	5.2596352E+03	37	19	0	1.0552635E+04	37	20	0	5.3402650E+03
37	21	0	1.6832991E+04	37	22	0	0.	37	23	0	1.1315051E+00	37	24	0	2.6661360E+03
37	25	0	-4.9534269E+01	37	26	0	-3.6311530E+00	37	27	0	1.1263737E+02	37	28	0	1.4218349E+03
37	29	0	4.7370975E+03	37	30	0	4.1112217E+03	37	31	0	4.3712103E+03	37	32	0	5.9976975E+03
37	37	0	1.5963499E+06	37	38	0	-2.7240036E+05	37	39	0	-7.2142933E+05	37	40	0	7.5726312E+04
37	41	0	-2.4213229E+02	37	50	0	0.	37	51	0	-7.7694939E+05	37	52	0	1.1382852E+05
38	1	0	-2.7531245E+05	38	2	0	0.	38	3	0	-8.3674875E-01	38	4	0	2.4319607E+04
38	5	0	9.6414722E+01	38	6	0	3.9356792E+02	38	7	0	-5.6803345E+02	38	8	0	-1.1306854E+04
38	9	0	-1.0593744E+04	38	10	0	-4.8424725E+03	38	11	0	-1.4298754E+03	38	12	0	0.
38	13	0	-4.3483745E-01	38	14	0	3.2938706E+03	38	15	0	3.3496731E+01	38	16	0	8.7552610E+03
38	17	0	1.1633668E+03	38	18	0	5.1898304E+03	38	19	0	1.7147353E+03	38	20	0	-3.3730615E+02
38	21	0	-7.3463155E+02	38	22	0	0.	38	23	0	-4.9166248E-01	38	24	0	-5.8257461E+03
38	25	0	2.1508828E+01	38	26	0	1.2519711E+02	38	27	0	4.5227727E+02	38	28	0	6.3230569E+02
38	29	0	1.8944333E+03	38	30	0	5.3282788E+02	38	31	0	2.6902369E+02	38	32	0	8.3338218E+01
38	37	0	-2.7248868E+05	38	38	0	5.6587862E+05	38	39	0	6.6411838E+04	38	40	0	-8.3216608E+04
38	41	0	1.8513838E+02	38	50	0	0.	38	51	0	3.9189817E+05	38	52	0	-2.3194331E+04
39	1	0	-4.1988058E+04	39	2	0	0.	39	3	0	6.4598405E-01	39	4	0	-1.8775144E+04
39	5	0	-6.9261579E+01	39	6	0	-3.1461697E+03	39	7	0	-7.5766918E+03	39	8	0	-4.2048454E+04

39	9	0	-6.4327523E+03	39	10	0	2.6229643E+03	39	11	0	3.775+136E+03	39	12	0	0.				
39	13	0	1.3572179E-01	39	14	0	-1.4316315E+02	39	15	0	-2.586[37E+01	39	16	0	-8.66683[2E+02				
39	17	0	2.3344283E+02	39	18	0	2.5279672E+03	39	19	0	2.181[464E+03	39	20	0	1.8536795E+03				
39	21	0	7.1653700E+03	39	22	0	0.	39	23	0	3.7957157E-01	39	24	0	1.8197642E+04				
39	25	0	-1.6666936E+01	39	26	0	-4.4891841E+01	39	27	0	-1.2527J75E+02	39	28	0	2.2926621E+02				
39	29	0	9.8893109E+02	39	30	0	3.3484652E+02	39	31	0	1.252[025E+03	39	32	0	1.8808541E+03				
39	37	0	-7.2142993E+05	39	38	0	2.6+11883E+04	39	39	0	1.182+656E+06	39	40	0	-3.5932943E+05				
39	43	0	-9.1214911E+01	39	50	0	0.	39	51	0	-5.4426232E+05	39	52	0	9.9833792E+04				
40	1	0	-2.9982648E+05	40	2	0	0.	40	3	0	-7.5237359E-01	40	4	0	2.1867438E+0.				
40	5	0	4.1296121E+01	40	6	0	-4.8972212E+02	40	7	0	-5.8835219E+03	40	8	0	-3.6503794E+04				
40	9	0	-5.9755722E+05	40	10	0	-1.3509177E+04	40	11	0	-4.7307625E+02	40	12	0	0.				
40	13	0	-3.9099238E-01	40	14	0	4.5945861E+03	40	15	0	3.0113224E+01	40	16	0	7.1974864E+02				
40	17	0	1.6438931E+03	40	18	0	3.1929411E+03	40	19	0	6.2575697E+03	40	20	0	2.0262427E+03				
40	21	0	2.9668225E+02	40	22	0	0.	40	23	0	-4.4205769E-01	40	24	0	-1.4450892E+04				
40	25	0	1.9412086E+01	40	26	0	1.5908133E+02	40	27	0	5.6628951E+02	40	28	0	1.0598370E+03				
40	29	0	2.4564373E+03	40	30	0	1.9564532E+03	40	31	0	1.6386617E+03	40	32	0	1.6676991E+03				
40	37	0	7.5726312E+04	40	38	0	-3.3216663E+04	40	39	0	-3.5931943E+05	40	40	0	6.9525488E+05				
40	43	0	3.4591129E+01	40	50	0	0.	40	51	0	5.3953601E+05	40	52	0	-5.8515586E+04				
41	33	0	5.7254206E+02	41	34	0	-3.2363883E+02	41	35	0	-2.0514492E+04	41	36	0	9.2422967E+03				
41	41	0	5.7369305E+04	41	42	0	-1.9434503E+03	41	43	0	-3.2133573E+04	41	44	0	1.0611373E+04				
41	45	0	-1.8662959E+03	41	46	0	-1.7980331E+03	41	47	0	-9.8203221E+02	41	48	0	-1.6441534E+03				
41	49	0	5.8874632E+02	41	50	0	-1.8296294E+02	41	51	0	-4.6191321E+03	41	52	0	-4.3269112E+03				
42	33	0	8.9671239E+02	42	34	0	-3.6172827E+02	42	35	0	-3.5354833E+02	42	36	0	5.6812741E+02				
42	41	0	-1.9434509E+03	42	42	0	3.8198988E+03	42	43	0	2.7587539E+03	42	44	0	-1.9718405E+03				
42	45	0	-4.4359956E+02	42	46	0	-7.4557249E+02	42	47	0	-5.6249218E+02	42	48	0	-9.5821752E+02				
42	49	0	2.8252843E+02	42	50	0	-4.4449095E+02	42	51	0	-1.3023539E+03	42	52	0	-1.6888982E+03				
43	33	0	-2.4159868E+02	43	34	0	-1.8418781E+03	43	35	0	-2.2896542E+04	43	36	0	1.1389653E+04				
43	41	0	-3.2139573E+04	43	42	0	2.7587633E+03	43	43	0	6.4490753E+04	43	44	0	1.2172231E+04				
43	45	0	-1.6376354E+03	43	46	0	-2.7552745E+03	43	47	0	-1.9773297E+03	43	48	0	-3.3667068E+03				
43	49	0	5.7285944E+02	43	50	0	-1.1595419E+03	43	51	0	-5.1713244E+03	43	52	0	-6.6046902E+03				
44	33	0	-7.2608458E+02	44	34	0	-3.3242284E+03	44	35	0	-1.0940561E+04	44	36	0	7.5899409E+03				
44	41	0	1.3511073E+04	44	42	0	-1.9718405E+03	44	43	0	1.2172231E+04	44	44	0	2.5320655E+04				
44	45	0	-1.9365525E+03	44	46	0	-3.2696104E+03	44	47	0	-2.9290336E+03	44	48	0	-5.0403605E+03				
44	49	0	3.9892383E+02	44	50	0	-4.0513281E+03	44	51	0	-3.7100595E+03	44	52	0	-7.6695035E+03				
45	33	0	-3.5306791E+04	45	34	0	-3.4451375E+04	45	35	0	-1.6481610E+04	45	36	0	-2.4993905E+04				
45	41	0	-2.6662959E+03	45	42	0	-4.4359955E+02	45	43	0	-1.6372334E+03	45	44	0	-1.9365950E+03				
45	45	0	1.6911061E+05	45	46	0	1.6734813E+05	45	47	0	-9.4094491E+03	45	48	0	-1.6225875E+04				
45	49	0	-1.8534363E+03	45	50	0	-3.5381051E+03	45	51	0	7.8753334E+03	45	52	0	-4.6577593E+04				
46	33	0	-5.7957448E+04	46	34	0	-3.2360455E+04	46	35	0	-3.1306636E+04	46	36	0	-4.1991796E+04				
46	41	0	-1.7983330E+03	46	42	0	-7.4557209E+02	46	43	0	-2.7552245E+03	46	44	0	-3.2696164E+03				
46	45	0	1.6734819E+05	46	46	0	2.9361913E+05	46	47	0	-1.5861523E+04	46	48	0	-2.7447062E+04				
46	49	0	-3.6897261E+03	46	50	0	-5.9289902E+03	46	51	0	1.4233355E+04	46	52	0	-8.0391427E+04				
47	33	0	-1.3741204E+04	47	34	0	-2.5354662E+04	47	35	0	-4.3031474E+04	47	36	0	-4.8872460E+04				
47	41	0	-9.8228221E+02	47	42	0	-3.8249219E+02	47	43	0	-1.9773297E+03	47	44	0	-2.9290306E+03				
47	45	0	-3.4394491E+03	47	46	0	-1.5861521E+04	47	47	0	9.9600322E+04	47	48	0	1.6695216E+05				
47	49	0	-1.8286016E+03	47	50	0	-1.6899222+E+03	47	51	0	1.0296321E+04	47	52	0	-3.7219733E+04				
48	33	0	-2.3736571E+04	48	34	0	-4.2513071E+04	48	35	0	-7.1083036E+04	48	36	0	-8.6915652E+04				
48	41	0	-1.6441534E+03	48	42	0	-3.5521752E+02	48	43	0	-3.3662368E+03	48	44	0	-5.0403605E+03				
48	45	0	-1.6225475E+04	48	46	0	-2.7+47902E+04	48	47	0	1.6695216E+05	48	48	0	2.9612113E+05				
48	49	0	-1.7716573E+03	48	50	0	-2.8747397E+03	48	51	0	1.9213437E+04	48	52	0	-6.4327506E+04				
49	1	0	-5.4191780E+01	49	2	0	0.	49	3	0	-1.1173685E+02	49	4	0	-1.3850857E+03				
49	5	0	1.2393187E+04	49	6	0	-2.5312531E+04	49	7	0	-5.1647669E+01	49	8	0	5.0504617E+01				
49	9	0	8.1385008E+03	49	10	0	+.5269265E+00	49	11	0	7.8601451E+00	49	12	0	0.				
49	13	0	-5.8398835E+01	49	14	0	-1.7368451E+02	49	15	0	4.4754323E+03	49	16	0	-4.4059229E+03				
49	17	0	-9.3467302E-01	49	18	0	-1.4116613E-03	49	19	0	-5.3063542E+03	49	20	0	-1.7665861E+04				
49	21	0	-4.6509855E-01	49	22	0	0.	49	23	0	-6.5E9.3495E+01	49	24	0	-1.4643198E+02				
49	25	0	2.8844516E+01	49	26	0	1.1718874E-02	49	27	0	-2.8191305E+03	49	28	0	-3.0857101E+01				

49	29	0	-2.7481693E+02	49	30	0	-1.0727d1aE+0d	49	31	0	-6.800d+12E-01	49	32	0	-4.7793851E-01				
49	33	0	-2.5319693E+04	49	34	0	+.475+02+E+03	49	35	0	-2.3452827E+04	49	36	0	8.2017431E+02				
49	37	0	-2.4210229E+02	49	38	0	1.0519833E+02	49	39	0	-8.1214311E+01	49	40	0	9.4591129E+01				
49	41	0	5.8174602E+02	49	42	0	2.8252843E+02	49	43	0	5.7285944E+02	49	44	0	3.9892363E+02				
49	45	0	-1.8334363E+03	49	46	0	-3.8597261E+03	49	47	0	-1.0108016E+03	49	48	0	-1.7716573E+03				
49	49	0	-3.8115732E+04	49	50	0	-5.9225175E+04	49	51	0	-2.9634238E+03	49	52	0	-1.8558354E+04				
50	33	0	3.6698757E+04	50	34	0	-1.5376573E+04	50	35	0	1.6816381E+04	50	36	0	-7.8335647E+03				
50	41	0	-9.8296294E+02	50	42	0	-+.++49095E+02	50	43	0	-1.153+419E+03	50	44	0	-1.0613281E+03				
50	45	0	-3.5381851E+03	50	46	0	-5.9289902E+03	50	47	0	-1.6899224E+03	50	48	0	-2.8747397E+03				
50	49	0	-6.9225175E+04	50	50	0	2.3664355E+05	50	51	0	7.4975139E+04	50	52	0	2.4425632E+04				
51	1	0	-1.5727716E+05	51	2	0	).	51	3	0	1.5721647E+01	51	4	0	-4.5694618E+05				
51	5	0	-1.6988211E+03	51	6	0	+.6182234E+03	51	7	0	4.8186426E+04	51	8	0	2.4176371E+05				
51	9	0	1.6252885E+04	51	10	0	-1.2120633E+04	51	11	0	-1.7239502E+04	51	12	0	0.				
51	13	0	6.1782518E+00	51	14	0	-2.8244925E+05	51	15	0	-6.2937739E+02	51	16	0	1.2927696E+03				
51	17	0	1.1834188E+03	51	18	0	-1.3022671E+03	51	19	0	-5.8575784E+03	51	20	0	-4.7495481E+05				
51	21	0	-1.8487094E+04	51	22	0	).	51	23	0	9.2379492E+00	51	24	0	-1.2866747E+05				
51	25	0	-4.6563788E+02	51	26	0	1.9357141E+02	51	27	0	1.0670344E+03	51	28	0	-1.0786054E+01				
51	29	0	-2.6384534E+03	51	30	0	-2.8663576E+03	51	31	0	-3.6251917E+03	51	32	0	-5.7151910E+03				
51	33	0	-1.8612387E+05	51	34	0	2.2625762E+04	51	35	0	-1.5706567E+05	51	36	0	4.6964739E+04				
51	37	0	-7.7694939E+05	51	38	0	5.9189817E+05	51	39	0	-5.4428202E+05	51	40	0	5.3958601E+05				
51	41	0	-4.6191021E+03	51	42	0	-1.3829539E+03	51	43	0	-5.1713244E+03	51	44	0	-3.7108956E+03				
51	45	0	7.8793324E+03	51	46	0	1.4230355E+04	51	47	0	1.0296321E+04	51	48	0	1.9213437E+04				
51	49	0	-2.9634298E+03	51	50	0	7.4975139E+04	51	51	0	3.2981933E+06	51	52	0	-1.3307727E+05				
52	1	0	-1.2258774E+05	52	2	0	).	52	3	0	3.2360330E-01	52	4	0	-9.4852510E+03				
52	5	0	-3.4966547E+01	52	6	0	7.7515203E+03	52	7	0	1.3944312E+04	52	8	0	3.4265719E+04				
52	9	0	3.6785273E+02	52	10	0	-1.4536641E+05	52	11	0	-5.1527085E+05	52	12	0	0.				
52	13	0	1.6816706E-01	52	14	0	-3.9511942E+03	52	15	0	-1.2954369E+01	52	16	0	4.4844198E+03				
52	17	0	3.3786282E+03	52	18	0	7.7503036E+03	52	19	0	9.2522078E+03	52	20	0	1.0025598E+04				
52	21	0	1.3529864E+04	52	22	0	).	52	23	0	1.9014325E-01	52	24	0	3.9418682E+03				
52	25	0	-8.3491622E+00	52	26	0	5.6414866E+02	52	27	0	2.4241755E+03	52	28	0	2.8035905E+05				
52	29	0	4.7561400E+03	52	30	0	5.6290663E+03	52	31	0	7.8502263E+03	52	32	0	5.4645053E+03				
52	33	0	-1.2519205E+05	52	34	0	-1.2537693E+05	52	35	0	-1.1436132E+05	52	36	0	-8.5262510E+04				
52	37	0	1.1382852E+05	52	38	0	-2.3194331E+04	52	39	0	9.9833732E+04	52	40	0	-5.8515586E+04				
52	41	0	-4.5269112E+03	52	42	0	-1.6488982E+03	52	43	0	-6.6046902E+03	52	44	0	-7.6695065E+03				
52	45	0	-4.6577593E+04	52	46	0	-5.0391427E+04	52	47	0	-3.7213733E+04	52	48	0	-6.4327506E+04				
52	49	0	-1.8558354E+04	52	50	0	2.4425632E+04	52	51	0	-1.3387727E+05	52	52	0	1.3708804E+06				
1	1	2	2.0260080E+08	2	2	2	1.2940000E-01	3	3	2	1.2940300E-01	4	4	2	1.4230000E-01				
5	5	2	1.4230000E-01	6	6	2	+.2930000E-01	7	7	2	1.7030000E-01	8	8	2	1.5420000E-01				
9	9	2	1.2940000E-01	10	10	2	1.2940000E-01	11	11	2	8.6700300E-02	12	12	2	1.2940000E-01				
13	13	2	1.2940000E-01	14	14	2	1.4750000E-01	15	15	2	1.4750300E-01	16	16	2	3.5230000E-01				
17	17	2	1.6153000E-01	18	18	2	1.4100000E-01	19	19	2	1.2503000E-01	20	20	2	1.2500000E-01				
21	21	2	8.8800000E-02	22	22	2	1.2740000E-01	23	23	2	1.2943030E-01	24	24	2	1.4230000E-01				
25	25	2	1.4230000E-01	26	26	2	1.7490000E-01	27	27	2	6.8580300E-01	28	28	2	4.0940000E-01				
29	29	2	2.4590000E-01	30	30	2	2.6960000E-01	31	31	2	2.8963030E-01	32	32	2	1.1620000E-01				
2	2	2	0.	3	3	2	).	4	4	2	0.	5	5	2	0.				
12	12	2	0.	13	13	2	).	14	14	2	0.	15	15	2	0.				
22	22	2	0.	23	23	2	).	24	24	2	0.	25	25	2	0.				